CISTER
Research Centre in
Real-Time & Embedded
Computing Systems

PhD Thesis

Synchronous Intelligent Intersections for Sustainable Urban Mobility

Radha Reddy

CISTER-TR-231002

2023

Synchronous Intelligent Intersections for Sustainable Urban Mobility

Radha Reddy

CISTER Research Centre

Polytechnic Institute of Porto (ISEP P.Porto)

Rua Dr. António Bernardino de Almeida, 431

4200-072 Porto

Portugal

Tel.: +351.22.8340509, Fax: +351.22.8321159

E-mail: reddy@isep.ipp.pt

https://www.cister-labs.pt

Abstract

According to the United Nations urbanization report 2018, 55% of the world's population lives in urban areas and is expected to reach 68% by 2050. Current urban transportation services (except during COVID-19) are already strained, causing fossil fuel dependency, environmental pollution, and associated human health. For instance, in the United States of America, urban dwellers lost 8.7 billion hours and almost 3.5 billion gallons of fuel due to traffic congestion in 2019 alone. In the case of the European Union, member states lost an estimated 110 billion euros annually for similar reasons. As per the European Environment Agency, 80% of European urban dwellers are exposed to dangerous vehicular emissions, particularly at intersections, bus stops, and other points of traffic confluence. This exposure can cause heart disease, cancer, respiratory disease, and, in the worst case, death. Therefore, in the worst-case scenario, the urban future would bring disastrous consequences, including transportation and mobility, human health, and environmental challenges. Hence, sustainable transportation is a major concern, requiring affordable energy-efficient transportation and emitting low to zero air pollutants, including alternate energy sources like electricity.

Intelligent transportation systems (ITS) incorporating communication, electric and autonomous technologies provide new opportunities for sustainable urban mobility (SUM). In the USA, the National Highway Traffic Safety Administration (NHTSA) anticipates that autonomous vehicles (AVs) would reduce nearly 50 minutes of average commuter delay daily. However, autonomous-only urban transportation is not expected before 2045, and transitioning from human-driven internal combustion engine (ICE) vehicles to communicating and electric AVs will take long. Therefore, ITS-based solutions of the near future must support mixed traffic of AVs and human-driven vehicles (HVs).

Motivated by these facts, we identify the vital role that road intersections play in urban transportation, where growing trends in queue length, waiting delays, and associated adverse effects can be observed. Existing intersection management (IM) strategies permit vehicles to access intersections sequentially from one road at a time or parallelly from opposite road lanes while blocking the traffic of other roads and lanes. This behavior imposes unnecessary waiting delays at intersections. Thus, this thesis introduces a reactive synchronous framework for maximizing vehicle intersection access from all non-conflicting roads based on their arrival at the intersection entrance instead of reserving lengthy time slots or imposing strong differentiation between HVs and AVs.

To study the practicality and performance of the synchronous framework, we resort to the Simulation of Urban MObility (SUMO) microscopic traffic simulator throughout this thesis. The synchronous framework is then applied to both isolated intersections (single-lane and multi-lane) and networks of multi-lane intersections. Two left-lane (dedicated and shared) configurations for multi-lane intersections are considered. The performance metrics, such as the throughput, average travel time loss, and associated fuel consumption, are measured for low-speed urban conditions. The simulation results of the tested scenarios show that synchronizing vehicles intersection access improves throughput between 3 to 30%, reduces travel time loss between 56 to 129%, and minimizes associated fuel consumption between 18.2 to 67.4% against the next best baseline approaches.

We also evaluate the operational efficiency of the IM systems in what concerns the worst-case reaction to given traffic scenarios described statistically. For this purpose, we borrowed a service metric from real-time systems concepts namely the Worst-Case Response Time (WCRT). The WCRT evaluates the maximum time a vehicle may experience since it enters an input road (i.e., origin) until it leaves the last intersection in its path before heading to the respective destination. The commonly available parameters such as the geographical settings of the road networks (road lanes length and intersection space within), traffic-related information (average speed, maximum

queue length, and capacity), and IM-specific parameters (green phase time and total cycle time) are utilized to formulate the WCRT. The analytical WCRT values are validated with simulation studies. On average, the computed WCRT values in diverse traffic conditions were up to 20% and 18% higher than the observed WCRT values at isolated single-lane and multi-lane intersections, respectively. In the case of networks of intersections, these values were up to 86.7% (64.5%), 49.5% (34.2%), and 47.6% (30.25%) higher for crossing single, two, and three dedicated (and shared) left lane intersections, respectively. This means the pessimism of estimated WCRT values gradually reduces for increasing number of crossed intersections and it also reduces from dedicated to shared left lane intersections.

Finally, we study the transportation sustainability of introducing growing penetration rates of AVs, either considering propulsion systems with gasoline ICE or with electric batteries (BEVs). Energy savings and emissions reduction are considered as performance metrics. The results show that our \textitsynchronous framework is more sustainable than the benchmark approaches in all the tested scenarios, speeds, and intersections, mainly when human-driven ICE vehicles are mixed with BEVs. In the networks of intersections case, the overall energy savings when increasing the AVs penetration from 10% to 90% are up to 43% (gasoline) and 1.45% (electricity), and emissions reduction is up to 42.6% (CO_2), 48.2% (NOx), 64.9% (PMx), 79.5% (HC), and 89.45% (CO). In the isolated intersections cases, these improvements are even more significant.

Overall, our research shows that the proposed synchronous framework has a high potential to improve the performance of intersections in urban scenarios during the transition period of human-driven to autonomous-only vehicles.

Faculdade de Engenharia da Universidade do Porto

Synchronous Intelligent Intersections for Sustainable Urban Mobility

Radha Krishna Reddy Pallavali

Doctoral Program in Electrical and Computer Engineering

Supervisor: Prof. Eduardo Manuel Medicis Tovar

Co-Supervisor: Prof. Luís Miguel Pinho de Almeida

Co-Supervisor: Prof. Pedro Miguel Salgueiro dos Santos

October 24, 2023

Synchronous Intelligent Intersections for Sustainable Urban Mobility

Radha Krishna Reddy Pallavali

Doctoral Program in Electrical and Computer Engineering

Approved by:

President: Prof. Dr. José Nuno Moura Marques Fidalgo, FEUP, Portugal
External Referee: Prof. Dr. Thidapat Chantem, Virginia Tech, USA
External Referee: Prof. Dr. Samia Saad-Bouzefrane, CNAM, France
External Referee: Prof. Dr. Joaquim José de Castro Ferreira, ESTGA-UA, Portugal
Internal Referee: Prof. Dr. Pedro Alexandre Guimarães Lobo Ferreira Souto, FEUP, Portugal
Supervisor: Prof. Dr. Eduardo Manuel Medicis Tovar, ISEP, Portugal
Co-Supervisor: Prof. Dr. Luís Miguel Pinho de Almeida, FEUP, Portugal
Co-Supervisor: Prof. Dr. Pedro Miguel Salgueiro dos Santos, FEUP, Portugal

---

October 24, 2023

Abstract

According to the United Nations urbanization report 2018, 55% of the world population lives in urban areas and is expected to reach 68% by 2050. Current urban transportation services (except during COVID-19) are already strained, causing fossil fuel dependency, environmental pollution, and associated human health. For instance, in the United States of America, urban dwellers lost 8.7 billion hours and almost 3.5 billion gallons of fuel due to traffic congestion in 2019 alone. In the case of the European Union, member states lost an estimated 110 billion euros annually for similar reasons. As per the European Environment Agency, 80% of European urban dwellers are exposed to dangerous vehicular emissions, particularly at intersections, bus stops, and other points of traffic confluence. This exposure can cause heart disease, cancer, respiratory disease, and, in the worst case, death. Therefore, in the worst-case scenario, the urban future would bring disastrous consequences, including transportation and mobility, human health, and environmental challenges. Hence, sustainable transportation is a major concern, requiring affordable energy-efficient transportation and emitting low to zero air pollutants, including alternate energy sources like electricity.

Intelligent transportation systems (ITS) incorporating communication, electric and autonomous technologies provide new opportunities for sustainable urban mobility (SUM). In the USA, the National Highway Traffic Safety Administration (NHTSA) anticipates that autonomous vehicles (AVs) would reduce nearly 50 minutes of average commuter delay daily. However, autonomous-only urban transportation is not expected before 2045, and transitioning from human-driven internal combustion engine (ICE) vehicles to communicating and electric AVs will take long. Therefore, ITS-based solutions of the near future must support mixed traffic of AVs and human-driven vehicles (HVs).

Motivated by these facts, we identify the vital role that road intersections play in urban transportation, where growing trends in queue length, waiting delays, and associated adverse effects can be observed. Existing intersection management (IM) strategies permit vehicles to access intersections sequentially from one road at a time or parallelly from opposite road lanes while blocking the traffic of other roads and lanes. This behavior imposes unnecessary waiting delays at intersections. Thus, this thesis introduces a reactive *synchronous framework* for maximizing vehicle intersection access from all non-conflicting roads based on their arrival at the intersection entrance instead of reserving lengthy time slots or imposing strong differentiation between HVs and AVs.

To study the practicality and performance of the *synchronous framework*, we resort to the Simulation of Urban MObility (SUMO) microscopic traffic simulator throughout this thesis. The *synchronous framework* is then applied to both isolated intersections (single-lane and multi-lane) and networks of multi-lane intersections. Two left-lane (dedicated and shared) configurations for multi-lane intersections are considered. The performance metrics, such as the throughput, average travel time loss, and associated fuel consumption,

are measured for low-speed urban conditions. The simulation results of the tested scenarios show that synchronizing vehicles intersection access improves throughput between 3 to 30%, reduces travel time loss between 56 to 129%, and minimizes associated fuel consumption between 18.2 to 67.4% against the next best baseline approaches.

We also evaluate the operational efficiency of the IM systems in what concerns the worst-case reaction to given traffic scenarios described statistically. For this purpose, we borrowed a service metric from real-time systems concepts namely the Worst-Case Response Time (WCRT). The WCRT evaluates the maximum time a vehicle may experience since it enters an input road (i.e., origin) until it leaves the last intersection in its path before heading to the respective destination. The commonly available parameters such as the geographical settings of the road networks (road lanes length and intersection space within), traffic-related information (average speed, maximum queue length, and capacity), and IM-specific parameters (green phase time and total cycle time) are utilized to formulate the WCRT. The analytical WCRT values are validated with simulation studies. On average, the computed WCRT values in diverse traffic conditions were up to 20% and 18% higher than the observed WCRT values at isolated single-lane and multi-lane intersections, respectively. In the case of networks of intersections, these values were up to 86.7% (64.5%), 49.5% (34.2%), and 47.6% (30.25%) higher for crossing single, two, and three dedicated (and shared) left lane intersections, respectively. This means the pessimism of estimated WCRT values gradually reduces for increasing number of crossed intersections and it also reduces from dedicated to shared left lane intersections.

Finally, we study the transportation sustainability of introducing growing penetration rates of AVs, either considering propulsion systems with gasoline ICE or with electric batteries (BEVs). Energy savings and emissions reduction are considered as performance metrics. The results show that our *synchronous framework* is more sustainable than the benchmark approaches in all the tested scenarios, speeds, and intersections, mainly when human-driven ICE vehicles are mixed with BEVs. In the networks of intersections case, the overall energy savings when increasing the AVs penetration from 10% to 90% are up to 43% (gasoline) and 1.45% (electricity), and emissions reduction is up to 42.6% (CO_2), 48.2% (NOx), 64.9% (PMx), 79.5% (HC), and 89.45% (CO). In the isolated intersections cases, these improvements are even more significant.

Overall, our research shows that the proposed *synchronous framework* has a high potential to improve the performance of intersections in urban scenarios during the transition period of human-driven to autonomous-only vehicles.

Keywords: Sustainable urban mobility, intelligent transportation systems, synchronous intelligent intersections, intersection management systems.

Resumo

De acordo com o relatório de urbanização das Nações Unidas de 2018, 55% da população mundial vive em áreas urbanas e espera-se que atinja 68% até 2050. Os actuais serviços de transporte urbano (excepto durante a COVID-19) já estão sobrecarregados, causando dependência de combustíveis fósseis e problemas ambientais com poluição e degradação da saúde humana. Por exemplo, nos Estados Unidos da América, os habitantes de zonas urbanas perderam 8,7 mil milhões de horas e quase 3,5 mil milhões de galões de combustível devido ao congestionamento do tráfego só em 2019. Nos estados membros da União Europeia, as perdas pelas mesmas razões ascenderam a cerca de 110 mil milhões de euros anualmente. De acordo com a Agência Europeia do Ambiente, 80% dos habitantes urbanos europeus estão expostos a emissões veiculares perigosas, especialmente em cruzamentos, paragens de autocarro e outros pontos de confluência de tráfego. Esta exposição pode causar doenças cardíacas, cancro, doenças respiratórias e, no pior dos casos, morte. Portanto, na pior das hipóteses, o futuro urbano poderá trazer consequências desastrosas, quer no transporte e mobilidade, quer na saúde humana e desafios ambientais. Assim, o transporte sustentável é uma grande preocupação, exigindo transportes acessíveis e eficientes em termos energéticos e com emissões baixas ou nulas de poluentes atmosféricos, incluindo fontes alternativas de energia como a eletricidade.

Os sistemas de transporte inteligentes (ITS) que incorporam tecnologias de comunicações, tração elétrica e autonomia apresentam novas oportunidades para a mobilidade urbana sustentável (SUM). A National Highway Traffic Safety Administration (NHTSA) prevê que a utilização exclusiva de veículos autónomos (AVs) reduziria quase 50 minutos diários de atraso médio nas viagens dos passageiros. No entanto, o transporte urbano totalmente baseado em AVs não é esperado antes de 2045 e a transição de veículos com motor de combustão interna (ICE) conduzidos por humanos para AVs levará ainda algum tempo. Assim, as soluções baseadas em ITS do futuro próximo devem suportar o tráfego misto de AVs e veículos ICE conduzidos por humanos (HVs). Motivados por estes factos, identificámos o papel vital que os cruzamentos rodoviários desempenham no transporte urbano, onde podem ser observadas tendências crescentes no comprimento das filas, tempos de espera e efeitos adversos associados. As estratégias existentes de gestão de cruzamentos (IM) permitem que os veículos acedam aos cruzamentos sequencialmente por faixas de acesso ou paralelamente a partir de faixas opostas, enquanto bloqueiam o tráfego de outras estradas e faixas rodoviárias. Este comportamento impõe atrasos de espera desnecessários nos cruzamentos. Assim, esta tese propõe uma abordagem síncrona reativa para maximizar o acesso de veículos ao cruzamento provenientes de todas as faixas que não apresentem conflitos, em vez de reservar longos intervalos de tempo ou impor uma forte diferenciação entre HVs e AVs.

Para estudar a praticabilidade e o desempenho da abordagem síncrona recorremos ao longo desta tese ao simulador de tráfego a nível microscópico chamado Simulation of Urban

MObility (SUMO). A abordagem síncrona é então aplicada tanto a cruzamentos isolados (de faixa única ou de faixas múltiplas) e a redes de cruzamentos de faixas múltiplas. São consideradas duas configurações de faixa esquerda (dedicada e partilhada) para cruzamentos com múltiplas faixas. As métricas de desempenho, como rendimento, perda média de tempo de viagem e consumo de combustível associado, são medidas para condições urbanas de baixa velocidade. Os resultados da simulação dos cenários testados mostram que a sincronização do acesso aos cruzamentos de veículos melhora o rendimento entre 3 a 30%, reduz a perda de tempo de viagem entre 56 a 129% e minimiza o consumo de combustível associado entre 18,2 a 67,4% em relação às melhores abordagens de comparação.

Para avaliar a eficiência operacional dos sistemas IM fazemos ainda uso duma métrica de serviço comum em sistemas de tempo real, nomeadamente o Worst-Case Response Time (WCRT). O WCRT avalia o tempo máximo que um veículo pode passar desde que entra numa estrada de acesso ao sistema rodoviário até sair do último cruzamento atravessado em direção ao respetivo destino. Os parâmetros comumente disponíveis, como as configurações geográficas das redes rodoviárias (comprimento das faixas rodoviárias e espaço interno dos cruzamentos), informações relacionadas com o tráfego (velocidade média, comprimento máximo da fila e capacidade das faixas) e parâmetros específicos de IM (tempo da fase verde e total tempo de ciclo) são utilizados para formular o WCRT. Os valores analíticos do WCRT são validados através de estudos de simulação. Em média, os valores WCRT calculados em condições saturadas foram até 20% e 18% superiores aos valores WCRT observados nos cruzamentos isolados de faixa única e de múltiplas faixas, respetivamente. No caso das redes de cruzamentos, esses valores foram até 86,7% (64,5%), 49,5% (34,2%) e 47,6% (30,25%) maiores para redes com um, dois e três cruzamentos com duas faixas e para faixas esquerdas dedicadas (e partilhadas), respetivamente. Isto significa que o pessimismo dos valores WCRT estimados reduz gradualmente com o aumento do número de cruzamentos atravessados e também reduz quando os cruzamentos usam a faixa esquerda partilhada.

Finalmente, estudamos a sustentabilidade do transporte com a introdução de taxas crescentes de penetração de AVs, quer usando propulsão ICE quer elétrica com baterias (BEVs). As métricas de desempenho consideradas são a poupança de energia e a redução de emissões. Os resultados mostram que a nossa estrutura síncrona é mais sustentável do que as abordagens de referência em todos os cenários, velocidades e cruzamentos testados, principalmente quando veículos ICE conduzidos por humanos são misturados com BEVs. No caso das redes de cruzamentos, a poupança global de energia ao aumentar a penetração dos AVs de 10% para 90% é de até 43% (gasolina) e 1,45% (eletricidade), e a redução de emissões é de até 42,6% (CO2), 48,2% (N Ox), 64,9% (P M x), 79,5% (HC) e 89,45% (CO). Nos casos de cruzamentos isolados, essas melhorias são ainda mais significativas.

No geral, a nossa investigação mostra que a abordagem síncrona proposta tem um elevado potencial para melhorar o desempenho dos cruzamentos em cenários urbanos durante o período de transição de veículos conduzidos por seres humanos para veículos exclusivamente autónomos.

Palavras-chave: Mobilidade urbana sustentável, sistemas de transporte inteligentes, cruzamentos inteligentes síncronos, sistemas de gestão de cruzamentos.

Acknowledgments

First, I would like to express my deepest gratitude to my supervisors, Prof. **Eduardo Tovar**, Prof. **Luis Almeida**, and Prof. **Pedro Santos**, for their strong support during my **doctoral** thesis and related research. I am exceptionally grateful to my supervisors for providing research independence, funding, and guidance in securing the FCT fellowship (**2021.05004.BD**). This made my time fruitful and enjoyable - a Ph.D. student couldn't expect more.

Especially to my GURU Prof. **Luis Almeida**, who not only provided me with scientific knowledge but also wisdom, motivation, and support without whom this milestone couldn't have been achieved.

To all the co-authors for their support in refining the research studies, the **DaRTES** team at FEUP for hosting me for the CRUAV project internship, and the ADACORSA and FLOYD project teams for funding.

I am so grateful to Prof. **Samia Bouzefrane**, CEDRIC Lab, CNAM-Paris, France, for her strong support with whom I achieved my first conference paper, consequent European Ph.D. life, shared ten years of bonding, and still counting.

Special thanks to **Sandra**, **Filipe**, **Marwin**, **Cristiana**, **Inês**, **Benilde**, and **Henrique** for their extraordinary administrative and technical support. To my friends and colleagues of CISTER Research Center, including **Miguel, Shardul, Jatin, Harrison, Isfaq, Mubarak, Yousef**, and among others, who patiently tolerated me all these years. To my previous research employers **Inria-Paris** and **COPELABS-Lisbon**, because of whom I reached the current position.

To my buddies with whom I have twenty years of friendship, **Raja**, **Pavan**, **Sadiq**, and **Srikanth**, and **Ruben** and **Miguel** (Lisbon), and all other teachers, lecturers, and professors, including Prof. **A.R. James** and Prof. **B.S. Varma**, who shaped me with their knowledge. To the Carnatic and Hindustani vocalists/musicians and Telugu speakers (Garikapati and Chaganti) for their music and teachings that immensely helped me during my darkest period. To all others who intentionally/unintentionally journeyed along with me.

Last but not least, to my odd family, including my nieces (**Sathvika** and **Navya**).

Porto, 2023

Radha Krishna Reddy PALLAVALI

क्रिया-सिद्धिः सत्त्वे भवति महतां नोपकरणे ||

Kriyāsiddhih satve bhavati mahatām nopakarane||

(The secret of success in materializing intentions lies in one's inner strength but not in the instruments and devices utilized).

Mahakavi Kalidasu
(4^{th} century CE).

To my odd family:

Subhadramma Pallavali (mother)

Viswanadha Reddy Pallavali (father)

Dr. Rojarani Pallavali, Ph.D. (sister)

Thesis Publications

Journal Papers

[1] **Reddy, R**., Almeida, L., Kurunathan, H., Santos, P. and Tovar, E., 2023. Comparing Energy Savings and Emissions Efficiency of Mixed ICEVs and BEVs at Complex Intersections. Under submission in the **Elsevier Transportation Research Part D: Transport and Environment**.

[2] **Reddy, R**., Almeida, L., Kurunathan, H., Gaitan, M., Santos, P. and Tovar, E., 2023. Comparing the Worst-Case Response Time of Complex Intersections Management. Under revision in the **IEEE Open Journal of Intelligent Transportation Systems**.

[3] **Reddy, R**., Almeida, L., Gaitan, M., Santos, P.M. and Tovar, E., 2023. Synchronous Management of Mixed Traffic at Signalized Intersections towards Sustainable Road Transportation. In **IEEE ACCESS**, Vol.11, pp.64928-64940.

Conference Papers

[4] **Reddy, R**., Almeida, L., Santos, P.M. and Tovar, E., 2023. Advantages of Synchronizing Vehicles Intersection Access. Accepted In Euro Working Group on Transportation Meeting (**EWGT 2023**), **Transportation Research Procedia**, pp.1-8.

[5] **Reddy, R**., Almeida, L., Santos, P.M., and Tovar, E., 2023. Waiting Time Analysis for a Network of Signalized Intersections. In International Conference on Ambient Systems, Networks and Technologies (**ANT 2023**), **Procedia Computer Science**, 220C, pp.503-510.

[6] **Reddy, R**., Almeida, L., Santos, P.M., Bouzefrane, S. and Tovar, E., 2021. Synchronous Intersection Management to reduce Time Loss. In Euro Working Group on Transportation Meeting (**EWGT 2020**), **Transportation Research Procedia**, 52, pp.364-372.

[7] **Reddy, R**., Almeida, L., Santos, P.M. and Tovar, E., 2020, September. Comparing the Ecological Footprint of Intersection Management Protocols for Human/Autonomous Scenarios. In IEEE International Conference on Intelligent Transportation Systems (**ITSC 2020**), pp.1-6.

Work-in-Progress Papers

[8] **Reddy, R**., Almeida, L., Santos, P. and Tovar, E., 2022, December. Work-in-Progress: Exploring the Composition of Synchronous Intelligent Intersections.

In 2022 IEEE Real-Time Systems Symposium (**RTSS 2022**), pp.523-526.

[9] **Reddy, R**., Almeida, L., Gaitan, M., Kurunathan, H., Santos, P. and Tovar, E., 2021, December. Work-In-Progress: Worst-Case Response Time of Intersection Management Protocols. In 2021 IEEE Real-Time Systems Symposium (**RTSS 2021**), pp.556-559.

[10] **Reddy, R**., Almeida, L. and Tovar, E., 2019, December. Work-in-Progress: Synchronous Intersection Management Protocol for Mixed Traffic Flows. In 2019 IEEE Real-Time Systems Symposium (**RTSS 2019**), pp. 576-579.

Extended Abstracts & Posters

[11] **Reddy, R**., Almeida, L., Santos, P.M. and Tovar, E., 2023. Quality of Service of IM Approaches under Saturated Traffic. Accepted In Euro Working Group on Transportation Meeting (**EWGT 2023**), pp.1-3, Santander, Spain.

[12] **Reddy, R**., Almeida, L., Santos, P.M. and Tovar, E., 2023. Complex Intersections with a Dedicated Road Lane per Crossing Direction. In 5th Doctoral Congress in Engineering (**DCE 2023**), Porto, Portugal.

[13] **Reddy, R**., Almeida, L., Gaitán, M.G., Santos, P.M. and Tovar, E., 2021. Synchronous Framework Extended for Complex Intersections. In Euro Working Group on Transportation Meeting (**EWGT 2021**), Book of Abstracts, pp.107, Aveiro, Portugal.

[14] **Reddy, R**., Almeida, L., Gaitán, M.G., Santos, P.M. and Tovar, E., 2021. Sustainability Analysis of Complex Multi-Lane Intelligent Signalized Intersections. In 4th Doctoral Congress in Engineering (**DCE 2021**), Porto, Portugal.

[15] **Reddy, R**., Almeida, L., and Tovar, E., 2020. Synchronous Intersection Management to reduce Time Loss. In Euro Working Group on Transportation Meeting (**EWGT 2020**), pp.1-3, Paphos, Cyprus.

[16] **Reddy, R**., Almeida, L., Gaitán, M.G., Santos, P.M. and Tovar, E., 2020, September. Impact of Intersection Management on Energy-Efficiency when Mixing Electric and Combustion Vehicles. In 23rd EURO Working Group on Transportation Meeting (**EWGT 2020**), pp.1-3, Paphos, Cyprus.

[17] **Reddy, R**., Almeida, L. and Tovar, E., 2019. An intersection management protocol for mixed autonomous and legacy vehicles. In 3rd Doctoral Congress in Engineering (**DCE 2019**), pp.7-8, Porto, Portugal.

Other Publications

[1] Gaur, S., Almeida, L., Tovar, E. and **Reddy, R**., 2019, September. Cap: Context-aware programming for cyber physical systems. In 2019 24th IEEE International Conference on Emerging Technologies and Factory Automation (**ETFA 2019**), pp.1009-1016.

Contents

List of Figures

List of Tables

List of Abbreviations

ACC	Adaptive Cruise Control
AV	Autonomous Vehicle
BEV	Battery-Electric Vehicle
BEAV	Battery-Electric Autonomous Vehicle
CAV	Connected and Autonomous Vehicles
CFM	Car Following Model
CV	Connected Vehicles
HV	Human-driven Vehicle
ICT	Intersection Crossing Time
IM	Intersection Management
IIM	Intelligent Intersection Management
IIMA	Intelligent Intersection Management Architecture
IST	Intersection Service Time
ITLC	Intelligent Traffic Light Control
ITS	Intelligent Transportation Systems
QTLC	Q-learning based Traffic Light Control
TTLC	Trivial Traffic Light Control
SIMP	Synchronous Intersection Management Protocol
SUM	Sustainable Urban Mobility
SUMO	Simulation of Urban MObility
RR	Round-Robin
WCIST	Worst-Case Intersection Service Time
WCRT	Worst-Case Response Time
WT	Waiting Time

Chapter 1

Introduction

This chapter first introduces the motivation signifying the need for *Intelligent Transportation Systems* (ITS) to achieve *Sustainable Urban Mobility* (SUM) and the general context of "What can be an ITS?". Then briefly present the related works on signalized intersections management dealing with urban mobility, on top of which our research questions are framed to pursue the *Intelligent Intersection Management* (IIM) paving the way towards ***ITS-based SUM***. The remaining sections explicitly state the thesis scope, statement, and key contributions and conclude with the thesis organization.

1.1 Motivation

According to the United Nations (UN) urbanization report 2018 [186], 55% of the world population is living in urban areas, and forecasts that by 2050, it will reach 68%. Furthermore, it is projected that countries like India, China, and Nigeria will be highly concentrated, with 416, 255, and 189 million urban populations. This concentration can potentially bring disastrous consequences to cities, including transportation and mobility, human health, and environmental challenges. It takes the collective effort of the UN member states to develop sustainable urban futures respecting urban mobility and avoid a worst-case scenario[1].

Current transportation practices pose severe challenges from multiple perspectives, such as economic, environmental, and health, by straining urban mobility [129], namely:

Fossil fuel dependency: According to the International Energy Agency (IEA), between 50 and 75% of the total produced energy is consumed by transportation, and it forecasts that by 2040 the transportation fuel requirement will be worth more than $2 trillion [30]. The INRIX[2] global traffic scorecard survey shows that the cost of traffic congestion, fuel wastage, and vehicular emission for France, Germany, the UK, and the US in 2013 was $200 billion (0.8% of global GDP); and can reach $300 billion by 2030.

[1] https://unhabitat.org/wcr/
[2] http://inrix.com/products/ai-traffic/

Pollutant emissions: The European Environment Agency (EEA) reported that above 80% of European urban dwellers are exposed to dangerous vehicular emissions of carbon monoxide (CO), particulate matter (PM_x), and nitrogen oxides (NO_x) due to their higher concentration levels than the annual limit, mainly observed at traffic stations [70].

Human health: Many research studies have focused on finding the relationship between urban transportation and mobility, environmental pollution, and human health [47; 79; 209; 235; 203; 149; 148; 150; 121]. In the worst case, exposure to dangerous emissions causes death, but it can also cause heart disease, stroke, lung cancer and respiratory diseases. These complications are expected to worsen in high-income and middle-income countries and transition in low-income countries [156; 98].

During the lockdown due to the novel coronavirus (COVID-19) pandemic, the delays and fuel wastage were reduced by 51%, including emissions of 50% each in the USA [190]. In the European Union (EU) [70], the levels of CO (-61.8%), NO_x (-60%), and PM_x (-30%) are considerably reduced from road transportation, the primary contributor to EU emissions. The research on post-pandemic traffic patterns suggests that urban commuters opt for private vehicles rather than public transit or ride-sharing services [44]. Thus, the traffic congestion conditions are expected to be even worse than the pre-pandemic conditions [44]. Therefore, providing urban mobility in such high-density scenarios is challenging for urban planners and transportation engineers to minimize delays and energy consumption and reduce air pollutants emissions. These challenges set a rationale towards transportation sustainability, a goal of UN sustainable development[3].

> As per the United States Department of Energy[a], transportation sustainability requires affordable energy-efficient transportation and emitting low- to zero-air pollutants, including electric and renewable fuels.
>
> [a] https://www.energy.gov/eere/sustainable-transportation

Accordingly, the fundamental objective of this thesis is to address the future trends of urban traffic conditions to achieve SUM relying on ITS. The following section discusses the significant role of ITS in achieving SUM.

1.2 Intelligent Transportation Systems

ITS refers to many modes of intelligent transportation, from road to air, rail, and maritime systems. Our primary focus is on the road ITS systems, also called road telematics, that employs Information and Communication Technologies for safer, more efficient, and

[3] https://sdgs.un.org/goals/goal11

sustainable road transportation to tackle growing traffic congestion, fuel wastage, and associated ever-increasing emissions [193].

As reported by the European ITS standards[a], ITS utilize real-time traffic information to achieve SUM by applying advanced electronics, information, and telecommunication technologies to roads, automobiles, and goods.

[a]https://www.itsstandards.eu/

Therefore, the success of SUM principally depends on the ITS platform. The generic components of ITS are intelligent sensing systems, communication networks, decision-making units, and connected, electric, and autonomous vehicular technologies. The sensing platforms can be intra-vehicle that collect the individual vehicles conditions (e.g., speed, engine performance, etc.), an essential system for developing advanced driver assistance systems (ADAS) [58]. The ADAS is divided into six levels from 0 (human-driven vehicles - HVs) to 5 (autonomous vehicles - AVs) [29]. The National Highway Traffic Safety Administration (NHTSA) in the USA projected that AVs could reduce nearly 50 minutes of average commuter delay daily [145].

The inter-vehicle sensing is used to sense the nearby vehicles utilizing cameras, radar, lidar, GPS (Global Positioning System), and On-Board Units (OBU) that enable inter-vehicles communications, either based on Dedicated Short-Range Communication (DSRC) [94] or the Wireless Access in a Vehicular Environment (WAVE) protocol stacks [18] and/or cellular [144]. Finally, the urban sensing platforms employ IP cameras, induction loop detectors and other road sensors (e.g., traffic volume, speed, weather detectors, etc.) to collect traffic-related information. The collected sensory data is then sent to the decision-making unit via Vehicle-to-Vehicle (V2V) and Vehicle-to-Infrastructure (V2I) communications. After processing the data, the decision-making unit disseminates the decisions back to vehicles via I2V or V2V communications [72].

We consider a real-world road network to motivate our research toward ITS-based SUM. Figure 1.1a displays an OpenStreetMap of the real-world road network in Portland, Oregon, USA. In this road network, the signalized (or unsignalized) intersections are arranged to form a grid road network. This kind of grid road network can be found in many cities, including Lisbon (Portugal), Barcelona (Spain), Berlin (Germany), New York (USA), Tokyo (Japan), etc.

In these road networks we can find two typical intersection types, namely conventional at-grade intersections (e.g., four-legged and three-legged or T-intersections) and unconventional continuous flow intersections with different geographic settings and several road lanes. In conventional at-grade intersections, multiple roads diverge, cross, and merge at the same height [152]. The three basic at-grade conventional road intersection types found in the real world are signalized intersections, roundabouts, and unsignalized intersections with stop signs. Unlike conventional at-grade intersections, continuous flow intersections

operate with displaced left turn lanes which can be bridges or tunnels that separate roads at different heights [152].

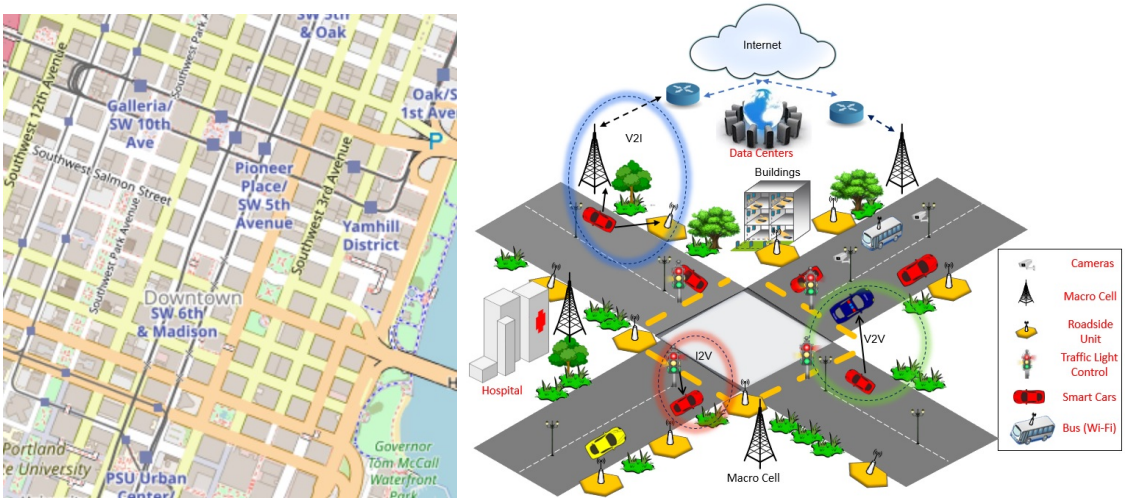

(a) Real world road network Portland. (b) Typical ITS-based intersection.

Figure 1.1: Motivational road network from the real world Portland, Oregon retrieved using the OpenStreetMap and the ITS-based intersection with various sensing objects, vehicles, and communications.

Fig. 1.1b shows a typical ITS-based intersection management (IM) system (or intelligent intersection management system - IIM) for an at-grade four-legged intersection, incorporating IP cameras, road sensors, roadside units (RSUs), smart cars and buses (AVs), traffic light control (TLC) units, and macro and micro cells for providing the V2V and V2I communications, etc. Here, TLC signals can be physical (for serving HVs) or virtual (for serving AVs). The following section discusses the crucial aspects and operations of IM approaches.

1.3 Signalized Intersection Management

In urban transportation networks, signalized intersections are traffic bottlenecks where the growing trends in queue lengths, waiting delays, and associated adverse effects can be observed [124]. From now onwards, we will use the intersection to represent the signalized intersection. For instance, Schrank et al., [190] reported that Americans lost 8.7 billion hours and almost 3.5 billion gallons of fuel due to traffic congestion in 2019. In the case of the EU, traffic congestion and inefficient transportation cost member states an estimated 110 billion euros each year [153]. As per the NHTSA [145], one-third of all intersection fatalities in the USA are associated with intersections. In the case of EU-27, 43% of all road injuries occur at intersections [234]. Even after a century of improvements that the IM has gone through since 1920's [140], intersections are still major contributors to traffic congestion and accidents involving 40% fatalities [67].

Hence at any intersection, the intersection area is a common resource that must be efficiently shared among vehicles with conflicting maneuvers from different road lanes. Thus, the adverse consequences of traffic congestion should be minimized. Over the past century, IM systems have been improved. Nevertheless, they are known to be significant contributors to traffic congestion and associated adverse effects like delays, fuel wastage, accidents, and emission of air pollutants. Numerous IM approaches were introduced to address these traffic issues at intersections. In those IM systems, TLC signal (defined below) operations are either local at each intersection, centralized for a network of intersections connected to a centralized controller, or cooperative through the cooperation between road users, infrastructure, and control centers.

The TLC signals definitions we use are adopted from the Highway Capacity Manual (HCM) [125].
Cycle - a complete sequence of TLC signal (Green, Yellow, Red) indications.
Cycle length - the total time assigned to complete a TLC cycle.
Signal/Phase - the part of the TLC cycle allocated to any combination of traffic movements.
Green time - the green phase duration (s) for a given road lane traffic movement at signalized intersections.
Red time - the red phase duration (s) in which the traffic movements are blocked.
Yellow time - the yellow phase duration (s) to clear the intersection traffic but not to permit intersection access.

Based on the TLC operations, the IM can be categorized as conventional, actuated, and adaptive [54; 166], including a novel class of IIM approaches [142].

1.3.1 Conventional IM Approaches

Conventional IM approaches were introduced initially for managing constant traffic with arbitrary arrival at intersections. These kinds of IM strategies control green phases in a pre-defined sequence for a predetermined time. For example, a fixed-time IM approach TLC settings are shown in Fig. 1.2, where N, E, S, and W indicate the roads named after the cardinal direction points of North, East, South, and West. This separation of TLC signals per road allows for analyzing each road individually.

In this research line, Clayton [39] published one of the first papers dating back to 1941, assuming constant arrival and departure times. Another notable work is Webster's approximations [228]. Newell also studied approximations for fixed TLC settings and binomially distributed arrivals [143]. Round-Robin (RR) IM approach [8; 34] and Trivial Traffic Light Control (TTLC) [24] strategies are the most frequent strategies of fixed-time. The RR and TTLC IM approaches will be further discussed in section 3.6 as we

employ them within the baseline IM approaches to compare the performance of our IIM approach. These conventional IM approaches can also be tuned for specific time-invariant traffic patterns. Optimization software like TRANSYT or SYNCHRO sets the cycle length and green phase duration accordingly [57; 64; 167; 187; 170]. As typical in fixed-time approaches, these are agnostic to the type of traffic, AV or HV, providing extra versatility and ease of deployment when both types are present.

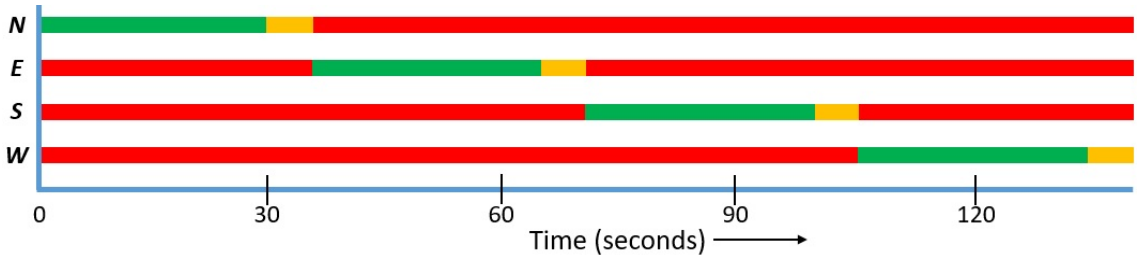

Figure 1.2: An example of a fixed-time Green, Yellow, and Red phases allocated to the four-legged intersection with roads N (North), E (East), S (South), and W (West).

However, these approaches are less efficient under time-varying traffic arrival patterns since their service does not adjust to the dynamic fluctuations of the vehicles arrivals. Therefore, the IM approaches that actuate green phases based on the traffic inflow might be practical and favorable. For instance, skipping the green phase to an empty lane thus takes us to the traffic-actuated IM approaches domain discussed in the following subsection.

1.3.2 Traffic-Actuated IM Approaches

From the literature, we can find various types of traffic-actuated IM approaches. One case occurs when traffic permits from one road at a time, in which the green phase changes once the traffic of that road is served. The same can apply to a case where multiple road lanes are given a green phase. In the other case, a minimum, a maximum, or a threshold green time will be assigned. Thus, the green phase changes though the traffic is queueing on that road. The former case can be referred to as the exhaustive type [27], while the latter can be referred to as a limited type of traffic-actuated IM approach. Note that traffic-actuated IM strategies employ sensory data and a simple logic of green time extension [52], a threshold between green phases, or a maximum green phase time to manage the traffic inflow [54]. The green time extension depends on the traffic flow information and will be prolonged or terminated based on the threshold.

Traffic-actuated IM approaches can be either fully-actuated or semi-actuated [62]. The fully-actuated IM approaches operate in variable sequence phasing, i.e., when no vehicles are present, the actuated controller skips green phases or terminates certain movements. Hence, sensors must be placed on all road lanes. Intrinsically, fully actuated IM approaches indicate the intersection where all roads are major. In the semi-automated IM approaches, the green phase is always present for major roads through movement (or straight-crossing),

and whenever the sensors detect vehicles on the minor roads, the green phase will be changed. In other words, the major roads have green phase priority than the minor roads. Thus, sensors are only required on minor roads [107; 40].

Since they first appeared, traffic-actuated IM strategies have consistently been applied in transportation research [69; 36; 199; 147; 211]. However, actuated IM approaches are not generally preferred due to the maintenance requirements and installation costs amounting to two to three times those of the conventional IM approaches. These types of IM approaches do not bring any advantages to regular or irregular (e.g., accidents, sports events, etc.) traffic patterns. Newell claims that the conventional fixed-time IM approach performs better than the traffic-actuated IM approach when two road lanes receive a green phase simultaneously [143]. Consequently, the adaptive IM approaches were introduced to tackle the limitations of the traffic-actuated IM approaches, which will be discussed in the next subsection.

1.3.3 Adaptive IM Approaches

Adaptive IM approaches are similar to the traffic-actuated IM approaches, but the green time adaptation depends on the changing traffic inflow patterns and eases traffic congestion. The benefits of employing the adaptive IM approach over conventional and traffic-actuated IM approaches can be a continuous distribution of green phase time to all roads based on their traffic levels to improve travel time reliability and reduce traffic congestion by extending the green time to impose smoother traffic flows. Miller presented the first adaptive IM approach in 1963 [134]. After that, numerous adaptive IM approaches have been developed, including SCOOT (Split Cycle Offset Optimisation Technique [78]), SCATS (Sydney Coordinated Adaptive Traffic [201]), RHODS (Real-Time Hierarchical Optimized Distributed Effective System [135]), OPAC (Optimized Policies for Adaptive Control [61]), and UTOPIA (Urban Traffic OPtimization by Integrated Automation [127]).

These adaptive IM approaches differ in the way they adjust TLC signal timings. For instance, SCOOT assigns incrementally over time; SCATS groups intersections into subsystems and then optimizes the TLC signals; and RHODES employs the estimated traffic demand for allocating the green time. However, their adaptation depends mostly on induction loop detectors to find current traffic patterns. Therefore, improvements to these adaptive IM approaches are a must. InSync is an example of this kind, and its TLC decisions depend on the actual traffic demand and the delay of individual movements [80]. InSync employs state-of-the-art sensor technologies (e.g., IP Cameras and loop detectors) and image processing techniques for measuring the queue lengths in real time and artificial intelligence for TLC signals optimization both locally and cooperatively.

On the other hand, some adaptive approaches operate with fixed minimum and/or maximum green/cycle times. For instance, the Max-pressure Control Algorithm (MCA) has a minimum green phase time [216], while the adaptive version of Webster's approach

employs both minimum and maximum cycle times [64]. We use these two adaptive approaches among the benchmark approaches for comparing against our IIM approach, and will be discussed further in section 3.6.

As the fixed-time IM approaches, the adaptive IM approaches are also agnostic to the type of traffic, AV or HV, providing extra versatility and ease of deployment in the presence of both types. Although the aforementioned adaptive IM approaches may perform better in many situations, there is still potential for substantial improvements due to the emergence of communications, electric and autonomous vehicular technologies to achieve SUM.

1.3.4 Intelligent IM Approaches

As mentioned in Section 1.2, the ITS platform for SUM involves many advanced and intelligent systems, including sensors (e.g., induction loop detectors, IP cameras, and other roadside sensors), RSUs, communication technologies (e.g., V2I and V2V), and autonomous/self-driving control of AVs. Numerous IIM approaches were presented using these intelligent technologies to tackle one or more SUM objectives. For instance, Dresner and Stone presented the reservation-based Autonomous Intersection Management (AIM) relying on multi-agent systems (MAS) to reduce delays [48; 49]. Subsequent reservation-based AIM protocols attempted to tackle the inequality of waiting between major and minor roads [194]; providing coordination between AVs and AIM [90]; vehicle motion planning and intersection crossing [108]; speed failure and vehicle safety [38]; simultaneous management of approach spillbacks, pedestrians and collision avoidance [223]; cooperation between AVs and road infrastructure [111]; and lane and trajectory optimization incorporating vehicle size [237], are a few.

> However, these approaches are for AV-only scenarios. As experts and scientists anticipate, the transition towards AV-only scenarios will be long and not before 2045 [19; 207]. Therefore, there is a need to support mixed traffic-flow scenarios of AVs and HVs coexisting.

Over the past few years, very few IIM approaches were introduced to manage the mixed traffic of HVs and AVs. Initially, Qian et al. introduced HVs as priority vehicles and stopped AVs until HVs left the intersection [168]. The IM in [20] used pre-sorting and pre-signaling techniques.

Some approaches improved the existing IM or AIM protocols. For instance, Yang et al. improved the Intersection Traffic Control Algorithm (ITCA) for minimizing total delay using optimal departure sequence and AV trajectories information [243]. Similarly, Dresner and Stone improved the AIM [48; 49] to support HVs using AVs sensing capabilities naming it as the Hybrid-AIM (H-AIM) [196]. Some IIM algorithms optimized vehicle trajectories, TLC signals, or both [164; 114; 118].

Overall, the research studies on mixed traffic management of HVs and AVs are minimal. Secondly, the existing approaches impose strong differentiation between AVs and HVs with throughput and travel time penalties. Therefore, new IIM strategies should consider multiple objectives in achieving SUM, i.e., providing traffic fluidity at intersections, minimizing traffic congestion and associated delays, while considering environmental factors and human health conditions in their design, given their impact on fuel wastage and the emission of dangerous air pollutants. In this direction, the following section presents the scope of this thesis.

1.4 Scope of the Thesis

The scope of this thesis is the design and operation of a reactive IIM system on various types of intersections (isolated intersections or networks of intersections) where vehicle-to-vehicle interactions are more prevalent, i.e., no pedestrians. Here, the IIM system reactivity indicates the system responsiveness for inflow traffic to provide traffic fluidity at intersections and reduce delays, fuel wastage, and associated emissions of air pollutants. We consider the typical real-world intersections, including those with four legs and three legs (T - intersections), which can be simple with a single inflow/outflow road or complex with multiple inflow/outflow road lanes. The proposed reactive IIM system can be used to control different vehicles of type (e.g., HVs or AVs) and size/length (e.g., car or bus) as it will deal with each vehicle individually.

We also employ the routes and traffic assignment between the origins and destinations of the road networks. We consider the same and static route and traffic assignments across experiments to avoid bias and influence against the baseline approaches (presented in section 3.6). We generate the spatio-temporal trajectories of individual vehicles whenever necessary, particularly when analyzing the worst-case traffic scenarios.

The main scope of this thesis is a mixed traffic scenario with HVs and AVs; thus, we employ two different car-following models (CFM) indicating HVs (Krauss CFM) and AVs (Adaptive Cruise Control - ACC CFM). These CFMs mimic human and autonomous driving behaviors, which will be discussed in section 3.2. We assume the fundamental difference between HVs and AVs is the driving control and communications, but not the hardware or types of equipment. Thus, the technical specifications of mixed vehicles, RSUs, Sensors, and TLC units are out of the scope of this thesis. Such issues were only considered at certain moments since the target was to implement the devised IIM approach in a microscopic traffic simulation environment discussed in section 3.1.

We also study the increasing rates of electric propulsion penetration to understand their performance in achieving the SUM. To analyze transportation sustainability we use a fuel consumption model for gasoline Internal Combustion Engine (ICE) vehicles and the associated emissions model, and an energy consumption model for Battery-operated Electric Vehicles, possibly Autonomous (i.e., BEVs/BEAVs). These models will be discussed

in sections 3.3, 3.5, and 3.4, respectively.

1.5 Thesis Statement

As mentioned in previous sections, current urban transportation practices bring severe challenges straining urban mobility, referring to traffic congestion, increased delays, fuel wastage, and emissions of dangerous air pollutants, mainly observed at intersections. Future urbanization brings even worse traffic conditions suggesting the need for intelligent solutions. On the other hand, with the advancements in communication, electric and autonomous technologies, it is possible to serve HVs mixed with AVs at intersections before adopting fully AV-based approaches. However, the IIM approach must react naturally and intelligently to the arriving traffic rather than synthetically reserving time slots or imposing strong differentiation between HVs and AVs. Therefore, we propose synchronizing vehicles intersection access from all non-conflicting road lanes simultaneously based on their presence at the intersection entrance. This is a ***synchronous framework*** that combines an *intelligent intersection management architecture* (IIMA) with an associated *synchronous intersection management protocol* (SIMP). Accordingly, our thesis statement is as follows:

> ***A reactive synchronous framework can provide smoother and more efficient intersection access for any percentage of AVs mixed with HVs to achieve improved throughput, reduced delays, and minimized fuel wastage and associated emissions of dangerous air pollutants, paving the way toward sustainable urban mobility.***

To verify the correctness of this statement, we test the operational performance of the *synchronous framework* at various types of isolated intersections and networks of intersections supporting mixed HV/AV traffic scenarios through simulations. We introduce an analytical model for estimating the IM performance under worst-case traffic scenarios and its validation using simulation studies. Finally, we study the transportation sustainability of introducing growing rates of ICE AVs and alternate-fueled vehicles, like BEVs and BEAVs.

The rest of the chapter provides the key contributions and the organization of the remaining thesis.

1.6 Contributions

The primary focus of this thesis is developing the reactive IIM approach (i.e., *synchronous framework*) supporting mixed HV/AV traffic scenarios of future urban settings for SUM. In this context we provide three major contributions: i) the *synchronous framework* for managing mixed HV/AV traffic scenarios at various types of intersections; ii) the analytical

model for estimating the IM system performance during worst-case traffic scenarios, and iii) the analysis of transportation sustainability with respect to the growing penetration rates of BEVs, AVs (gasoline ICE based) and BEAVs.

1.6.1 Synchronous Framework

Current transportation practices strain urban mobility, and AVs-only scenarios are not expected before 2045 [19; 207]. Moreover, existing IIM protocols strongly differentiate HVs and AVs with imposed throughput and travel time penalties. Therefore, the first contribution is the reactive *synchronous framework* presented in Chapter 4. *Synchronous framework* is a combination of the *intelligent intersection management architecture* (IIMA) and associated *synchronous intersection management protocol* (SIMP) to support any percentage of AVs mixed with HVs. Note that both *synchronous framework* and SIMP are utilized interchangeably. SIMP synchronizes vehicle intersection access smoothly from all road lanes relying on the *Conflicting Directions Matrix* (CDM) to increase traffic fluidity. SIMP serves HVs using physical TLC signals and AVs using virtual TLC signals via messages. We evaluate the performance of the *synchronous framework* against conventional, intelligent, and adaptive IM approaches at isolated single-lane and multi-lane intersections (Chapter 5) and networks of multi-lane intersections (Chapter 6). Two intersection crossing configurations are tested for multi-lane intersection scenarios, namely using lanes dedicated to a specific crossing direction (i.e., left, straight/through, and right) or lanes that are shared between different crossing directions (i.e., left and straight, and straight and right). Various traffic arrival rates are utilized representing low, medium, and saturated conditions at low-speed urban settings. The experimental evaluations suggest that our *synchronous framework* increases the traffic throughput and decreases traffic congestion, travel delays, fuel consumption, and the associated emission of dangerous air pollutants in average case [171; 172; 174; 176; 177; 178; 179].

1.6.2 Vehicles Worst-Case Response Time

In the previous contribution, only the average case is covered. However, as mentioned in the motivation section, the time a vehicle takes to cross an intersection in the worst-case for different traffic scenarios is also relevant in evaluating the quality of service of IM systems, apart from the average case. For analyzing worst-case behavior in traffic scenarios, we introduce a new service measure named *Worst-Case Response Time* (WCRT), inspired on real-time systems concepts. We present analytical models to estimate vehicles maximum waiting time and WCRT per road lane in Chapter 7. We employ commonly available parameters for devising the WCRT models, like the geographic settings of roads (road length and intersection space within), traffic information (average speed, maximum queue length, and capacity), and IM parameters (green phase time and total cycle time). The response time of vehicles (s/veh) is measured between the path origin and until exiting

the last intersection in the path before reaching the destination. This metric includes what we call the waiting time (s/veh), which is the time spent in a queue, measured when the vehicles speed is below $1.5m/s$ or wholly stopped with zero speed. We validate the analytical estimations using the simulation results at isolated single-lane ([175]) and multi-lane ([182]) intersections and networks of multi-lane intersections [181; 184].

1.6.3 Transportation Sustainability

To minimize air pollutants emissions, on the one hand, EVs already occupied 4.6% of the US market share in 2021, and projections show that by 2030 they can occupy around 50%[4]. Similarly, Europe also witnessed 34% EVs in 2021[5] and projected 70% by 2030. On the other hand, Bansal and Kockelman [19] and Talebian and Mishra [207] suggested that adopting AVs exclusively will take a longer period (only after 2045) based on their availability via technological innovation, user acceptance, and urban policies. Therefore, studying the transportation sustainability of introducing AVs and BEVs, at different market penetration rates is necessary to determine whether they bring what they projected. Hence, we study the performance behavior of introducing ICE AVs and BEVs in Chapter 8. BEVs can be driven by human drivers (BEVs) or be autonomous (BEAVs). We designed several scenarios for growing rates of ICE AVs, BEVs, and BEAVs mixed with ICE HVs at isolated single-lane and multi-lane intersections as well as road networks of multi-lane intersections. Our contribution analyses the AVs/BEVs/BEAVs and IM operations involvement towards transportation sustainability, a UN sustainable development goal[6]. The findings are presented in [174; 173; 183].

1.7 Thesis Organization

The rest of this thesis is organized as follows. Chapter 2 studies the background and related work. Chapter 3 discusses the simulation tools and models and the baseline IM approaches employed to compare the performance against our reactive *synchronous framework*. Chapter 4 introduces the design and development of the reactive *synchronous framework* for managing various types of intersections. Chapters 5 and 6 compare the performance of the reactive *synchronous framework* at isolated single-lane and multi-lane intersections and road networks of multi-lane intersections against the baseline IM approaches. Chapter 7 presents the response time analysis during worst-case traffic conditions at isolated as well as networks of intersections. Chapter 8 studies the transportation sustainability of introducing various market penetration rates of AVs, BEVs, and BEAVs, again at isolated and networks of intersections. Chapter 9 concludes this thesis and provides possible future research directions.

[4] IEA, 2021. Global EV Data Explorer. Paris, France: IEA.
[5] https://theicct.org/wp-content/uploads/2022/06/global-ev-update-2021-jun22.pdf
[6] https://sdgs.un.org/goals/goal11

Chapter 2

Background and Related Work

This chapter presents the background and related work on the three following topics: (i) signalized intersections management, (ii) operational efficiency of IM approaches from a worst-case response time perspective, and (iii) transportation sustainability when introducing growing rates of AVs, BEVs, and BEAVs in a HV context.

2.1 Signalized Intersections Management

Concerning the geographic settings, the signalized intersections can be divided into three-legged or T-intersections, four-legged, and multi-legged (more than four legs) intersections. Many years of research and development have established significant contributions to the state-of-the-art in IM strategies to manage isolated intersections or networks of intersections (i.e., arterial, grid, or general). Isolated intersections operate solely without considering the neighboring intersections. According to the HCM, intersections that are more than 1.6km away from each other and managed independently can be considered isolated [125]. In arterial networks, multiple intersections are closer together and/or managed together and arranged sequentially. In these networks, vehicles cannot change roads, i.e., they can only do straight/through-crossing. When the intersections are closer together and/or managed together and arranged as a matrix, and allow vehicles to change roads taking any turn (except U-turns), they form a grid network. Otherwise, other possible arrangements of multiple intersections that are close together and/or managed together but do not fit the previous cases are called general road networks.

First, we focus on four-legged isolated intersections, both simple, i.e., a single inflow/outflow lane per road (Section 2.1.1), or complex, i.e., with multiple (more than one) inflow/outflow lanes per road (Section 2.1.2), and then we analyze the T-intersections (Section 2.1.3). Then we focus on a grid network of complex signalized intersections, with multiple inflow/outflow lanes (Section 2.1.4). After introducing these road networks, we discuss the related works.

2.1.1 Isolated Single-lane Intersections

Figure 2.1 sketches an isolated single-lane intersection right-angled with four legs. Therefore, each leg is with a single inflow and outflow road. The four legs can be identified with the four cardinal directions (North - n, East - e, South - s, West - w). The inflow lane serves the upstream approaching traffic, and the outflow lane serves the downstream traffic, and their indexes change based on the left-hand or right-hand driving conditions. Furthermore, each road can have a separate TLC unit or a single central TLC unit managing all roads.

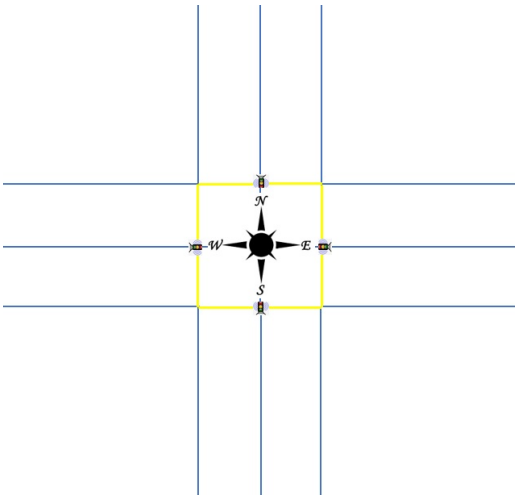

Figure 2.1: Sample layout of single-lane signalized intersection with four legs.

Conventional IM approaches like the linear control algorithm were presented to manage the traffic at intersections assuming constant traffic arrival [52]. Many studies employed the Round-Robin (RR) IM approach, which relied on the RR process scheduling [139]. With RR the TLC operations do not depend on the approaching traffic but on the allocated green phase time. A sequence of vehicles is permitted to access and cross the intersection from one road at a time for a predefined green time and shifts to the next road either clockwise or anti-clockwise forming a cycle. These can also be configured to support different allocated times for different day periods.

However, in these fixed-time approaches, the vehicles suffer longer waiting delays due to fixed green phase or cycle time. A few approaches targeted the TLC signals optimization based on the traffic inflow instead of the fixed cycles. For instance, TLC signals optimization [191; 45; 33], and reinforcement learning-based signal adaptation [232]. To increase the robustness, wireless communication technologies are utilized for gathering real-time traffic data that feeds a smart traffic load balancing, minimizing delays [247].

The approaches referred to in the previous paragraph were devised considering HVs, only. Consequently, new optimization techniques began targeting mixed CAV and non-CAV (or HVs) traffic after introducing wireless communications and autonomous technologies and studying various performance metrics like delays and energy efficiency. In this research line, [87] proposed an eco-driving system for optimizing speed profiles in a partial

CAV environment to achieve fuel efficiency. In [250], authors presented an optimal control framework for improving energy efficiency, and in [77], both TLC signal timing and approaching vehicles speed were optimized to minimize energy consumption. Differently, in [65], presignals and speed control were introduced to prioritize buses and minimize the number of stops of cars that follow buses. These approaches impose strong differentiation between CAVs and non-CAVs with throughput and travel time penalties.

As opposed to the previous works, we introduced the *synchronous framework* that simply reacts to the traffic at the intersection entrance independently of being HVs or AVs, synchronizes their intersection access and we confirmed it performs better against various configurations of the RR IM approach concerning intersection throughput, delays, fuel consumption, and tailpipe emissions [172; 171; 174; 178]. This dissertation details this contribution in chapter 4.

After our work, a few more authors tackled mixed traffic management to minimize delays. For example, the game-theory-based priority control algorithm [21] employs the V2I communications for information exchange between AVs and RSUs; thus, the TLC makes an appropriate decision to allow either AV or HV. In [244], a decentralized control model was presented for CAV trajectory optimization in mixed traffic scenarios considering travel time, fuel consumption, and safety. In their approach, the original decentralized model was simplified using time discretization to find the exact near-optimal solution.

In future work, we plan to compare the performance of our *synchronous framework* against these approaches.

2.1.2 Isolated Multi-lane Intersections

Multi-lane intersections also called complex intersections, have multiple inflow and outflow lanes on every road. Each lane is either dedicated to a specific crossing direction or shared between directions namely right, straight/through, and left. Figure 2.2 exhibits a four-way intersection with two-lanes (Fig. 2.2a) and three-lanes (Fig. 2.2b) per inflow/outflow road.

Traditional IM approaches like RR are also introduced to manage complex signalized intersections [34; 176]. Like RR, the trivial traffic light control (TTLC) mechanism is also traditional. Unlike RR, TTLC permits vehicles from two opposite road lanes parallelly and then shifts to the next pair of opposite road lanes [24]. More information on the RR and TTLC IM approaches for complex multi-lane signalized intersections can be found in section 3.6, as we employ them as the baseline against our synchronous approach. For improving HVs fluidity at signalized intersections, many adaptive IM approaches were presented, like optimal signal timing [33] and the Q-learning-based traffic light control (QTLC) that rely on multi-agent systems (MAS) [3]. Adaptive load-balancing techniques are also introduced for energy efficiency in urban signalized intersections where the stop-and-go, lower speeds, and lower gears are more prevalent [219; 220]. In [253], the authors studied the dynamic utilization of left-crossing lanes for straight-crossing vehicles to balance the traffic between inflow and outflow lanes.

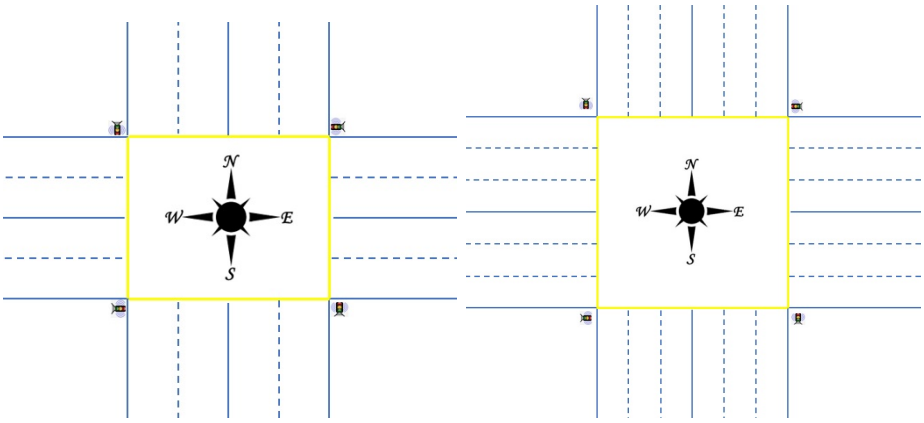

(a) Two-lane signalized intersection. (b) Three-lane signalized intersection.

Figure 2.2: Typical multi-lane (two and three) signalized intersections with four legs.

A wealth of solutions are reported in the literature relying on CV abilities (communicating position, speed, length, etc.). For instance, [240] proposed a cooperative method for optimizing traffic signals and vehicle speed for energy efficiency. The authors of [136] presented a user-based signal timing (UST) strategy to maximize user throughput. Then they introduced the user-based signal timing optimization (UBSTO) strategy with the same target, i.e., serving a maximum number of passengers [137]. In [208], Trajectory-Based Signal Control for delay optimization using trajectory information of CVs is presented.

Various recent surveys comprehensively studied the utilization of reinforcement learning techniques [231]; model-predictive control [245]; metaheuristic algorithms [85]; and others [166; 110] in optimizing TLC signals.

A branch of TLC protocols relies only on full-AV technologies and virtual traffic signals for managing multi-lane complex intersections. First [48; 49] introduced the Autonomous Intersection Management (AIM) system relying on MAS. In this system, AVs request the AIM to reserve a conflict-free time slot to cross the intersection; in turn, AIM processes requests in a "First-Come-First-Served"(FCFS) manner. Subsequently, numerous reservation-based AIM protocols were introduced to tackle various problems like the inequality of waiting between major and minor roads [194]; providing coordination between AVs and AIM [90]; multi-vehicle motion planning and intersection crossing [108]; targeting speed failure and vehicle safety [38]; AIM employing V2I communications [113]; simultaneous management of approach spillbacks, pedestrians and collision avoidance [223]; optimal intersection crossing of CAVs [248]; cooperation between AVs and road infrastructure [111]; lane and trajectory optimization incorporating vehicle size [237]; and trajectory-based AIM (T-AIM) [123].

For more information on AVs-only IIM approaches, see the following surveys that were carried out based on the cooperative methods [35]; longitudinal motion control [226]; deep reinforcement learning [73]; graph, prediction, optimization, and machine learning-based approaches [110]; and others [142; 255; 1].

However, AVs-only approaches can be identified as unsignalized intersections due to no physical traffic signals. Moreover, it was projected that complete penetration of AVs would not occur before 2045 [19; 207]. Until then, AVs must co-exist with HVs in mixed-traffic scenarios. The remaining section discusses the IIM approaches to managing the mixed traffic of HVs and CVs or AVs. For instance, Li et al. in [112] targeted the oversaturated traffic conditions by formalizing multi-objective optimization to improve throughput and minimize the average queue ratio. In [246], the Intelligent Traffic Light Control (ITLC) algorithm uses vehicle movement information (queue length, speed, acceleration, and distance) for traffic signal optimization and waiting delay minimization. Differently, Yang et al. developed an Intersection Traffic Control Algorithm (ITCA) for minimizing total delay using optimal departure sequence and vehicle position information [243].

Some authors modified AVs-only-based IM approaches to support mixed HV/AV scenarios. For instance, the AIM [48; 49] is improved to support HVs using AVs sensing capabilities and named the Hybrid-Autonomous Intersection Management (H-AIM) [196]. Moreover, the primary goal is to avoid congestion regardless of vehicle type, HVs, or AVs. In [164], the authors presented an Intelligent Intersection Control Algorithm (IICA) to optimize TLC signal phase timing and vehicle trajectories based on arrival data (including the randomness in traffic arrival) to reduce travel times. In [53], H-AIM and IICA were compared for various AV penetration rates and headways. The IICA shows the highest throughput and the lowest delays in the considered scenarios. Liu et al. in [118] introduced a Safe Intersection Management system for mixed HV and AV scenarios using the model predictive controller, in which HVs follow worst-case driving behavior while the AVs follow strict driving behavior.

Another optimization approach uses mixed-integer nonlinear programming (MINLP) to optimize vehicle trajectories and TLC signal timings [151]. Their approach continuously optimizes AV trajectories and introduces a white phase to instruct HVs to follow the front vehicle. Thus, groups of HVs follow an AV during the white phase. On the other hand, [14] evaluated mixed traffic safety (i.e., rear-end crashes) using longitudinal control of AVs and CAVs. Real-world connected vehicle data is fed to consider the acceleration/deceleration of HVs. The longitudinal conflicts and speed volatility of mixed traffic are analyzed to understand the safety performance of various AVs/CAVs penetration rates.

Liang et al. presented a joint traffic signal control optimization algorithm using the information from CAVs for optimizing traffic signal phasing and timing and speed guidance to individual AVs and HVs (enforcing strict speed guidance) [114]. Then it extended for minimizing connected and non-connected vehicle delays [115], in which a central controller collects real-time vehicle information. Then the control algorithm optimizes the signal phase and time to discharge a sequence of platoons of vehicles based on their proximity. Similarly, [206] formulated the coordinated Signal Timing and Trajectory Optimization (STTO) for both trajectory and signal optimization at complex intersections.

The efficiency and safety at intersections for penetration of two types of AVs (aggressive and discrete) are studied in [161]. The simulation results suggest that an increase in aggressive AVs percentage can increase the intersection capacity; however, the safety risks are high as the distance between consecutive vehicles is narrowed. On the contrary, increasing discrete AVs decreases the intersection capacity to improve safety, but HVs may trigger risky behavior due to extra delays. Unlike others, [138] improved the conventional RR to support platoons while prioritizing special vehicles (e.g., emergency vehicles) with the help of CAV technologies.

The challenge with these IIM approaches is that they impose strong differentiation between HVs and AVs. Accordingly, the applicability of these IIM approaches is limited. To tackle this, another section of novel IIMs available in the literature is based on synchronizing the movement of AVs, possibly considering HVs. For instance, [76] shows that the synchronous movement of traffic can considerably impact the energy efficiency of vehicles even during over-saturated traffic conditions. In [212], a synchronization-based intersection control mechanism was introduced that employs local vehicle information to synchronize AVs movements at individual intersections, acting on vehicles speed to enforce inter-vehicle gaps. Therefore, AVs maintain some gaps by reducing their speed. This synchronization significantly reduced total delays and associated fuel consumption compared to non-synchronized mechanisms.

Similarly, Aoki et al. introduced the Configurable Synchronous Intersection Protocol (CSIP) using inter-vehicle distance for AVs management at complex intersections accounting for GPS errors [13]. CSIP reduces the number of collisions at the cost of extra average trip delays. Conversely, its predecessor, the Ballroom Intersection Protocol (BRIP) [17], enforces the synchronized AVs arrival for maximum usage of intersection capacity, thus allowing vehicles from all inflow lanes to continue as they arrive. The authors claimed that BRIP improved throughput by 96.24% against competing approaches. In [12], the Distributed Synchronous Intersection Protocol (DSIP) for mixed HV/AV management was introduced to synchronize AVs in the absence of HVs. In the presence of HVs, AVs cooperate and share the sensed information at the intersection. The performance of DSIP shows that the trip delay is high for growing AV penetration rates.

Concisely, previous studies on mixed traffic management of HVs and AVs are limited, particularly the synchronized ones in low-speed urban conditions. In the synchronous approaches, the synchronization is among AVs only, requires high AV penetration for higher efficiency, and is based on inter-vehicle coordination, which is limited by interoperability issues specific to each AV type and manufacturer. In addition, urban transportation policymakers also suggest lower speed limits in urban areas.

Addressing these challenges, our *synchronous framework* tackles mixed traffic seemingly with any ratio of AVs and HVs using sensory data to increase the concurrent traffic management at complex intersections and using physical traffic lights to control the HVs. Therefore, the vehicles can be fully independent of among them, just coordinated by SIMP

[176; 177]. SIMP performance, when applied to complex intersections, is compared against fixed-time RR and TTLC approaches and adaptive ITLC and QTLC approaches. Section 3.6 presents more information on these baseline approaches, showing improved throughput and a strong reduction of delays, fuel/energy consumption, and polluting emissions.

2.1.3 T - Intersections

Figure 2.3 illustrates a three-legged or three-way or T - intersection, one of the common road intersections with three arms. T - intersections can be either signalized or unsignalized. The figure indicates that no road is ahead from the South; only left- or right-crossing directions are possible—similarly, there is no right-crossing from the East and no left-crossing from the West.

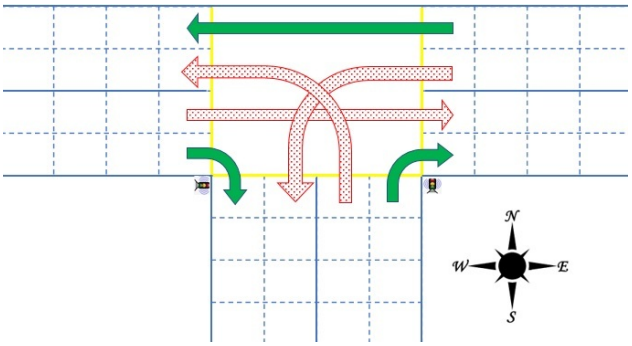

Figure 2.3: Three-legged or T - Intersection.

We found many related works on unsignalized T-intersections [25]; however, we focus on signalized T-intersections for which fewer works are available. For instance, Kumara et al. analyzed the road accidents at 104 signalized T-intersections in Singapore, focusing on underreporting through the Poisson model [102]. On the other hand, Gomes et al. estimated the safety performance of signalized and unsignalized intersections, including 44 T-intersections in the Lisbon area [68]. The study considered several crash predictive models using the Poisson-gamma modeling framework and noted responsible geometric design characteristics. Differently, Kumar et al. studied a real-world T-intersection in the Indian city of Vellore to find traffic congestion by analyzing the traffic video [101]. Differently, Warchol et al. analyzed the gap acceptance data-based guide to finding initial signalization needs for intersections. The idea is to guide traffic engineers in installing signalized intersections [227].

Again, all these works did not consider a synchronous framework and we will show that T-intersections managed with SIMP and included in networks of intersections still exhibit performance advantages over the considered competing IMs.

2.1.4 Networks of Signalized Intersections

Figure 2.4 illustrates a 2×2 grid network of signalized intersections. Here, each signalized intersection (I_0, I_1, I_2, and I_3) is associated with an IM unit for implementing the TLC operations. Each intersection has two inflow roads connecting the outside road network and two inflow roads connecting the neighboring intersections. Hence, each origin can have seven destinations passing through one, two, or three intersections.

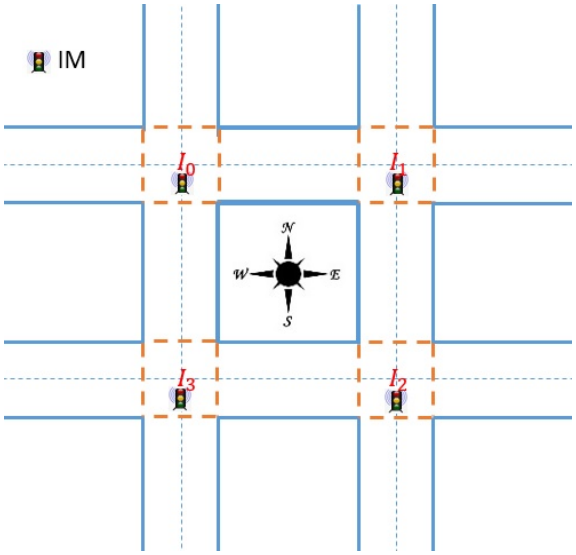

Figure 2.4: 2×2 - Network of signalized intersections.

The computational complexity of analyzing networks of intersections grows dramatically when the number of road lanes and intersections increases. In an initial work Gazis [63] studied an arterial of 1×2 intersections with multiple lanes in 1964. Then many works focused on analyzing similar arterial networks D'ans and Gazis [42], Michalopoulos and Stephanopoulos [131], and Lin and Wang [116]. With the advancements in simulation software tools, the size of the intersections network that can be analyzed has increased significantly in recent decades, enabling the simulation of urban traffic management. Wong [236] analyzed a general road network of 15 signalized intersections with one or more road lanes per leg, McKenney and White [128] successfully analyzed a 9×7 grid network of signalized intersections in Ottawa, Canada, and Aslani et al. [15] studied a general network of 50 intersections in Tehran city, Iran.

Broadly, the two fundamental ways of managing a network of intersections are controlling each intersection individually or all intersections together cooperatively. All the conventional fixed-time IM approaches can be categorized under individually operating intersections, as their TLC operations consider time-invariant constant traffic arrivals. Differently, Boon and van Leeuwaarden [26] presented a network algorithm that decomposes networks of intersections into isolated intersections that are managed independently based on the fixed cycle traffic light model. Similarly, Terraza et al. [210] proposed an hourly

green split mechanism for minimizing delays at individual intersections towards the network level optimization hour-by-hour to track varying traffic inflows. In the same direction, Varaiya [216] introduced the fixed minimum MCA to stabilize the network traffic without requiring knowledge of the traffic demand, just controlling adjacent lanes traffic movement at individual intersections. In [230], Wei et al. combined the MCA with reinforcement learning to minimize delays and maximize throughput in an arterial network.

On a different branch, related works employed metaheuristic algorithms for TLC signals optimization. For instance, Gao et al. [60] targeted the heterogeneous network of signalized and unsignalized intersections to minimize the overall delay. Jamal et al. [84] employed Genetic Algorithm and Differential Evolution for delay optimization and intelligent control of individual intersections in a network of two intersections in Dhahran, Saudi Arabia. Shirke et al. [198] presented a metaheuristic robust plan approach that identifies robust TLC fixed signals in an arterial network of intersections. A detailed review on employing metaheuristics for TLC signals optimization can be found in Jamal et al. [85]; Jalili et al. [83]; Shaikh et al. [195].

Cooperative IM can be centralized or decentralized. In the centralized cooperative IM, a central traffic monitoring system observes the network traffic and optimizes TLC operations at all intersections to improve the system-wide performance. In the decentralized cooperative IM, each intersection is managed separately and autonomously through cooperation between multiple neighboring intersection agents. In this direction, most works are based on MAS. For instance, Belbachir et al. [22] utilized MAS for self-adaptive intersections that cooperate to minimize traffic congestion, while Darmoul et al. [43] designed an intelligent distributed and adaptive TLC system using MAS and biological immunity systems to minimize delays and queue lengths by providing coordination among neighboring intersections.

Jin and Ma [89] introduced a decentralized hierarchical MAS framework, in which the network is decomposed into regions where each region represents a group of intersections. At each intersection, the reinforcement learning algorithm optimizes the TLC operations. Liu et al. [119] presented a MAS-based Q-learning approach to optimize the trajectories of vehicles. The algorithm calculates optimal control actions by considering the local and neighboring intersection traffic information. Torabi et al. [213] developed the Distributed Agent-based traffic LIghts (DALI) based on the Traffic Signal Timing system (TST) for highly dynamic and congested traffic conditions. In DALI, the traffic light agents directly communicate with neighboring agents to collaborate by sharing incoming traffic flow information. Jiang et al. [88] presented an accumulated exponentially weighted waiting time-based adaptive traffic signal control to calculate the road priorities and then applied the distributed MAS-based reinforcement learning with a graph decomposition approach. The decomposition divides a network-level traffic control problem into sub-problems based on the average residual capacities.

Other works used a diversity of intriguing approaches from microscopic traffic models

to self-organization concepts, particle swarms optimization, trajectory control, etc. For example, Osorio and Nanduri [157] combined a stochastic microscopic traffic simulation model with an instantaneous vehicular fuel consumption model and embedded them within a simulation-based optimization algorithm to minimize travel time and fuel consumption at nine intersections. In [91], the authors proposed an autonomous decentralized control scheme for adapting the TLC signals to unpredictable changes in traffic relying on virtual impulses, a physics concept. These impulses are estimated using the optimal velocity model. Wang et al. [225] introduced a self-organized traffic signal control system using fuzzy control for minimizing traffic congestion and oversaturation in a network of four signalized intersections. The traffic-related information input to this system is collected using the VANET. Qi et al. [167] proposed a coordinated intersection signal decision that uses particle swarm optimization to obtain optimal cycle length and green time duration. Agafonov et al. [4] introduced the cooperative control of CAV trajectories via coordination and traffic signal phases optimization to improve transportation systems efficiency and safety in three real-world road networks through reduced traffic congestion, travel time, and fuel consumption.

Overall, some of these works propose collaborating intersections, some rely on global information, some support AVs only, and generally use cyclic slot-based intersection management. However, communication among intersections is not always supported, global information is frequently unavailable, and hybrid AV/HV traffic will likely persist for a significant time. Thus, we target compositions of independent synchronous intersections in Chapter 6, particularly assessing fluid synchronous AV/HV traffic management, which is still an open research line compared to cyclic slot-based approaches.

2.2 Worst-Case Traffic Scenario

As discussed in previous sections, the literature related to signalized intersections management primarily focuses on improving the average performance, e.g., throughput, energy efficiency, waiting and travel delays, and emission of air pollutants. Nonetheless, an important metric of the quality of service of the IM policies is the worst-case waiting time they may imply given certain statistical traffic conditions (e.g., Poisson arrivals), i.e., how long a vehicle may expect to wait in the worst-case since it enters the road system until it departs from the last intersection in the path knowing the vehicles arrival follows some known statistical law. In this research direction, we found a few relevant related works that are discussed below.

Boon et al. [27] studied the vehicle-based actuated traffic signal control for saturated and under-saturated traffic conditions that follow *Poisson* and general renewal arrival patterns. Exact limiting distributions for vehicle delays were derived with closed-form approximations achieved by interpolating heavy and light traffic distributions.

Oza and Chantem in [158] studied the closely spaced intersections prone to queue spillbacks. They present an adaptive real-time server-based approach for dynamically adjusting signal timings to minimize queue spillbacks. They also provide worst-case analysis with bounds on wait times. As a continuation, the work in [160] introduces an optimal algorithm to maximize the traffic flow and eliminate the queue spillbacks simultaneously. Accordingly, they complimented the time bounds on worst-case wait time and associated recovery time. Further research by [159] covered the worst-case wait time bounds for non-emergency vehicles during the presence of emergency rescue vehicles.

In [130], Miao et al. studied traffic signal scheduling to reduce average wait time and guarantee certain worst-case wait times for CAVs. First, the best-case and the worst-case wait time bounds of CAVs were derived. Then by utilizing these bounds, two adaptive signal control mechanisms were proposed to assign deadlines to CAVs and adapt traffic signals to meet the deadlines.

A bi-level programming model to study the network performance and network flow distribution during uncertain link capacity using the worst-case mixed traffic (HVs and CAVs) assignment model was presented in [222]. For this, the network equilibrium is estimated based on the fixed road capacity and then find the optimal input for all road capacities within their ranges. In [50], the authors studied the reliability of user route choice and how the cascading failures spread traffic congestion over the road network; thus, the outcome can be used in future traffic management. Young and Sharon [162] extended the fixed-time H-AIM scheme by combining it with the actuated and adaptive approaches for computing safety bounds on signal timing in the case of demand uncertainty.

Differently, in [221], the authors analyzed the worst time-to-collision metric for AVs relying on driving dynamics and physical possibilities and, in the case of uncertainties, stochastic predictions are employed by [23]. Sontges et al. in [204] studied time-to-react (TTR) in worst-case traffic scenarios to mitigate collisions. The authors presented a deterministic upper bound to the TTR used to find a feasible emergency maneuver or to trigger a collision mitigation system.

Distinctly, we defined a service measure of TLC operations of IM inspired by real-time systems concepts. We named it *worst-case response time* (WCRT) that the IM approaches can guarantee to vehicles from their origin until exiting the intersection system, knowing the traffic statistical arrival pattern [175]. To our best knowledge, this is the only work so far specifically providing worst-case traversal time guarantees in low-speed urban settings with mixed traffic scenarios.

2.3 Transportation Sustainability

As mentioned in the introduction chapter, transportation sustainability indicates intelligent, affordable, energy-efficient transportation that minimizes emissions, utilizing alternate fuels like electricity. Therefore, introducing connected, electric, and autonomous

technologies into the transportation systems is significant [10; 188]. The AVs and BEVs are part of this effort. BEVs can be controlled by either human drivers (simply BEVs) or be autonomous (BEAVs), with the main difference being that human driving tends to be more inefficient than autonomous driving, as human sensing is less accurate and human decision-making involves other criteria and objectives than mere optimization of traffic fluidity and sustainability. However, both BEVs and BEAVs are energy-efficient through regenerative braking and are environment friendly due to zero-emission of toxic air pollutants.

In this direction, several research studies focused on introducing AVs, EVs, BEVs, and BEAVs, and the associated impacts when mixing with ICE HVs. Examples include the lifecycle assessment to study the energy efficiency, emissions characterization, and environmental effects [11; 93; 105; 218; 219; 220; 238]; well-to-wheel-based estimation of energy efficiency and emissions (from the energy extraction to the consumption in the vehicle) [55; 16; 6]; environmental feasibility of using electric vehicle taxis [202]; a city/region (network of intersections) level comparison [126; 74; 163]; and at isolated intersections [5; 251]. The effect on emissions by introducing BEVs in 29 EU countries between 2010 and 2020 is also analyzed in [59]. These works analyzed mixed BEVs and ICE vehicle scenarios, generally considering human drivers. On the other hand, just a few research works study autonomous electric vehicles. Some examples include energy-efficient cruise driving [117; 122], trajectory control [109], energy optimization [249], and ride-sharing [81]. However, most of these works focused on studying CO_2 emissions only, and only a few studies characterized other more dangerous emissions (CO, NOx, and PMx) as per the WTO. The remaining section elaborates on these studies.

In [220], the authors presented a traffic control algorithm for urban areas where vehicles exhibit stop-and-go behavior with low speeds in low vehicle gears. They employed traffic intensity detectors that tune the TLC signals to reduce fuel consumption and CO_2 emission. In [238], the authors applied a Lagrangian model to predict the traffic and air pollutants in Hong Kong, especially CO, NOx, and PMx; the predicted data were compared with real-time data showing a good correlation.

Vreeswijk et al. [219] described *eCoMove*, an energy-efficient traffic management and control approach that uses an adaptive balancing and control mechanism. The authors study various traffic conditions such as rerouting, green priority, and speed advice, showing that *eCoMove* reduces fuel consumption and CO_2 and NOx emissions while increasing PMx emissions.

In [11], the authors proposed the Intelligent Green Traffic Congestion (IGTC) model for urban traffic management. IGTC combines traffic flow, vehicle emission, and air quality modeling. An extensive analysis of IGTC results indicates a considerable reduction in all significant vehicular emissions (CO_2, CO, PMx, NOx) in urban areas.

Faria et al. compared the sustainability of BEVs against ICE vehicles with various energy sources [55]. This work discussed the CO_2 emissions during electricity production from traditional fuels, the ownership cost, and the impact of BEV driving cycles, i.e., the

BEVs performance during various speed conditions respecting the electricity consumption and associated emissions.

Athanasopoulou et al. [16] also compared the emission of CO_2 in a mixed scenario of ICE vehicles and BEVs. In their approach, the authors found that the estimated CO_2 emissions are higher than the approved ones, regardless of vehicle type. Particularly the gasoline ICE vehicles exceed the diesel ones, and BEVs produced CO_2 emissions are lower than the ICE vehicles.

The authors in [6] investigated the energy efficiency of EVs over ICE vehicles. They compared various energy sources for both EVs and ICE, and their findings show that renewable energy for EVs provides the highest efficiency than the other sources of electricity, such as gasoline, coal, and diesel, then ICE with gasoline and diesel.

In [126], the authors compared the impact of human-driven EVs at lower and higher rates to understand the behavioral impacts on the road network and the electricity grid. Two driver behavioral models (unaware and aware) were tested in an activity-based trip pattern. They found direct and indirect impacts on traffic congestion, the electric grid, and charging infrastructure.

He et al. studied a mixed traffic platoon of ICE and EVs over a network of intersections [74]. An optimal control model was developed to provide eco-driving suggestions. The proposed model relies on connected vehicle technologies to obtain the platoon characteristics and share the speed advisory. For this purpose, two eco-driving advisory strategies were developed. One provides the acceleration profile for the leader vehicle, while the other provides cruising speeds for followers. From the authors perspective, the first advisory is more suitable for autonomous leaders, while the other is for human leaders.

Patella et al. [163] presented the simulated footprint of CO_2 for the city of Rome, for which 100% of BEAVs introduction is considered. The results were compared with the current real-world scenario of Rome to extract the positive environmental effects of adopting 100% BEAVs. The results outline improved travel time and average speed for reduced CO_2 emissions over the life cycle of BEAVs.

Kawamoto et al. [93] utilized the lifecycle assessment methodology for comparing the CO_2 emissions of ICE (gasoline and diesel) and BEVs. For CO_2 estimation, the USA, European Union, Japan, China, and Australia were selected as the reference regions. The estimated CO_2 emissions of BEVs are higher than that of ICE due to the addition of CO_2 emissions from battery production. When renewable energy sources were considered, the BEVs CO_2 emissions were lesser than ICE.

Liu et al. [117] presented a low-emission-oriented speed guidance model for reducing energy consumption and associated emissions (PM_x, NO_x, and CO) while minimizing travel delays at an isolated intersection under mixed ICE and EVs. The numerical analysis shows the better performance of their approach in reducing energy consumption and associated emissions at high traffic volumes. It is found that the energy/emission reduction effects under-speed guidance will increase with an increasing share of EVs.

Lu et al. [122] presented an energy-efficient electric driving model for BEAVs in a mixed traffic stream of BEVs and ICE vehicles. The proposed model aims to adjust the distance between leaders and followers of the mixed stream to maintain high energy efficiency via regenerative braking. The authors also presented a power-based energy consumption model for BEVs energy consumption estimation considering the ambient temperature and load. The mixed fleet was simulated in a long single lane of 7.45 miles. The proposed approach outperforms its counterparts in energy efficiency. The authors claim that the higher rates of BEAVs penetration may not be energy efficient due to decreasing regenerative energy. The combination of BEVs and BEAVs in the mixed ICE shows higher energy efficiency results.

Ahn et al. [5] studied the impact of intersection (roundabout, traffic signal, and two-way stop) control on BEVs energy consumption when mixing with ICE due to their differences in fuel consumption patterns. The BEVs are energy efficient at high-speed roundabouts and traffic signal control, while ICE at a two-way stop sign. The main reason is the regenerative braking of BEVs.

Zhao et al. [251] aims at analyzing the influence of signal timing on the CO_2 emission of ICE when mixing with BEVs. To achieve this, they use a set of CO_2 incremental emission (statistical regression) models depending on stop rate and control delay. The outputs are referred to for signal timing optimization, and in this paper, these outputs are collected from simulation data. Their findings suggest that the models timing optimization can balance the CO_2 emissions generated by vehicles during the control and idling stages. They also find that the road section speed and the mixed proportion of BEVs directly impact the vehicle delay at intersections.

The subsequent studies focused on adopting AVs and their impacts, respecting various factors. For instance, Duarte and Ratti [51] studied the impacts of adopting AVs concerning the need for road infrastructures, parking space, and the number of vehicles on future roads, while Zhong et al. [254] studied the long-term effects of shared AVs concerning the land usage and transportation integration, electrification and its impacts on emissions. Taiebat et al. [205] reviewed the implications of introducing CAVs concerning energy, environment, and sustainability. Kopelias et al. [99] studied the related works of the last 10 years anticipating the impacts of introducing CAVs and EVs on fuel consumption and tailpipe emissions. Similarly, Silva et al. [200] reviewed the impacts of introducing AVs on the environment—differently, Dirsehan and Can [46] surveyed 391 individuals acceptance of adopting AVs concerning trust and sustainability. The results indicate the relationship between AV technologies acceptance, ease of use, and behavioral intention.

In summary, different studies have employed various methodologies to understand the impacts of introducing AVs, EVs, BEVs, and BEAVs at the city/region, network of intersections, and isolated intersections. These works mainly focused on energy efficiency and CO_2 emissions using specific IM systems. We complement these studies by analyzing the sustainability of our proposed protocol SIMP, including fuel/energy efficiency and analysis

of dangerous air pollutants such as PM_x, NO_x, and CO which need to be given more attention. We compared against different IM approaches at isolated and networks of intersections under various traffic conditions and observed the benefits that SIMP introduces, also in this dimension.

2.4 Summary

This chapter presented the background and an extensive survey of related works concerning signalized intersections management, worst-case traffic situations, and transportation sustainability. We approached the IMs in the related works from the signalized intersections viewpoint: isolated intersections and networks of intersections with single/multiple inflow/outflow lanes per road. Then, we also considered the working behavior of IM approaches, i.e., whether they were based on fixed-time, actuated, adaptive, and intelligent. Another perspective we considered was the type of vehicles the IM approaches could serve, i.e., HVs-only, AVs-only, and mixed HV/AV scenarios. Considering the worst-case traffic scenarios, the related works addressed a diversity of conditions, particularly in networks of intersections, such as spillback conditions. The studies on transportation sustainability focused on introducing AVs, BEVs, and BEAVs to improve traffic throughput, reduce congestion, improve energy efficiency, and mostly minimize CO_2 emissions. As we have referred to in the chapter, our proposed protocol SIMP showed significant performance improvements in all referred dimensions, with novel mechanisms and analysis in some cases.

The following chapter presents the simulation tools, models, and baseline approaches that we have considered in our work.

Chapter 3

Simulation Tools, Models, and Baseline Approaches

This chapter describes the SUMO (Simulation of Urban MObility) simulator employed throughout this dissertation for (i) building road networks and IM strategies, (ii) car-following models (CFM) indicating HVs and AVs driving behavior, (iii) fuel consumption and (iv) tailpipe emissions models for ICE vehicles, and (v) electricity consumption model for BEVs/BEAVs. The remaining of the chapter presents the baseline IM approaches for comparing the performance of our reactive *synchronous framework*. The notation used in the models presented in this chapter is the same as presented in original works where they were proposed. In some cases it collides with the notation we use in the following chapters for our own analysis, but we believe there is no risk of confusion since we will be addressing different aspects.

3.1 Simulation of Urban MObility - SUMO

On the one hand, the queueing theory and HCM models focus mainly on aggregated traffic behavior. On the other hand, individual vehicle driving behaviors and their interactions in a larger environment can be modeled using micro traffic simulators like *Simulation of Urban MObility* (SUMO). This section briefly describes the SUMO simulator developed by the Institute of Transportation Systems at the German Aerospace Center [120]. SUMO has gone through tremendous improvements since its development in 2000. SUMO is licensed under EPL 2.0 and is an open-source, microscopic, space-continuous, time-discrete traffic simulator that is highly portable for handling from small isolated road segments to large city-wide road networks.

The road networks can be imported from external sources like VISUM, Vissim, Shapefiles, OSM, RoboCup, MATsim, OpenDRIVE, and XML-Descriptions or designed and developed by using the NETCONVERT tool. Then NETCONVERT converts the imported or developed road network data into a SUMO-usable format, including simplifying the road

geometric settings, creating road network topology, assigning default speed limits, etc. This tool also permits users to update/modify the default parameter values. After building the road network, the user must provide: i) other configuration files (like .sumocfg), ii) routes, flows, and trips definitions, iii) vehicle/user-specific definitions (maximum speed, acceleration, deceleration, etc.), and iv) TLC strategies of user interest.

SUMO supports the concept of inter-modal simulation, i.e., simulating various road users like private vehicles (e.g., private cars or taxis), public transportation (e.g., buses and trains), heavy vehicles (e.g., goods and delivery trucks), pedestrians, bicycles, and other road users on road networks. The analysis can be of individuals/groups of vehicles, lanes, edges, or even the entire scenario.

To handle the behavior of the simulating objects and obtain the simulation values, SUMO provides a powerful tool named TraCI (Traffic Control Interface) [229]. TraCI is a communication interface between external software and the SUMO simulator to interact and manage the simulations in real-time. It follows the client-server architecture, in which external software acts as a client requesting to modify the simulation state, and SUMO acts as a server with appropriate updates on the simulation. This includes adding or removing vehicles, adjusting vehicle speeds, and modifying TLC signals based on their working nature. The external software can be built using various programming languages, including Python, Java, C++, etc.

SUMO offers various features, including vehicle types and driving behaviors, road intersection and network types, and TLC systems. It also provides a range of output formats for visualizing simulation results and performance metrics.

SUMO has been widely used by researchers, academicians, and practitioners from various domains of transportation engineering and urban mobility to evaluate various traffic management strategies, including optimizing TLC phases and timing, road capacity improvements, public transportation planning, and the impact of new or improvements to the existing road infrastructure towards SUM.

The following section presents different car-following models employed in our simulations and their working nature.

3.2 Car-Following Models

Based on traffic flow theory, the car-following model (CFM) describes how one car follows another on a road lane in an uninterrupted flow. CFMs are major contributors to simulation studies and are mathematical models that describe the behavior of individual vehicles and traffic flow. Examples include capturing the interaction between the driver and the corresponding vehicle, the vehicles in front of them, and the traffic environment. CFMs employ different parameters to describe their working nature, such as speed, acceleration,

deceleration, braking, emergency braking, gap, and other relevant factors. We employ the CFMs in the SUMO simulator to understand the driving behavior of individual vehicles and traffic flows; thus, better planning of TLC signals can improve traffic flow and reduce congestion safely. Some of the most commonly used CFMs are the Intelligent Driver Model (IDM) [214], the Gipps Model [66], the Wiedemann model [233], the Krauss Model [100], General motors [31], Adaptive Cruise Control (ACC) [132; 239], and Cooperative ACC (CACC) [133].

We employ the Krauss CFM indicating HVs and the ACC CFM indicating AVs.

3.2.1 Krauss Car-Following Model

The Krauss CFM aims at letting cars drive as fast as possible while maintaining a safe distance. In this model, every vehicle can have two types of motion: free and interactive. In free motion, the vehicle velocity is determined by its maximum velocity $v \leq v_{max}$. In interactive motion, the vehicle (follower) interacts with the vehicle ahead (leader) to adjust its velocity to avoid collisions. In this situation, the vehicle velocity is determined by a safe velocity $v \leq v_{safe}$.

The desired velocity of a vehicle is estimated using Eq. 3.1:

$$v_d(t) = Min(v_f(t) + a_{max}\tau, v_{safe}, v_{max}) \tag{3.1}$$

The safe velocity for every time step is calculated using Eq. 3.2:

$$v_{safe}(t) = v_l(t) + \frac{g(t) - v_l(t)\tau}{\frac{v_l(t)+v_f(t)}{2b} + \tau} \tag{3.2}$$

In equations 3.1 and 3.2, t is the time step, $v_l(t)$ is the velocity of the leading vehicle at time t, $v_f(t)$ is the velocity of the following vehicle at time t, $g(t)$ represents the gap between vehicles in t, τ is the driver reaction time (default $1s$), a_{max} is the maximum acceleration, and b is the deceleration function.

The speed of the follower vehicle after the reaction time τ is $v_f(t+\tau) = Max(0, v_d - \epsilon a \eta)$, where ϵ is the noise amplitude, a is the acceleration, and η is a random number.

We use this Krauss CFM to represent the HV driving behavior due to its jerkiness. The jerkiness is defined as the derivative of acceleration to time by [189].

3.2.2 Adaptive Cruise Control

The ACC CFM is a vehicle longitudinal control system in which a vehicle adapts its speed (via brake and throttle actions) in a pre-selected time gap (default $1s$) whenever it detects a vehicle ahead using its sensors. The distance and speed errors of a vehicle were used to

model the acceleration in Eq 3.3:

$$a_k = k_1(X_{k-1} - X_k - t_{hw}v_k) + k_2(v_{k-1} - v_k) \tag{3.3}$$

where, a_k, X_k, and v_k indicate the acceleration, position, and velocity of k^{th} vehicle respectively; X_{k-1} and v_{k-1} are the position and velocity of preceding vehicle, t_{hw} is the selected time-gap; and k_1 and k_2 are the gains from both the position and speed errors [132; 239].

3.2.3 Simulation Settings

The SUMO simulator v1.6.0 is used on an Intel Core i3-4160 CPU, 3.60Ghz × 4 cores, NVIDIA RTX 2070, 8GB RAM, and 64-bit Ubuntu 18.04.4 LTS OS to build the isolated single-lane and multi-lane intersections, and networks of multi-lane intersections over flat urban road settings, to generate synthetic traffic conditions and to execute the IM protocols. The simulation parameters and assigned values are listed in Table 3.1.

Table 3.1: Simulation Parameters and assigned values.

Parameters	**Values**
Isolated intersection road area	$1020 \times 1020\ m^2$
Vehicle Length	5 meters
Safety Distance	5 meters
Vehicle Type	HVs (Krauss CFM) and AVs (ACC CFM)
AVs Percentage	50%
Target Maximum Speeds	$30km/h$ (i.e., $8.33m/s$) and $50km/h$ (i.e., $13.89m/s$)
Acceleration	$2.6m/s^2$
Deceleration	$-4.5m/s^2$
Emergency Deceleration	$-9m/s^2$
Minimum Time Headway	$1s$
Drivers Imperfection	0.5

Each road is set to $500m$ long until the intersection entrance in the isolated intersections scenarios. The space within the intersection is set to $20m^2$; thus, the total road network area is $1020m^2$. In the case of networks of intersections also, the road length and intersection space are similar to the ones mentioned in the case of the isolated intersection, but the route length depends on the number of intersections that the vehicles cross to exit the road network.

The vehicle length is set to $5m$ long, indicating the average passenger car length and the safety distance between consecutive vehicles is set to $5m$ long. The other simulation parameters of vehicles and associated values are the following - a maximum acceleration of $2.6m/s^2$, a maximum deceleration of $-4.5m/s^2$, an emergency deceleration of $-9m/s^2$,

a minimum $1s$ time headway between vehicles and a driving imperfection factor of 0.5. These values are the SUMO-provided default values for passenger cars[1].

Two typical maximum speeds of $30km/h$ and $50km/h$ are employed, indicating the low-speed urban settings throughout the thesis. We specify when different speeds are employed other than these two speeds.

Using these simulation parameters, the jerky driving behavior of a passenger car with the Krauss CFM running at a free-flow maximum speed of $30km/h$, i.e., $8.33m/s$ to cross $1020m$ road is presented in Figure 3.1. This driving behavior provides some level of confidence in using the Krauss CFM for HVs.

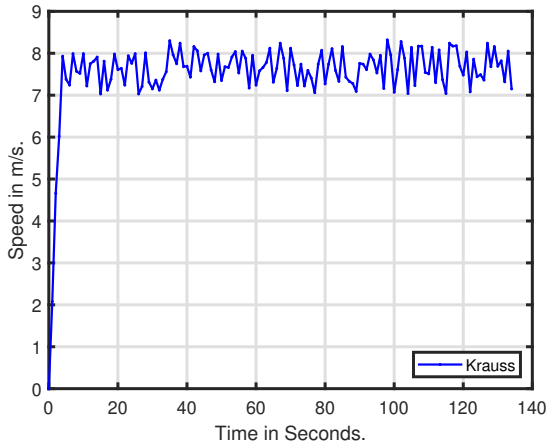

Figure 3.1: Jerky driving behavior of Krauss CFM

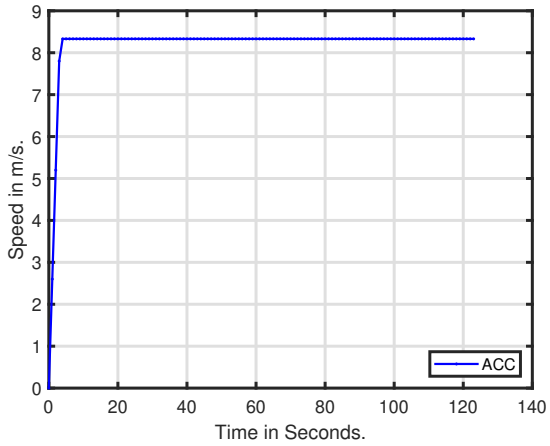

Figure 3.2: Smooth driving behavior of ACC CFM

To test the driving behavior of ACC CFM, we employed similar settings to the Krauss CFM presented earlier. The achieved result speed over time is presented in Fig. 3.2. The

[1] https://sumo.dlr.de/docs/Vehicle_Type_Parameter_Defaults.html

result shows that the ACC CFM provides smooth driving behavior and can be used to indicate AVs with some degree of confidence.

3.3 Fuel Consumption Model

The SUMO simulator quantifies fuel consumption based on the Handbook on Emission Factors for Road Transport (HBEFA3.1[2]). HBEFA 3.1 is a widely used reference guide for estimating air pollutants. It supports 45 emission classes respecting passenger cars, light-duty to heavy-duty vehicles, and buses, including one zero-emissions class, meaning that this class does not produce emissions. This guide includes the fuel consumption model to estimate the amount of fuel a vehicle consumes under different driving conditions by considering various factors (vehicle weight, engine size, and driving speed) affecting fuel consumption.

This fuel consumption model is for the internal combustion engine (ICE) vehicle that burns fuel inside a combustion chamber, generating heat and pressure to power the vehicle. Most ICE vehicles use gasoline or petrol/diesel fuel as their primary energy source, and ICE vehicles have dominated transportation for many decades.

According to HBEFA 3.1 and European Emissions Standard IV, the emission class PC_G_EU4 characterizes a passenger car (e.g., AVs and HVs) with gasoline fuel. Following HBEFA 3.1, the total fuel utilization F for every vehicle trajectory is estimated using Eq 3.4.

$$F = \int_{t_i}^{t_j} Q(t)dt. \tag{3.4}$$

where t_i and t_j indicate the starting and the ending time instants while $Q(t)$ represents the fuel flow. Here, the fuel flow over time t is estimated using the velocity $v(t)$ and acceleration $a(t)$, i.e., $Q(t) = Q(v(t), a(t))$ [215].

ICE vehicles are the transportation sector's primary source of air pollution and greenhouse gas emissions. The following section presents the tailpipe emissions model for ICE vehicles.

3.4 Tailpipe Emissions Model

The HBEFA is developed and maintained by the European Commissions Joint Research Centre. The HBEFA supports the estimation of various types of emissions such as carbon monoxide (CO), nitrogen oxides (NOx), particulate matter (PMx), carbon dioxide (CO_2), hydrocarbons (HC), etc., from different types of road vehicles using type and age of the vehicle, the driving cycle, and the fuel type. Here, the driving cycle indicates the pattern of

[2]https://www.hbefa.net/e/index.html

acceleration, deceleration, and steady-state driving a vehicle experiences during a typical journey.

> The tailpipe emissions of ICE vehicles are estimated using **F** × **Emission Factor** (E_F).

The E_F factor is a continuous real number that depends directly on the velocity and indirectly on the acceleration [106], as expressed in Eq. 3.5:

$$E_F(v, \alpha) = \frac{e_0 + e_{va_1} va + e_{va_2} va^2 + e_1 v + e_2 v^2 + e_3 v^3}{\text{total simulation time in seconds}} \tag{3.5}$$

Note that $\alpha = arctan(\frac{rs}{100})$ represents the slope of the road in degrees (rs is the slope of the road in %), the acceleration a is evaluated from α using $a = \sin(\alpha) g_0$ (g_0 is the standard gravity), and e_{va_1}, e_{va_2}, e_0, e_1, e_2 and e_3 are specific parameter values for the PC_G_EU4 vehicle emission class.

As per [106], different tailpipe emissions that HBEFA produced have different relationships with fuel consumption. For instance, the correlation between energy consumption and emission of PM_x, NO_x, and CO_2 is directly proportional. For CO and HC emissions estimation, vehicle engine parameters (temperature, speed, and gear) play a significant role, so the relationship between CO and HC to fuel consumption is not directly proportional and less accurate than other emissions.

However, the ICE vehicles are set to be phased out to reduce human health risks from dangerous air pollutants like PMx and NOx [155] and to meet the international agreements on reducing greenhouse gases like the Paris agreement [192].

> Various countries proposed to ban ICE vehicles at different periods. For example, the European Union agreed to ban ICE vehicles by 2035, and all new cars and vans registered will be zero-emission vehicles [28].

Zero-emission vehicles (ZEV) do not emit tailpipe emissions, and at present, all types of Electric Vehicles (EVs), including Battery Electric Vehicles (BEVs), are commonly available ZEV vehicles. The following section presents the electricity consumption model of BEVs.

3.5 Electricity Consumption Model

At every discrete time step, the battery-electricity consumption of BEVs (E_{BEV}) is calculated by aggregating the following energy components: kinetic (E_k), potential (E_p), and rotational (E_r) and deducting the energy loss (ΔE_l) due to resistance components, such as air, rolling, and curve resistance, including the constant consumers such as air conditioning

or heating [104]. Therefore, equation 3.6 can be used to estimate the BEVs energy at time t:

$$E_{BEV}(t) = E_k(t) + E_p(t) + E_r(t) \tag{3.6}$$

This energy can be equalized based on the known vehicle parameters such as mass (m), speed over time ($v(t)$), gravitational acceleration (g), altitude over time ($h(t)$), and internal rotating moment of inertia (I_i), as in Eq. 3.7.

$$E_{BEV}(t) = \frac{m}{2} \cdot v^2(t) + m \cdot g \cdot h(t) + \frac{I_i}{2} \cdot v^2(t) \tag{3.7}$$

From the time step t to $t+1$, the energy gain (ΔE_g) can be estimated using the following equation 3.8:

$$\Delta E_g(t) = E_{BEV}(t+1) - E_{BEV}(t) - \Delta E_l(t) \tag{3.8}$$

For more information on resistance components, check [104]. At $t+1$, the energy variation of BEV can be further estimated using the energy gain or consumption ($\Delta E_g(t)$), regeneration (η_r where $\Delta E_g(t) > 0$), and propulsion (η_p where $\Delta E_g(t) < 0$) constant efficiency factors, as in Eq. 3.9.

$$\begin{aligned} E_{BEV}(t+1) &= E_{BEV}(t) + \Delta E_g(t) \cdot \eta_r \\ E_{BEV}(t+1) &= E_{BEV}(t) + \Delta E_g(t) \cdot \eta_p^{-1} \end{aligned} \tag{3.9}$$

here, $\Delta E_g(t)$ represents both consumed and retained energy due to its movements.

Previously, we have presented the CFMs that mimic HVs and AVs driving behavior, fuel consumption and emissions models for ICE vehicles, and the electricity consumption model for BEVs. The following section presents the baseline IM approaches we employed to compare the performance against our *synchronous framework*.

3.6 Baseline Approaches

This section presents the state-of-the-art baseline approaches considered for validating the proposed reactive SIMP protocol in three cases: average-case (AC), worst-case (WC), and market penetration rate case (MPR). Based on the complexity and applicability of tackling the intersection, various IM approaches are employed against SIMP. For instance, the RR IM approach is employed in all the cases, i.e., isolated single-lane and multi-lane intersections and networks of multi-lane intersections. The TTLC is utilized only in complex multi-lane intersections (isolated and networks of intersections). The IIM approaches ITLC and QTLC are used in the isolated two-lane intersections. Finally, the MCA and WTLC are applied only to the multi-lane intersections. We improved all IM

strategies by permitting all non-conflicting right-crossing lanes. A description of each baseline approach is presented below and summarized in Table 3.2.

3.6.1 Round-Robin Intersection Management - RR

The RR IM strategy was developed based on the RR scheduling algorithm of Operating Systems (OS). The RR IM strategy is a pre-timed IM system that switches green phases in a circular order for a fixed allocated time assigned to each road direction in equal amounts [8; 34]. The RR IM approach is also called the uniform TLC due to the uniformly distributed green and yellow phases, as shown in Fig. 1.2. This strategy creates a cycle that we consider to rotate in a clockwise direction.

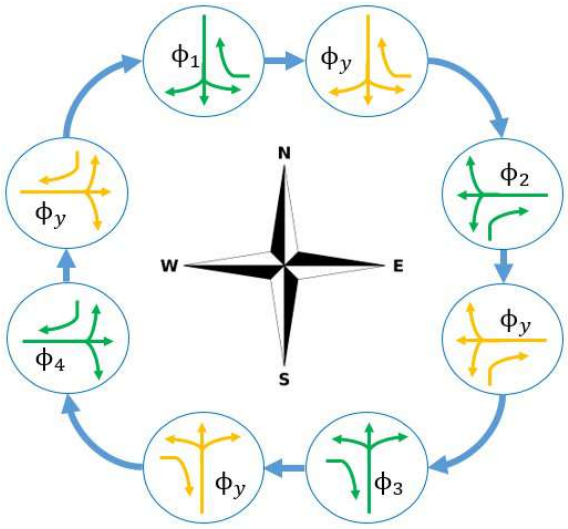

Figure 3.3: Round-Robin IM control phases for single-lane intersections.

Figure 3.3 illustrates the RR IM strategy for the isolated single-lane intersection presented in Fig. 2.1. It comprises four green control phases (ϕ_1, ϕ_2, ϕ_3, ϕ_4) followed by a yellow phase (ϕ_y) in between green phases. While one inflow lane is in one of these phases, the other lanes are blocked by a red traffic light. In the single-lane case, we tested different green phase time settings, i.e., 5s (RR-5), 10s (RR-10), 20s (RR-20), and 30s (RR-30), and found that RR IM with 30s green time provides the best results. Here, each green phase is followed by a 4s yellow phase. We also tested higher green time values, but the performance is inferior to the RR-30.

Hence, we employ the 30s of green phase time configuration in the remaining cases of multi-lane isolated and networks of multi-lane intersections. Figures 3.4a, 3.4b, and 3.4c illustrate the green phase configurations for a two-lane intersection with dedicated and shared left lanes and a three-lane intersection with dedicated lanes, respectively. These figures indicate the green phase ϕ_1 from the North. Rotating this phase clockwise, followed by a yellow phase, generates a TLC cycle. In the network of intersections, these TLC

signals operate individually, each locally, without cooperation or coordination with the neighboring intersections.

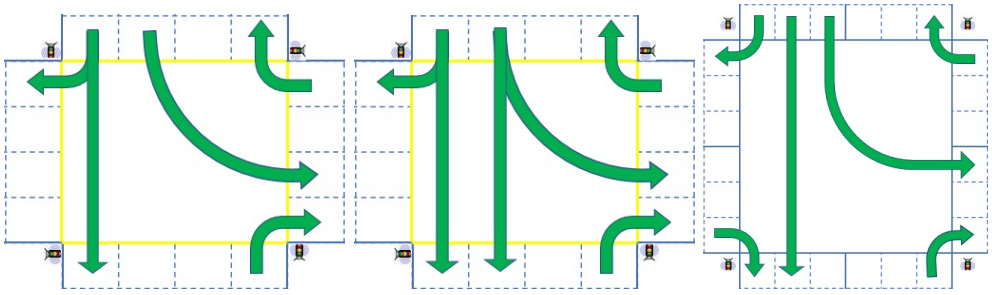

(a) Dedicated left-lane. (b) Shared left-lane. (c) All dedicated lanes.

Figure 3.4: RR IM approach green phase layout for a). dedicated and b). shared left-lane intersections with two inflow/outflow lanes, and c). every lane is dedicated to a specific crossing direction in a three-lane intersection.

3.6.2 Trivial Traffic Light Control - TTLC

The TTLC strategy is also a pre-configured IM mechanism. This strategy controls traffic by authorizing vehicles from opposing directions at the same time, instead, thus alternating between North-South and East-West [24]. Originally, the decision to cross left was given to vehicles rather than the TLC itself, as they are parallelly permitted with the straight-/right-crossing vehicles. We split the left-crossing signals into separate phases thus, the control is given to the TLC. This operation can also be represented by four circular phases (ϕ_1, ϕ_2, ϕ_3, ϕ_4) as shown in Fig. 3.5. ϕ_1 and ϕ_3 are set with $30s$ of green time and $4s$ of yellow time, while ϕ_2 and ϕ_4 are set with $15s$ of green time also followed by $4s$ of yellow time. These values are those used in [24] except for the duration of ϕ_2 and ϕ_4 that was increased from $12s$ to $15s$ to cope with a higher flow rate of left-turning vehicles.

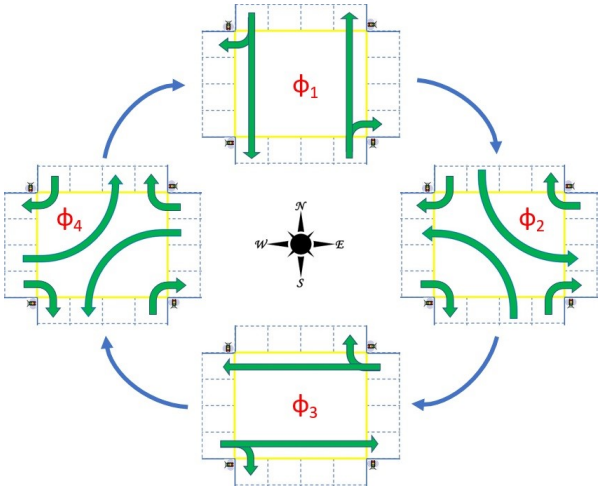

Figure 3.5: TTLC green phases for two-lane intersections with dedicated left crossing lanes.

In the case of shared left lane configuration, phases ϕ_1 and ϕ_3 will have an additional straight-crossing green phase from North and South and East and West. For three-lane intersections also, only ϕ_1 and ϕ_3 phases will change. The example green phase ϕ_1 for the shared left lane and three-lane intersections are presented in Figs. 3.6a and 3.6b.

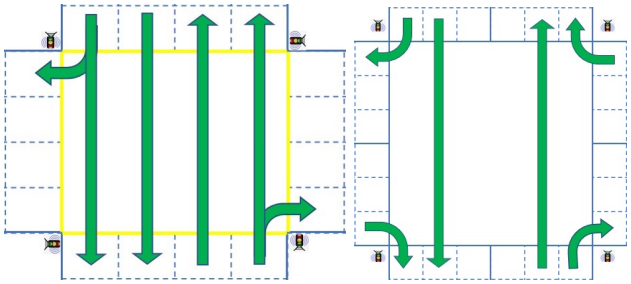

(a) Shared left-lane. (b) All lanes dedicated.

Figure 3.6: TTLC approach green phase layout for shared left-lane intersections with two inflow/outflow lanes, and every lane is dedicated to a specific crossing direction in a three-lane intersection.

3.6.3 Intelligent Traffic Light Control Protocol - ITLC

Younes and Boukerche presented the ITLC algorithm [246]. The ITLC mechanism uses the real-time traffic characteristics from roadside sensors, namely queue length in vehicles, vehicle speed, and associated acceleration, to determine the green time applied to the respective lane, their order, and execution length. Using these real-time traffic characteristics, ITLC can improve traffic fluidity and reduce waiting time. This adaptation is made per cycle, thus making the protocol highly reactive. Nevertheless, given that two opposite lanes are served at a time, the green time used is always the maximum of those two lanes. For the dedicated left-crossing lane intersection, the TLC phases of ITLC are similar to the ones of TTLC as in Fig. 3.5. In this, the green time for the straight-/right-crossing lane is bounded between 5 and 60s, and for the left lane, it is fixed to 15s; again, both cases are followed by 4s of yellow time, while the vehicles from adjacent inflow lanes are stopped. Like TTLC, ITLC is also applied to the isolated shared left lane intersection, as shown in Fig. 3.6a.

3.6.4 Q-learning based Traffic Light Control - QTLC

The QTLC protocol was presented by Abdulhai [2] for minimizing travel delays relying on multi-agent systems. The QTLC employs vehicle queue length and phase duration to estimate TLC decisions. It either chooses to continue with the present phase or change to the next phase to minimize travel delays. This adaptation, done by means of Q-learning, is relatively slow and tracks long-term average traffic arrival rates. QTLC has also been implemented for isolated two-lane intersections, which are configured with dedicated and

shared left lanes permitting traffic from opposing road directions, similar to TTLC and ITLC. The QTLC control phases of the dedicated left-lane intersection are also similar to TTLC, and ITLC, as in Fig. 3.5. The shared left-lane TLC signals are also similar to the shared left-lane model of TTLC and ITLC, as in Fig. 3.6a. Nonetheless, the green time of phases ϕ_1 and ϕ_3 is adjusted between $20s$ and $60s$ accompanied by $4s$ yellow time as suggested in [2]. The duration of phases ϕ_2 and ϕ_4 is kept equal to $15s$ green time followed by 4s of yellow time. Note that, similarly to ITLC, there is a coupling between opposite lanes, and the green time applied to each in each cycle is the maximum of their individual values.

3.6.5 Max-pressure Control Algorithm - MCA

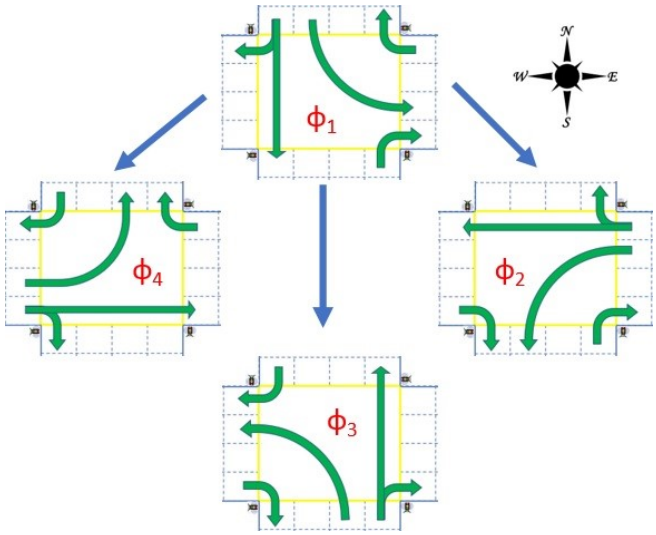

Figure 3.7: MCA control phases of a dedicated left-lane intersection.

MCA was initially employed in communication networks for message scheduling. The same idea has been applied in managing signalized intersections [216; 169]. MCA optimizes TLC signals by measuring adjacent lanes traffic inflow (number of vehicles) and assigning weights to turn movements. MCA improves the intersection throughput by stabilizing the traffic pressure at individual intersections. Thus, the sequence of green phases and associated maximum timing are estimated based on the instantaneous traffic inflow to the intersection. Hence, MCA is an adaptive approach with a minimum green phase time. Due to its acyclic nature, the green phases of MCA can jump to any road with maximum pressure. We have tested several control configurations and minimum green times ($5s$, $15s$, and $30s$) and found that the control phases shown in Fig. 3.7 with $30s$ of green time followed by $4s$ yellow time to be the most efficient for the dedicated left-lane intersections. The same TLC configurations and acyclic adaptations apply to the shared left-lane intersections but with the TLC phases of shared left-lanes shown in Fig. 3.4b.

3.6.6 Webster's Traffic Light Control - WTLC

The original Webster's method is similar to the RR IM approach but with optimal TLC signals. In this dissertation, we employed the adaptive version of the WTLC presented in [64]. Therefore, WTLC follows a cycle-based TLC for a fixed minimum and maximum allocated time and employs traffic flow data for traffic signal optimization [228]. WTLC collects the traffic flow data for a specified time interval. Then Webster's method calculates the cycle time and green phase duration for that time interval. The adaptive form of WTLC utilizes the most recent time interval to collect data and then assumes that the traffic demand will be the same for the upcoming time interval. In WTLC, the time interval selection is crucial as it can result in various trade-offs. Smaller values can result in frequent adaptations to changing traffic demands, and larger values adapt less frequently. This thesis utilizes different TLC cycle lengths with different time intervals based on traffic densities. The WTLC control phases for the dedicated and shared left-lane intersections are the same as in Fig. 3.4a and 3.4b.

Table 3.2: Baseline IM approaches employed against SIMP to compare the performance at single-/multi-lane isolated and networks of intersections.

IM	**Isolated Intersections**							**Road Networks**		
	Single-lane			**Two-lane**			**Three-lane**	**Two-lane**		
	AC	WC	MPR	AC	WC	MPR	AC	AC	WC	MPR
RR-5	✓	✓	✓							
RR-10	✓	✓	✓							
RR-20	✓	✓	✓							
RR-30	✓	✓	✓	✓	✓	✓	✓	✓	✓	✓
TTLC				✓	✓	✓	✓	✓	✓	✓
ITLC				✓	✓	✓				
QTLC				✓	✓	✓				
MCA					✓	✓	✓	✓	✓	✓
WTLC						✓	✓	✓	✓	✓

3.7 Summary

This chapter briefly presented the open-source micro traffic simulator SUMO employed throughout the thesis for simulation studies. The two CFMs Krauss and ACC, representing HVs and AVs driving behaviors, are also presented showing their speed over time at $30km/h$ maximum speed. The SUMO simulator employed HBEFA 3.1-based fuel consumption, associated tailpipe emission models for ICE vehicles, and the electricity consumption model for BEVs are also presented. The baseline conventional, intelligent, and adaptive IM approaches for comparing the performance against the *synchronous framework* are also described.

The following chapter presents the first contribution of this thesis, the *synchronous framework* for managing the mixed traffic of HVs and AVs at single-lane and multi-lane intersections.

Chapter 4

Synchronous Framework

This chapter presents the primary contribution of the thesis, the ***synchronous framework***, a combination of *intelligent intersection management architecture* (IIMA) and *synchronous intersection management protocol* (SIMP). As mentioned in previous chapters, we consider isolated single-lane and multi-lane intersections from which a road network of intersections can be built. Therefore, first, we present the IIMA for isolated single-lane and multi-lane intersections. The *Conflicting Directions Matrix* (CDM) designed from single-lane and multi-lane intersections will be presented. The CDM plays a significant role in SIMP's decision-making. Then the SIMP protocol and its adjustments from single-lane to multi-lane intersections are presented. Note that the *synchronous framework* and SIMP terms are occasionally used interchangeably.

The majority of the content of this chapter is obtained from the following scientific publications:

- **Reddy, R.**, Almeida, L. and Tovar, E., 2019, December. Work-in-Progress: Synchronous Intersection Management Protocol for Mixed Traffic Flows. In 2019 IEEE Real-Time Systems Symposium (**RTSS 2019**), pp. 576-579.
- **Reddy, R.**, Almeida, L., Santos, P.M., Bouzefrane, S. and Tovar, E., 2021. Synchronous Intersection Management to reduce Time Loss. In Euro Working Group on Transportation Meeting (**EWGT 2020**), **Transportation Research Procedia**, 52, pp.364-372.
- **Reddy, R.**, Almeida, L., Gaitan, M., Santos, P.M. and Tovar, E., 2023. Synchronous Management of Mixed Traffic at Signalized Intersections towards Sustainable Road Transportation. In **IEEE ACCESS 2023**.

4.1 Introduction

Signalized intersections are significant in urban transportation where multiple road paths cross and are available in various shapes and geographic settings. As mentioned in the

introduction chapter, typical signalized intersections can have three, four, or more legs. Again each leg can have a lane group indicating a set of inflow/outflow road lanes at the intersection entrance. Without loss of generality, Figure 4.1 shows the four typical lane groups and vehicle movements in those lane groups, designed relying on the HCM [125].

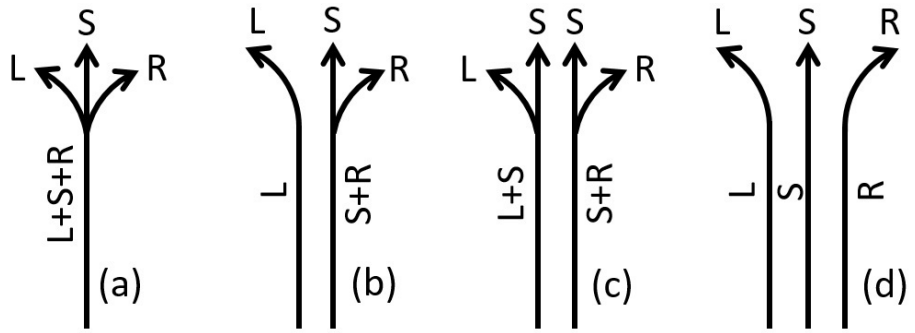

Figure 4.1: Typical lane groups

In Fig. 4.1, L, S, and R indicate the left, straight, and right-crossing directions within intersections. The figure also shows the traffic movements. For instance, Figure 4.1a indicates a single-lane approach with L+S+R traffic. Figure 4.1b and 4.1c indicate a two-lane approach with dedicated L and shared S+R traffic and shared L+S and S+R traffic. Finally, Figure 4.1d shows a separate lane for each L, S, and R traffic. Therefore, using the four typical lane groups mentioned above, we design single-lane and multi-lane intersections with four approaches and the IIMA associated with each intersection type. In the case of T-intersections, each inflow lane will be configured with any two of the three L+S+R traffic movements, i.e., in some cases there will be no L traffic, in other cases no S traffic or no R traffic.

The next section presents the IIMA for single-lane and multi-lane intersections built using the lane groups shown in Fig. 4.1.

4.2 Intelligent Intersection Management Architecture - IIMA

This section presents the assumptions, components, and communications between the components forming the IIMA for single-lane and multi-lane intersections, supporting mixed HV/AV traffic detection. The IIMA is composed of a set of fixed components, namely RSUs, TLC units with communication capabilities (i.e., IM units), road sensors (i.e., induction loop detectors and camera sensors), and a set of non-fixed (mobile) users, namely communicating AVs and communicating HVs. We also briefly discuss the assumed V2V, V2I, and I2V communications between the IIMA components.

The following notation is used in this chapter:

- Road index $i = 1, .., n$ ($n = 8$ for four-legged intersections). Odd indexes represent inflow roads and even indexes outflow roads;

- Road lane index $j = 1, 2, 3$, from the outermost to the innermost lane;
- R_{ij} stands for road i lane j;
- Direction codes index $m = 1, 2, 3$ for Right, Straight and Left, respectively.
- $D_{ij,m}$ is the arrival from lane R_{ij} with direction m;
- $\Phi(IM)$ is the set of phases that compose the intersection control cycle under a given IM protocol, including green $(\phi_1, \phi_2, \phi_3, \phi_4)$ and yellow (ϕ_y), as appropriate.

4.2.1 IIMA Components

Figure 4.2 illustrates an IIMA for a four-way intersection with a single lane per road and roads arranged orthogonally. The inflow/outflow road lanes are referred as R_{ij}, where $i = 1, .., 8$ clockwise starting from the North and $j = 1$. For this kind of intersection we omit the j for simplicity, given it is constant. Thus, inflow road lanes are R1, R3, R5, and R7, and outflow lanes are R2, R4, R6, and R8. In this intersection, each inflow lane convey vehicles with all three crossing directions (R,S,L) as in Fig. 4.1a. Figure 4.2 also highlights the three possible crossing directions within the intersection, identified with three codes assigned to a direction variable m. As shown, $m = 1$ refers to the Right-crossing, $m = 2$ refers to the Straight-crossing, and $m = 3$ refers to the Left-crossing.

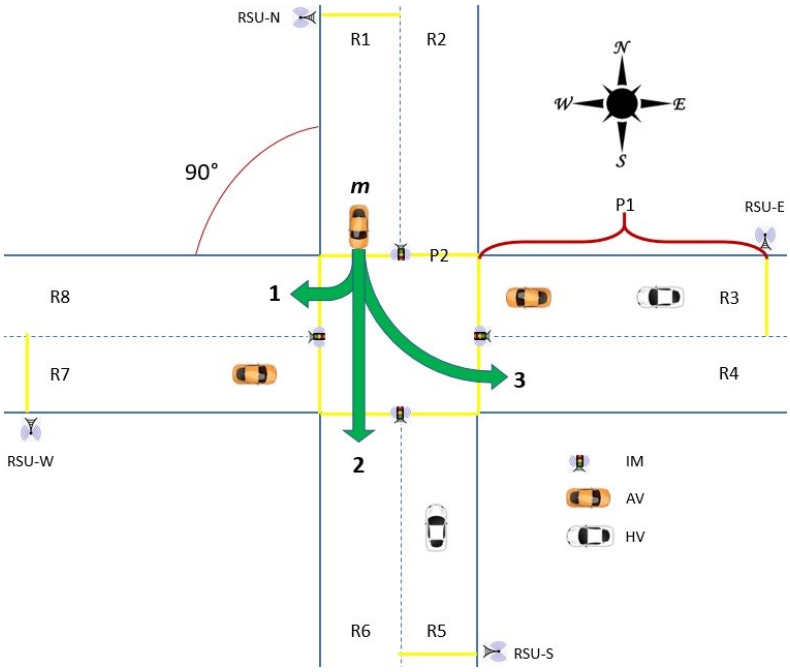

Figure 4.2: IIMA for a four-way single-lane intersection with direction codes ($\boldsymbol{m}$): ***1***-Right-crossing; ***2***-Straight-crossing; and ***3***-Left-crossing movements.

Figure 4.2 also depicts a basic scenario consisting of RSUs, IM units, road sensors ($P1$ and $P2$), AVs (yellow cars), and HVs (white cars). In the IIMA, each road is equipped

with RSU units ($RSU-N$, $RSU-E$, $RSU-S$, and $RSU-W$). The RSU is a DSRC transceiver mounted along a road for providing connectivity and information support to AVs, including safety alerts and other traffic-related information [92]. The IM unit is where the TLC operations occur based on the SIMP protocol control logic, probably an edge node [146].

Each inflow road of the IIMA is equipped with $P1$ road sensors, which are complex with multi-entry/exit induction-loop detectors combined with camera sensors. The entry point of this $P1$ sensor is placed at a certain distance from the intersection, and the exit point is at the intersection entrance. The area that the sensor $P1$ covering is called the intersection area. The outflow lanes are equipped with P2 road sensors at intersection exit points, which are simple induction-loop detectors. These $P1/P2$ road sensors detect vehicles arriving at the intersection entrance and crossing and exiting the intersection [37; 9]. The induction loop detectors can also be employed to identify rear-end collisions [154], CO_2 emissions [71], speed [97], etc., [224]. Vehicle movements are detected using the cameras installed at intersections under $P1$ sensor and image processing techniques in real-time [56; 217; 86]. All these road infrastructures are connected via a wired medium assumed to have no losses and no latency.

AVs are assumed to have the standard components, such as localization and path planning navigation systems, autonomous driver controller, wireless communication interface (DSRC or WAVE, 5G or IEEE 802.11p), and many sensors [196; 12; 252]. It is also possible to use the AVs camera sensors to detect the blinking lights of other vehicles (AVs/HVs) to identify turning movements at intersections [165; 242]. HVs are equipped with all sensors and communication devices as AVs, except humans drive them.

Four-way two-lane dedicated and shared left-lane intersections are built using two lane groups, as shown in Figs. 4.1b and 4.1c. Figures 4.3 and 4.4 illustrate the IIMA for dedicated and shared left-lane intersections, respectively. In both cases the outermost lanes convey traffic that crosses right or straight, i.e., R_{ij} with $j = 1$ can have direction codes $m = 1, 2$, respectively. The innermost lane, i.e., $j = 2$, is different for the two types of intersections. For dedicated left lanes (Figure 4.3) the direction code is constant ($m = 3$) while for shared left lanes (Figure 4.3) the direction code can be either $m = 2, 3$ for straight or left crossing, respectively.

Figure 4.4 shows the IIMA for a four-way two-lane shared left-crossing intersection. This one is similar to the dedicated left-crossing intersection (Fig. 4.3) in every aspect except the straight-crossing vehicles ($m = 2$) are shared between road lanes $j = 1$ and $j = 2$.

Similar to the single-lane IIMA shown in Fig. 4.2, these two IIMAs also depict a basic scenario consisting of RSUs, IM units, roadside sensors ($P1$ and $P2$), AVs, and HVs. The only difference is that the lane with dedicated ($j = 2$) direction does not need complex $P1$ sensors with cameras, but simple induction loop detectors since these are sufficient to detect vehicles present at the intersection entrance and their direction (implicit direction).

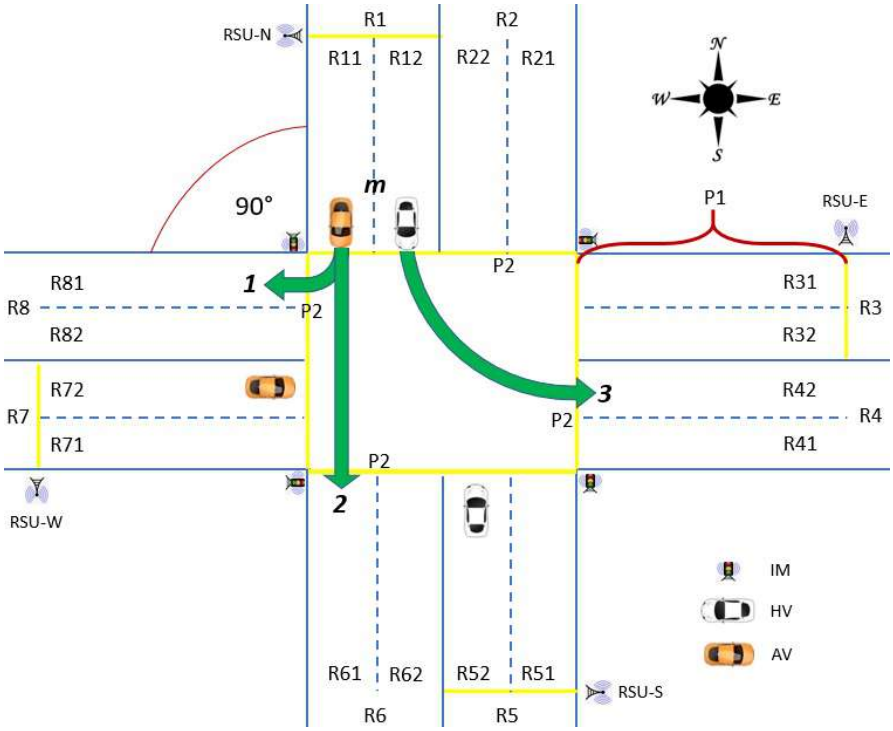

Figure 4.3: IIMA for a four-way two-lane dedicated left-crossing intersection with the direction codes ($\boldsymbol{m}$): ***1***-Right-crossing; ***2***-Straight-crossing; and ***3***-dedicated Left-crossing movements.

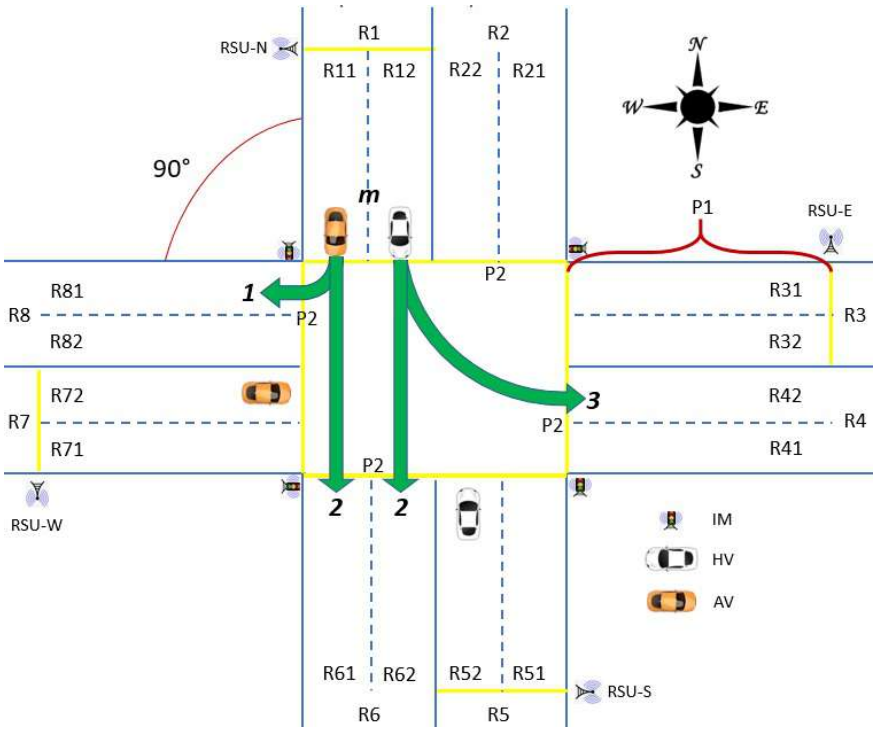

Figure 4.4: IIMA for a four-way two-lane shared left-crossing intersection with the direction codes ($\boldsymbol{m}$): ***1***-Right-crossing; ***2***-Straight-crossing; ***3***-Left-crossing movements.

Figure 4.5 shows the IIMA for a four-way three-lane intersection, in which each traffic movement has a separate lane j, as shown in Fig. 4.1d. Here, the road index R_i is similar to the previous ones and $j = 1$ is for the right ($m = 1$), $j = 2$ is for the straight ($m = 2$), and $j = 3$ is for the left-crossing ($m = 3$) lanes, i.e., an exclusive direction code m for each lane j (directions are implicit). Therefore, all right-crossing lanes are conflict-free, and vehicles have the right-of-way, just stopping for synchronization; only straight- and left-crossing lane vehicles may be yielded by the IM operations. The IIMA does not need the complex roadside sensors combined with the cameras for these dedicated lane intersections, as each lane group hosts vehicles of one crossing direction. Hence, simple induction loop detectors are sufficient to detect vehicles present at the intersection entrance and their direction.

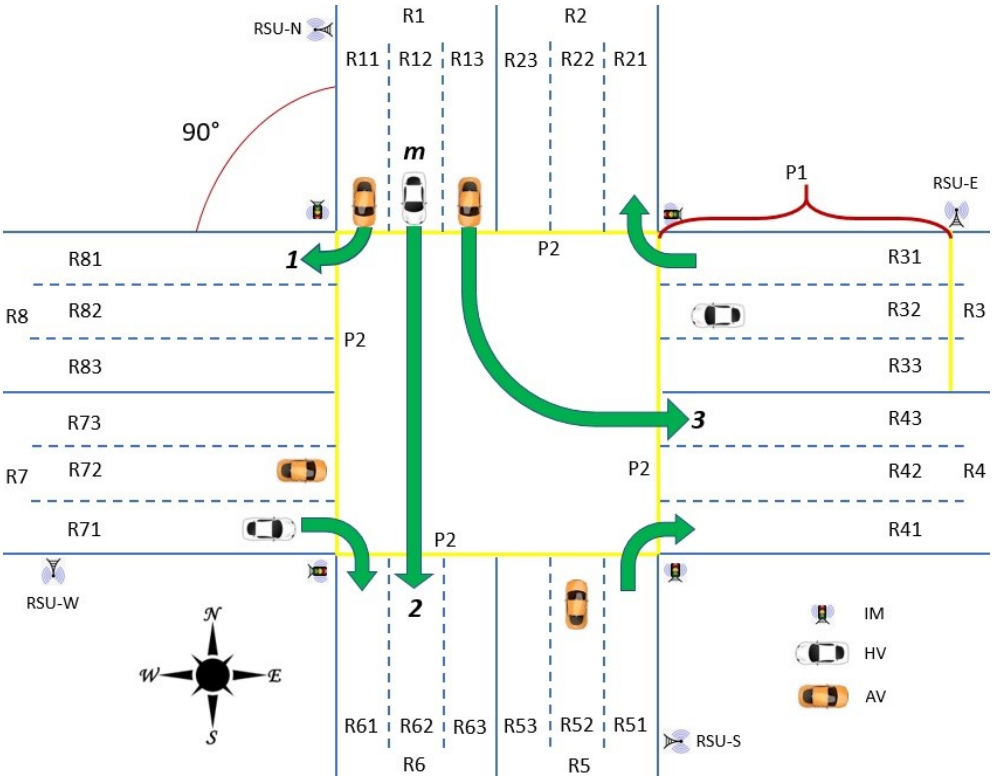

Figure 4.5: IIMA for a four-way three-lane dedicated crossing intersection with the direction codes ($\boldsymbol{m}$): ***1***-Right-crossing; ***2***-Straight-crossing; and ***3***-Left-crossing movements.

The following subsection discusses the communications, i.e., V2V, V2I, and I2V, between the components of the IIMA.

4.2.2 IIMA Communications

The AV and wireless technologies advancements provide subsequent communications between the IIMA components. Now consider a scenario in which the IIMA is set to function, and AVs arrive within the communication range of RSUs. Thus, AVs directly communicate with the road infrastructure (RSUs and IM units) via V2I to access the intersection by

sharing their arrival information and the desired departure direction. If the requests are sent to the RSUs, then the RSUs send these requests to the IM unit via wire communication due to ultra-low communication delays. $P1$ sensors detect the vehicles (AVs or HVs) when they pass over them toward the intersection, and this vehicular information is also shared with the IM units.

As mentioned in the previous section, the IM unit already has the geographic settings of signalized intersections (R_{ij}) and associated CDM (which will be discussed in the coming section). The IM leverages the information provided by the RSUs and roadside sensors. Consequently, the IM unit can allow/block the access/crossing of vehicles to the intersection through the well-defined set of conflict-free vehicle maneuvers and direction codes (m) discussed in the previous section. These IM decisions are shared with the AVs through direct communication (or via RSUs) using I2V as messages and HVs with the physical TLC signals. Therefore, the RSUs behave like brokers between AVs and other road infrastructure (i.e., IM units) by transmitting AV requests and IMs responses. In the end, AVs confirm their exit of the intersection through V2I communication, while P2 detects the exit of HVs. In this scenario, AVs and communicating HVs exchange information via V2V communications. The information can be safety alerts, such as emergency brakes, collision warnings, intersection crossing assistance, blind spot, and lane changing.

The following section presents the CDM, a major component the SIMP protocol utilizes in decision-making.

4.3 Conflicting Directions Matrix - CDM

This section presents the CDMs for single-lane and multi-lane intersections considered in the previous section. The CDM is static for a given intersection and will be employed by the SIMP for permitting or blocking the vehicles. The CDM indicates the conflicts among vehicles that want to access the intersection from several road lanes simultaneously.

4.3.1 Single-lane Simple Intersections

In Figure 4.2, the IIMA for a single-lane four-way intersection is presented along with the direction codes that the vehicles take while crossing the intersection, namely right ($m = 1$), straight ($m = 2$), and left ($m = 3$). Before accessing the intersection, the vehicles must diverge as the lane group hosts the vehicles of all three crossing directions, then cross the intersection and merge with the vehicles from other lane groups after exiting the intersection. Thus, these three events trigger three types of conflicts - diverging, crossing, and merging, as shown in Fig. 4.6 designed relying on Chandler et al. [32].

As shown in Fig. 4.6, the four-way single-lane intersection comprises 8 diverging, 8 merging, and 16 crossing conflicts. Diverging conflicts, marked with half-grey circles, occur when two vehicles from the same inflow lane go to two different outflow lanes. Crossing conflicts, marked with black dots, occur when two vehicles coming from different inflow

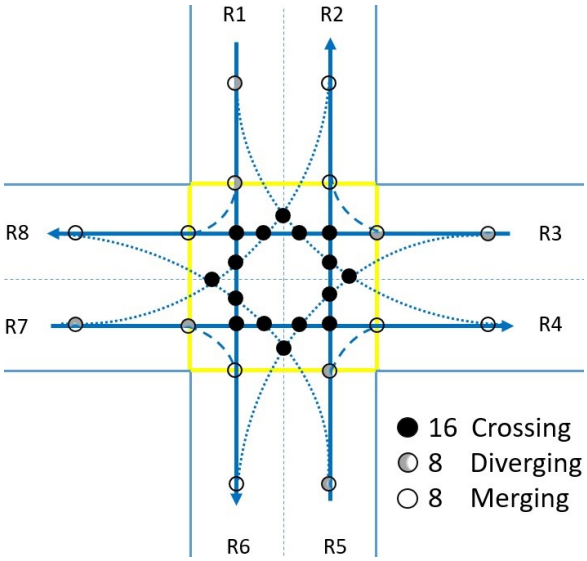

Figure 4.6: Crossing, diverging, and merging conflicts of a four-way single-lane intersection.

lanes and going to two different outflow lanes must cross their trajectories. Merging conflicts, marked with white circles, occur when vehicles from different inflow lanes go to the same outflow lane. Merging and diverging conflicts can lead to rear-end and sideswipe collisions that may occur at the intersection exit or entrance lanes, respectively.

Based on these conflicts and the condition that any conflicting point cannot be used by more than a vehicle at any time, we derived the CDM presented in Table 4.1, where 0 represents a conflict-free direction, and 1 indicates a conflicting direction, between two vehicles at the entrance of the intersection in any two distinct incoming lane groups. Note that for single-lane intersections, R_{ij} becomes R_i, as $j = 1$ intrinsically.

Table 4.1: CDM for a four-way single-lane intersection (0 - no conflict and 1 - conflict).

$D_{i.m}$		$D_{1.m}$			$D_{3.m}$			$D_{5.m}$			$D_{7.m}$		
	m	1	2	3	1	2	3	1	2	3	1	2	3
$D_{1.m}$	1				0	1	1	0	0	1	0	0	0
	2				**0**	**1**	**1**	**0**	**0**	**1**	**1**	**1**	**1**
	3				0	1	1	1	1	1	1	1	1
$D_{3.m}$	1	0	0	0				0	1	1	0	0	1
	2	1	1	1				0	1	1	0	0	1
	3	1	1	1				0	1	1	1	1	1
$D_{5.m}$	1	0	0	1	0	0	0				0	1	1
	2	0	0	1	1	1	1				0	1	1
	3	1	1	1	1	1	1				0	1	1
$D_{7.m}$	1	0	1	1	0	0	1	0	0	0			
	2	0	1	1	0	0	1	1	1	1			
	3	0	1	1	1	1	1	1	1	1			

In Table 4.1, the empty positions represent impossible situations due to the vehicle

arrival lane groups sources. For example, line 2 in Table 4.1 represents the conflicts with direction $D_{1,2}$ (a vehicle arriving from lane R_1 and going straight $m = 2$). This direction has no conflict with another vehicle arriving from lane R_3 and turning right ($m = 1$), or arriving from lane R_5 and turning right ($m = 1$) or going straight ($m = 2$). Vehicles arriving from any lane (R_3, R_5, R_7) with other directions will cause a conflict.

4.3.2 Multi-lane Complex Intersections

Previously, the IIMA for complex multi-lane (two-/three-lanes) four-legged intersections are presented in Figs. 4.3, 4.4, and 4.5, respectively. For those complex intersections, the potential conflicts, i.e., diverging, crossing, and merging, are presented first. Then by employing these conflicts, the CDMs are obtained.

Figure 4.7 shows the potential conflicts of the dedicated left-lane intersection shown in Fig. 4.3 with lane groups as in Fig. 4.1b. This intersection configuration has 16 crossing (black dots), 4 diverging (half-gray circles), and 4 merging (white circles) conflicts. The CDM for this intersection is presented in Table 4.2 reflecting the conflicts as in Fig. 4.7.

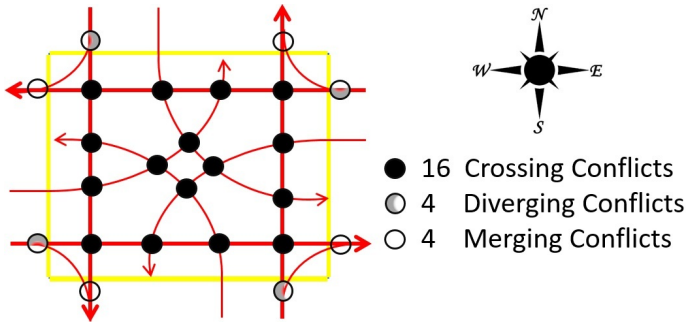

Figure 4.7: Dedicated left-turn movement with shared straight/right movements and conflicts (crossing, diverging, and merging).

In Table 4.2, the road lanes $j = 1$ and $j = 2$ represents the two lane groups in which the former one hosts both right- and straight-crossing vehicles ($m = 1, 2$) while the latter one is dedicated to left-crossing vehicles ($m = 3$). Like in the single-lane intersections CDM, the values 0 and 1 encode the absence or presence of a conflict.

This CDM clearly shows that all the right-crossing movements are conflict-free. In addition to the right-crossings, left-crossings from opposite road lanes (R_{12} and R_{52} or R_{32} and R_{72}) are also conflict-free. Only the straight-crossing movements have the highest possible conflicts, permitting vehicles from opposite road lanes.

For a shared left lane intersection as shown in Fig. 4.4 with the lane group as in Fig. 4.1c, the potential conflicts are presented in Figure 4.8 in which 36 are crossing (black dots), 8 are diverging (half-gray circles), and 8 are merging (white circles). In this case, we may always have situations where the vehicle at the intersection entrance is not given access. In contrast, the following vehicle in that lane, going in a different direction, could have gotten access. A consequence of this blocking is that it also increases the chances of

Table 4.2: CDM of a four-way two-lane intersection assigned with a dedicated left lane (1 - conflict and 0 - no conflict).

$D_{ij,m}$			$D_{1j,m}$			$D_{3j,m}$			$D_{5j,m}$			$D_{7j,m}$		
			R_{11}		R_{12}	R_{31}		R_{32}	R_{51}		R_{52}	R_{71}		R_{72}
		m	1	2	3	1	2	3	1	2	3	1	2	3
$D_{ij.m}$	R_{11}	1				0	1	0	0	0	0	0	0	0
		2				0	1	0	0	0	1	1	1	1
	R_{12}	3				0	1	1	0	1	0	0	0	1
$D_{3j.m}$	R_{31}	1	0	0	0				0	1	0	0	0	0
		2	1	1	1				0	1	0	0	0	1
	R_{32}	3	0	0	1				0	1	1	0	1	0
$D_{5j.m}$	R_{51}	1	0	0	0	0	0	0				0	1	0
		2	0	0	1	1	1	1				0	1	0
	R_{52}	3	0	1	0	0	0	1				0	1	1
$D_{7j.m}$	R_{71}	1	0	1	0	0	0	0	0	0	0			
		2	0	1	1	0	0	1	1	1	1			
	R_{72}	3	0	1	1	0	1	0	0	0	1			

rear-end collisions between the vehicles in this lane. It is also visible in the figures (4.7 and 4.8) that the shared left lane case has a higher complexity, with more conflicts of all kinds, particularly crossing ones.

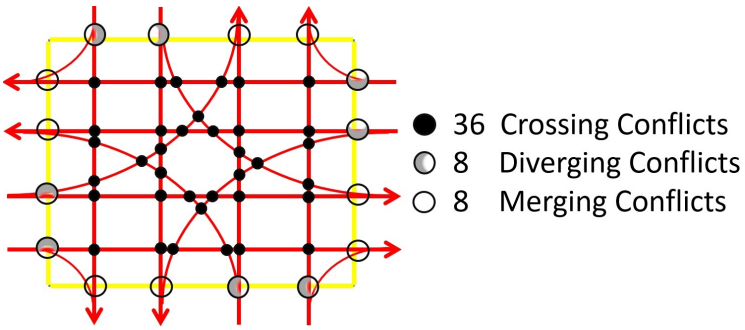

Figure 4.8: Conflicts of a shared left-lane intersection with left/straight and straight/right movements.

In this intersection type, any lane R_{ij} with $j = 1, 2$ may convey vehicles of two crossing directions, i.e., $j = 1$ accepts $m = 1, 2$ and $j = 2$ accepts $m = 2, 3$. Table 4.3 presents the CDM for this shared left lane intersection. In the shared left-lane intersection, all the right-crossing vehicles have conflict-free movements similar to the dedicated left-lane intersection. Then the number of conflicting movements increases based on the crossing direction and lane group in which the vehicles are present.

Finally, the three-lane intersection with a separate lane for each crossing direction is shown in Fig. 4.5. Due to dedicated lanes, only the crossing conflicts exist for this intersection type, as presented in Fig. 4.9. Compared to the previously presented single-lane and two-lane intersections, the three-lane intersection with dedicated road lanes has

Table 4.3: CDM of a four-way two-lane intersection with shared left lanes (1 - conflict and 0 - no conflict).

$D_{ij,m}$			$D_{1j,m}$				$D_{3j,m}$				$D_{5j,m}$				$D_{7j,m}$			
			R_{11}		R_{12}		R_{31}		R_{32}		R_{51}		R_{52}		R_{71}		R_{72}	
		m	1	2	2	3	1	2	2	3	1	2	2	3	1	2	2	3
$D_{1j.m}$	R_{11}	1					0	1	0	0	0	0	0	0	0	0	0	0
		2					0	1	1	0	0	0	0	1	1	1	1	1
	R_{12}	2					0	1	1	1	0	0	0	1	0	1	1	1
		3					0	1	1	1	0	1	1	0	0	0	1	1
$D_{3j.m}$	R_{31}	1	0	0	0	0					0	1	0	0	0	0	0	0
		2	1	1	1	1					0	1	1	0	0	0	0	1
	R_{32}	2	0	1	1	1					0	1	1	1	0	0	0	1
		3	0	0	1	1					0	1	1	1	0	1	1	0
$D_{5j.m}$	R_{51}	1	0	0	0	0	0	0	0	0					0	1	0	0
		2	0	0	0	1	1	1	1	1					0	1	1	0
	R_{52}	2	0	0	0	1	0	1	1	1					0	1	1	1
		3	0	1	1	0	0	0	1	1					0	1	1	1
$D_{7j.m}$	R_{71}	1	0	1	0	0	0	0	0	0	0	0	0	0				
		2	0	1	1	0	0	0	0	1	1	1	1	1				
	R_{72}	2	0	1	1	1	0	0	0	1	0	1	1	1				
		3	0	1	1	1	0	1	1	0	0	0	1	1				

fewer crossing conflicts, 8 in this case. As mentioned earlier, only the straight- and left-crossing vehicles can be yeilded by the TLC signals, as all the right-crossing vehicles can only be stopped for synchronization reasons. The CDM for this intersection is listed in Table 4.4.

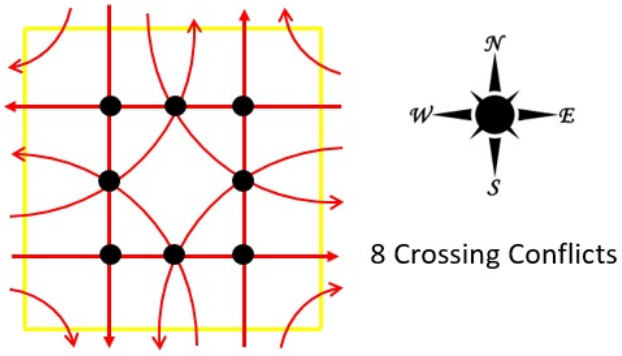

Figure 4.9: Dedicated left, straight, and right movements with crossing conflicts.

The IIMA, conflicting movements within intersections, and associated CDMs are presented for single-/two-/three-lane intersections. The following section presents the SIMP protocol.

Table 4.4: CDM for a four-way single-lane intersection (0 - no conflict and 1 - conflict).

$D_{ij.m}$			$D_{1j.m}$			$D_{3j.m}$			$D_{5j.m}$			$D_{7j.m}$		
			R11	R12	R13	R31	R32	R33	R51	R52	R53	R71	R72	R73
		m	1	2	3	1	2	3	1	2	3	1	2	3
$D_{1j.m}$	R11	1				0	0	0	0	0	0	0	0	0
	R12	2				0	1	0	0	0	1	0	1	1
	R13	3				0	1	1	0	1	0	0	0	1
$D_{3j.m}$	R31	1	0	0	0				0	0	0	0	0	0
	R32	2	0	1	1				0	1	0	0	0	1
	R33	3	0	0	1				0	1	1	0	1	0
$D_{5j.m}$	R51	1	0	0	0	0	0	0				0	0	0
	R52	2	0	0	1	0	1	1				0	1	0
	R53	3	0	1	0	0	0	1				0	1	1
$D_{7j.m}$	R71	1	0	0	0	0	0	0	0	0	0			
	R72	2	0	1	0	0	0	1	0	1	1			
	R73	3	0	1	1	0	1	0	0	0	1			

4.4 Synchronous Intersection Management Protocol - SIMP

SIMP primarily aims to handle a centralized non-conflicting traffic flow operation between AVs and HVs at signalized intersections. As mentioned earlier, SIMP works on top of the intelligent architecture IIMA, enabling synchronous movement of vehicles in cycles. The current cycle is triggered by the end of the previous cycle to enable a smooth (non-conflicting) behavior at each cycle. At every cycle, the operation of SIMP involves several stages: **detecting the total number of vehicles within the intersection area** access lanes using $P1$ sensors; **identifying the vehicles crossing direction** at the intersection entrance - HVs crossing directions are detected by using $P1$ sensors and AVs sensing capabilities, and AVs via wireless communications; and **performing intersection access decisions** using the CDM. In previous sections, these components and the communications between them are discussed.

Now we present how the SIMP protocol invokes the intersection access decisions depending on the CDM and vehicle crossing direction information with an illustrative example. Figure 4.10 shows four vehicles at the entrance of a four-way single-lane intersection, in which two are HVs (white color - North and East), and two are AVs (yellow color - South and West). Every vehicle can have three possible intersection crossings - right (Fig. 4.10a), straight (Fig. 4.10b), or left (Fig. 4.10c), as this lane group hosts the vehicles of all crossing directions.

From the North side HV case, right-crossing conflicts with the vehicle movements of straight-crossing from the East and left-crossing from the South, and the remaining crossing directions are conflict-free. In the case of straight-crossing, only the right-crossing from the East and straight/right-crossing from the South are conflict-free, and the remaining crossing movements raise conflicts. In the case of left-crossing, the right-crossing from East/West and the left-crossing from the South are conflict-free, and the remaining crossing

movements raise conflicts.

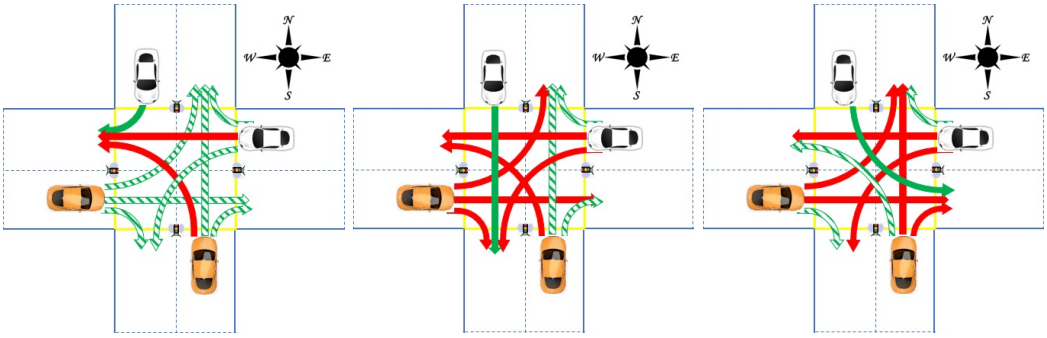

(a) Right crossing. (b) Straight crossing. (c) Left crossing.

Figure 4.10: An illustrative example of conflict-free and conflicting maneuvers of vehicles at single-lane four-way intersections.

Four crossing situations emerge when these three crossing directions are applied to all four vehicles. All vehicles crossing their right are conflict-free and can be served in a single TLC phase. All vehicles crossing straight have four conflicts, which can be resolved by permitting opposite roads in two TLC phases (North/South and East/West). All vehicles crossing left also have four conflicts, which can be solved similarly by permitting vehicles of opposite roads in two TLC phases. These three situations are unusual. Finally, the random crossing in which the vehicles opt for any crossing direction. To address this random crossing situation, we designed a cycle of control phases (ϕ_1, ϕ_2, ϕ_3, and ϕ_4) for SIMP shown in Fig. 4.11 based on the CDM (Table 4.1). Note that the TLC phases order changes at any point based on vehicle presence information from roadside sensors and AV requests.

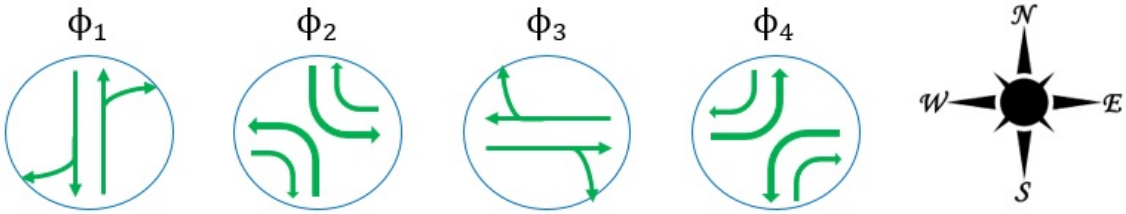

Figure 4.11: Best possible composition of green phases.

We allocated the green time for each control phase, i.e., 2.5s for right/straight-crossing and 3s for left-crossing (due to the longer path), and the remaining directions are closed with red signals. This allocated green time is sufficient for a vehicle to accelerate (if stopped), enter, cross, and exit the intersection was identified through extensive simulation studies. When all four phases are executed in order, they form a TLC cycle of 11s, the lowest cycle time to serve one vehicle from each non-conflicting road.

Figures 4.12, 4.13, and 4.14 illustrate the control phases of SIMP for two-lane intersections with dedicated and shared left lanes and three-lane intersection with dedicated

lanes, respectively. In these multi-lane intersections, SIMP checks one road lane at a time in a circular fashion to arbitrate between vehicles trying to access the intersection from different road lanes simultaneously, unlike roads in single-lane intersections. If a vehicle is present in that lane, it is admitted to access the intersection with the vehicles at the entrance of the intersection in other lanes that have no conflicts with it and among them. For instance, starting from the North as in Fig. 4.12 (bottom), SIMP checks the right lane (phase ϕ_1) and then the left lane (phase ϕ_2), followed by the right and left lanes of East (phases ϕ_3 and ϕ_4), South (phases ϕ_5 and ϕ_6) and West roads (phases ϕ_7 and ϕ_8). In Fig. 4.12 (top), we also presented the remaining conflict-free directions (dashed red lines) when permitting right, straight, and left crossing vehicles (solid green lines) during ϕ_1 and ϕ_2 phases.

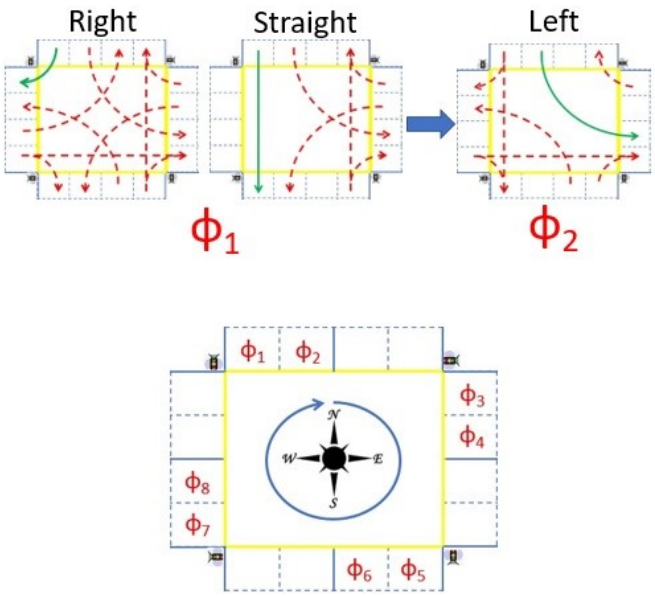

Figure 4.12: Control phases of SIMP for a dedicated left lane intersection.

Similarly, in each phase at each intersection, SIMP checks the right lane (phase ϕ_1) and then the left lane (phase ϕ_2), followed by the right and left lanes of East (phases ϕ_3 and ϕ_4), South (phases ϕ_5 and ϕ_6) and West roads (phases ϕ_7 and ϕ_8).

Like in single-lane intersections, four crossing situations occur in two-lane intersections also - all vehicles cross right, straight, left, or random. Unlike the single-lane case, all right-crossing vehicles have a conflict-free path along with the left-crossing vehicles from the opposite lanes. Therefore, only straight-crossing vehicles impose higher conflicts. In the case of random crossing, SIMP iterates the same steps in cycles and can mimic the patterns shown in Figs. 3.5 and 3.6a, but only the green phases.

Similar crossing situations occur with the three-lane intersections when an exclusive

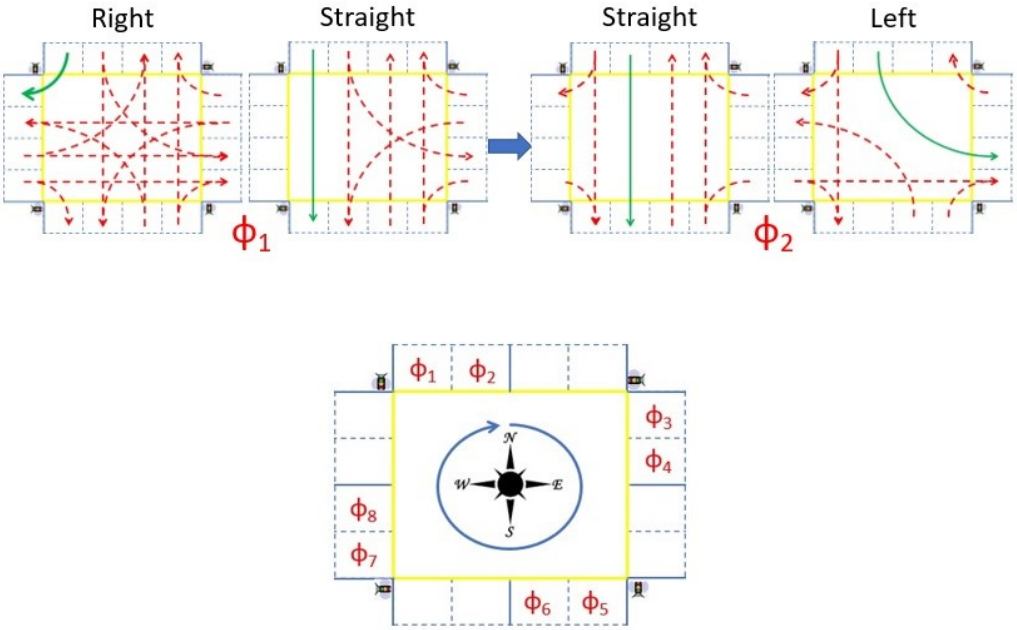

Figure 4.13: Control phases of SIMP for a shared left lane intersection.

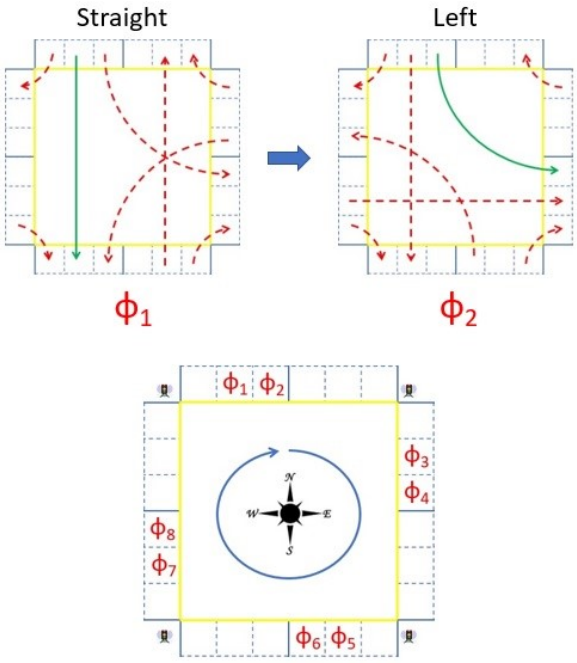

Figure 4.14: Control phases of SIMP for a three-lane intersection.

lane per crossing direction is permitted. As mentioned earlier, all right-crossing lanes have the right-of-way; thus no yielding or stopping on those lanes; only the vehicles on straight- and left-crossing lanes raise conflicts to be managed by the IM protocol.

When an AV fails to notify its crossing direction, it will be treated as an HV, and SIMP employs the same procedure to serve it as an HV. Suppose a rouge vehicle accesses the intersection in a slot that is not provided to it. In that case, the SIMP protocol blocks the vehicles of other lanes until the rouge vehicle is exited the intersection, known by the sensor $P2$. A specific situation in which SIMP halts its functioning is when a vehicle stops at the intersection. A final note is that this framework can be equally applied to other intersection types as long as the CDM is properly configured.

4.5 Summary

This chapter presented the first contribution of this thesis, namely the *synchronous framework*, a combination of IIMA and SIMP. The *synchronous framework* is presented in a way that by configuring the lane groups, conflicts (diverging, crossing, and merging), and the CDM, it can easily be applied to any intersection. The single-/two-/three-lane intersections are presented as examples. The main idea is to synchronize mixed vehicles (HVs and AVs) intersection access from all non-conflicting road lanes in phases.

In each phase, SIMP allows the vehicle in the checked lane and one vehicle in each of the other lanes with no conflicts. When all admitted vehicles exit the intersection, i.e., at the end of a cycle, SIMP checks the next lane to start a new cycle. If no vehicle is found in the lane, SIMP immediately checks the next one. Thus, crossing cycles are triggered fairly and fluidly whenever there are vehicles at the entrance of the intersection. In summary, SIMP assigns slots on-demand to individual vehicles, unlike all other protocols that handle groups of vehicles at once.

In the following chapter, the working performance of the *synchronous framework* is evaluated in low-speed urban traffic settings at isolated single-/two-/three-lane intersections.

Chapter 5

Evaluating Synchronous Framework at Isolated Intersections

The previous chapter introduced the *synchronous framework* for managing mixed HV/AV traffic at signalized intersections. This chapter evaluates the performance of the *synchronous framework* and compares it with the baseline IM approaches presented earlier in Section 3.6. In this direction, this chapter first defines the three common and relevant performance indicators of SUM: intersection throughput, travel time loss, and fuel consumption, which are defined as follows.

- **Intersection throughput** (veh/h) is determined as the number of vehicles that concluded their trip by crossing the intersection in an hour.
- **Travel time loss** (s/veh) is the time the vehicles lost due to driving slower than the maximum allowed speed from the origin to the destination because of traffic congestion and TLC signals. In other words, the travel time loss combines stopped delay, approach delay, time-in-queue delay, and intersection control delay [197].
- **Fuel consumption** (ml/veh) is the fuel the vehicles consume to travel from the origin to the destination. The fuel consumption model for ICE vehicles is presented in Section 3.3.

The majority of the results of this chapter are obtained from the following scientific publications:

- **Reddy, R.**, Almeida, L., Santos, P.M., Bouzefrane, S. and Tovar, E., 2021. Synchronous Intersection Management to reduce Time Loss. In Euro Working Group on Transportation Meeting (**EWGT 2020**), **Transportation Research Procedia**, 52, pp.364-372.
- **Reddy, R.**, Almeida, L., Gaitan, M., Santos, P.M. and Tovar, E., 2023. Synchronous Management of Mixed Traffic at Signalized Intersections towards Sustainable Road Transportation. In **IEEE ACCESS 2023**, Vol.11, pp.64928-64940.

The following sections introduce the traffic scenarios and simulation settings for each single-/two-/three-lane intersections and discuss the achieved results.

5.1 Single-lane Intersections

5.1.1 Simulation Scenarios

To characterize the performance of the SIMP at a four-way single-lane intersection, a realistic traffic scenario is considered in which vehicles cross the intersection in all three possible directions (left, straight, and right), as shown in Figs. 4.1a and 4.2. The crossing direction to vehicles is assigned equally (i.e., 33% to each crossing direction) and randomly at the intersection entrance. The SIMP protocol is compared against the RR-x schemes (RR-5, RR-10, RR-20, and RR-30) which were described in Section 3.6 of Chapter 3, where x indicates the green phase time.

The comparisons are carried out under two typical maximum speeds allowed in urban areas, notably $30km/h$ and $50km/h$, and four traffic arrival rates per road: $0.05veh/s$, $0.1veh/s$, $0.2veh/s$ and $0.4veh/s$. These arrival rates represent low to medium and congested (i.e., saturated) traffic conditions. In each experiment, we injected 50% AVs and 50% HVs. The *Uniform* distribution process executed every second on each road and added a vehicle randomly, respecting the referred average rates. The simulation parameters and assigned values are listed in Table 3.1.

The simulations were run six times with different random seeds for the same set of parameters in all scenarios; thus, the results are the average of the six runs. The intersection throughput is measured for $1h$, i.e., $3600s$ after the warm-up period of $60s$ ($30km/h$) and $36s$ ($50km/h$), the time for a vehicle to reach the intersection entrance. The remaining performance indicators are an average of 1000 vehicles.

5.1.2 Experimental Results

5.1.2.1 Intersection Throughput (veh/h)

Figure 5.1 shows the intersection throughput results in veh/h for $30km/h$ (Fig. 5.1a) and $50km/h$ (Fig. 5.1b) maximum speeds for the tested traffic arrival rates. The first observation is that the results at both maximum speeds show similar patterns, with a slight growth for increased speed. Overall, SIMP exhibits the best throughput values of up to 29.5% and 54.1% compared to the best and worst IM approaches, i.e., RR-30 and RR-5, respectively. The remaining IM approaches (RR-10 and RR-20) show intermediary performance. The higher throughput values of SIMP can be attributed to its reactive nature in serving vehicles from all non-conflicting roads based on their arrival at the intersection entrance rather than the synthetic way of serving a set of vehicles sequentially per road while blocking the other road vehicles.

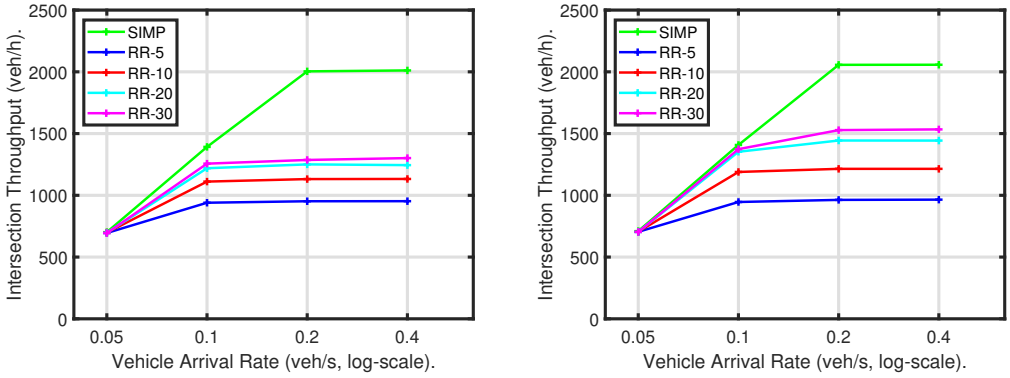

(a) Intersection throughput at $30km/h$. (b) Intersection throughput at $50km/h$.

Figure 5.1: Intersection throughput results in veh/h of the comparing IM approaches for $30km/h$ and $50km/h$ maximum speeds for various traffic arrival rates.

In both cases, all RR-x approaches saturated at the lowest arrival rate of $0.1veh/s$ (except RR-30 at $50km/h$), while the SIMP saturated at the highest arrival rate of $0.3veh/s$. At $50km/h$, the RR-30 saturates at $0.2veh/s$. The increased speed improved the throughput values of RR-30, with the highest value of 150 vehicles. At the same time, SIMPs improvements are slight, with an increase of 31 vehicles, due to the working nature of SIMP permitting one vehicle per green phase rather than the speed. These results indicate that the synchronous intersection access of vehicles has the advantage of serving a higher number of vehicles than the sequentially serving IM approaches like RR-x.

5.1.2.2 Average Travel Time Loss (s/veh)

Figure 5.2 displays the average travel time loss results for the simulations mentioned earlier for $30km/h$ (Fig. 5.2a) and $50km/h$ (Fig. 5.2b) maximum speeds. Each data point indicates an average of 1000 vehicle travel time loss values.

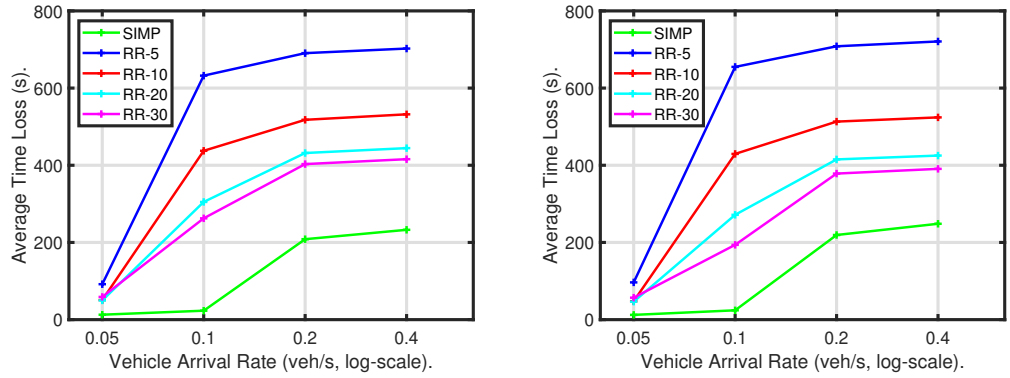

(a) Avg. travel time Loss at $30km/h$. (b) Avg. travel time Loss at $50km/h$.

Figure 5.2: Average travel time loss results of 1000 vehicles for $30km/h$ and $50km/h$ maximum speeds.

Firstly, SIMP exhibits the best travel time loss results with the lowest values than the competing RR-x schemes. Overall, SIMP achieves up to 83% and 126% travel time improvements over the following best and worst IM approaches, i.e., RR-30 and RR-5, respectively. The remaining RR-x schemes show intermediary performance. A major portion of the travel time loss is the waiting time at the intersection entrance due to red signals and traffic congestion. Though the SIMP protocol serves one vehicle at a time (from all non-conflicting roads), waiting before accessing the intersection is short due to the short cycle time. In contrast, the sequentially operating RR-x schemes let vehicles wait longer as they serve one road at a time.

The increased speed slightly reduced the travel time loss values for all IM approaches except SIMP and RR-5. In the case of SIMP, the travel time values were slightly reduced for lower traffic arrival rates of up to $0.1veh/s$, then increased for higher traffic arrival rates. In the case of RR-5, the increase in travel time loss is observed for all traffic arrival rates. This is due to the increased speed that vehicles arrive faster at the intersection entrance but must wait longer due to red signals.

5.1.2.3 Average Fuel Consumption (ml/veh)

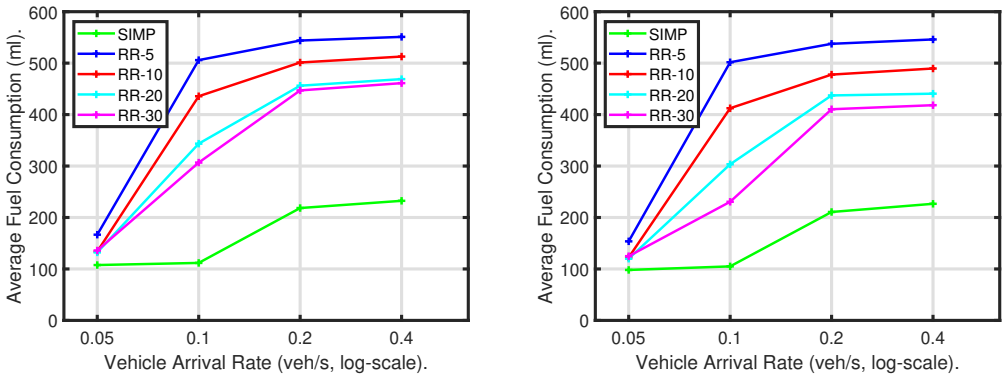

(a) Average fuel consumption at $30km/h$. (b) Average fuel consumption at $50km/h$.

Figure 5.3: Average fuel consumption results for 1000 vehicles at $30km/h$ and $50km/h$ maximum speeds.

Figure 5.3 shows the fuel consumption results corresponding to the previously mentioned simulation scenarios. The results show that the SIMP protocol is more energy efficient than the conventional RR-x schemes. Overall, SIMP saves 67.4% and 90% fuel than the conventional RR-30 and RR-5 approaches at $30km/h$ maximum speed. A slight reduction in fuel consumption is observed with the increased speed of $50km/h$. In this case, SIMP saves 60% and 68% fuel than the same RR-30 and RR-5 approaches.

For SIMP, the results tend to be worse given the diversity of directions, many of which are conflicting and thus forcing serialization of the access to the intersection. Curiously, the performance we observed was not worse than the best RR configuration, i.e., RR-30,

which indicates that SIMP can perform well in all realistic scenarios. The fuel consumption results show the opposite behavior concerning the travel time loss, meaning that low-speed conditions consume more fuel (i.e., $232.4ml$) than high-speed scenarios (i.e., $225ml$).

5.1.3 Discussion

The results shown in the previous section indicate that SIMP achieves higher throughput and lower time loss than the best RR configuration, namely RR-30. It does so for both speed limits, i.e., $30km/h$ and $50km/h$, for all traffic arrival rates. A similar result was observed for fuel consumption. Given that the access-decision-making of SIMP is carried out on a per vehicle-basis, multiple vehicles are allowed to enter the intersection if their target directions do not conflict (according to the CDM). This means that, under SIMP, vehicles have an inferior probability (and periods) of idling, leading to vehicles engaging in smoother and momentum-preserving driving behavior. Conversely, the RR promotes longer alternate periods of consecutive idling and motion, incurring lower throughput, higher travel time, and fuel penalty.

We also observed a particular situation that increases fuel consumption. By nature, HVs have a jerky speed profile. When an AV follows an HV at a certain controlled distance, the latter inherits speed jerkiness, increasing fuel consumption. This is typically called leader-follower behavior. It turns out that RR management policies accumulate vehicles during the red light periods, promoting the leader-follower situations, while SIMP, by processing vehicles one by one, breaks the leader-follower situations.

Finally, another observation from the results is that a small intersection like the one we used has a relatively low saturation point. In this case, this point was achieved with as low as $0.1veh/s$ injected in each road. Above this value, the vehicles accumulate in unbounded lines along the roads. We also observed that, when using the RR management, there was no benefit in increasing the green window beyond $30s$. We believe this is also associated with the intrinsic capacity of the intersection.

In summary, we conclude that SIMP fits well intersections in urban residential areas where the traffic frequency is typically below $0.1veh/s$, and the vehicles seldom go above $30km/h$ speed.

In this section, we evaluated the performance of SIMP at an isolated four-way single-lane intersection and compared it with the conventional RR IM approach for several green phase configurations. In the coming section, SIMPs performance is evaluated at four-way two-lane intersections.

5.2 Two-lane Intersections

As discussed in the introduction section of Chapter 4, the four-way two-lane intersection is configured with two left lane groups (see Figs. 4.1b and 4.1c). Therefore, the SIMP protocol is referred to as SIMP-D referring to the dedicated left lane intersection, and SIMP-S

referring to the shared left lane intersection. For evaluating the two-lane intersections, we employed the same simulation settings (parameters and assigned values) similar to those in Table 3.1. Additionally, three more traffic arrival rates (0.067, 0.133, 0.3) are employed to the ones tested (0.05, 0.1, 0.2, 0.4) in the single-lane intersections case. Several baseline approaches (RR, TTLC, ITLC, and QTLC) are employed to compare the performance of the SIMP protocol, as discussed in Chapter 3, Section 3.6.

5.2.1 Simulation Scenarios

We injected vehicle flows per road with average arrival rates from 0.05 to $0.4veh/s$, covering non-saturated to saturated traffic conditions and using approximately regular points in a logarithmic scale. The vehicle traffic is also randomly dispersed across lanes with uniform distribution and balanced portions of AVs and HVs, i.e., 50% each. For assessing the intersection throughput, simulations were run for $1h$ of intersection operation; 1000 vehicles are considered for other metrics, similar to the single-lane intersections case. In all scenarios, simulations were run five times over a range of random seeds for the same parameter values, and hence the results represent the average of those five simulation runs.

To reduce possible bias on the IM systems performance, in both scenarios, caused by the asymmetric distribution of directions in intersection crossing, we make vehicles take a random direction distributed uniformly for left, straight, and right crossings, i.e., 1/3 for each crossing direction. In the case of SIMP-S, the vehicles doing a straight crossing are evenly distributed to each lane, i.e., 1/6 to each.

Two traffic generation scenarios are defined to compare the performance of the IM approaches:

- Scenario-1: **Continuous upstream traffic - the traffic is continuously injected in four inflow directions, randomly, with the specified average rates, following a time-invariant approach**;
- Scenario-2: **Interrupted upstream traffic - to represent real-world road intersections, the traffic is interrupted for every** $250s$ **in a circular fashion starting from the North. This creates a time-varying pattern in each lane**.

The interrupted upstream traffic scenario provides insights into the adaptivity of these IM approaches to sustained variations in traffic patterns, either caused by road blockage, e.g., due to accidents or changes in road usage. To avoid inserting a bias on the performance of a single lane, we apply a $250s$ traffic interruption to all lanes, one at a time, in a cyclic fashion, starting from North and rotating clockwise. The duration of the traffic interruption corresponds to the longest time required by a stream of vehicles to exit the network under ITLC and QTLC in their worst cases. This is the highest value of all protocols. These protocols also couple every pair of opposing lanes by forcing the same green time in both every cycle. This needs to be taken into account when analyzing the

results. For completeness, we also checked a few cases of simultaneous traffic blocking on opposite lanes, but we considered these to be less realistic, and thus we did not expand them. For saturated traffic conditions, the interruption periods may not be visible due to the presence of queued vehicles in all lanes. A sample video of SIMP working at a dedicated left-turn lane intersection can be seen in the YouTube link[1].

5.2.2 Experimental Results

Here, we will occasionally refer to SIMP-D and SIMP-S as SIMP protocols and to TTLC, ITLC, and QTLC as the xTLC protocols for the sake of simplicity.

5.2.2.1 Intersection Throughput (veh/h)

Figure 5.4 shows the intersection throughput results of two simulation scenarios with a maximum speed of $30km/h$, where the X-axis is the vehicle arrival rate in veh/s at each road on a log scale, including all three directions and both types of vehicles, as referred before. Throughput results show that each IM strategy results in a different saturation point in these tested scenarios. For instance, RR and xTLC protocols saturate at approximately $0.2veh/s$, and SIMP protocols at approximately $0.3veh/s$. Notably, SIMP-S exhibits the highest saturation throughput values in both scenarios as the straight-crossing vehicles are distributed by both inflow road lanes, enhancing their crossing opportunities in the intersection. Contrarily, SIMP-D piles up more straight/right-crossing cars on the right-most lane, reaching saturation faster and showing lower saturation throughput. RR achieves the lowest saturation throughput being the worst-performing IM approach. The differences in throughput results are minor for arrival rates of $0.133veh/s$ and below. These differences become evident at $0.2veh/s$ and above.

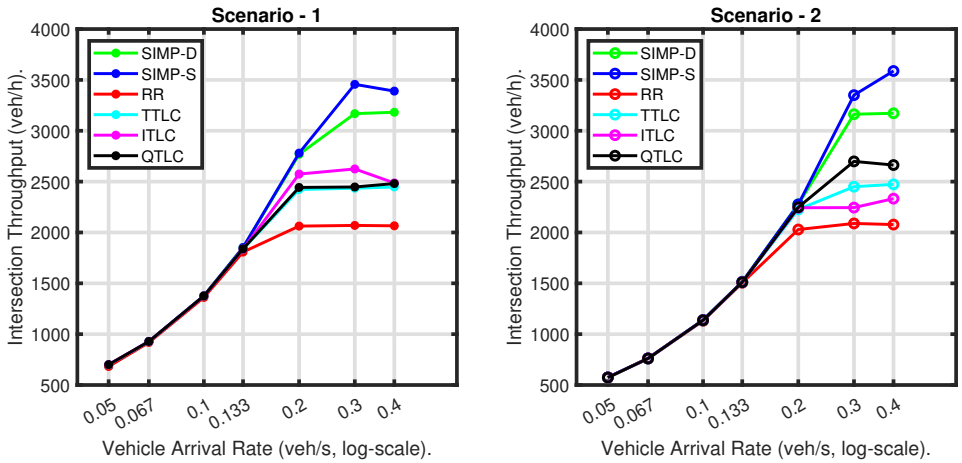

Figure 5.4: Intersection throughput (no. of vehicles) of continuous (scenario-1) and interrupted (scenario-2) upstream traffic flows for 30 km/h maximum speed.

[1] https://youtu.be/ut5MfFqHawY

The interruption in upstream traffic influences the throughput results. Note that the vehicle arrival rates apply to periods of vehicle injection only, without accounting for the interruptions. However, due to the interruptions, there are less injected vehicles overall in scenario-2. This can be observed in Fig. 5.4, with lower throughput results for scenario-2 than for scenario-1 for traffic arrival rates until $0.2veh/s$, when saturation starts to occur. Upon saturation, each IM exhibits different behavior.

RR and TTLC are agnostic to changes in traffic inflow, thus, when the saturation level is sufficient to mask the traffic interruptions with queuing, they offer the same saturation throughput in both scenarios, namely a little more than $2000veh/h$ for RR and a little less than $2500veh/h$ for TTLC.

ITLC and QTLC have to be analyzed per scenario. In scenario-1 (left graph in Fig. 5.4), ITLC provides longer green times on average, resulting in a slightly improved saturation throughput. In turn, QTLC converges to green times that are close to those used in TTLC, leading to similar saturation throughput. However, all xTLC protocols converge as saturation increases to the same saturation throughput near $2500veh/h$.

In scenario-2 (right graph in Fig. 5.4), ITLC shows an unexpected degradation. This is caused by coupling the green times of both opposing lanes being served in each phase. Thus, ITLC is unable to adapt to the interruption in a single lane, and it will continue offering long green times for fewer vehicles, thus effectively reducing throughput. Conversely, QTLC tracks long-term average arrival rates, influenced by a time window that captures the interruptions in both opposite lanes. This allows it to effectively adjust the green times to the actual arrival rates, thus improving throughput.

Finally, as expected, SIMP protocols show the highest saturation throughput since they explore parallelism in crossing the intersection per vehicle. They are also reactive at the vehicle resolution, thus accommodating instantaneously any change in arrival patterns. As discussed before, SIMP-D saturates faster due to the accumulation of traffic on the right lanes, reaching approximately $3200veh/h$ in both scenarios. SIMP-S goes beyond, reaching around $3500veh/h$. The difference between the two scenarios in SIMP-S is still being analyzed, whether it is an artifact of the simulation conditions or a fundamental aspect of the protocol. In any case, SIMP-S is the protocol that achieves the highest sustained throughput, saturating with almost twice the saturation throughput of RR.

For scenario-1, we also measured the lane throughput (veh/s) for linearly increasing traffic arrival rates between 0.01 to $0.11veh/s$. Note that we only tested the SIMP-D in this case, but not the SIMP-S. The lane throughput can be defined as the number of vehicles that completed their journeys by crossing the intersection either straight or right (S/R-crossing lane) or left (L-crossing lane) from their injection point in one hour. We used $30h$ long-run FCD data to observe the achieved lane throughput. Figure 5.5 shows the throughput of both lanes (S/R-crossing and L-crossing).

The throughput results show a similar behavior among all IM approaches until $0.05veh/s$ for both S/R-crossing and L-crossing lanes, with just a small difference of $1-3veh$ among

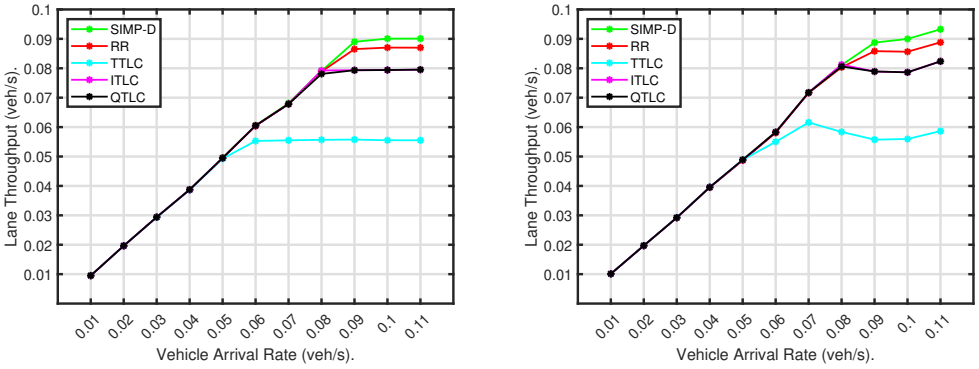

Figure 5.5: Lane throughput in veh/s against the vehicle arrival rate in veh/s for L-crossing (left) and S/R-crossing (right) lanes at $30km/h$ maximum speed.

IM approaches. The performance of TTLC starts decreasing with increasing arrival rates and saturates at $0.06veh/s$, the poorest IM approach in serving dense traffic. The next saturating approaches are ITLC and QTLC at $\sim 0.08veh/s$, followed by the RR conventional IM approach achieving between $0.08veh/s$ and $0.09veh/s$. SIMP shows the highest lane throughput with at least $0.09veh/s$.

5.2.2.2 Average Travel Time Loss (s/veh)

The average travel time loss results for both scenarios for $30km/h$ maximum speed are presented in Fig. 5.6. The X-axis shows the vehicle arrival rate in veh/s on each road, while the Y-axis shows the average travel time loss (s) of 1000 vehicles. RR and TTLC show the highest time losses, with a small disadvantage for RR. In these protocols, the time loss is similar in both scenarios, with a slight decrease in scenario-2. This is caused by traffic interruptions leading to queue size reductions in the respective lanes. Thus, the vehicles that arrive after the interruptions suffer smaller time losses.

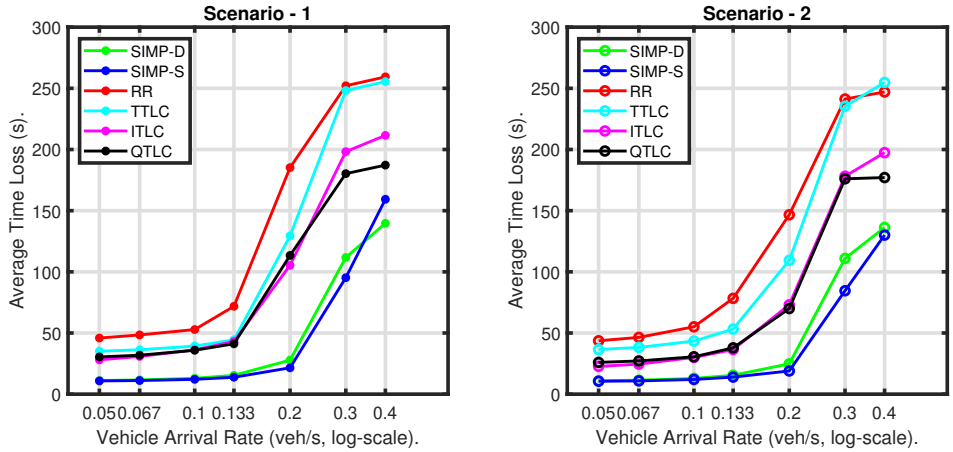

Figure 5.6: Average travel time loss (s) of 1000 vehicles for Scenario-1 and Scenario-2 at $30km/h$ maximum speed.

ITLC and QTLC show very similar behavior between them and lower time loss than the previous two protocols. The only visible difference is under strong saturation, as we have already seen that ITLC becomes less effective than QTLC. These protocols show the largest reduction from scenario-1 to scenario-2, given their adaptive features that increase the green times and serve more vehicles per cycle. However, this is non-trivial as longer green times also increase the cycle time, but this effect seems to be less impactful.

Again, the SIMP protocols offer the lowest time loss, which also maintains almost similar behavior between scenarios. There is a small difference for SIMP-D, which shows a slightly higher time loss in scenario-1 under strong saturation. This is due to the accumulation of traffic in two directions in the right lanes (right and straight crossings).

5.2.2.3 Average Fuel Consumption (ml/veh)

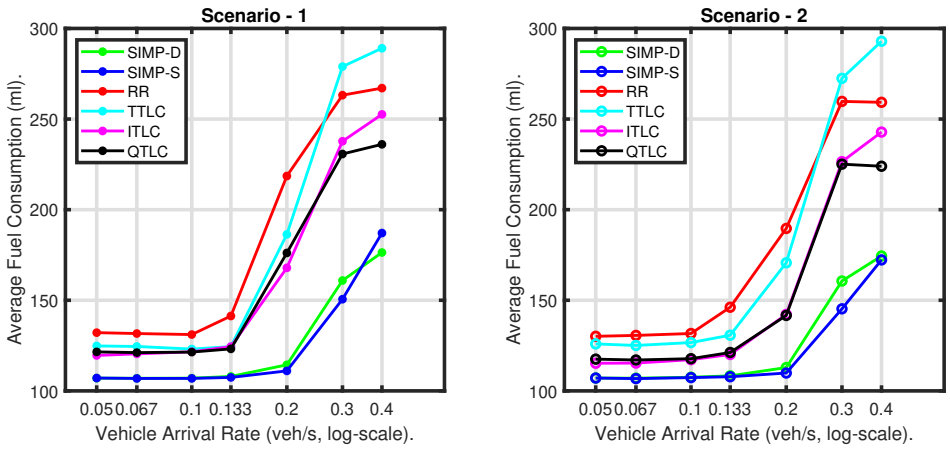

Figure 5.7: Average fuel consumption (ml) of 1000 vehicles for Scenario-1 and Scenario-2 at $30km/h$ maximum speed.

Figure 5.7 illustrates the average fuel consumption results of the same experiments as mentioned earlier. The first observation is that fuel consumption behavior correlates with the corresponding behavior of travel time loss in each scenario. This is expected since the higher the time lost, the longer the engines work with slow movements or even idling, and more fuel is consumed. Thus, similar comments apply. There is just one particular note concerning TTLC, in which fuel consumption increases significantly for strong saturation traffic, surpassing RR. This is due to a higher number of start-stop queue maneuvers that TTLC allows per cycle.

5.2.3 Discussion

The experiments with both continuous (time-invariant) and interrupted (time-varying) upstream traffic scenarios explored the performance of IMs at a four-way two-lane isolated intersection respecting throughput, travel time loss, and associated fuel efficiency. In general terms, with time-invariant balanced traffic patterns (scenario-1), the protocols can

be classified into three groups according to their performance. RR is alone as the worst-performing protocol. Then, the xTLC protocols show an intermediate performance, with a slight advantage of QTLC under strong saturation and a general disadvantage of TTLC. Then, SIMP protocols exhibit a similar performance but are significantly better than the other protocols.

Under time-varying traffic patterns (scenario-2), the capacity of the protocols to adapt dynamically impacts the performance. This is visible for ITLC and QTLC, generally improving their metrics when traffic interruptions occur. The only exception is throughput, in which ITLC actually degrades its performance, as explained before. In general, the rigidity of TTLC makes it depart from the xTLC group and exhibit a performance that now approaches and even falls behind that of RR in terms of fuel consumption. SIMP protocols exhibit their inherent reactivity capability and perform best across all scenarios, metrics, and traffic intensities. We hypothesize these benefits emerge from the synchronous movement of vehicles upon their arrival at the intersection one by one, which may lead to an emerging behavior of a slowly moving queue with fewer starts/stops.

Finally, we also experimented with the original configurations of TTLC, ITLC, and QTLC with the shared left lanes handled as presented by their authors. These allow left and straight-crossing vehicles from opposing lanes to enter the intersection simultaneously and conflicts are avoided by the vehicles. The simulation results are comparable, plus a minimal increase in intersection throughput, travel delays, and fuel consumption because the left-turning vehicles yield to let the vehicles through movement from the opposing roads cross first. This kind of operation is less safe than the dedicated left-turn movement due to its dependency on cars to prevent collisions. We also experimented with a speed limit of $50km/h$, having reached similar results, despite a slightly lower relative advantage of SIMP concerning the other protocols.

In this section, we evaluated the performance of SIMP at two-lane intersections with two left-lane configurations (dedicated and shared). In the coming section, we evaluate the performance of SIMP when a lane group is dedicated to a specific crossing direction.

5.3 Three-lane Intersections

In this section, the performance of SIMP is evaluated at a four-way three-lane intersection and compared against the baseline approaches presented in Section 3.6. Figure 4.5 illustrates the three-lane four-way intersection configured with a dedicated lane group for each crossing direction as shown in Fig. 4.1d.

5.3.1 Simulation Scenarios

The simulation settings are similar to the ones employed previously (see Table 3.1), including the traffic arrival rates (i.e., 0.05, 0.067, 0.1, 0.133, 0.2, 0.3 and $0.4veh/s$). Similar maximum speeds ($30km/h$ and $50km/h$) are employed, indicating the urban road settings.

The simulation scenarios are also identical to the ones employed in the single-lane intersections performance evaluation. This means the traffic is equally distributed (i.e., 33%) by randomly allocating the crossing direction (i.e., left, straight, and right) at the intersection entrance.

The RR and TTLC baseline approaches are employed against SIMP in this case. Because the applicability of the other baseline approaches (ITLC, QTLC, MCA, and WTLC) is in question as their TLC operations utilize the weights on turning movements which is different when a dedicated lane group per crossing direction is allocated.

5.3.2 Experimental Results

The same three performance indicators are measured, i.e., the intersection throughput (veh/h), average travel time loss (s/veh), and average fuel consumption ($liters$). Note that the travel time loss and fuel consumption results are measured for 1000 vehicles. The mixed traffic management of SIMP is presented in the YouTube video[2].

5.3.2.1 Intersection Throughput (veh/h)

Figure 5.8 exhibits the throughput curves of the comparing IM approaches, SIMP, RR, and TTLC for various traffic arrival rates at $30km/h$ (Fig. 5.8a) and $50km/h$ (Fig. 5.8b) maximum speeds.

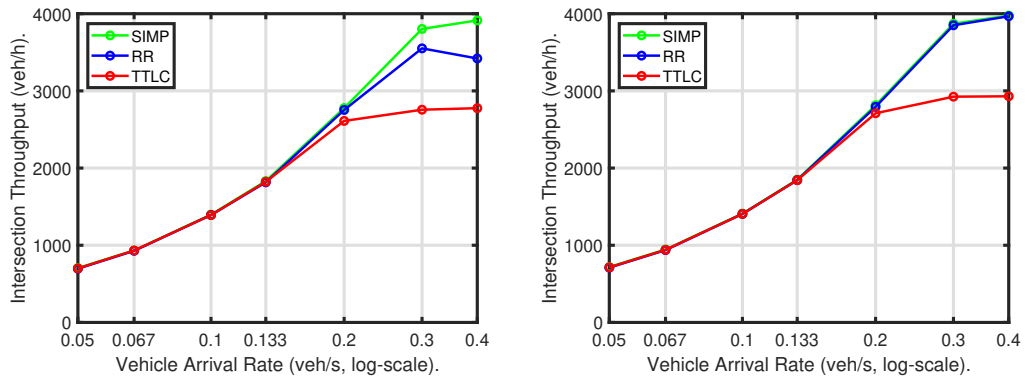

(a) Intersection throughput at $30km/h$. (b) Intersection throughput at $50km/h$.

Figure 5.8: Intersection throughput results in veh/h of the comparing IM approaches for $30km/h$ and $50km/h$ maximum speeds.

At the $30km/h$ maximum speed, the throughput difference between the IM approaches is the slightest until $0.133veh/s$, then a clear separation can be observed. Again the dominance of the SIMP protocol is observable, and the RR and TTLC follow the SIMP protocol. Overall, SIMP improves the throughput of up to 5.4% to the RR and 16.73% to the TTLC approaches. It is also observable that the TTLC approach is saturated

[2] https://youtu.be/1tnxBIx4tEc

just above $0.2veh/s$ while the RR is saturated at $0.3veh/s$, and SIMP reaches its highest throughput at $0.4veh/s$ and close to saturation.

The increased speed significantly improved the throughput results of the RR IM approach with just 0.5% away from the SIMP. In the case of TTLC, the performance difference with the SIMP is 14.6%. Overall, SIMP performs better. A particular observation about SIMP and RR is that they both are close to saturating at $0.4veh/s$. TTLC is the worst-performing approach saturated at $0.3veh/s$.

5.3.2.2 Average Travel Time Loss (s/veh)

Figure 5.9 shows the average travel time loss results for various traffic arrival rates of the comparing IM approaches at $30km/h$ (Fig. 5.9a) and $50km/h$ (Fig. 5.9b) maximum speeds.

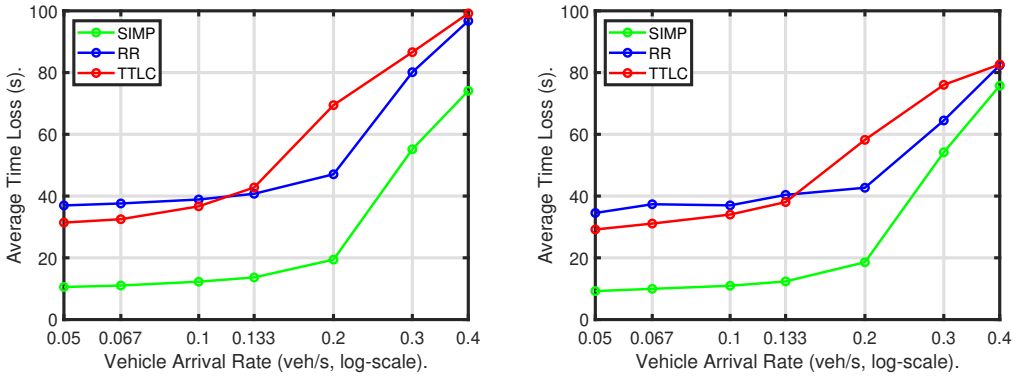

(a) Average travel time loss at $30km/h$. (b) Average travel time loss at $50km/h$.

Figure 5.9: Average travel time loss results in s/veh for various arrival rates and vehicle count of the comparing IM approaches for $30km/h$ and $50km/h$ maximum speeds.

The $30km/h$ maximum speed results show different performance behaviors for different IM approaches. For instance, the TTLC performs better than RR until $0.1veh/s$, and then the RR performs better. RR and SIMP show similar performance behaviors with a difference of up to $29s$ at every traffic arrival rate. A steady increase until $0.2veh/s$ and a sharp increase after it can be observed. The lowest travel time loss values are observed with the SIMP protocol, as it serves vehicles based on their arrival at the intersection and the lowest cycle time. Conversely, the TLC cycle times of RR and TTLC are fixed and higher, so thus, their time loss values. Overall, SIMP improved by 63.4% and 68% when compared to the RR and TTLC approaches.

The increased speed eventually reduced the travel time loss values for all IM approaches, except for the SIMP at a higher traffic arrival rate of $0.4veh/s$. At higher traffic densities, SIMP imposes synchronous movement among vehicles, thus they travel at lower speeds, leading to higher time loss values. The advantage of SIMP is that it significantly minimizes the waiting time to access the intersection. Therefore, for SIMP, the time loss values

increased with the increased speed. However, SIMP improved by 55.75% and 58.7% more than the RR and TTLC approaches, respectively.

5.3.2.3 Average Fuel Consumption (*liters*)

Figure 5.10 displays the fuel consumption results of comparing IM approaches at $30km/h$ (Fig. 5.10a) and $50km/h$ (Fig. 5.10b) maximum speeds for 1000 vehicles at each traffic arrival rate.

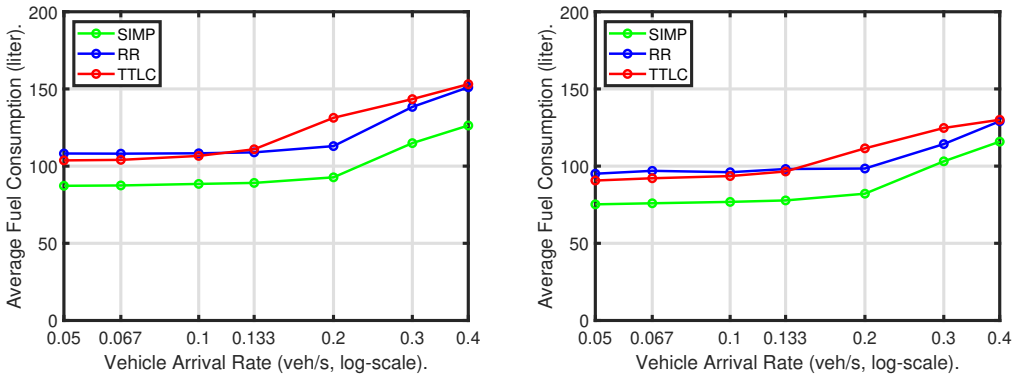

(a) Average fuel consumption at $30km/h$. (b) Average fuel consumption at $50km/h$.

Figure 5.10: Average fuel consumption results in *liters* for various arrival rates and vehicle count of the comparing IM approaches for $30km/h$ and $50km/h$ maximum speeds.

The $30km/h$ fuel consumption results correlate with the travel time loss results. This means that until $0.133veh/s$, SIMP and RR IM approaches exhibit similar fuel consumption patterns with a difference of up to 24 liters. They grow almost linearly to increasing traffic arrival rates. TTLC performs better than RR until $0.1veh/s$, then lead to the worst-performing approach with the highest fuel consumption results. Overall, SIMP improved by 19.6% and 21.7% fuel consumption over the following conventional IM approaches RR and TTLC.

The increased speed positively affected all IM approaches by reducing the fuel consumption values. The maximum and minimum fuel that SIMP saved with the increased speed is 12 and 10 liters at 0.05 and $0.4veh/s$ accordingly. RR and TTLC's highest fuel saved is 24 liters ($0.3veh/s$) and 23 liters ($0.4veh/s$), respectively. Overall, SIMP is 18.2% and 19.7% more energy efficient than RR and TTLC at $50km/h$ maximum speed.

5.3.3 Discussion

The results of intersection throughput, travel time loss, and associated fuel consumption provide some level of confidence that the SIMP protocol performs better than the benchmark approaches, even when an exclusive lane per crossing direction is allocated.

In the throughput results, a clear separation between IM approaches performance curves is visible at higher arrival rates of $30km/h$. With the increased speed, SIMP performs

better, but the improvements are slight. This is expected as the SIMP protocol serves vehicles based on the CDM rather than their speed. At both speeds, SIMP is close to saturation at the highest traffic arrival rate of $0.4veh/s$, while others perform differently at different speeds. The TTLC saturates at $0.3veh/s$ at both maximum speeds showing the worst performance.

Similar performance behaviors can be observed with the travel time loss and fuel consumption results; however, a clear separation between performance curves can be observed for all tested traffic arrival rates at both maximum speeds. Compared to the benchmark approaches, SIMP reduced between 56% to 68% travel time. In the case of fuel consumption, SIMP saves up to 19.7%. These results indicate that applying SIMP can improve travel time and reduce unnecessary fuel wastage.

We also ran the same simulations to answer the question of applying other baseline approaches like the MCA and WTLC for dedicated three-lane intersections. The results were identical to the ones achieved with the conventional RR IM approach. This indicates that these approaches do not adapt their TLC cycles when permitted by an exclusive lane per crossing direction. Thus, there is no point in applying these complex protocols in this specific case with dedicated lanes.

5.4 Summary

This chapter evaluated the performance of the *synchronous framework* presented in Chapter 4 and compared it against various benchmark approaches based on their applicability at single-/two-/three-lane intersections. Various traffic arrival rates under low-speed urban conditions (30 and $50km/h$) are tested. The intersection throughput, travel time loss, and associated fuel consumption results are studied as they represent the relevant performance indicators of SUM.

From the SUMO simulation results, the following observations were made.

- SIMP shows the best throughput performance in the tested single-lane and multi-lane intersections and traffic scenarios. A clear dominance of SIMP can be observed, particularly at higher traffic arrival rates. The improvements are modest at lower traffic arrival rates.

- SIMP significantly minimized travel time loss values in all the tested traffic scenarios, intersections, and speeds. The travel time improvements are greater than the best of benchmark approaches.

- The fuel consumption results are proportional to the travel time loss values, and SIMP is more energy efficient than the compared IM approaches.

The performance of all IM approaches increases with the increased number of road lanes. It is apparent that the complexity of intersections is also increased when the road lanes share vehicles of different crossing directions.

The following chapter will address the composition and evaluation of networks of synchronous intersections employing complex two lanes intersections.

Chapter 6

Evaluating Networks of Synchronous Intersections

The *synchronous framework* for simple and complex isolated intersections was introduced in Chapter 4, and its performance was evaluated in Chapter 5. However, the larger picture of controlling a network of intersections is increasingly important and complex due to the interdependencies between adjacent intersections within the road network. The complexity is also brought by the multiple road lanes, particularly when shared by vehicles of different crossing directions. In this direction, this chapter introduces road networks composed of synchronous intelligent intersections and evaluates and compares the performance with the benchmark approaches.

A significant amount of the content of this chapter is obtained from the following scientific publications:

- **Reddy, R**., Almeida, L., Santos, P. and Tovar, E., 2022, December. Work-in-Progress: Exploring the Composition of Synchronous Intelligent Intersections. In 2022 IEEE Real-Time Systems Symposium (**RTSS 2022**), pp.523-526.
- **Reddy, R**., Almeida, L., Santos, P. and Tovar, E., 2023. Advantages of Synchronizing Vehicles Intersection Access. Accepted In Euro Working Group on Transportation Meeting (**EWGT 2023**), **Transportation Research Procedia**, pp.1-8.

6.1 Composing Networks of Intersections

Two road networks with four signalized intersections were composed. The first indicates a homogeneous road network (see Fig. 6.1), in which all four intersections have four legs that can be either dedicated or shared left-lane intersections. The second indicates a heterogeneous road network of four-legged and three-legged (or T) intersections. These configurations were chosen because they are widespread in urban settings. The IIMA

for the four-way two-lane intersections is presented in Figs. 4.3 and 4.4. The IIMA for T-intersections is presented in Fig. 6.2.

Without loss of generality, Figure 6.1 illustrates the homogeneous road network with a grid of $M \times M$ (with $M = 2$) intersections spanning over a squared area of size $L \times L$. In such a configuration, the distance between neighboring intersections is regular and given by $l = L/(M+1)$. This grid road network can be easily changed to a general one by applying varying road lengths and other geographic settings. Four cardinal directions (n, e, s, w) indicate four sides of the grid network. Each side of the grid connects the external road system through M roads to M intersections. For $M = 2$, the grid north side connects n_1 and n_2 roads with I_0 and I_1 intersections. Similarly, the set of intersections and outer roads of the grid network is $\mathcal{I} = \{I_0, I_1, I_2, I_3\}$ and $\mathcal{O} = \{w_2, n_1, n_2, e_1, e_2, s_1, s_2, w_1\}$, respectively. Therefore, the set $\mathcal{O}$ represents the outer edges, which are of particular relevance since they are the points of traffic injection (inflow lanes) and traffic egress (outflow lanes). As in Fig. 6.1, the internal roads are indexed with the IDs of intersections based on the edge direction between intersections $(I_{01}, I_{10}, I_{03}, I_{30}, I_{12}, I_{21}, I_{23}, I_{32})$. All intersections are equipped with an IM unit for implementing the SIMP protocol and associated control signals for managing traffic inflows.

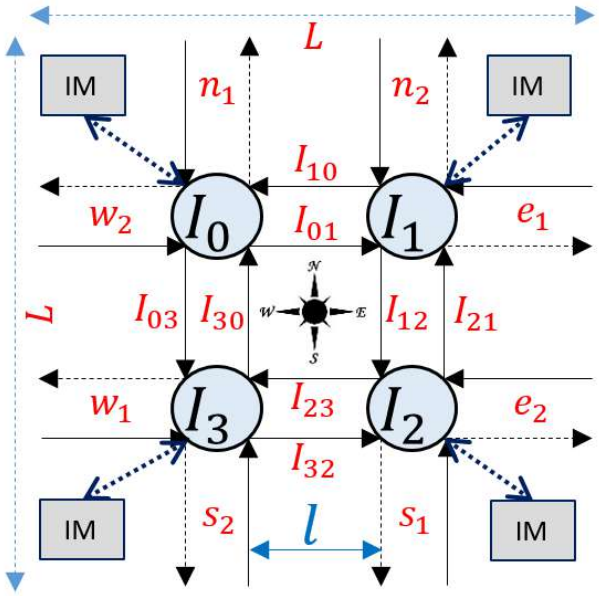

Figure 6.1: 2x2 Grid network of signalized intersections.

In the heterogeneous road network, the two left-side intersections (I_0 and I_3) are four-legged similar to the homogeneous road network, and the remaining two intersections (I_1 and I_2) on the right side are three-legged. Figure 6.2 shows the three-legged intersection, in which the rightmost lane is a free-flow lane; thus, the traffic does not yield or stop on that specific road lane. All the non-conflicting right-crossing directions are permitted. Hence, the IM approaches only need to manage the traffic of left-crossing lanes from the South and the West and the straight-crossing lane from the North. Therefore, on these

road lanes, the simple induction loop detector sensors are sufficient to detect the vehicles presence.

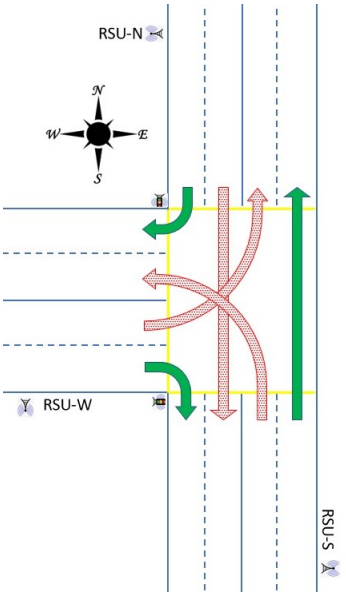

Figure 6.2: T-intersection with two lanes.

6.2 Traffic Routes

Two traffic routes per homogeneous and heterogeneous road networks were designed using the dedicated and shared left-lane configurations as in Figs. 4.1b, 4.1c, and 6.2. When a vehicle is injected into the homogeneous road network, its path is statically defined at that moment, picked randomly and uniformly among the $4 * M - 1$ possible destinations (assuming U-turns are forbidden and considering preset routes). For $M = 2$,

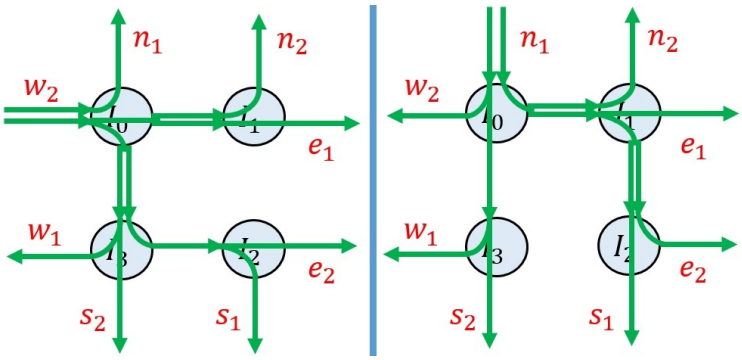

Figure 6.3: Dedicated left-lane routes for destinations reachable from w_2 (left) and n_1 (right) via intersection I_0.

Figs. 6.3 and 6.4 show the traffic routes for the dedicated and shared left-lane intersections, respectively. Those figures present the seven reachable destinations from w_2 (left)

and n_1 (right) via intersection I_0. We follow the same procedure for all the outer edges of all intersections, rotating the patterns as needed. The pattern on the left applies to all $*_2$ outer edges, while that on the right applies to all $*_1$ outer edges ($*$ stands here for any cardinal direction). Since we generate patterns from all four cardinal directions to all respective destinations with similar stochastic properties, all edges have a similar and time-invariant stochastic traffic load.

As shown in Fig. 6.3, from n_1 road, the rightmost lane hosts the traffic of three exit lanes w_2, w_1, and s_2 while the centermost lane hosts the traffic of the remaining four exit lanes n_2, e_1, e_2, and s_1. This means that by design, the centermost lane of all $*1$ roads will host more traffic than their rightmost lane. Conversely, it will be the rightmost lane of all $*2$ roads hosting the traffic of six exit lanes, while the centermost lane is completely dedicated to a single exit lane.

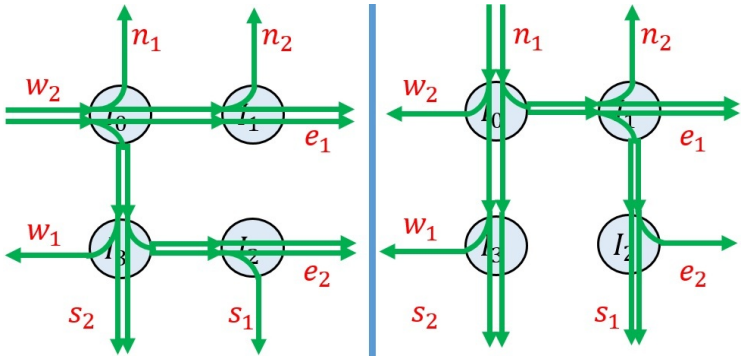

Figure 6.4: Shared left-lane routes from w_2 (left) and n_1 (right) to the reachable destinations via intersection I_0.

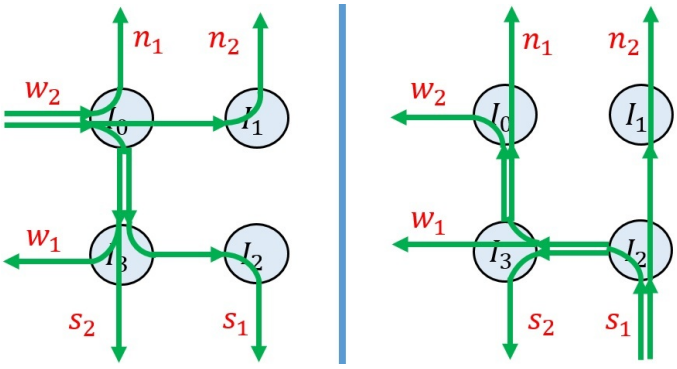

Figure 6.5: Dedicated left-lane routes from w_2 (left) and T-intersection routes from s_1 (right) to the reachable destinations.

The shared left lane routes are shown in Fig. 6.4, and the difference with the dedicated left lane routes (Fig. 6.3) is the additional straight-crossing route. Therefore, the traffic load of straight-crossing vehicles is shared among both lanes reducing the strain on any particular lane. In the heterogeneous road network, intersections I_0 and I_3 are four-way two-lane intersections that can be either dedicated or shared left-lane intersections. The

other two intersections, I_1 and I_2, are T-intersections, as shown in Fig. 6.2. For heterogeneous road networks, the traffic routes are presented in Fig. 6.5. The left side of the figure shows the five possible routes from w_2 via intersection I_0 (dedicated left lane model). The five possible routes from a T-intersection I_2 are presented on the right side of the figure. In the case of the shared left-lane model, an additional straight-crossing route will exist for four-way intersections, while T-intersections routes remain the same.

6.3 Simulation Scenarios

Two simulation scenarios for each homogeneous and heterogeneous road network were designed depending on previously designed routes.

- ***Scenario-1***, all intersections are homogeneous and are configured with dedicated left lanes.
- ***Scenario-2*** is similar to scenario-1, but the shared left lanes replace the dedicated left lanes (i.e., the straight-crossing vehicles share both road lanes).
- ***Scenario-3***, intersections I_0 and I_3 are the same as in scenario-1, with the dedicated left lanes and intersections I_1 and I_2 being T-intersections.
- ***Scenario-4*** is similar to scenario-3, but the dedicated left lanes are replaced by the shared left lanes at intersections I_0 and I_3; thus, the intersections I_1 and I_2 are T-intersections.

We set the intersection width[1] and road length to $20m$ and $l = 500m$, respectively. Thus $L = 1540m$ in the homogeneous road network scenarios. In the case of the heterogeneous road network, the vertical distance is the same as $L = 1540m$, but the horizontal distance is $L - l = 1040m$. Five traffic arrival rates ($0.025veh/s$, $0.05veh/s$, $0.067veh/s$, $0.1veh/s$, and $0.133veh/s$) are employed each for 1h, representing the low, moderate, and (below) saturated traffic conditions. *Poisson distribution* generates traffic on all external inflow lanes and lets the simulations run until all the generated vehicles exit the network. Moreover, the injected cars can be HVs or AVs with equal probability. In the homogeneous networks, the external inflow lanes are eight, i.e., n_1, n_2, e_1, e_2, s_1, s_2, w_1, and w_2; thus the generated traffic is equally distributed to seven outflow lanes at 0.143% without U-turns to the outflow lane of the source. For the heterogeneous networks, the external inflow lanes are six, i.e., n_1, n_2, s_1, s_2, w_1, and w_2; hence the generated traffic is again equally distributed to the five external outflow lanes at 0.2% without U-turns to the outflow lane of the source.

To study the above-mentioned scenarios in urban road settings, we tested two different maximum speeds, 30 and $50km/h$. The remaining simulation parameters and assigned values are similar to the ones presented in Table 3.1.

[1] We consider each lane to be $5m$ wide.

6.4 Experimental Results

We measured the number of vehicles left the road network in $1h$, as the road network throughput (veh/h). We also measured the average results of waiting time, travel time loss, and fuel consumption for 2500 vehicles. Therefore, for lower arrival rates, the simulations ran accordingly. The results of dedicated left lane approaches are identified with $* - D$ and shared left lane approaches with $* - S$.

6.4.1 Network Throughput (veh/h)

The network throughput results of both homogeneous (scenarios 1 and 2) and heterogeneous (scenarios 3 and 4) road networks are presented in Fig. 6.6 for $30km/h$ and Fig. 6.7 for $50km/h$ maximum speeds.

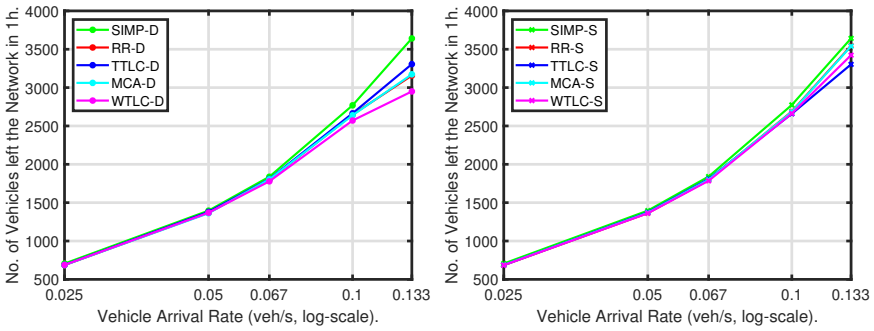

(a) Scenario-1 at $30km/h$. (b) Scenario-2 at $30km/h$.

(c) Scenario-3 at $30km/h$. (d) Scenario-4 at $30km/h$.

Figure 6.6: Network throughput (veh/h) of homogeneous (top plots) and heterogeneous (bottom plots) road networks at $30km/h$ maximum speed of comparing IM approaches.

The results of homogeneous road networks show that all the shared left-lane intersections (scenario 2) serve the highest number of vehicles than the dedicated left-lane intersections (scenario 1), except for TTLC. The TTLC with the dedicated left lanes serves more vehicles than its shared left lane configuration, and this is because the straight-crossing vehicles block the left-crossing vehicles and vice versa. Indeed the increased speed improved the throughput of all IM approaches in both scenarios.

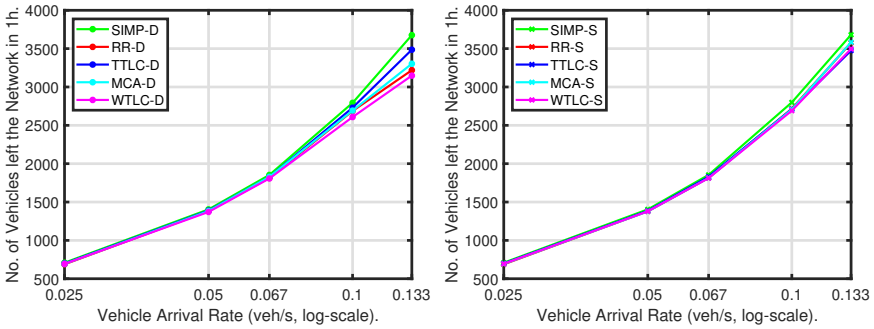

(a) Scenario-1 at $50km/h$. (b) Scenario-2 at $50km/h$.

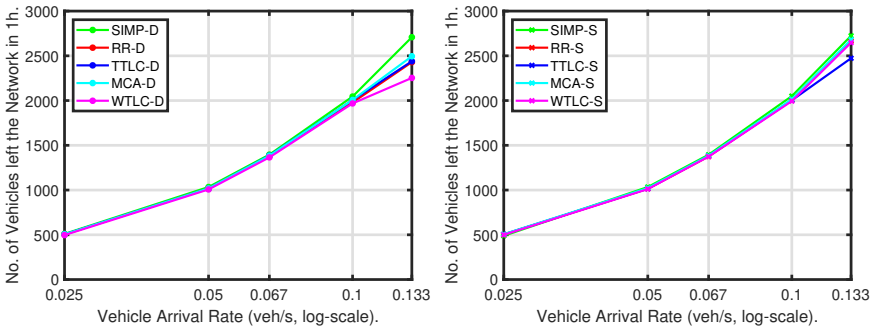

(c) Scenario-3 at $50km/h$. (d) Scenario-4 at $50km/h$.

Figure 6.7: Network throughput (veh/h) of homogeneous (top plots) and heterogeneous (bottom plots) road networks at $50km/h$ maximum speed of comparing IM approaches.

In the case of heterogeneous road networks, all the shared left lane intersections (scenario 4) perform better than the dedicated left lane intersections (scenario 3) for both maximum speeds, similar to the homogeneous networks. Moreover, the TTLC-S also performs better in this scenario. These results are due to T-intersections, i.e., two intersections without lane blocking, the right-of-way of right-crossing from the North and West, and the straight-crossing from the South to the North.

Overall, SIMP exhibits the highest throughput values in both homogeneous and heterogeneous road networks and maximum speeds (i.e., $30km/h$ and $50km/h$). SIMPs throughput improvements are slightest for lower traffic arrival rates and highest for higher traffic arrival rates. These results provide higher confidence levels that the vehicles synchronous intersection access can significantly reduce traffic congestion and improve throughput.

On the other hand, WTLC is the worst-performing approach in all scenarios and speeds with the lowest network throughput values except at $0.133veh/s$ in the shared left lane road networks. This behavior can be related to the inadequate adaptation of WTLC as shown in Figs. 6.6b, 6.6d, 6.7b, and 6.7d. In these cases and at the rate of $0.133veh/s$, TTLC is the worst-performing approach because sharing the left lane in TTLC raises conflicts between straight- and left-crossing vehicles and blocks the opposite road lanes.

The other IM approaches show intermediary performance. The throughput improvements of these approaches are due to the sharing of straight-crossing vehicles between lanes

and the sequential TLC operations that utilize the left lane at its highest level, including the right-of-way in the T-intersections of heterogeneous road networks. Overall, SIMP improved the network throughput by up to 3% than the following best approach MCA.

All IM approaches saturate above $0.1veh/s$ (see the slight inflection of the respective lines), except SIMP-S (which was observed to be at $0.2veh/s$). SIMP shows dominance over the other IM protocols for both intersection configurations, particularly at higher traffic intensities near/at saturation. For low traffic intensity, the global throughput is very similar for all IM protocols.

Between the two configurations, the shared left lane shows a higher traffic saturation point (thus higher throughput), resulting in two lanes serving the traffic going straight at each intersection. The differences between the IM protocols at a traffic arrival rate of $0.133veh/s$ (saturated traffic) are already significant for the dedicated left lane configuration. At this arrival rate, the global throughput of SIMP-D is $\sim 300veh/h$ ($\sim 10\%$) higher than that of TTLC-D, the second best performing protocol with dedicated left lanes. With SIMP-S, the difference to the second performing protocol with shared left lanes, RR-S, is smaller, $\sim 100veh/h$ ($\sim 3\%$).

6.4.2 Average Travel Time Loss (seconds)

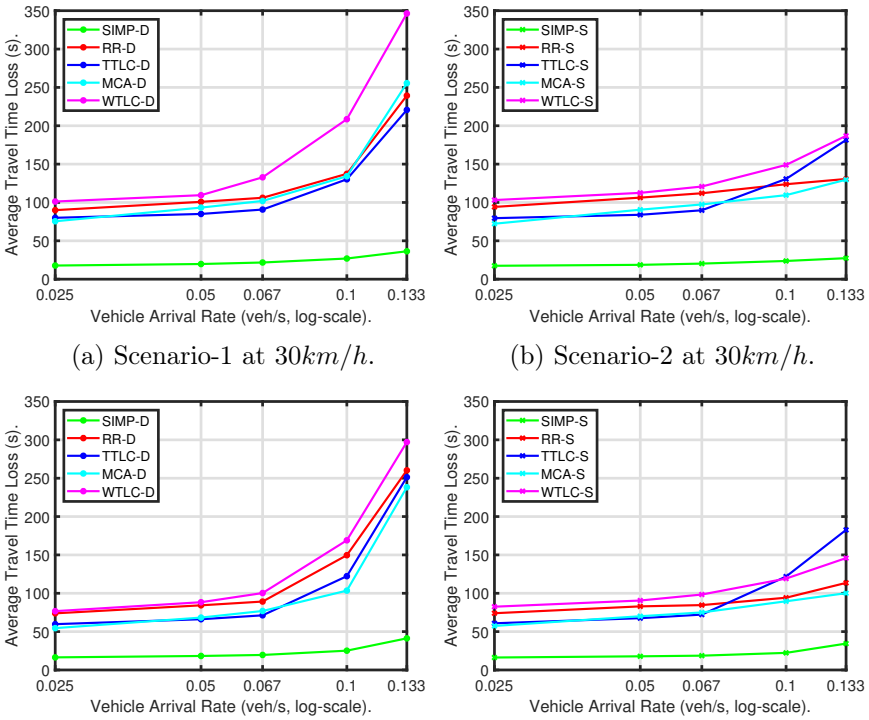

(a) Scenario-1 at $30km/h$.

(b) Scenario-2 at $30km/h$.

(c) Scenario-3 at $30km/h$.

(d) Scenario-4 at $30km/h$.

Figure 6.8: Average travel time loss (s/veh) of 2500 vehicles for homogeneous (top plots) and heterogeneous (bottom plots) road networks at $30km/h$ maximum speed imposed by the comparing IM approaches in both dedicated and shared left lane intersections.

The average travel time loss (s) of 2500 vehicles for the same scenarios, arrival rates, and speeds are presented in Figs. 6.8 ($30k/h$) and 6.9 ($50km/h$). The travel time loss combines the waiting time at intersections and the time lost due to speed deviations in the journey between the origin and the destination. Speed deviations occur when vehicles travel in close proximity, and the following vehicle adapts its speed depending on the front vehicle for safe passage and to avoid collisions. Whenever there is a red signal, vehicles must decelerate before stopping and accelerate to access the intersection during the green signal; thus, some time will be lost in these situations too.

In all the tested scenarios, arrival rates, and speeds, SIMP's maximum waiting time is below $8s$. This means that, on average, the vehicles wait for less than one control cycle of SIMP, i.e., $11s$. This shows the advantage of employing SIMP in urban settings that effectively reduces the waiting time of vehicles due to synchronous intersection access from multiple lanes and the lowest control cycle time.

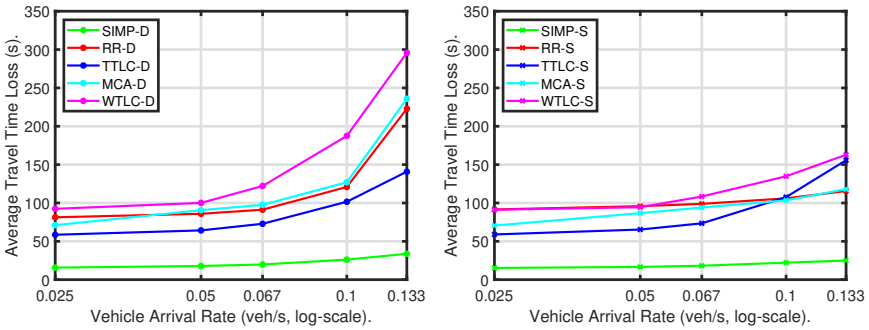

(a) Scenario-1 at $50km/h$.

(b) Scenario-2 at $50km/h$.

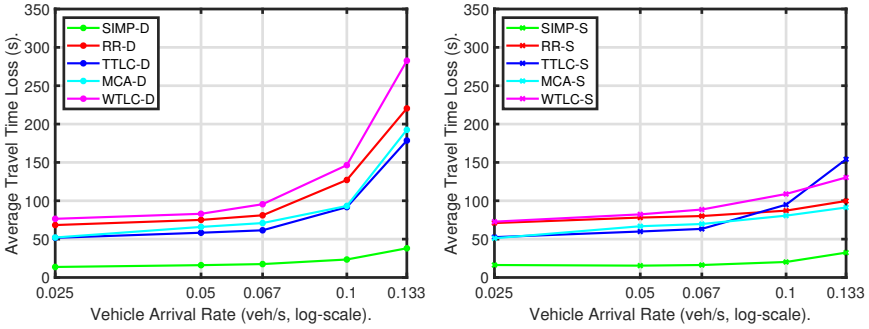

(c) Scenario-3 at $50km/h$.

(d) Scenario-4 at $50km/h$.

Figure 6.9: Average travel time loss (s/veh) of 2500 vehicles for homogeneous (top plots) and heterogeneous (bottom plots) road networks at $50km/h$ maximum speed imposed by the comparing IM approaches in both dedicated and shared left lane intersections.

On the contrary, WTLC-D is the worst-performing approach with the highest waiting time values due to its poor adaptations in serving arriving vehicles sequentially. The drawback of serving a sequence of vehicles sequentially is that the vehicles of the remaining lanes must wait until their turn. Compared to SIMP, vehicles in the WTLC-D lost more than $200s$ on average in waiting to access the intersections. In the same dedicated left-

lane scenarios, the remaining IM approaches show intermediary behavior with around $50s$ higher waiting time than SIMP until $0.067veh/s$ and then keep growing for increasing arrival rates. TTLC is the following best approach in most cases.

The homogeneous road network results (scenarios 1 and 2) at both maximum speeds show the advantages of employing the SIMP protocol with the lowest travel time loss values of $27s$ (SIMP-S at $30km/h$) and $25s$ (SIMP-S at $50km/h$) at the arrival rate of $0.133veh/s$. The worst-performing approach is again the WTLC-D in scenario 1, where vehicles lost $\sim 100s$ due to the speed deviations reaching $350s$ compared to the waiting time of $250s$.

Overall, the travel time loss results of shared left lane approaches are lower than the dedicated left lane results, except for the TTLC-S, due to the lane blocking of straight-crossing vehicles in shared between lanes, again. The increased speed minimized the time loss values for all IM approaches. Similar to the waiting time results, scenario 4 at $50km/h$ maximum speed, all IM approaches show their best travel time loss results. These results can be attributed to the fewer crossing conflicts and more right-of-way permissions at the T-intersections. In total, SIMP minimized up to 129.2% travel time loss compared to the following best approach again MCA.

6.4.3 Average Fuel Consumption (liters)

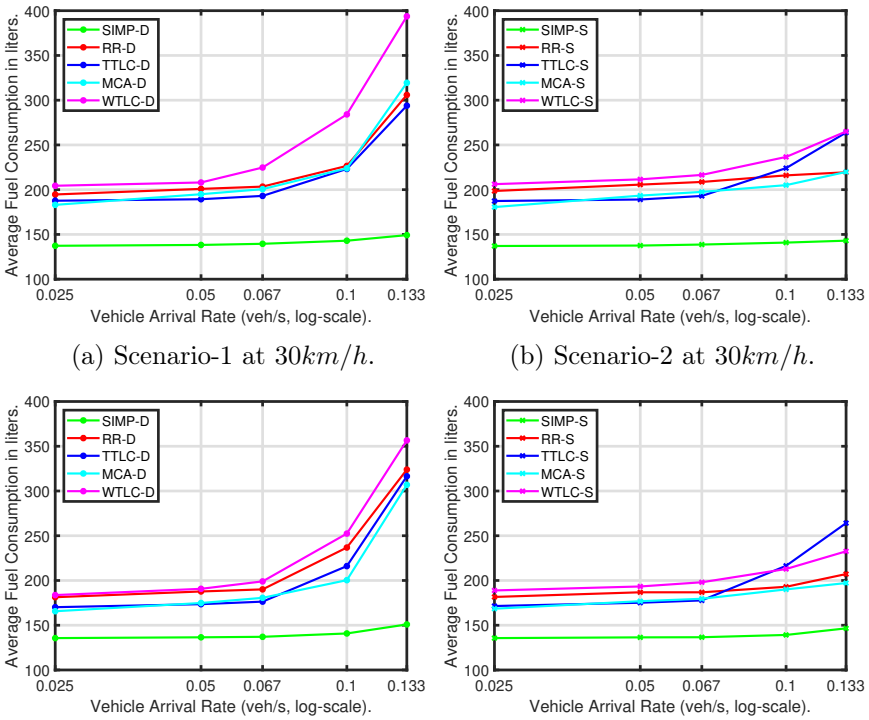

(a) Scenario-1 at $30km/h$. (b) Scenario-2 at $30km/h$.

(c) Scenario-3 at $30km/h$. (d) Scenario-4 at $30km/h$.

Figure 6.10: Average Fuel Consumption (*liters*) of 2500 vehicles for comparing IM approaches at $30km/h$ and $50km/h$ maximum speeds of both homogeneous (top plots) and heterogeneous (bottom plots) road networks.

The average fuel consumption results for the same simulation scenarios are presented in Figs. 6.10 ($30km/h$) and 6.11 ($50km/h$) for the same 2500 vehicles. The vehicles let their engine in idling mode when waiting at intersections, leading to more gasoline consumption than when they are in cruising mode. Similar to the waiting and travel time loss results, the shared left-crossing intersections show better fuel consumption results. Particularly scenario 4 at $50km/h$ maximum speed shows the best results for all IM approaches. Again SIMP shows the best energy efficiency results. The reason is the synchronous intersection access that imposes smooth driving between consecutive vehicles—secondly, less waiting time at intersections due to the short TLC cycle time. Consequently, gasoline consumption is reduced.

In the case of sequential (RR, MCA, and WTLC) and parallel (TTLC) vehicle intersection access, the higher gasoline consumption is associated with their waiting time results due to the engine idling mode. Once again, the highest fuel consumption values are with the WTLC-D being the worst option, while the other approaches show intermediary performance. Overall, SIMP is up to 35.4% more energy efficient than the following best approach, MCA.

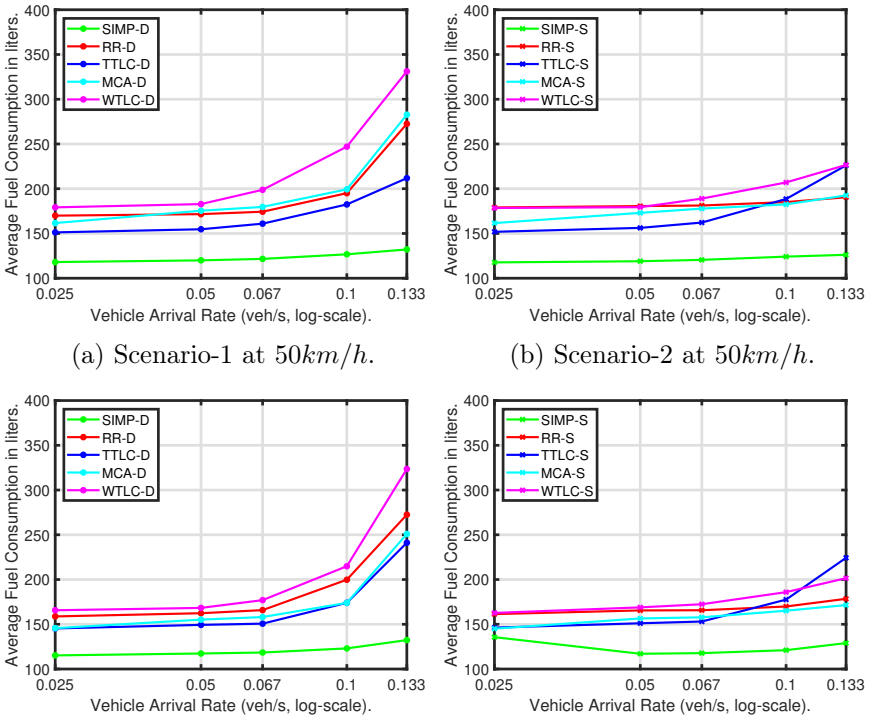

(a) Scenario-1 at $50km/h$. (b) Scenario-2 at $50km/h$.

(c) Scenario-3 at $50km/h$. (d) Scenario-4 at $50km/h$.

Figure 6.11: Average Fuel Consumption (*liters*) of 2500 vehicles for comparing IM approaches at $30km/h$ and $50km/h$ maximum speeds of both homogeneous (top plots) and heterogeneous (bottom plots) road networks.

6.5 Summary

This chapter presented the composition of homogeneous and heterogeneous road networks with four intersections. The homogeneous road networks are designed to form a grid with four-legged intersections. The heterogeneous road networks are designed to form a partial grid combining four-legged and three-legged intersections. These road networks can easily be adapted to represent real-world general road networks by applying exact geographic settings. The traffic route patterns on these road networks are designed so that vehicles cross single/two/three intersections to exit the road networks. Two maximum speeds, 30 and $50km/h$, were tested, indicating the low-speed urban settings. The advantage of synchronous intelligent intersections is a multitude concerning the network throughput, travel delays, and associated fuel consumption. A clear dominance of the synchronous SIMP over the counterparts can be observed, especially when the shared left lane intersections are mixed with the T-intersections, i.e., scenario-4 at $50km/h$.

We also tested scenarios 1 and 2 at $70km/h$ maximum speed to study the applicability of SIMP in high-speed urban conditions. The results are promising, with overall improvements in network throughput (up to 3%), travel delays (up to 125.5%), and associated fuel efficiency (up to 34.6%). These results are presented in [185].

Up to now, the applicability of the *synchronous framework* has only been tested in the average case. However, the average values do not represent the actual values, which are affected by variations caused by the irregular arrival of vehicles, thus generating a time series. In this research direction, an endeavor relevant to traffic planning and safety is assessing for each given traffic scenario the worst-case service level that can be expected. This is addressed in the next chapter.

Chapter 7

Worst-Case Response Time

This chapter presents analytical expressions for evaluating the Worst-Case Response Time (WCRT) of IM approaches given defined traffic scenarios. The concept of WCRT is borrowed from real-time systems. The WCRT for one vehicle is the worst-case time a vehicle may take since it enters the road system until it exits the last intersection before reaching the destination. We estimated the WCRT utilizing the commonly available geographical settings of the road networks (road lanes length and intersection space within), traffic-related information (arrival rate, average speed, maximum queue length, and capacity), and IM-specific parameters (green phase time and total cycle time). As defined in [175], the WCRT is a service measure of the TLC operations given statistically defined traffic conditions.

For the moment, we just know the traffic statistics at the traffic injection points, e.g., traffic injected according to a uniform distribution or a Poisson distribution. Once this traffic enters an intersection, the statistics at the output are altered, thus the same analysis cannot be simply applied to the following segments in a network of intersections. Consequently, the analysis in this chapter concerns, essentially, isolated intersections both single-lane and multi-lane, and we generate the so-called local WCRT values.

Nevertheless, in a network of intersections we can assume pessimistic conditions in which all intermediate segments are filled up with vehicles up to their capacity, i.e., saturated. By simulation it is possible to determine a region of traffic injection rates that generate under-saturation conditions across the network. In these circumstances an upper bound to the global WCRT value of a network of intersections, i.e., from injection to exit from the last intersection in the route, is the summation of all local WCRT values considering saturated intermediate segments. This global WCRT analysis is pessimistic but simple and it can be utilized in the strategic planning of urban transportation. More accurate analysis is left for future work. Thus, this chapter also presents at the end the analytical models for estimating the WCRT of networks of multi-lane intersections.

A significant amount of the content of this chapter is obtained from the following scientific publications:

- **Reddy, R.**, Almeida, L., Gaitan, M., Kurunathan, H., Santos, P. and Tovar, E., 2021, December. Work-In-Progress: Worst-Case Response Time of Intersection Management Protocols. In 2021 IEEE Real-Time Systems Symposium (**RTSS 2021**), pp.556-559.

- **Reddy, R.**, Almeida, L., Santos, P.M., and Tovar, E., 2023. Waiting Time Analysis for a Network of Signalized Intersections. In International Conference on Ambient Systems, Networks and Technologies (**ANT 2023**), **Procedia Computer Science**, 220C, pp.503-510.

- **Reddy, R.**, Almeida, L., Kurunathan, H., Gaitan, M., Santos, P. and Tovar, E., 2023. Comparing the Worst-Case Response Time of Complex Intersections Management. Under revision in **IEEE Open Journal of Intelligent Transportation Systems**.

7.1 Notation

To facilitate the understanding of the analysis presented in this chapter, we introduce here the most relevant notation used. We skip here other notation with obvious semantics, which is just incorporated in the text.

- R_{ij} is the road lane in the intersection (for $i = 1, ..., 8$ and $j = 1, 2$);
- m is the crossing direction ($m = 1, 2, 3$ for right, straight, left);
- l is the road length to, from and between intersections;
- v_z is the velocity v of vehicle z;
- l_z is the length l of vehicle z;
- d_s is the minimum safe distance between consecutive vehicles;
- $C = \frac{l}{l_z + d_s}$ is the road capacity;
- Q_{max} is the maximum number of vehicles that queue up across all road lanes;
- S_{max}, S_F, and S_R are the maximum, free-flow, and running speeds, respectively;
- $WCRT_{IM_{R_{ij}}}$ is the worst-case response time (WCRT) provided by the concerned IM protocol for road lane R_{ij};
- $WCIST_{IM_{R_{ij}}}$ is the worst-case intersection service time (WCIST) provided by the concerned IM protocol for road lane R_{ij};
- $QT_{R_{ij}}$ is the vehicle queue joining time on road lane R_{ij};

- $WT_{IM_{R_{ij}}}$ is the vehicle waiting time imposed by the IM on road lane R_{ij};
- ICT_m is the intersection crossing time of crossing direction m;
- $\Phi(IM)$ is the set of phases that compose the intersection control cycle under a given IM protocol, including green $\phi_g = (\phi_1, \phi_2, \phi_3, \phi_4)$ and yellow (ϕ_y), as appropriate;
- $T_\Phi(IM)$ is the time required for the execution of one complete intersection control cycle $\Phi(IM)$;
- n is the number of control cycles that vehicles must wait before being served;
- $\mathcal{D}_{IM_{R_{ij}}}$ is the number of vehicles that the IM approach serves per road lane R_{ij} during the green phase.
- $\alpha(t)$ is the cumulative arrival function of vehicles at an intersection;
- $\mu(t)$ is the cumulative service function of vehicles dispatched from an intersection;
- λ is the long-term average arrival rate;
- s is the saturation flow rate;
- x is the number of vehicles in a queue under analysis;
- x_s is the number of queued vehicles needed to trigger saturation;

7.2 Worst-Case Response Time

The key components of the WCRT estimation are the queue joining time (QT) and the worst-case intersection service time (WCIST). The WCIST is a combination of waiting time (WT) and intersection crossing time (ICT).

First, we present the three possible speed conditions of vehicles passing through an arbitrary intersection I. Figure 7.1 presents the time-space trajectory diagram of a vehicle passing through I considering its maximum target speed (S_{max}), free flow speed (S_F), and the running speed (S_R). The maximum target speed is the theoretical maximum speed assigned to vehicles or road lanes. The free-flow speed is the average speed of a vehicle when no vehicles are present on inflow road lanes and without intersection delays. Running speed is also the average speed of a vehicle but includes various types of delays (acceleration/deceleration, leader-follower, and waiting delays) in accessing and crossing intersection I. The leader-follower delay occurs when a group of vehicles traveling in close proximity and follower vehicles reduce their speed according to the vehicle ahead for safe travel [141]. Suppose vehicle z is initiated at origin d_0 and time t_0. To reach the destination, vehicle z goes through various points in time (t_1, t_2, t_3, t_4) and space (d_1, d_2, d_3) associated with changes in its speed, as portrayed in Fig. 7.1.

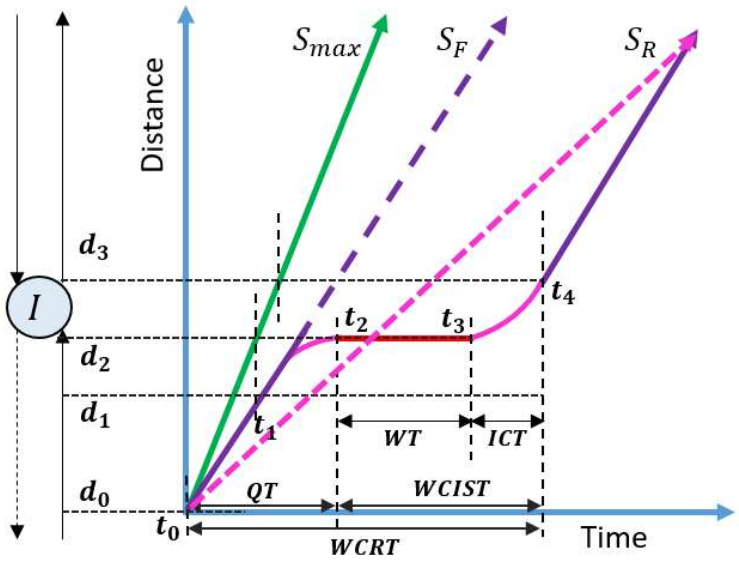

Figure 7.1: Time-space trajectory of a vehicle and various components of the WCRT in a signalized intersection I.

The figure also shows the three major components of WCRT, i.e., QT, WT, and ICT. The analytical expression of WCRT is exhibited in Eq. 7.1, and its components are defined subsequently.

$$WCRT_{IM_{R_{ij}}} = QT_{R_{ij}} + WT_{IM_{R_{ij}}} + ICT_m \tag{7.1}$$

Queue joining time (QT in s/veh) on any road lane R_{ij} is the time a vehicle takes from the injection point to the queue tail, including the deceleration time. In Fig. 7.1, the QT is shown between t_0 and t_2 at d_0 and d_2, and calculated using Eq. 7.2 with an average speed v_z.

$$QT_{IM_{R_{ij}}} = \frac{l - Q_{max} \times (l_z + d_s)}{v_z} \tag{7.2}$$

The second component is the **waiting time** (WT in s/veh), which is measured from when vehicles arrive at a queue and stop (t_2) until they restart moving (t_3) at d_2 distance from the injection point. When the maximum queue length (Q_{max}) is less than the number of vehicles that the IM approach serves during a green phase ($\mathcal{D}_{IM_{R_{ij}}}$), two situations can happen. Either an arriving vehicle crosses in that phase and its $WT = 0$ (we refer to this condition as ϕ_g) or, if the phase ends before that vehicle crosses, it will have to wait for the next green phase in the following cycle, thus $WT = T_{\Phi_{IM}} - \phi_g$. If, under sufficiently dense traffic, the Q_{max} grows beyond the number of vehicles that can be served in a single TLC cycle ($\mathcal{D}_{IM_{R_{ij}}}$), then a vehicle may have to wait stopped for $n-1$ full TLC cycles plus the maximum time to the next green phase, where n is the number of TLC cycles needed to serve the Q_{max} vehicles ($n = \left\lceil \frac{Q_{max}}{\mathcal{D}_{IM_{R_{ij}}}} \right\rceil$). These three cases are expressed in Equation 7.3.

$$WT_{IM_{R_{ij}}} = \begin{cases} 0, & \text{if } Q_{max} \leq \mathcal{D}_{IM_{R_{ij}}} \& \ \phi_g \\ T_{\Phi_{IM}} - \phi_g, & \text{if } Q_{max} \leq \mathcal{D}_{IM_{R_{ij}}}; \\ (n-1) \times T_{\Phi_{IM}} + (T_{\Phi_{IM}} - \phi_g), & \text{if } \mathcal{D}_{IM_{R_{ij}}} < Q_{max} \leq n\mathcal{D}_{IM_{R_{ij}}}. \end{cases} \tag{7.3}$$

The third component of the WCRT is the **intersection crossing time** (ICT s/veh), which is the time required to traverse the intersection. The ICT is measured between t_3 and t_4 at d_2 and d_3 as in Fig. 7.1 and Eq. 7.4 and it is different for different crossing directions, thus we use index m to express this dependence.

$$ICT_m = (t_4 - t_3) - \frac{d_3 - d_2}{v_z} \tag{7.4}$$

For the sake of simplification, we consider two different crossing times, to turn right (shorter) and to cross straight or turn left (longer). Using two-lane intersections (Figs. 4.3 and 4.4) with $20m$ width, the observed ICT values are under $\sim 1s$ (R-crossing) and $3s$ (L/S-crossing) for both AVs and HVs at $S_{max} = 30km/h$ and $v_z = S_F$. When the vehicles are stopped and waiting to access the intersection, it takes approximately $2s$ for the first vehicle to react to the green signal. The following vehicles add up a gradually smaller reaction time, which is called the start-up lost time [241]. Altogether, we consider $\text{ICT}_1 \leq 3s$ (R-crossing) and $\text{ICT}_{2,3} \leq 5s$ (S- and L-crossing). For convenience, we later do a pessimistic assumption and consider $\text{ICT}_m \leq 5s, \forall_m$ to estimate the WCIST value at all speeds. Combining WT (Eq. 7.3) and ICT (Eq. 7.4) leads to the WCIST as in Eq. 7.5.

$$WCIST_{IM_{R_{ij}}} = WT_{IM_{R_{ij}}} + ICT_m \tag{7.5}$$

7.3 Isolated Single-lane Intersections

First, we evaluate the WCRT for the isolated four-way single-lane ($j = 1$) intersection with $l = 500m$ (see Fig. 4.2). The comparing IM approaches are SIMP and RR-x schemes (RR-5, RR-10, RR-20, and RR-30) and we consider $S_{max} = 30km/h$ (i.e., $8.33m/s$). The other main SUMO simulation parameters are similar to the ones presented in Table 3.1. Therefore, the road capacity $C = \frac{l}{l_z + d_s} = \frac{500}{5+5} = 50$ vehicles, as we consider vehicles of equal length with $l_z = 5m$ and the safety distance among consecutive vehicles is $d_s = 5m$. These values lead to $Q_{max} \leq 50$ vehicles, i.e., for stability of the intersection, Q_{max} should not grow beyond 50 vehicles. To test worst-case conditions, we inject 50 vehicles on each inflow road following a uniform distribution executed every second with an average rate of $0.2veh/s$, which already creates some level of traffic saturation, i.e., several vehicles are injected faster than the intersection can serve them and a queue builds up at the intersection entrance. When a vehicle is injected, it comes with a crossing direction, which

is assigned randomly with uniform distribution among the all crossing directions, i.e., 33% of the traffic to the right, straight, and left directions.

As presented in Chapter 4.4, SIMP uses $2.5s$ and $3s$ as green time for right/straight crossing and left crossing, respectively. Also, to complete a TLC cycle by serving one vehicle from each road lane, SIMP takes $11s$. For RR-x (RR-5, RR-10, RR-20, and RR-30), the control cycle times are $36s, 56s, 96s$, and $136s$. The corresponding number of vehicles that can cross the intersection in each green phase at $S_{max} = 30km/h$ is given by $\mathcal{D}_{RR-x} = 2, 4, 8$, and 12, respectively. These values are exhibited in Table 7.1.

Table 7.1: IM specific cycle and green times, and the corresponding number of vehicles that can be served.

IM	Cycle Time (s)	Green time (s)	No. of vehicles
SIMP	11	2.5/3	1
RR-5	36	5	2
RR-10	56	10	4
RR-20	96	20	8
RR-30	136	30	12

Figure 7.2 shows the worst-case intersection service time $WCIST_{IM}$ as a function of the maximum queue length Q_{max} for all IMs (using Eq. 7.5). All $WCIST_{RR-x}$ curves show the typical step-wise behavior corresponding to the green phases of the control cycles. Note that Eq. 7.5 considers whole phases only, even if the last cycle uses just a part. This introduces some pessimism for the sake of simplification, which essentially affects the left side of each step. The right side is accurate, representing the situation in which the last phase is fully used, too. $WCIST_{SIMP}$ is linear, given that SIMP cycles handle vehicles from each lane one at a time. Fig. 7.2 also shows that $WCIST_{SIMP}$ is lower than all $WCIST_{RR-x}$ curves (lower worst-case service time) for any queue length Q_{max}.

Figure 7.3 shows the observed maximum response time of 50 vehicles at $0.2veh/s$ for 100 simulation runs using SUMO. The following WCRT values are observed $274s$ (SIMP), $781s$ (RR-5), $607s$ (RR-10), $536s$ (RR-20), and $541s$ (RR-30). These observed WCRT values are below the analytical values given by Eq. 7.1, i.e., $550s$ (SIMP), $900s$ (RR-5), $728ss$ (RR-10), $672s$ (RR-20), and $680s$ (RR-30), which can be taken from Fig. 7.2.

For these SUMO produced WCRT values, Fig. 7.4 shows the intersection queue dynamics, displaying the queue length in one inflow lane for all IMs during the simulation. Until $t \approx 350s$, we observe the queue building up given an arrival rate higher than the service rate. When the vehicle injection stops, the queue is served until exhaustion. During the service periods, the whole queue moves forward, and SUMO does not detect it as a queue until the vehicles stop again and re-queue. This causes the deep valleys that can be observed in the figure.

We assessed the last vehicle WCRT with all IMs as a preliminary validation. SUMO reports a queue length of 16 (SIMP) and 37 (RR-5 to RR-30) upon vehicle arrival at the

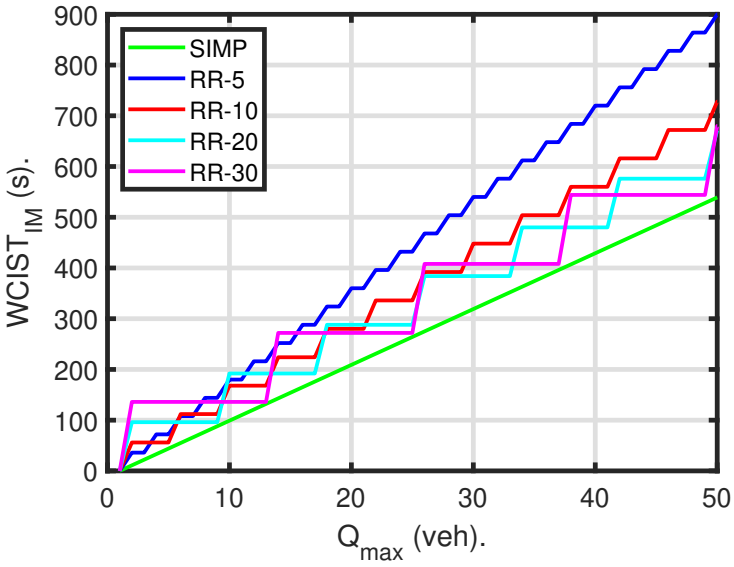

Figure 7.2: Worst-case intersection service time for Q_{max} queued vehicles.

intersection. With these observed values of Q_{max}, we estimate a WCRT upper bound using the equations above. The observed response times were the following, in the same order of IMs, with the respective analytical WCRT in parenthesis: 274s (313s), 713s (780s), 542s (620s), 369s (540s) and 328s (468s). The observed values are below the WCRT, as expected. Similar observations were made for random vehicles in the simulation.

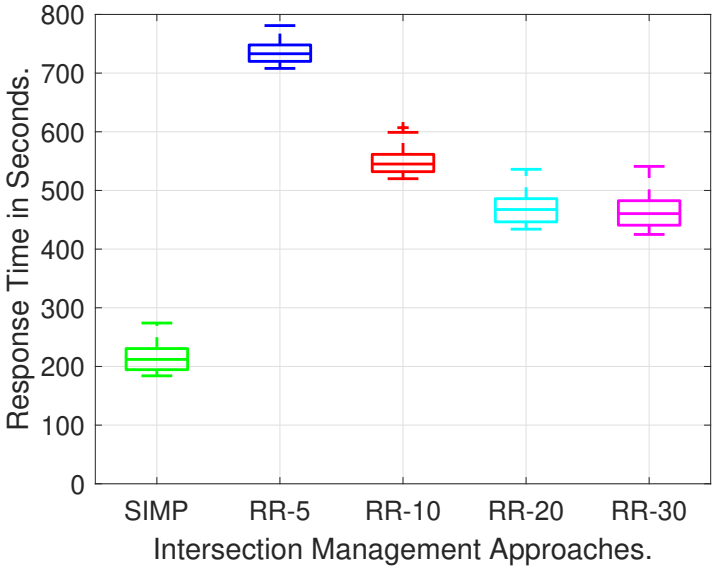

Figure 7.3: Observed response time of 50 vehicles for 100 simulation runs, with an average traffic injection rate of $0.2veh/s$.

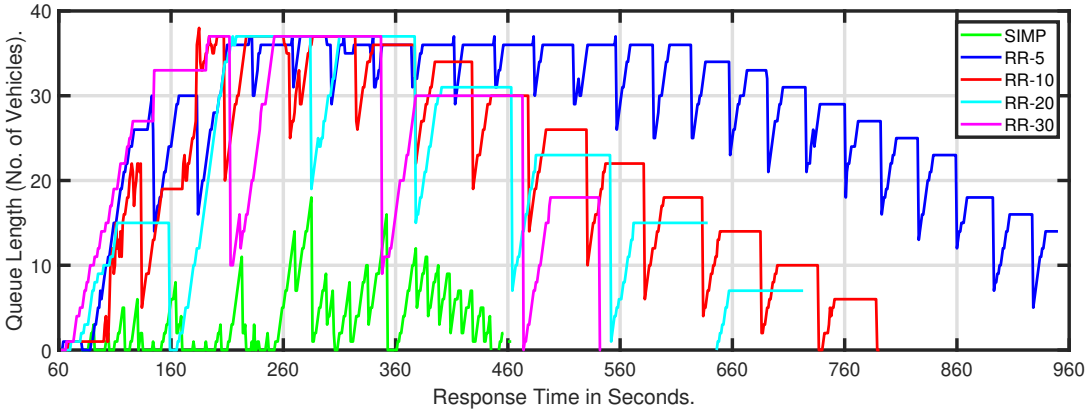

Figure 7.4: Queue length (number of vehicles) along time, with an average traffic injection rate of 0.2veh/s.

7.4 Isolated Multi-lane Intersections

This section estimates the WCRT for isolated multi-lane intersections, particularly two-lane intersections with dedicated left lanes, as shown in Fig. 4.3. However, in this section, we also introduce another WCRT analysis. Instead of determining Q_{max} empirically, which is not always possible (requires a simulator or actual experimentation), we use an analytical method to derive an upper bound to Q_{max}. In particular, we resort to flow analysis and queuing theory, which have long been used to compute queue length and service time estimates in traffic scenarios [41]. Once we to determine the referred Q_{max} upper bound we can derive the associated WCRT. We then validate these analytical WCRT results using the SUMO simulations in non-saturated and saturated traffic flow conditions.

7.4.1 Arrival and Service Curves per Inflow Lane

Flow analysis and queuing theory use arrival and service curves per inflow road lane, e.g., the Network Calculus framework. Considering an intersection with a given IM protocol, a cumulative service function tells us how many vehicles the intersection can serve from a given lane up to time t. Moreover, a cumulative traffic arrival function per inflow lane provides the number of vehicles arriving at the intersection in that lane up to time t. The difference between the arrival and the service curves at time t gives us the number of vehicles queued at the intersection in that lane, waiting to be served. Similarly, the IST for a given number of vehicles can be computed by the difference between the time they arrive together at the queue and the time the last one is served.

The cumulative service function typically designated $\mu(t)$, is frequently easy to derive, knowing the control cycle of the specific IM protocol and its configuration parameters. On the other hand, the traffic arrival is normally stochastic and thus impossible to define precisely. However, it is frequently possible to upper bound it, even if with a residual probability of exceedance, if it follows a known distribution. A common arrival curve

upper bound, typically designated $\alpha(t)$, is shown in Eq. 7.6.

$$\alpha(t) = \begin{cases} s \cdot t \text{ if } t < x_s/s \\ x_s + \lambda \cdot t \text{ otherwise} \end{cases} \tag{7.6}$$

This upper bound arrival curve considers that x_s vehicles arrive initially in a burst, i.e., at the saturation flow rate s [125], thus causing vehicles queuing. Then, the following vehicles arrive equally spaced at a long-term average rate λ. Knowing the arrival upper bound and the service functions allows deducing an upper bound to the queue length as in Eq. 7.7, subject to $\alpha(t) > \mu(t)$, and to the $WCIST$ as in Eq. 7.8, subject to $\mu^{-1}(x) > \alpha^{-1}(x)$, where x stands the instantaneous number of vehicles in the queue.

$$Q_{max} = \max_t(\alpha(t) - \mu(t)) \tag{7.7}$$

$$WCIST = \max_x(\mu^{-1}(x) - \alpha^{-1}(x)) \tag{7.8}$$

Note that the value of Q_{max} provided by Eq. 7.7 also allows solving Eqs. 7.5 and 7.1 to deduce $WCIST$ and $WCRT$ values, respectively. Moreover, for the stability of the intersection system, it is necessary that the long-term average arrival rate λ is always lower than the average service rate $\bar{\mu}$.

7.4.1.1 Vehicle Arrival Patterns

Our concrete case considers all roads leading to the intersection having a length of $550m$. This road length is divided into the intersection area with $l = 500m$ and the traffic injection area with $50m$. Figure 4.3 illustrates the intersection area with two inflow/outflow lanes where the queue length Q can be measured. The traffic injection area is a single-lane road that initiates and distributes the arriving traffic to the two inflow lanes according to the target directions. We consider an equal distribution for the three directions, i.e., 33%. The aforementioned settings are identical to the ones employed in Reddy et al. [176]. Therefore, we utilize the throughput results of Reddy et al. [176] to select the saturation flow rate, in which different IM systems saturate at different rates between $0.2veh/s$ and $0.4veh/s$. Here we use $0.4veh/s$ as the saturation flow rate to enforce saturation for all IM systems. This rate is distributed among the two inflow lanes according to the traffic volume per direction and the directions served per lane. For the dedicated left lane $s = 0.133veh/s$ (33% left-crossing vehicles) and for the straight and right-crossing lane $s = 0.266veh/s$ (33% of straight-crossing plus 33% of right-crossing vehicles).

These flow rates are used to draw the arrival curves using Eq. 7.6. Since we do not know the saturation flow volume x_s, we consider just the saturation flow rate and not the long-term rate that is lower, thus upper bounding vehicles arrival. It is also important to recall the capacity of $500m$ long lanes, with $5m$ long vehicles and $5m$ safety distance, i.e., the maximum number of vehicles that can be queued in any one lane is $C = 50veh$.

7.4.1.2 Vehicle Service Patterns

The service the intersection can provide for crossing vehicles depends on the IM protocol used and the maximum speed allowed. The maximum speed makes a stronger impact in protocols with longer green times since more vehicles cross per green phase. On the other hand, for worst-case conditions, we consider that no vehicles are served in the yellow phases. These are used for flushing vehicles admitted at the end of the preceding green phases.

Therefore, based on the properties of the IM protocols described in Section 3.6 and the two speeds considered in urban environments ($30km/h$ and $50km/h$), we present in Table 7.2 how many vehicles each IM can serve from each lane per cycle.

Note that SIMP permits per cycle (Fig. 4.12) at least one vehicle per L lane and 3 vehicles per S/R lane. On the other hand, ITLC and QTLC adapt their green time based on the instantaneous queue length, waiting time, the distance from the intersection entrance, and their accelerations. In this case, we consider the maximum green time of $60s$, which would correspond to having no cars arriving on the other roads and leads to longer cycle time.

To draw the specific arrival and service curves that apply to our case, we consider that the system is empty at $t = 0$; thus, $Q(0) = 0$, and only then accumulates vehicles. Also, note that this is a worst-case traffic scenario. Thus each IM approach starts (at $t = 0$) at the beginning of the phase that immediately succeeds the phase of the respective lane, thus waiting for a control cycle to start serving vehicles.

Table 7.2: IM specific cycle and green times, and the corresponding number of vehicles that can be served at different maximum speed settings.

IM	**Cycle Time (s)**	Green time (s) (Lanes S/R and L)		No. of vehicles			
				30km/h		50km/h	
		S/R	L	S/R	L	S/R	L
SIMP	11	2.5	3	3	1	3	1
RR / MCA	136	30	30	12	12	14	14
TTLC	106	30	15	12	6	14	7
ITLC / QTLC	166	60	15	24	6	28	7

7.4.1.3 Arrival-Service Curves

Figure 7.5 shows the arrival curve $\alpha(t)$ and service curves $\mu(t)$ for the different IM protocols for both maximum speeds employed, i.e., $30km/h$ and $50km/h$. The vertical axis represents the cumulative number of vehicles that arrive/leave the intersection. Figure 7.5 also shows the case of the dedicated left lane intersection with $s = 0.133veh/s$ (left plots) and $s = 0.266veh/s$ (right plots).

Given the increments of just one vehicle at a time, we also represent the arrival and SIMP service curves as linear. Conversely, all other service curves have a clear step-wise

pattern with the step size given by the number of vehicles each IM processes per control cycle (Table 7.2).

Among all IM protocols, SIMP shows the highest average service rate. However, the case of SIMP shared right lane (S/R) requires clarification since the service rate of the right lane ($3veh/11s = 0.27veh/s$) would be higher than the arrival rate ($0.266veh/s$), thus violating the $\alpha(t) > \mu(t)$ condition needed to have traffic accumulation. In this case, we consider that the service rate is truncated to the arrival rate (naturally, the intersection cannot serve more vehicles than those arriving). All other IM protocols respect this condition, thus leading to traffic accumulation.

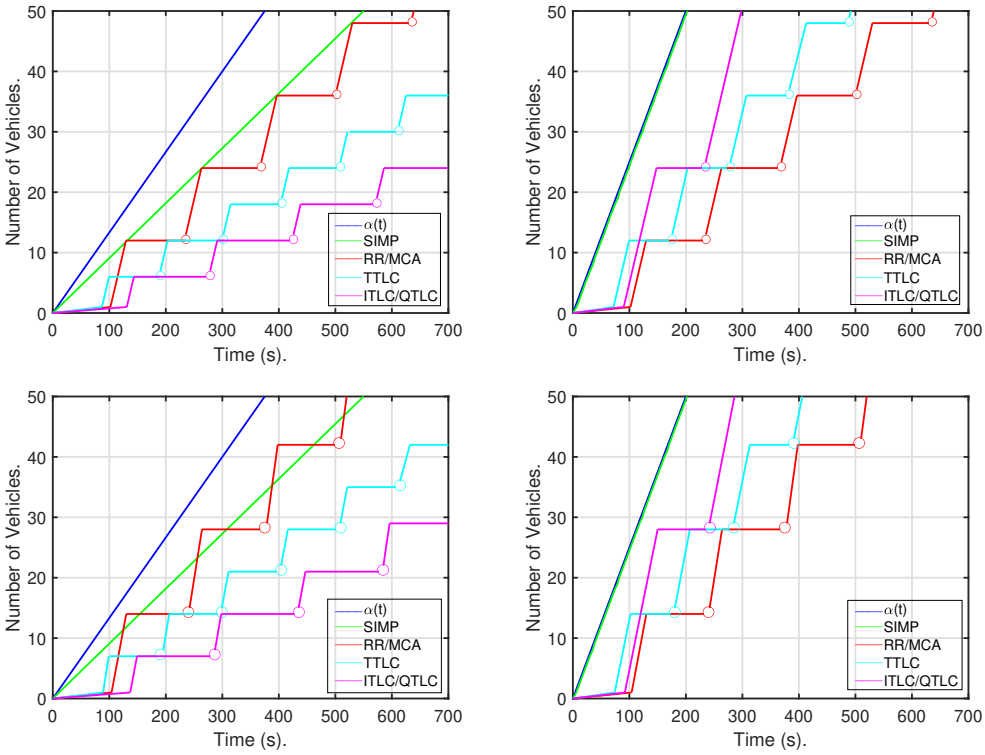

Figure 7.5: Arrival and service curves at $30km/h$ (top) and $50km/h$ (bottom), for the dedicated left lane (left) with $s = 0.133veh/s$, and a shared right lane (right) with $s = 0.266veh/s$.

Another important observation is the relative performance in the average service rate of the other IM protocols beyond SIMP. While RR and MCA serve equally ($12veh$ per cycle, for the left and right lanes, respectively), the left and right lanes (red traces), TTLC, ITLC, and QTLC show a significant asymmetry, which is more pronounced for ITLC and QTLC ($6veh$ against $24veh$ per cycle) than for TTLC ($6veh$ against $12veh$ per cycle). These differences invert the order of the average service rates of these protocols. On the left lane, both TTLC, ITLC, and QTLC are worse than RR/MCA, with ITLC and QTLC being the worst given their relatively poor service in the left lane. Conversely, in the right lane, both TTLC, ITLC, and QTLC are better than RR/MCA, with ITLC and QTLC being

the best given their relatively better service.

Figure 7.6 shows a more expressive version of the dedicated left lane at 30km/h maximum (upper left plot) of Fig. 7.5 in which we consider an arriving burst of $50veh$ injected. We then extended all service curves until they reach $50veh$ so that we can compute for all cases the $WCIST$ and Q_{max} according to Eqs. 7.7 and 7.8.

With SIMP, the last vehicle in each cycle suffers a longer waiting time, given the protocol serving just one vehicle per cycle per lane. Unlike SIMP, in all other IM approaches (RR, MCA, TTLC, ITLC, and QTLC), the first vehicle in each cycle suffers the longest waiting time compared to the other vehicles served in the same cycle (each step). The small circles in the service curves indicate the vehicles that suffer the worst service (Figs. 7.5 and 7.6), and it can be confirmed by visually inspecting the vehicles marked to have a larger time interval (X-axis distance) to the arrival curve (blue line) than those at the end of a cycle. The reason is that the first vehicle, in the worst case, arrives at the intersection entrance when the current red phase starts, thus having to wait for the green phase of the next cycle. Conversely, a vehicle arriving during the red phase when other vehicles are already queued will have to wait for less time for the beginning of the following green phase. Then, during the green phases, the waiting time is also reduced since the dispatch rate is at the maximum speed (see the inclination of the service curves when transitioning between steps). Since the dispatch rate is higher than the arrival saturation rate, traffic accumulation reduces during the green phases.

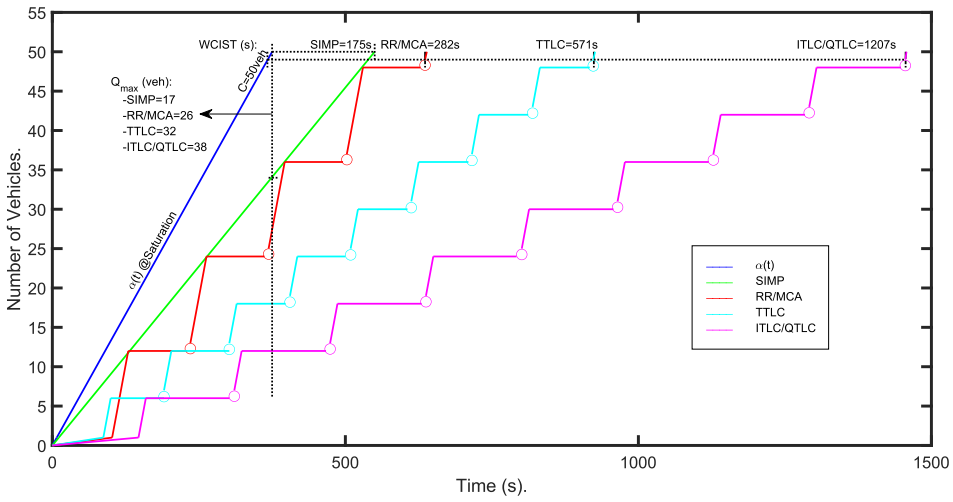

Figure 7.6: Blue: upper bound of the arrival curve at saturation flow conditions; other colors: lower bound of service curves of IM approaches. Dashed horizontal lines show the estimated WCIST with an injected burst of $50veh$. Dashed vertical lines show the estimated Q_{max} for each IM with the same injected burst for each IM.

The maximum vehicle queue length Q_{max} shows how congested the road lane is and specifies the efficiency of IM protocols in tackling the saturation flows. Due to its short control cycle length, SIMP is again the best IM in this aspect, with the lowest Q_{max} values

for all cases in the various tested arrival rates. The other IM approaches show different Q_{max} behaviors depending on their control cycle time.

Finally, we have also studied the arrival-service curves, Q_{max}, and $WCIST$ of all IM protocols at an increased maximum speed of $50km/h$ (lower plots of Fig. 7.5). The results achieved are similar for SIMP since it continues serving the same number of vehicles per cycle. For all other IM protocols, the service is increased since more vehicles can cross the intersection per phase of the control cycle (Table 7.2). Consequently, we observe a reduction in the respective values of Q_{max} and $WCIST$.

7.4.2 Determining Maximum Queue Length and WCIST

One possible way of finding Q_{max} directly consists of direct measurements with the help of deployed road infrastructure. Alternatively, if the distribution of the traffic arrival pattern is known, then it is possible to compute the maximum arrival of vehicles in a given interval with a certain probability. We call them sensor-based and stochastic-based approaches.

7.4.2.1 Sensor-based determination

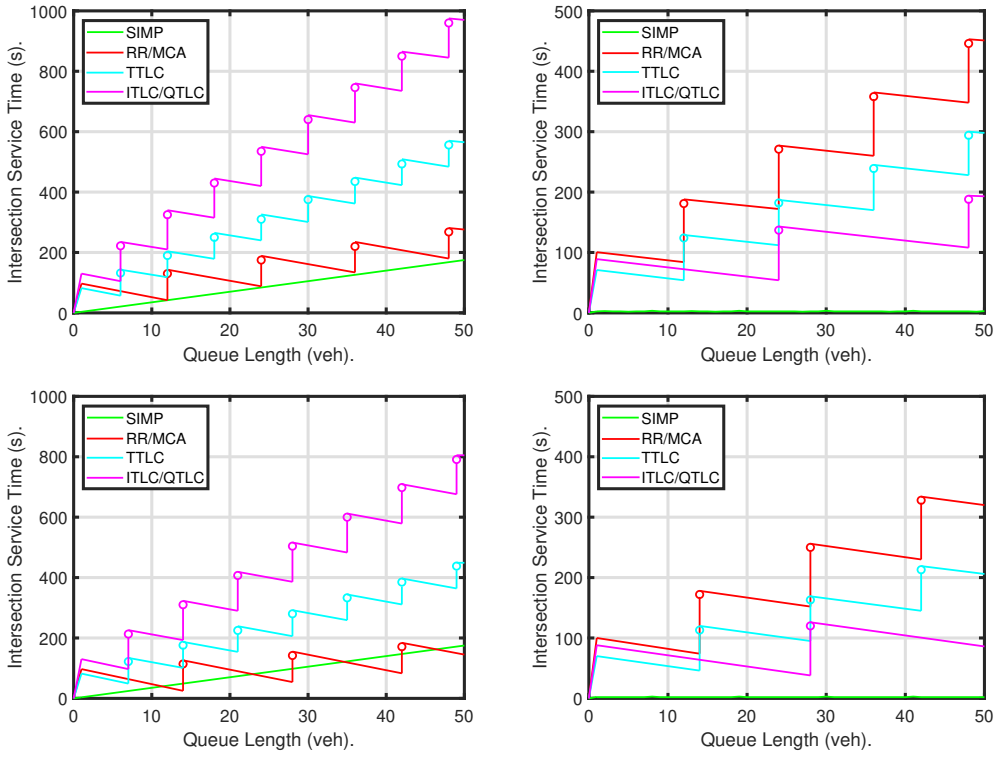

Figure 7.7: Intersection service time (IST) in seconds as a function of the queue length in veh for $30km/h$ (top) and $50km/h$ (bottom) maximum speeds and for the dedicated left lane (left) and shared right lane (right).

In this approach, the queue length is measured using deployed sensors, such as induction loop detectors and cameras, as well as vehicle-to-infrastructure (V2I) communications if available. Then, Q_{max} is estimated after observing the queue length for a sufficiently long interval. Knowing Q_{max}, $WCIST$ can be obtained directly from Eq. 7.5.

Figure 7.7 displays the IST for the last vehicle in the queue as a function of the queue length for all IM protocols and both dedicated left and shared right lanes (corresponding to the same cases in Figure 7.5). The results indicate that the vehicles in the left lane (left plots) suffer longer waiting times for all IM approaches than vehicles in the right lane (right plots), except RR and MCA. This is due to the lower bandwidth of the service provided by the IM protocols in the left lane, except for the two referred. Remember that SIMP, in the right lanes (right plots) is able to serve the saturation arrival rate without queuing, thus the IST is constant and the lowest possible, at $4s$.

Finally, Figure 7.7 also shows the effect that IST reduces during service phases, as we discussed already. The $WCIST$ per service phase occurs for the first vehicle of that phase (queue sizes immediately after the small open circles).

7.4.2.2 Stochastic-based burst determination

In this case, we consider that the traffic arrival pattern follows a known distribution. In this case, we consider a Poisson distribution (Eq. 7.9) since the vehicles arrive independently of each other. Knowing the distribution, we can compute the maximum number of vehicles (x) arriving in a specific interval t given the desired probability. We use this to determine the saturation volume x_s with two desired probabilities (or confidence levels), namely 99% and 99.9%. Then we can deduce Q_{max} using Eq. 7.7.

$$P(x \text{ vehicles in interval } t) = \frac{(\lambda t)^x e^{-\lambda t}}{x!} \tag{7.9}$$

One interesting feature of this approach is that, for each desired probability, Q_{max} comes as a function of the long-term average vehicles arrival rate λ, with Q_{max} bounded by the lane capacity C and λ constrained to be less than the corresponding saturation flow rate s. Thus, knowing λ we can compute x_s and Q_{max}. To compute x_s, we increment the number of vehicles x one by one, computing for each number the time t corresponding to the arrival of x vehicles at the saturation flow rate s. We use these values in Eq. 7.9 and compute the associated probability. We increment x until the achieved probability exceeds the defined threshold (confidence level).

The left plot of Figure 7.8 presents the values of x_s using Eq. 7.9 with probability values of 99% and 99.9%. It also shows the observed maximum vehicle burst (via SUMO simulator) as a function of λ (left plot). We used a single inflow lane with a single injecting point to obtain these values. Note that these values, i.e., vehicle arrivals, are independent of the intersection. The maximum burst was observed in SUMO during a simulated time of 40h and using the vehicle parameters in Table 3.1. We observed a burst behavior that

grows for growing values of λ until $0.06veh/s$ and then saturates at $10veh$. We believe SUMO induces this saturation, but the concrete reason remains to be uncovered. More interestingly, the observed bursts for lower values of λ are between the value of x_s for the probabilities of 99% and 99.9%.

Figure 7.8 also presents the $WCIST$ values provided by the different IM approaches using Eq. 7.8 (center plot for the left lane and right plot for the right lane) and associated with x_s values of 99.9% confidence. Though not shown, the WCIST values for x_s values with 99% confidence are necessarily lower or equal, given that fewer cars arrive with this probability. For these WCIST values, first, we calculate the IST values for each vehicle on each road lane, which will serve as the WCIST based on the Q_{max} estimated earlier for each road lane. Thus the maximum value of the WCIST of all inflow lanes can be considered as the WCIST of the entire IM approach with respect to λ.

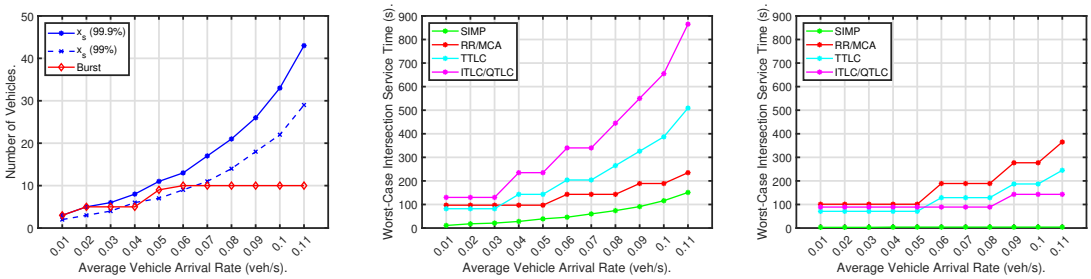

(a) x_s and burst (veh). (b) WCIST for the lane L. (c) WCIST for the S/R lane.

Figure 7.8: Maximum burst x_s (left) and $WCIST$ against the long-term average vehicle arrival rate in veh/s considering x_s values with 99.9% confidence for left lanes (center) and right lanes (right).

7.4.3 Simulation-based Characterization

7.4.3.1 Simulation Setup

To validate the analytical results, we ran simulations using the SUMO. As of our analytical analysis, the six IM protocols (SIMP, RR, MCA, TTLC, ITLC, and QTLC) were applied to an isolated four-way two-lane intersection. Two maximum speeds ($30km/h$ and $50km/h$) were tested with acceleration ($2.6m/s^2$), deceleration ($-4.5m/s^2$), and emergency deceleration ($-9m/s^2$) respecting typical urban mobility settings. The summary of simulation parameters and assigned values are similar to the ones presented in Table 3.1.

For Q_{max} (Fig. 7.9), the traffic generation follows the Poisson distribution similar to what we considered in the previous section. However, we separated the injection into the two lanes of each road instead of using a single injection as we described before. This separation was relevant, here, to fully respect the generation distribution per lane, avoiding the potential interference that the single injection point could create.

7.4.3.2 Maximum Queue Length

For Q_{max} analysis, we analyzed traces of $30h$ of simulated time with various long-term average arrival rates, namely $\lambda = 0.01$ to $0.11veh/s$. We measure Q_{max} by counting the vehicles from the intersection entrance until the last consecutive vehicle moving at or below $5km/h$. Figure 7.9 illustrates the observed Q_{max} for both maximum speeds, i.e., $30km/h$ (top) and $50km/h$ (bottom) for both the left lane (left) and the right lane (right).

At $30km/h$ maximum speed, SIMP shows the best performance on both lanes with lower Q_{max} values. Particularly, SIMP-produced Q_{max} is below $10veh$ with up to $0.06veh/s$ in the left lane and up to $0.07veh/s$ in the right lane. For the same arrival rates, the Q_{max} of TTLC reaches the lane capacity being the worst performing approach. The other IM approaches show, in the left lane, a closely interchangeable relation among RR, MCA, ITLC, and QTLC where ITLC reaches the lane capacity level first. In the right lane, QTLC is the second best-performing approach after SIMP for lower arrival rates. In general, most IM approaches start saturating for λ above $0.05veh/s$. After TTLC, the order IM approaches to reach the lane capacity are ITLC and MCA, QTLC and RR, and in the end, SIMP. Similar observations can be made with the maximum speed of $50km/h$.

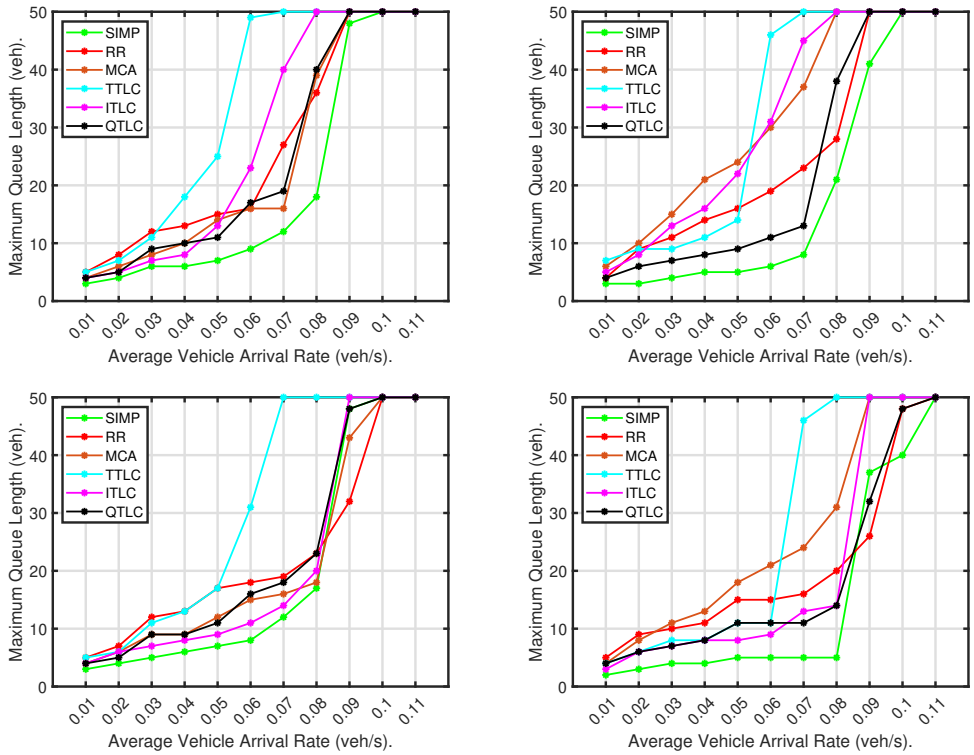

Figure 7.9: IM induced Q_{max} in veh against the long-term average vehicle arrival rate in veh/s for the left-crossing lane (left) and right lane (right) at $30km/h$ (top) and $50km/h$ (bottom) maximum speeds and capacity $C = 50veh$.

SUMO also provides a direct assessment of Q_{max} in each of the simulation traces. In most cases, both SUMO and our sensor-based approaches provide similar results with a

difference of one to two vehicles. In a few cases, the SUMO-produced Q_{max} results are much higher. A possible reason is that SUMO may consider vehicles moving below $5km/h$ speed on the entire road lane instead of consecutive from the intersection entrance.

7.4.3.3 Response Time of non-Saturated Traffic Flow

As defined earlier, the RT includes both the vehicle time to join the queue and the IST upon joining the queue. Note that the IST comprises both the queuing time and intersection crossing time. In this section, first, we present the queue joining time, then the IST, and in the end, the RT (QT + IST). For this non-saturated scenario, we use the same traffic generation as in the analytical characterization, with a single injection point per road, following a Poisson distribution. The crossing directions are uniformly distributed for left (33%), straight (33%), and right (33%).

Therefore, the right lane accommodates $0.067veh/s$ of the injected vehicles, and the left lane accommodates the remaining $0.033veh/s$. We generated the FCD data for these experiments using the same SUMO simulator for 1000 vehicles injected in each road at a long-term average arrival rate of $\lambda = 0.1veh/s$.

Queue Joining Time

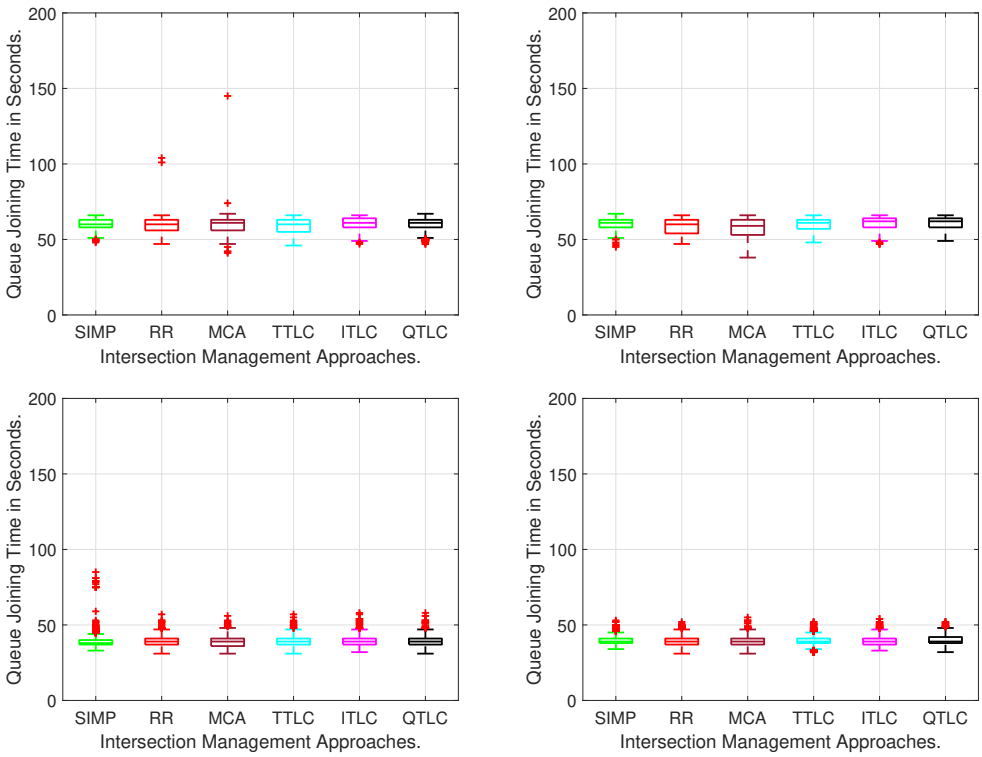

Figure 7.10: Observed queue joining time (s) of 1000 vehicles for $30km/h$ (top) and $50km/h$ (bottom), L-crossing (left) and S/R-crossing (right) at $\lambda = 0.033veh/s$ and $0.067veh/s$ respectively, and $C = 50veh$.

Queue joining time is when vehicles approach the intersection entrance or join the queue before accessing the intersection. We consider that in this period they travel close to the maximum speed. However, vehicles are injected with zero speed, taking about $4s$ to reach maximum speed. This may influence the following injected vehicles to comply with the safety distance. Whenever a burst of vehicles is injected with inter-injection times below $4s$, the following vehicles speed profiles are adjusted so they respect the minimum inter-vehicle distance. This creates a leader-follower dependency following the first vehicle in the burst. This may lower the actual travel speed of the vehicles, thus influencing the queue joining time.

Figure 7.10 illustrates with boxplots the observed queue joining time of 1000 vehicles for both L-crossing and S/R-crossing lanes at both maximum speeds. The joining times are naturally lower for higher speeds, so as their variation. There are occasional outliers that correspond to vehicles that find no queue. At lower speeds, the IM policies that generate longer queues also tend to generate shorter joining times.

Intersection Service Time

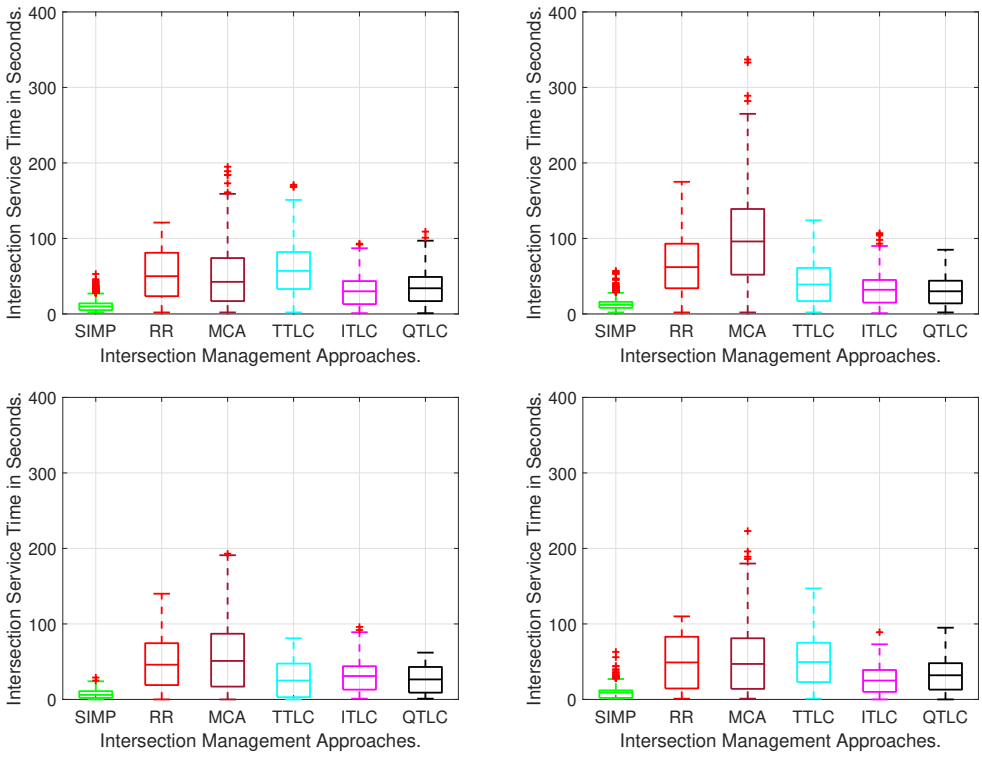

Figure 7.11: Observed intersection service time (s) of 1000 vehicles for $30km/h$ (top) and $50km/h$ (bottom), L-crossing (left) and S/R-crossing (right) lanes at $\lambda = 0.033veh/s$ and $0.067veh/s$ respectively, and $C = 50veh$.

Once vehicles join the queue, they take the IST to be served by each IM approach. From the FCD data, the observed intersection crossing times are below $4s$ depending on

the crossing directions, being shorter for right-crossing.

Figure 7.11 displays the IST results for both speeds and crossing lanes with different IM approaches showing different distributions. At both maximum speeds and crossing lanes, in all three cases (highest, lowest, and median), SIMP is the best performing approach with the lowest IST values. The following best approaches are ITLC and QTLC. Overall, MCA exhibits poor performance due to its working nature, since the green phase circulation is based on the instantaneous traffic flow. Thus, MCA may let vehicles of lanes with instantaneously less traffic wait for more cycles.

Response Time

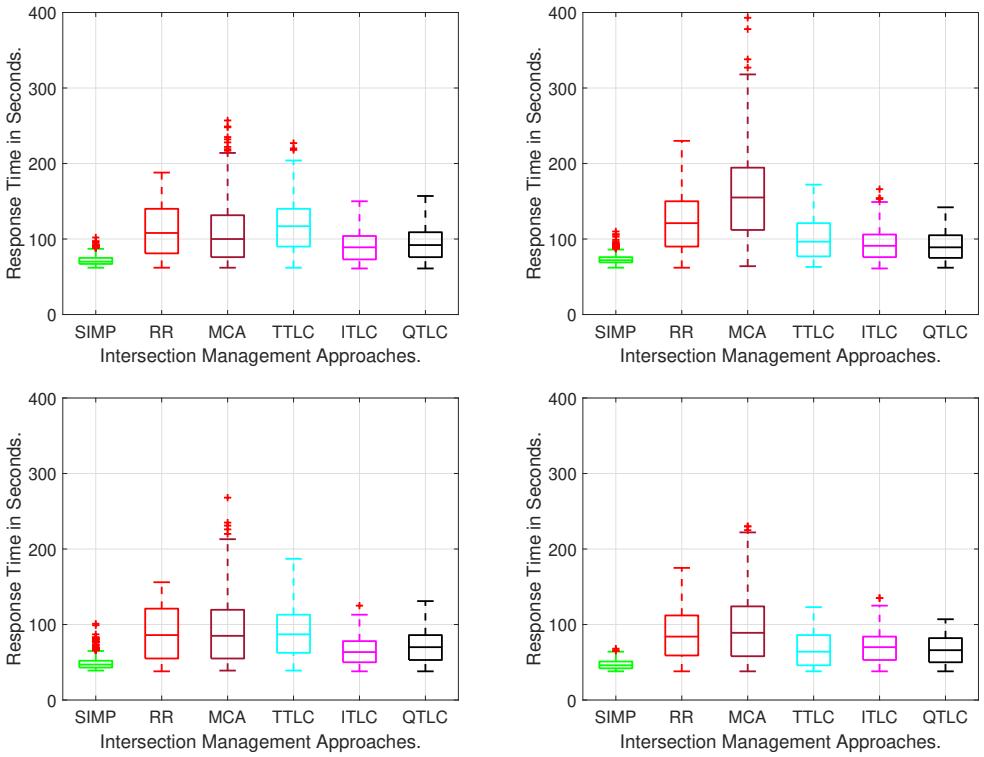

Figure 7.12: Observed response time (s) of 1000 vehicles for $30km/h$ (top) and $50km/h$ (bottom), L-crossing (left) and S/R-crossing (right) lanes at $\lambda = 0.033veh/s$ and $0.067veh/s$ respectively, and $C = 50veh$ (non-saturated traffic).

As specified earlier, RT is the combination of queue joining time and IST, and their individual results show the highest values that are imposed by the IST and the lowest values are imposed by the queue joining time; and different IM approaches behave differently for both measures. The RT results provide the overall efficiency of IM approaches in non-saturated traffic scenarios. The RT results for both maximum speeds and crossing lanes are presented in Fig. 7.12. From these results, the following observations can be made. SIMP is the best-performing approach on both crossing lanes and maximum speeds. The following best approaches are the ITLC and QTLC, and their performance order changes

from the L-crossing lane to the S/R-crossing lane. Similar behavior can be observed with the RR and TTLC, but it changes with the speed, i.e., from L-crossing $30km/h$ to S/R-crossing $50km/h$ and vice versa. In the end, MCA is the poorest-performing IM approach with the highest RT values. When we compare both the L-crossing and S/R-crossing results of MCA, the highest RT values at $30km/h$ can be noticed in the S/R-crossing lane, while at $50km/h$ it is in the L-crossing lane.

7.4.3.4 Response Time of Saturated Traffic Flow

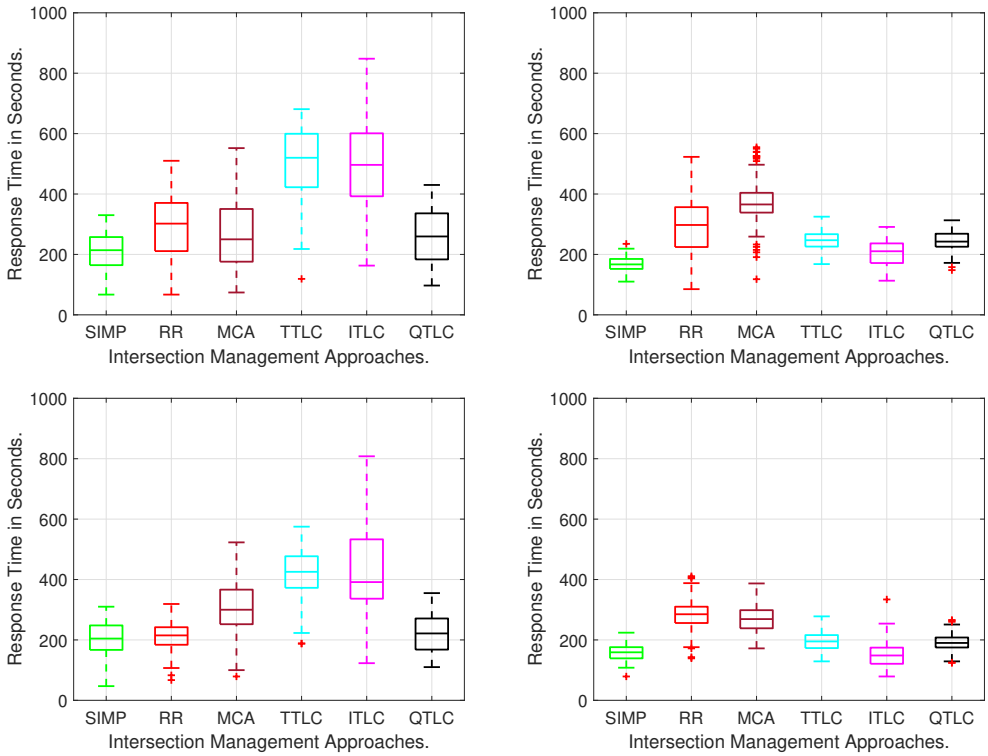

Figure 7.13: Observed response time (s) of 50^{th} vehicle for $30km/h$ (top) and $50km/h$ (bottom), L-crossing (left) and S/R-crossing (right) lanes at $\alpha(t) = 0.4veh/s$ and $C = 50veh$ (saturated traffic).

For analyzing response time during saturated traffic conditions, we ran 100 simulations at a long-term average rate of $0.4veh/s$ for $1000s$. We let the traffic flow during the first 100s to avoid bias caused by initialization and then we analyzed the response time of the 50^{th} vehicle injected after the initial 100s period. We believe the 50^{th} vehicle is close to a worst-case situation, being already unaffected by the initial conditions while the road capacity is not yet flooded in any of the protocols. For this scenario, the traffic generation follows the same pattern as the previous case but with a long-term average arrival rate of $\lambda = 0.4veh/s$, divided uniformly among the three crossing directions. Therefore, the S/R-crossing lane accommodates 67% of vehicles at $0.267veh/s$, and the L-crossing lane accommodates the remaining 33% of vehicles at $0.133veh/s$. The road capacity is also

considered to be $C = 50veh$. The achieved RT results for the 50^{th} vehicle in all scenarios are presented as boxplots in Figure 7.13 for L-crossing (left plot) and S/R-crossing (right plot) lanes for $30km/h$ (above) and $50km/h$ (below). The highest RT presented serves as the *observed* WCRT.

At 30km/h maximum speed, SIMP shows the lowest RT results for both the maximum and median cases in both S/R- and L-crossing lanes, similar to the non-saturated traffic flow results. TTLC and ITLC exhibit a significantly higher RT in the L-crossing lanes due to the lower bandwidth they offer to these lanes. Conversely, for S/R-crossing lanes, both RR and MCA show higher RT values. When we increase the maximum speed to 50km/h (lower plots) the RT values generally decrease in all IMs, approximately maintaining their relative behavior. However, in this case the advantage of SIMP over all other IMs is lost, performing similarly to RR in the L-crossing lanes (left plot) and to ITLC in the S/R-crossing (right plot) lanes.

7.4.3.5 Worst-Case Response Time

Since the WCRT values produced by Eqs. 7.1 and 7.5 are higher than those produced by Eqs. 7.1 and 7.8, given that Eq. 7.5 considers whole cycles, we use Eq. 7.5 for the sake of safety of the analysis.

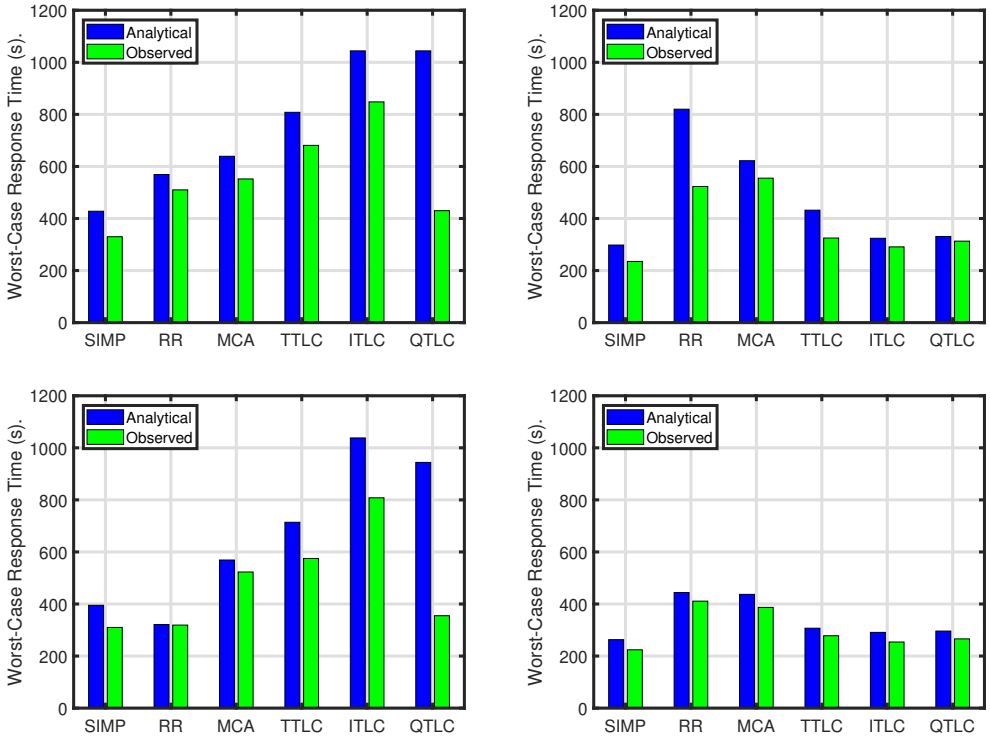

Figure 7.14: Worst-case response time (s) for L-crossing (left) and S/R-crossing (right) lanes at $30km/h$ (top) and $50km/h$ (bottom), $\alpha(t) = 0.4veh/s$, and $C = 50veh$ (saturated traffic).

Figure 7.14 shows the analytical and observed WCRT values (i.e., the highest RT values) for both $30km/h$ (above) and $50km/h$ (below) maximum speeds and L-crossing (left) and S/R-crossing (right) lanes. The first and primary remark is that the observed WCRT values of all IM approaches are below the analytical WCRT values, providing an empirical validation of the WCRT analysis we proposed earlier. Hence, we confirm to some degree of confidence that the analytical WCRT provides upper-bound values to RT, as no empirical observation from the simulations was higher than those values. A second conclusion is that the proposed WCRT analysis offers a level of pessimism that is different for the L-crossing and the S/R-crossing lanes, being particularly low in the second case. Nevertheless, two cases depart from the global pattern, QTLC in L-crossing lanes for both maximum speeds and RR in S/R-crossing lane for 30km/h maximum speed. We believe the pessimism of QTLC emerges from pessimistic assumptions in the analysis that did not capture its adaptation capacity. For RR we believe the pessimism results from a limited simulation time that did not capture worst-case conditions. Removing these outlying cases, on average the computed WCRTs in saturated conditions were 17.6% ($30km/h$) and 17.95% ($50km/h$) above the observed ones in the L-crossing lanes and 15.3% ($30km/h$) and 11.51% ($50km/h$) in the S/R-crossing lanes.

7.5 Networks of Multi-lane Intersections

In the previous section, we evaluated the WCRT for isolated four-way two-lane intersections when the left lane is dedicated by employing sensory- and stochastic-based approaches for determining Q_{max}. This section evaluates the WCRT for the same two-lane four-way intersections but for both dedicated and shared left-lane configurations in a network of four intersections. Accordingly, the maximum WT analysis will first be presented, then the WCRT analysis.

7.5.1 WCRT of Road Networks

We consider the same 2×2 grid network presented in Fig. 6.1 with multi-lane signalized intersections. The focus is only on the external inflow lanes, i.e., those receiving traffic from the outside grid. Since the target is to compare the WCRT of different IM approaches used in the intersections, the traffic must be balanced on all edges (lanes connecting intersections). We achieve this by fixing the routes for all possible destinations reachable from one intersection. For example, the routes of w_2 and n_1 from I_0 are presented in Figs. 6.3 (dedicated left lane configurations) and 6.4 (shared left lane configurations). We rotate the same route patterns and apply them to the traffic arriving at all four intersections. Moreover, we generate the destinations randomly and uniformly for each inflow lane among all seven possibilities.

As presented in Eq. 7.1, the WCRT is a combination of queue joining time, waiting time, and intersection crossing time. First, we analyze the maximum waiting time, as

specified earlier. The waiting time delay, also called the stopped delay, occurs when a vehicle stops at the intersection entrance due to red signals (empty roads) or waiting in the queue (non-empty roads) to access the intersection. In Fig. 7.1, this waiting time is shown in red color between t_2 (after deceleration) and t_3 (before acceleration); thus, the WT suffered by vehicle x at intersection I is $WT_{I(x)} = t_3 - t_2$. To characterize the intersection I, we compute the maximum waiting time overall for vehicles that cross it ($WT_I = max_x(WT_{I(x)})$) using Eq. 7.3. We can also define the maximum waiting time along a specific route of intersections $\mathcal{I}$ as $WT_{\mathcal{I}} = \sum_{\forall I \in \mathcal{I}} WT_I$. For the n_1 case of the dedicated left lane intersections (Figure 6.3), $\mathcal{I}_{n_1}$ may include I_0^R (turning right at I_0), I_0^L and $I_1^{L,S}$ (turning left at I_0 and then left or straight at I_1), I_0^S and $I_3^{R,S}$, or finally I_0^L, I_1^R and $I_2^{L,S}$. Eq. 7.10 gives the corresponding maximum waiting time.

$$WT_{\mathcal{I}_{n_1}} = \begin{cases} WT_{I_0^R}, & \text{if } \mathcal{I}_{n_1} = \{I_0\} \\ WT_{I_0^L} + WT_{I_1^{L,S}}, & \text{if } \mathcal{I}_{n_1} = \{I_0, I_1\} \\ WT_{I_0^S} + WT_{I_3^{R,S}}, & \text{if } \mathcal{I}_{n_1} = \{I_0, I_3\} \\ WT_{I_0^L} + WT_{I_1^R} + WT_{I_2^{L,S}}, & \text{if } \mathcal{I}_{n_1} = \{I_0, I_1, I_2\} \end{cases} \tag{7.10}$$

Equation 7.11 gives the maximum waiting time of w_2 route case for the shared left lane intersections (Figure 6.4).

$$WT_{\mathcal{I}_{w_2}} = \begin{cases} WT_{I_0^{L,S}}, & \text{at } \mathcal{I} = \{I_0\} \\ WT_{I_0^{L,S}} + WT_{I_1^{L,S}}, & \text{at } \mathcal{I} = \{I_0, I_1\} \\ WT_{I_0^{R,S}} + WT_{I_1^S}, & \text{at } \mathcal{I} = \{I_0, I_1\} \\ WT_{I_0^{R,S}} + WT_{I_3^{R,S}}, & \text{at } \mathcal{I} = \{I_0, I_3\} \\ WT_{I_0^{R,S}} + WT_{I_3^{L,S}}, & \text{at } \mathcal{I} = \{I_0, I_3\} \\ WT_{I_0^{R,S}} + WT_{I_3^{L,S}} + WT_{I_2^S}, & \text{at } \mathcal{I} = \{I_0, I_3, I_2\} \\ WT_{I_0^{R,S}} + WT_{I_3^{L,S}} + WT_{I_2^{S,R}}, & \text{at } \mathcal{I} = \{I_0, I_3, I_2\} \end{cases} \tag{7.11}$$

Similarly to the maximum waiting time delays (Eqs. 7.10 and 7.11), the WCRT over a specific route of intersections can be defined by adding the QT and ICT.

7.5.2 Analytical Results

Figures 7.15a and 7.15b present the maximum waiting time (s) of S/R-crossing ($j = 1$) and L-crossing ($j = 2$) lanes at a single intersection as a function of Q_{max}, using Eq. 7.3. Note that, in the case of the shared left-lane intersections, $j = 2$ hosts both straight- and left-crossing vehicles. We consider road lanes full capacity $C = 50$ and the IM-specific parameters presented in Table 7.3.

The results of Eq. 7.3 can then be used in Eqs. 7.10 and 7.11 to compute the maximum waiting time delay for each concrete route. The step size in the traces in Figs. 7.15b

Table 7.3: Summary of the IM approaches under comparison.

IM	**Cycle Time (s)**	Green time (s)		No. of vehicles (30km/h)	
		S/R	L	S/R	L
SIMP	11	2.5	3	3	1
RR	136	30	30	12	12
MCA*	136	30+	30+	12+	12+
TTLC	106	30	15	12	6
WTLC	[136 180]	[30 41]	[30 41]	[12 16]	[12 16]

and 7.15a depend on the number of vehicles that the IM approach serves during the green phase from each road lane, i.e., the higher green phase time leads to a bigger step size. From the graphs, it is clear that the lowest waiting time values are obtained with the SIMP protocol in both L and S/R lanes, and we represent it with a linear behavior because of its very short cycle time. Thus, the queues last vehicle (i.e., 50th) experiences maximum waiting delays. Conversely, for the other approaches, the first vehicle in every cycle undergoes maximum waiting delays as the following vehicles join the queue later.

Among all IMs but SIMP, none dominates the other ones for the full range of possible Q_{max}. However, for $Q_{max} \geqslant 18$ vehicles, TTLC exhibits lower maximum waiting delays than the others in the S/R lanes, while it presents higher maximum waiting delays in the L lanes due to offering a lower service time. Note that the acyclic nature of MCA will adapt the green phase time dynamically based on the traffic flow movements. Thus, in Figs. 7.15a and 7.15b, we represent the worst-case behavior of this IM approach. For WTLC, we explicitly represent the service with the minimum and maximum cycle times. Finally, the value of Q_{max} depends on the interaction between the IM approach and the arrival pattern in each lane. The two possible ways of finding the Q_{max} are either measured directly using road infrastructures or the distribution of traffic arrival patterns. In the analysis, we consider the Q_{max} values using the initial method while the work on the latter method is left for future work.

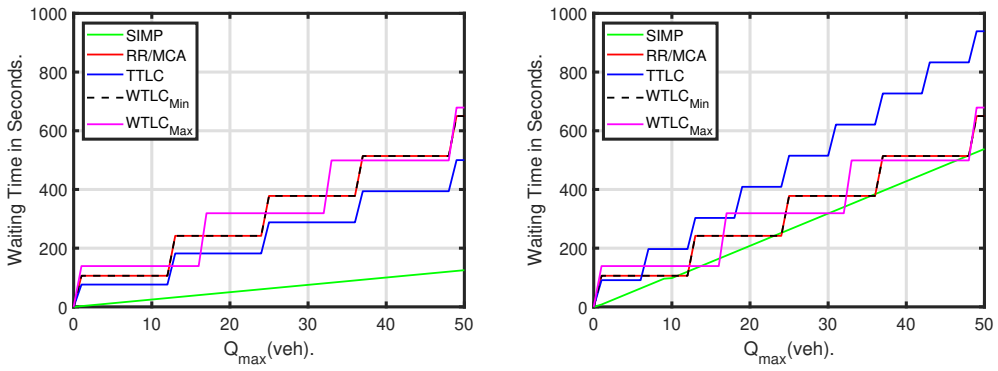

(a) Waiting time (s) on S/R lane.

(b) Waiting time (s) on lane L.

Figure 7.15: Waiting time delay (s) for various IM approaches with $C = 50$ on S/R- and L- lanes.

We present the analytical WCRT values on Fig. 7.16 for both S/R-crossing (Fig. 7.16a) and L (Fig. 7.16b) lanes at $Q_{max} = C = 50$ vehicles and for the IM specific values mentioned in Table 7.3.

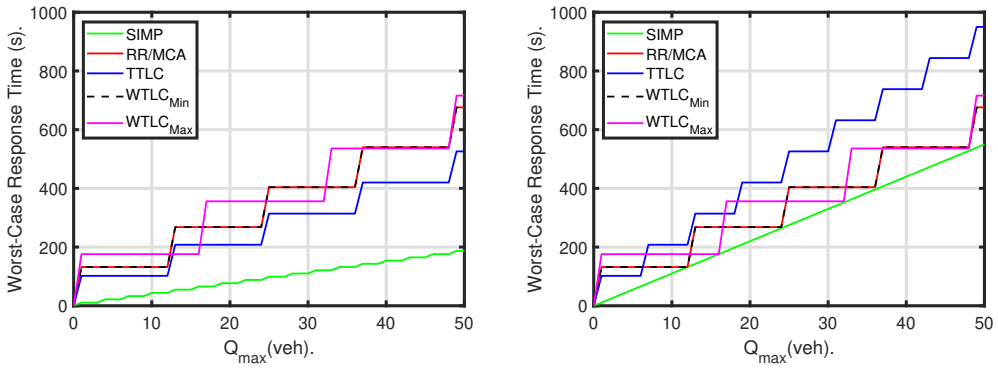

(a) WCRT (s) on S/R lane.

(b) WCRT (s) on lane L.

Figure 7.16: WCRT (s) for various IM approaches with $C = 50$ on S/R- and L- lanes.

In Fig. 7.16, we presented the RR, MCA (minimum green time), and WTLC (minimum cycle time) with a single line due to the traces achieved based on their green and cycle times. Different step sizes in the plots indicate the different numbers of vehicles that each IM discharges from L (L/S-) and S/R- lanes per green phase. The difference between the maximum WT results (Fig. 7.15) and WCRT results (Fig. 7.16) is the QT and ICT values that the WCRT consists of.

Overall, SIMP's WCRT values are the lowest with almost linear growth (smallest step sizes) as it serves one (L-crossing) or three (S/R-crossing) vehicles per shortest cycle time of $11s$. When the percentage of the R-crossing vehicles is lowest, we suggest using the L-crossing WCRT values for S/R-crossing lanes, too, as it serves one vehicle per cycle.

RR, MCA, and WTLC (min. and max.) show similar step sizes but interchange among them as these IM approaches permit vehicles from one road only (both L/S- and S/R-crossing lanes) at a time. Among this group, WTLC with maximum cycle time exhibits the lowest WCRT values for the queue length between 12 and 48 vehicles while the highest WCRT values for other queue length values.

7.5.3 Simulation Settings

Two simulation scenarios are designed to compare the waiting time performance of five state-of-the-art IM approaches presented in Table 7.3 (RR, TTLC, MCA, WTLC, and SIMP). In scenario-1, all intersections are configured with dedicated left lanes. In scenario-2, all intersections are configured with shared left lanes. Note the IM approaches operate at individual SIs without coordination and cooperation. The random traffic injection on all external inflow lanes in both scenarios follows the *Poisson distribution*. A set of four average traffic arrival rates (0.025, 0.05, 0.067, and 0.1) in veh/s are used in sequence, each

for $1h$; thus, the total simulated time is approximately $4h$. We simulate a long run until all the injected vehicles exit the road network. Once the last vehicle of the current arrival rate exits the grid network, then only the vehicles of the following arrival rate are injected. These rates cover from low to medium and near saturated traffic conditions. Note that at $0.133veh/s$, some of the IM approaches (e.g., TTLC) are already oversaturated [181], so the presented analytical WCRT models are no longer applicable, and additional parameters must be considered to analyze these oversaturated traffic conditions. The path of the injected vehicles follows predefined routes by picking them randomly and uniformly, as described in the previous chapter (Figs. 6.3 and 6.4). The simulation parameters and associated values are similar to the ones presented in Table 3.1 and scenarios 1 and 2 of the previous chapter (Section 6.3). We tested only the $30km/h$ maximum speed with 50% HVs and 50% AVs.

7.5.4 Maximum Waiting Time Results

The waiting time results of the two scenarios were presented by grouping vehicles according to the number of intersections they crossed. We show both analytical (using Eqs. 7.10, 7.11 and 7.3) and SUMO-provided waiting time results. For crossing a single intersection, our analysis provides a single analytical value (marked with $\times$). However, for WTLC and MCA, we provide two values (marked with $\times$ and $\times'$). These correspond to the minimum and maximum cycle times (WTLC) or an under or over-approximation of a cyclic behavior (MCA). When vehicles cross more than one intersection, Eq. 7.10 generates multiple results depending on the specific paths taken. We represent the lowest values obtained (marked with $\times$) and the highest ones (marked with a black $+$). For WTLC, we also represent the lowest value with the minimum cycle time (marked with $\times'$). Finally, we indicate the IM approaches with extension $*-D$ and $*-S$ for the dedicated (scenario-1) and shared (scenario-2) left lanes, respectively.

7.5.4.1 Scenario 1

Figure 7.17 shows the waiting time delays of scenario-1 (dedicated left lane intersections). SIMP exhibits the lowest waiting time values (overall below $135s$), dominating all three cases in analytical and simulation results. The observed (simulation) values are significantly lower, though, showing pessimism in the analysis, which decreases for longer paths. The difference between analytical and maximum observed values for three intersections is below $20s$. The same pattern of higher pessimism of the analysis for single intersection paths, reducing for longer paths, is visible in all IM approaches. Due to its adaptive behavior, MCA shows a larger spreading of values in simulation with a single intersection (Fig. 7.17a). This case also shows that the analysis can be optimistic when under-approximating the cyclic behavior. The analysis always provided upper bounds for the observed waiting times for all other IMs.

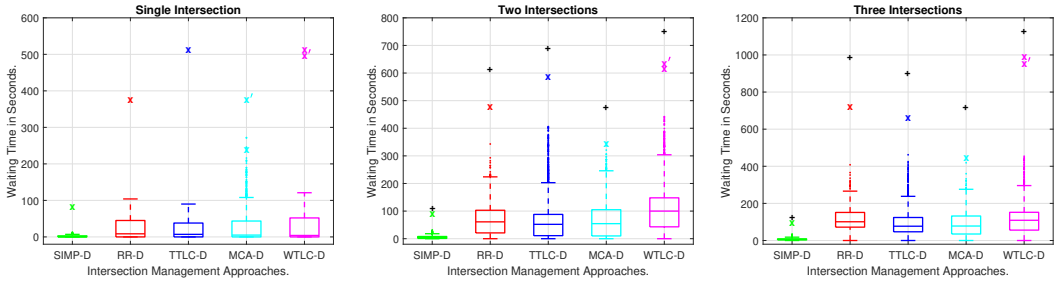

(a) WT (s) of 1039 vehicles. (b) WT (s) of 3993 vehicles. (c) WT (s) of 1948 vehicles.

Figure 7.17: Waiting Time (s) of scenario-1 for 6980 vehicles crossing one (a), two (b), and three (c) intersections.

Concerning the observed (simulation) results, SIMP stands out with significantly lower values and dispersion. The median value of SIMP in a single intersection (Fig. 7.17a) is $0s$, followed by WTLC with $4s$. When the vehicles cross two intersections (Fig. 7.17b), the median value of SIMP is $5s$, followed by TTLC with $52s$ (more than 10 times the median of SIMP). Crossing three intersections (Fig. 7.17c), SIMP median is $6s$, while the following best approaches are TTLC and MCA with $77s$ ($\sim$ 13 times more than that of SIMP). In all three cases, the worst-performing approaches are RR with $8.5s$ when crossing a single intersection and WTLC with $100s$ and $109s$ in the other two cases, respectively.

7.5.4.2 Scenario 2

Fig. 7.18 shows the waiting time delays of scenario-2, i.e., when the intersections use shared left lanes. As the left lane is shared by the straight and left crossing vehicles, the queue lengths and associated waiting time delays are generally reduced. The analysis becomes, then, less pessimistic. We also see this pessimism reducing when the paths include more intersections. The only exception is TTLC. It has specific phases with shorter green time to handle left lanes, which are served simultaneously from opposite roads. In this case, a straight-crossing vehicle can block a left crossing one or vice versa. This leads to increased pessimism about the analysis (single intersection) and a higher spread of the waiting times with two and three intersections.

As in the previous scenario, SIMP is the best-performing approach with the lowest waiting time delays, followed by RR, WTLC and MCA, with TTLC being the worst due to the aspects just referred.

Concerning the distribution of the simulation results, SIMP is the best-performing approach in all three cases with median values of $0s$ (single intersection), $4s$ (two intersections), and $5s$ (three intersections), respectively, and very tight dispersion. The following best approaches are WTLC with $1s$ median (single intersection) and MCA with $48s$ and $51s$ median with two and three intersections. The worst performing ones are TTLC with $7s$, WTLC with 82, and RR with $98s$ medians for one, two, and three crossed intersections, respectively.

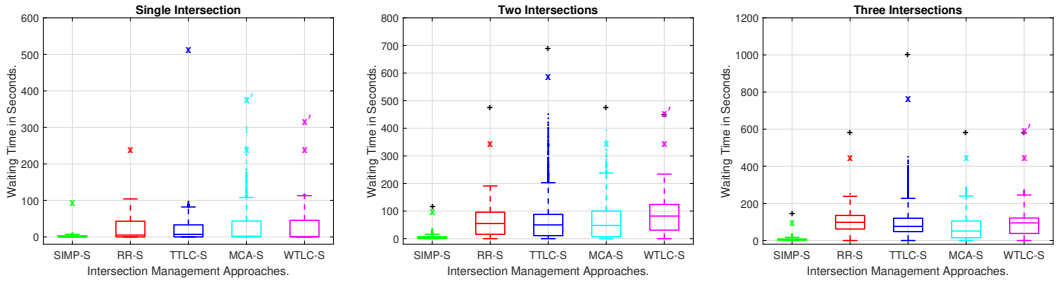

(a) WT (s) of 1039 vehicles. (b) WT (s) of 3993 vehicles. (c) WT (s) of 1948 vehicles.

Figure 7.18: Waiting Time (s) of scenario-2 for 6980 vehicles crossing one (a), two (b) and three (c) intersections.

7.5.5 Worst-Case Response Time Results

Figure 7.19 exhibits both analytical and observed (SUMO generated) WCRT results of road networks for dedicated and shared left lanes (scenarios 1 and 2) at $30km/h$ (i.e., $8.33m/s$) maximum speed. For analytical WCRT values, an average speed of $7m/s$[1] (below $8.33m/s$) is considered in Eq. 7.2, and the Q_{max} values are already known from the maximum waiting time analysis. As discussed earlier, a $5s$ ICT value per intersection crossing is considered; thus, the ICT values are $10s$ and $15s$ for crossing two and three intersections.

The primary observation is that the observed WCRT results are below the analytical WCRT values for all IM approaches in both scenarios, except for the MCA. MCA is a unique case due to its acyclic nature (as explained in 3.6), for which an additional control cycle time is added to the analytical values in both scenarios and the number of intersections crossing, except at three intersections configured with the shared left lanes (Fig. 7.19f). Therefore, to some degree of confidence, we confirm that the analytical WCRT is upper-bounded to RT. As in the previous cases (isolated intersections WCRT), the analytical WCRT values are pessimistic as Eq. 7.3 considers the full TLC cycle time. Regarding the dedicated left lanes scenario, TTLC exhibits the highest pessimism at single and two intersections, while at three intersections, it is the WTLC (Fig. 7.19e). Contrary behavior can be observed between WTLC and TTLC concerning the second-highest pessimism. The SIMP protocol shows the lowest pessimism. In the shared left lane configurations, TTLC and RR are the first and second approaches to show the higher pessimism levels. The WTLC (two and three intersections) and SIMP (single intersection) show the lowest pessimism. On average, the estimated WCRT values in saturated conditions were 86.7% (64.5%), 49.5% (34.2%), and 47.6% (30.25%) higher than the observed ones at single, two, and three dedicated and shared left lane intersections, respectively.

[1]Note that, even with $8m/s$ maximum speed, the QT differences are minimal.

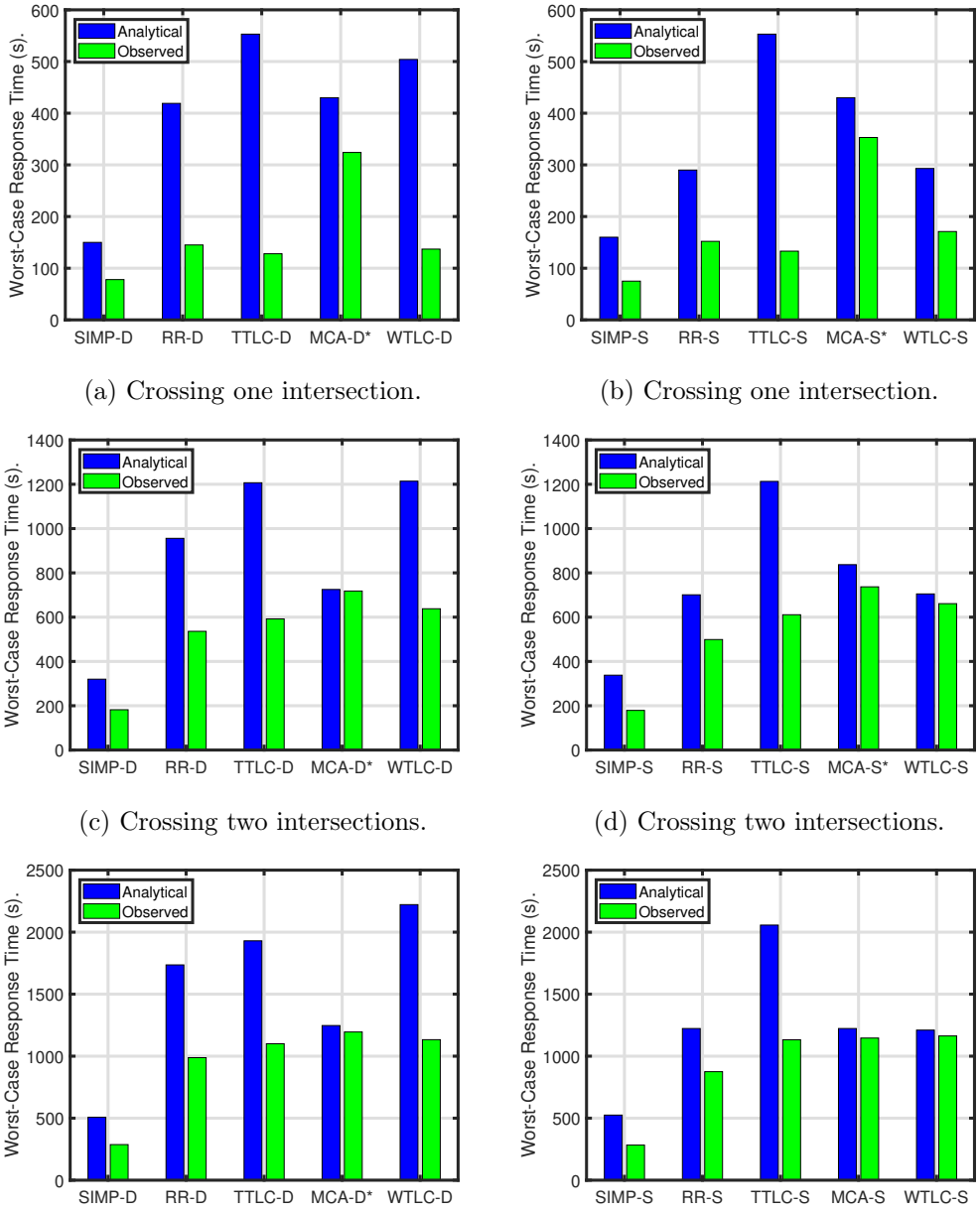

(a) Crossing one intersection.

(b) Crossing one intersection.

(c) Crossing two intersections.

(d) Crossing two intersections.

(e) Crossing three intersections.

(f) Crossing three intersections.

Figure 7.19: Worst-case response time (s) for crossing the single intersection (top), two intersections (middle), and three intersections (bottom). Dedicated left-crossing intersections (left) and shared left-crossing intersections (right). MCA* - added an extra TLC cycle time to analytical values.

7.5.6 Discussions

The lowest waiting time delays of SIMP are due to the lowest control cycle time and the efficiency of using the CDM that allows synchronous access of one vehicle from each non-conflicting road lane. This aspect allows respecting the leader-follower driving control without hard braking or complete stops leading to very short (in fact, the shortest) queue lengths. Moreover, the queues on the left lanes grow more than those on the right lanes. Note the left lanes serve only one vehicle per cycle, while the S/R lanes serve multiple vehicles due to non-conflicting right crossings. The results indicate that SIMP maintains its efficiency even when operating in a grid network.

Conversely, the remaining IM approaches admit multiple consecutive vehicles from single or multiple opposite lanes for longer green times, thus causing vehicles from other conflicting lanes to stop and wait until their turn. This behavior generates longer queues and waiting delays on red signals due to longer cycle times. We observed that RR and WTLC (dedicated left lane) showed longer queues on both external inflow and internal lanes forming the road network. For the same RR and WTLC (shared left lane), reduced queues are observed on all internal and external lanes due to the sharing of straight-crossing vehicles among the S/R and L lanes. Differently, both dedicated and shared left lane intersections of TTLC showed longer queues on particular external inflow lanes (n_2, e_2, s_2, w_2), while all other lanes showed shorter queues. In the case of MCA-D, only the external inflow lanes showed longer queues. In contrast, the internal lanes interestingly showed the same maximum queue lengths leading to the same waiting time delays. Reduced queue lengths are observed with the MCA-S, similar to RR-S and WTLC-S.

For all IM approaches, we compared the observed maximum waiting time delays and WCRT results against the analytical ones, giving a perception of the pessimism of the analysis. Except for MCA, for which case the analysis is not totally accurate, the observed values were consistently above the ones obtained, validating the worst-case character of the analysis. The pessimism was relatively growing for the increasing number of intersections the vehicles crossed, except for the WTLC in the shared left lane scenario (in fact, it exhibits the opposite behavior).

7.6 Summary

This chapter studied the worst-case response time to specific traffic scenarios defined statistically. This is a new service metric inspired on real-time systems concepts that assesses the maximum time a vehicle may experience since it is injected in the road system until it leaves the last intersection in its route. Commonly available parameters such as the geographical settings of the road networks (road lanes length and intersection space within), traffic-related information (average speed, maximum queue length, and capacity), and IM-specific parameters (green phase time and total cycle time) are employed to defining the WCRT. The analytical WCRT values are validated using the observed WCRT results

(SUMO-produced FCD data) at isolated single-lane and multi-lane as well as networks of multi-lane intersections. The validations provide some degree of confidence in employing the WCRT analysis for cycle-based IM approaches when the maximum queue length does not exceed the road capacity, i.e., saturated traffic conditions. The other primary observation is that the performance of the SIMP protocol dominates other competing benchmark approaches in the tested traffic scenarios.

Until now, we have studied the performance of the *synchronous framework*, in average-case as well as worst-case when HVs mixed with the AVs in equal amounts, i.e., 50% each. However, the transportation sustainability of introducing growing rates of AVs and other alternate energy vehicles (like BEVs) is still pending, and is the subject of the following chapter.

Chapter 8

Transportation Sustainability

As mentioned in the introduction chapter, transportation sustainability represents affordable energy-efficient transportation and emitting low- to zero-air pollutants, including alternative and renewable fuels, like electricity. To cope with road traffic issues and achieve transportation sustainability, introducing AVs, BEVs, and BEAVs technologies is significant [10; 188]. However, the full adoption of these vehicle technologies will take over an extended period of time and only after 2045. Thus, the research question is whether this adoption does bring any good as projected or otherwise. To answer this question, this chapter studies the growing rates of AVs, BEVs, and BEAVs at isolated single-lane and multi-lane intersections as well as networks of multi-lane intersections in low-speed urban settings.

The aim is to analyze transportation sustainability in terms of reducing the consumption of gasoline/electricity and lowering emissions brought by the introduction of AVs, BEVs, and BEAVs in scenarios of co-existence with mixed ICE vehicles. In the single-lane intersection case, we consider mixing ICE AVs and BEAVs with ICE HVs to understand the impact of introducing them. We consider the ICE HVs mixed with BEVs and BEAVs in the latter. We exclude ICE AVs from the study because taking as reference legislation such as that of the EU mandating that all vehicles produced from 2035 onwards must be electric [82] and that the foreseen temporal horizon for the introduction of Level 5 autonomy matches or even exceeds that date [95], we expect that the existence of ICE AVs will be residual or even null [7]. The IM operating in the intersection is a second dimension that we include in this study.

The majority of the content of this chapter is obtained from the following scientific publications:

- **Reddy, R.**, Almeida, L., Santos, P.M. and Tovar, E., 2020, September. Comparing the Ecological Footprint of Intersection Management Protocols for Human / Autonomous Scenarios. In IEEE International Conference on Intelligent Transportation Systems (**ITSC 2020**), pp.1-6.

- **Reddy, R.**, Almeida, L., Kurunathan, H., Santos, P. and Tovar, E., 2023. Comparing Energy Savings and Emissions Efficiency of Mixed ICEVs and BEVs at Complex Intersections. Under submission in the **Elsevier Transportation Research Part D: Transport and Environment**.

8.1 Isolated Single-lane Intersections

For analyzing isolated single-lane intersections, three traffic scenarios are designed. The first scenario is to test individual vehicles fuel consumption and associated emissions behaviors based on how the IM approaches serve vehicles. Both HVs and AVs (50% each) are ICE vehicles in this scenario. The second and third scenarios study the impact of introducing growing rates of ICE AVs and BEAVs mixed with ICE HVs. Simulation parameters and associated values are similar to the ones presented in Table 3.1 with $30km/h$ maximum speed. Similar to the performance analysis of average-case (Chapters 5 and 6) and worst-case (Chapter 7), we compare RR-x schemes (RR-5, RR-10, RR-20, and RR-30) against the SIMP protocol.

8.1.1 Scenario 1

In this scenario, three traffic cases are defined in which vehicles can cross only one direction (i.e., left or straight, or right), and they are meant to expose the intrinsic behaviors of the IM approaches. The three cases are defined as the following.

- Case-1: **Left-crossing** - all vehicles turn left at the intersection;
- Case-2: **Straight-crossing** - all vehicles cross through the intersection;
- Case-3: **Right-crossing** - all vehicles turn right at the intersection.

We carried out the comparisons under four traffic arrival rates (λ) per road: $0.05veh/s$, $0.1veh/s$, $0.2veh/s$, and $0.4veh/s$. In each experiment, we injected 1000 vehicles (50% AVs and 50% HVs). The injection process executed every second on each road, and added a vehicle randomly, respecting the referred average arrival rates. The simulations were run six times; thus, the results are the average of the six runs. We measured the average fuel consumption and associated emissions for 1000 vehicles, along with speed and fuel consumption over time of the 500^{th} vehicle, which is an AV.

8.1.1.1 Fuel Consumption

The behavior of average fuel consumption results of **cases-1,2,3** is similar to the ones shown in Fig. 5.3a with differences in quantitative values. Therefore, these results are exhibited in Table 8.1.

λ	**Case 1: Left Crossing**				
	SIMP	RR-5	RR-10	RR-20	RR-30
0.05	105.9	162.29	145.42	131.08	134.62
0.1	107.31	501.87	499.39	408.7	371.46
0.2	186.39	541.22	558.17	498.28	481.43
0.4	210	549.06	563.02	512.37	493.3
	Case 2: Straight Crossing				
0.05	105.9	158.7	129.6	127.2	131.1
0.1	107.3	504.8	420.6	316.6	274.7
0.2	189.7	544.2	493.7	448.3	428.2
0.4	211.3	552.3	503.5	460.7	446.4
	Case 3: Right Crossing				
0.05	100.1	158.2	129	126.7	130.7
0.1	97.3	505	416.4	315.8	279.3
0.2	92.3	543..1	493.7	446.1	432.
0.4	89.4	551.3	502.7	457.2	443.4

Table 8.1: Average fuel consumption (ml) for **Cases 1, 2**, and **3** at $30km/h$ maximum speed.

On average, vehicles consume more fuel on left-crossing, given the slightly longer path and longer waiting times (longer engine idling). Slight differences can be observed for SIMP and RR-5. We also observe that increasing green time in the RR configurations decreases fuel consumption in (near) saturated cases. This is expected, too, since shorter green windows imply more breaks in the traffic flow and, thus, more engine idling period. SIMP performs better than any RR configuration, and the improvement is distinctly significant for a high arrival rate of $0.4veh/s$. RR-x configurations consume two times (**cases-1, 2**) and four to five times (**case-3**) more fuel than SIMP. We observed that this advantage of SIMP arises from the synchronous access of the vehicles to the intersection, leading to smoother traffic handling with fewer stopping/idling periods than any RR-x configuration. Another observation concerns SIMP in **case-3**. Curiously, fuel consumption for low arrival rates is higher than for higher arrival rates. This is because, in this scenario, vehicles move at a speed superior to the cruising speed (a speed at which fuel consumption is optimal) that consumes more fuel in low densities.

Subsequently, we inspect individual fuel consumption patterns until the vehicles exit the road network by crossing the intersection. We selected an AV (500^{th} vehicle) from mid-simulation for the left-crossing (**case-1**) configuration from RR-5, RR-30, and SIMP with an average traffic arrival rate of 0.4 veh/s at which the IM system saturates (Fig. 8.1). For RR-5, the AV experiences consecutive phases of acceleration and deceleration, with several periods of stopping during which the vehicle is idling and consuming. The HBEFA3.1 model considers a significant idling consumption). In RR-30, we observe a similar behavior but with longer moments of motion and waiting. The jerky driving behavior in RR-30 indicates that the AV is following an HV. The total travel time and average consumption are lower

than for RR-5 (436s vs. 604s and 398.61ml vs. 429.98ml). For SIMP, we observe 512s for transit time and 321.87ml of fuel consumption in this case. The main takeaway for SIMP is that, by allowing vehicles one-by-one in the intersection instead of using fixed time periods, SIMP causes fewer stopping/idling periods than any of the RR options (in which stop times are always above 15s). The impact of idling on fuel consumption shows that Start/Stop systems may contribute significantly to fuel economy. We will address this possibility in future work.

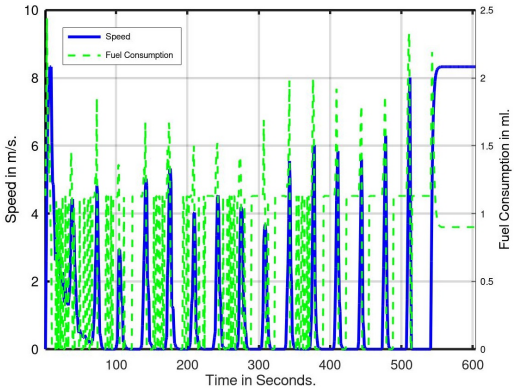

(a) RR-5.

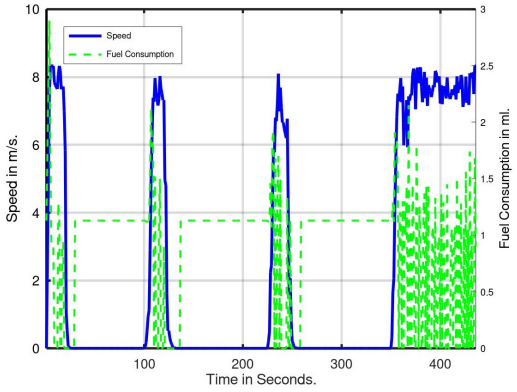

(b) RR-30.

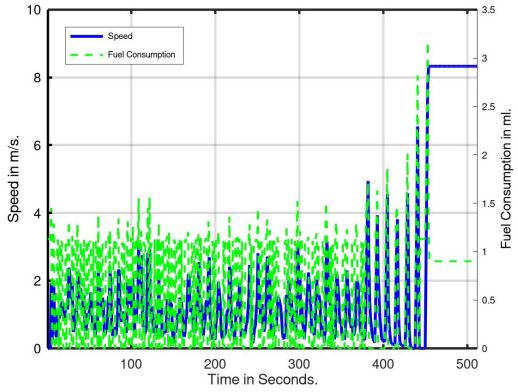

(c) SIMP.

Figure 8.1: Speed and fuel consumption of 500^{th} vehicle an AV in RR-5, RR-30, and SIMP protocol in which all vehicles cross their left.

8.1.1.2 Vehicular Emissions

The vehicular emissions (PMx, NOx, CO, CO_2, and HC) for the aforementioned experiments are presented in Table 8.2.

Particulate Matter

The average PMx emissions show that, in all three scenarios, SIMP leads to considerably lower emissions: at most 15.5mg for left crossing, 13.2mg for straight crossing, and 3.2mg

for right crossing. Note that the SUMO simulator does not consider the PMx emissions caused by braking.

Nitrogen Oxide

The average NOx emission results show that SIMP is superior to all RR configurations. The NOx emissions of SIMP for left crossing are $326mg$ for an arrival rate of 0.4veh/s, which is a saving of 40%, 44%, and 31% with respect to RR-5, RR10, and both RR-20 and RR-30. In the case of straight and right crossing, SIMP performs even better. Particularly, for right crossing, SIMP has three times lesser NOx emissions. This is due to the high traffic fluidity of SIMP in this scenario. SIMP also leads to inferior emissions as traffic density increases (from $96.1mg$ in the $0.05veh/s$ scenario to $89.24mg$ in the $0.4veh/s$ case).

Carbon Monoxide

In Table 8.2, the average CO emissions are represented in grams for left, straight, and right crossings accordingly. In all three cases, SIMP shows better performance with lower emission of CO, i.e., less than $35g$ for left, $30g$ for straight, and $5g$ for right crossing. As with NOx, this can be attributed to higher traffic fluidity. Likewise, average emissions decrease as traffic density increases.

Carbon Dioxide

The CO_2 results also show a better performance of SIMP. The highest CO_2 emission for this protocol is $754g$, $740g$, and $254.05g$ for left, straight, and right crossing, respectively; RR varies from $740g$ to $1299g$. In this case, the average emission values of SIMP in the right crossing are lower in the straight crossing case (unlike the two previous metrics, NOx and CO).

Hydro Carbons

Finally, the lower part of Table 8.2 represents the average HC in mg. Overall, for left crossing, SIMP shows a reduction of 36%, 39%, 28%, and 27% with respect to RR-5 through RR-30, respectively. For straight and right crossings, SIMP shows between 50% and 56% less HC emissions than RR configurations.

λ	Left Crossing					Straight Crossing					Right Crossing				
	SIMP	RR-5	RR-10	RR-20	RR-30	SIMP	RR-5	RR-10	RR-20	RR-30	SIMP	RR-5	RR-10	RR-20	RR-30
Average PMx Emission in mg.															
0.05	4.02	6.5	5.58	4.85	5.15	3.65	6.20	4.63	4.63	4.98	3.09	6.25	4.66	4.65	4.99
0.1	12.9	25.3	27.9	21	20.1	8.5	23.4	21.1	19.6	18.1	3.12	23.4	21.3	19.7	18
0.2	15.2	26.8	29.5	23.8	23.5	12.9	24.8	23.6	22.8	22.2	3.15	24.8	23.5	23	22.1
0.4	15.5	27	29.7	24	23.6	13.2	25.1	24	23.5	22.8	3.16	25.2	24.1	23.4	22.7
Average NOx Emission in mg.															
0.05	115.07	155.54	137.52	123.13	128.10	107.52	149.89	120.43	119.21	125.02	96.10	150.95	121.02	119.68	125.3
0.1	278	501	545	416	400	196	465	421	391	362	94.08	466	424	393	361
0.2	321	529	575	468	462	278	491	468	450	437	90.75	491	465	452	435
0.4	326	536	585	473	464	284	497	474	463	449	89.24	499	477	461	447
Average CO Emission in grams.															
0.05	6.9	12.96	10.8	9.1	9.8	6.12	12.22	8.6	8.6	9.5	4.9	12.3	8.6	8.6	9.5
0.1	28.3	58.2	64.4	47.9	46.2	17.1	53.3	47.5	44.7	41.2	4.85	53.4	47.9	44.9	42.9
0.2	34.1	62	68.3	54.8	54.5	28.2	56.8	53.6	52.6	51.3	4.76	56.7	53.3	52.8	51.1
0.4	34.8	62.4	68.8	55.2	54.7	28.9	57.5	54.5	54.3	52.9	4.74	57.7	54.8	53.97	52.7
Average CO_2 Emission in grams.															
0.05	297.32	379.5	338.95	306.61	316.8	280.14	367.07	302.31	298.3	310.29	254.05	369.47	303.7	299.3	311
0.1	649	1132	1226	942	906	740	1052	955	887	823	246.5	1055	962	891	822
0.2	743	1193	1290	1054	1040	649	1109	1056	1016	986	234.5	1109	1051	1021	982
0.4	754	1200	1299	1061	1044	661	1121	1070	1044	1012	229	1125	1076	1039	1008
Average HC Emission in mg.															
0.05	38.46	67.68	56.91	48.27	51.84	34.11	64	45.84	45.92	50.12	28.06	64.35	46	46.1	50.21
0.1	144	291	322	240	231	89	267	238	224	207	27.6	268	240	225	207
0.2	173	310	341	274	272	143	284	269	263	257	26.9	284	267	264	255
0.4	175.7	312	343	276	274	147	288	273	272	265	26.7	289	274	270	263

Table 8.2: Average emission of air pollutants.

8.1.2 Scenario 2

In this scenario, we test the growing rates of AVs (from 10% to 90%) mixed with HVs (decreasing from 90% to 10%), where both are ICE vehicles. The simulation parameters and associated values are exhibited in Table 3.1, and the maximum employed speed is $30km/h$. From Figure 5.1a, we can observe that RR-x configurations saturate at $0.1veh/s$; thus, we choose the same traffic arrival rate for this simulation study. The traffic is generated following a uniform distribution and randomly distributed for left (33%), straight (33%), and right (33%) crossings in all experiments. We measured the average speed (distance traveled by the time taken - m/s), travel time loss (s), fuel consumption (ml), and associated emissions of air pollutants (PMx, NOx, CO, CO_2, and HC) for 1000 vehicles.

8.1.2.1 Experimental Results

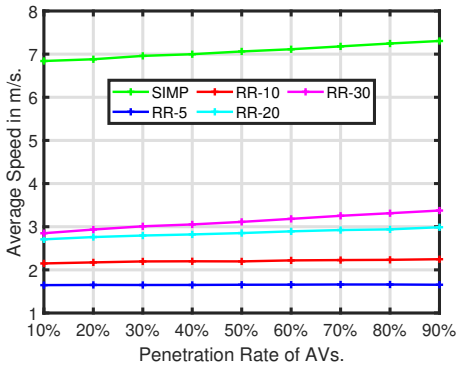

(a) Average speed (m/s).

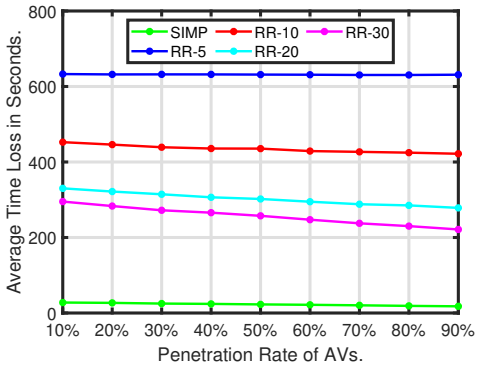

(b) Average travel time loss (s).

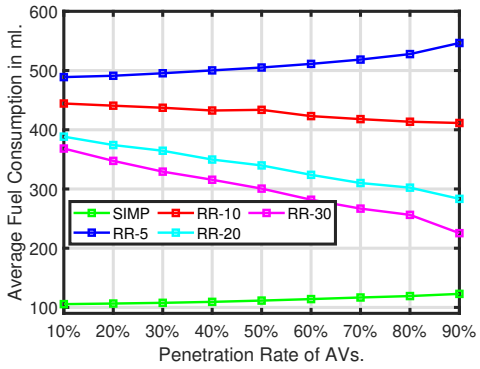

(c) Average fuel consumption in ml.

Figure 8.2: Average speed, travel time loss, and fuel consumption results of 1000 vehicles for growing AV rates of comparing IM approaches.

Figure 8.2 shows the results of average speed (Fig. 8.2a), travel time loss (Fig. 8.2b), and fuel consumption (Fig. 8.2c) for growing rates of AVs. The average speed results (Fig. 8.2a) show the dominance of the SIMP protocol with higher average speed values.

These values keep growing for the increasing rates of AVs. On the other hand, the RR-5 shows the worst performance with the lowest average speed values. Whatever the AV rate is, the RR-5 keeps the same average speed results. The best RR-x configuration is RR-30, which shows comparatively better results than other RR configurations. Slight improvements in the RR-30 results can be observed for growing rates of AVs. Overall, at 90% AV penetration, all IM approaches exhibit their best performance.

The travel time loss results (Fig. 8.2b) for increasing AV rates indicate the advantages of using the SIMP in reducing travel time loss against traditional RR-x IM strategies. From the results, we can observe the highest time loss values for RR-x configurations with 10% of AVs between 250s (RR-30) and 650s (RR-5). For growing rates of AVs, the time loss continues declining; however, still above 200s at 90% of AVs. On the contrary, SIMP retains the lowest time loss values among 31.6s (10%) and 20s (90%), in decreasing order. Similar to the average speed results, the travel time loss results are also kept the same for whatever the AV rate.

The fuel consumption results (Fig. 8.2c) indicate the advantages of synchronous intersection access against the traditional continuous flow from a single lane at signalized intersections. Firstly, the travel time loss results (Fig. 8.2b) and fuel consumption results (Fig. 8.2c) show a relative behavior. This means the more time vehicles lose, the more fuel they consume (e.g., RR IM configurations). On the other hand, SIMP's average fuel consumption is two to three times less than the RR IM strategies, as the time loss of vehicles in SIMP is comparatively less than in RR configurations. An observation is that the fuel consumption is proportional to the increasing AV rates for both the SIMP and RR-5, while the reverse effect can be observed in RR-10, RR-20, and RR-30. This is due to the strict driving rules the AVs follow for crossing the intersection, which lets them wait longer.

8.1.2.2 Vehicular Emissions

Figure 8.3 exhibits the average emission of dangerous air pollutants (CO, PMx, and NOx) for growing rates of AVs. The primary observation is that these results correlate with the fuel consumption results (Fig. 8.1) with varying absolute values. The other emissions, such as CO_2 and HC, also show similar patterns, so we presented them in Table 8.3.

The emissions results show that the SIMP is more environmentally friendly, with the lowest emissions. SIMP maintains approximately the same emissions values in most cases, and a slight increase can be observed in NOx and CO_2 emissions, similar to fuel consumption, regardless of the AV rate. On the other hand, RR-5 is the most unfriendly approach with the highest emissions values, and it keeps emitting higher values for increasing the rates of AVs. The RR-10 and RR-20 slightly and significantly reduce the emissions exhaust for growing rates of AVs. However, RR-30 is the best approach after SIMP, with the highest emissions reduction from 10% to 90%. All these emissions results are similar

to the fuel consumption results. Overall, SIMP performs 142% (CO), 94% (CO_2), 138% (HC), 125% (PMx), and 103% (NOx) better than the next best approach, RR-30.

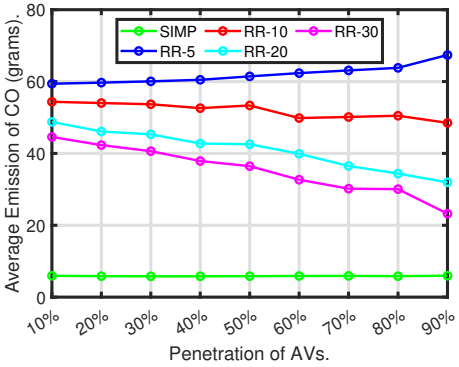

(a) Average emission of CO ($grams$).

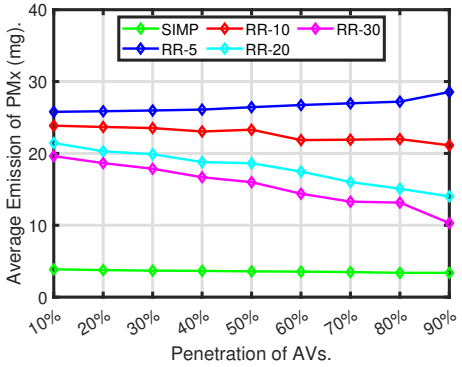

(b) Average emission of PMx (mg).

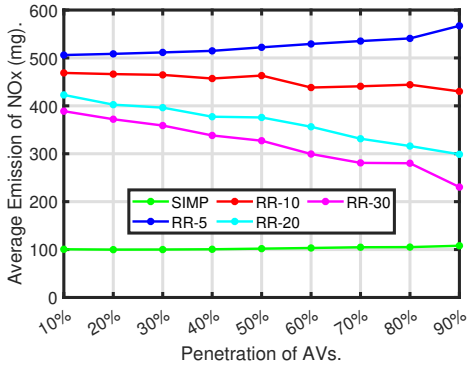

(c) Average emission of NOx (mg).

Figure 8.3: Average emission of CO, PMx, and NOx for 1000 vehicles for growing AV rates.

	Avg. emission of CO_2 ($grams$).					**Avg. emission of HC (mg).**				
	SIMP	RR-5	RR-10	RR-20	RR-30	SIMP	RR-5	RR-10	RR-20	RR-30
10%	251.3	1136.8	1054.4	953.7	879.5	32.8	296.9	272	244.3	223.4
20%	251.1	1143.4	1050.1	910.4	844.1	32.2	298.5	270.5	231	212.3
30%	253.6	1151.5	1048	898.4	817	32	300.3	268.8	227.2	204
40%	256.5	1159.8	1033	858.4	773	32.2	302.4	263.5	214.6	190.4
50%	262.5	1177.6	1048.3	857	751.2	32.4	307	267.3	213.7	183.4
60%	268	1195	995.8	816.8	692.8	32.8	311.7	250	200.5	164.8
70%	274.6	1210.1	1003.5	764.4	654.6	33	315.4	251.6	184	152.5
80%	278.2	1223.8	1012.8	733.5	655	32.7	319	253.4	173.5	152
90%	287.8	1283.4	984.7	698.7	549.6	33.5	336.6	243.6	161.5	118.4

Table 8.3: Average emission of CO_2 ($grams$) and HC (mg) for **scenario 2** at $30km/h$ maximum speed.

8.1.3 Scenario 3

This scenario analyzes the growing rates of BEAVs mixed with the ICE HVs. This study is also two-fold similar to the previous scenario, but the only difference is that the AVs are equipped with battery electricity. Thus, we only measure the consumption of gasoline and electricity and the emissions of air pollutants. We employed the same $0.1veh/s$ traffic arrival rate at $30km/h$ maximum speed. The traffic is generated following a uniform distribution and randomly distributed for left (33%), straight (33%), and right (33%) crossings in all experiments. The simulation parameters and associated values for AVs and ICE HVs are exhibited in Table 3.1. The battery electricity-related information is in Table 8.4 indicating the average passenger cars [103].

Table 8.4: Simulation Parameters and assigned values for BEAVs.

Parameters	**Values**
Max. Battery Capacity	$2000Wh$
Actual Battery Capacity	$1000Wh$
Max. Power	$1000W$
Constant Power Intake	$100W$
Internal moment of Inertia	$0.01Kg.m^2$
Air drag coefficient	0.6
Radial drag coefficient	0.5
Roll drag coefficient	0.01
Propulsion Efficiency	0.9
Recuperation Efficiency	0.9
Stopping Threshold	$0.1km/h$

Figure 8.4 shows the total gasoline and electricity consumption and HC emissions results for the growing rates of BEAVs. The fuel consumption behaviors are expected as the percentage of vehicles changes, i.e., growing BEAVs for decreasing ICE HVs.

Overall results show that SIMP is up to 115% (gasoline) and 10.15% (electricity) more energy efficient than the next best approach, the RR-30. The air pollutants emissions results also correlate with the gasoline consumption results (Fig. 8.4a), as the BEAVs emissions are zero. The absolute emissions values for CO, PMx, CO_2, and NOx are presented in Table 8.5. Concerning the emissions, the SIMP protocol produces up to 155% (CO), 115% (CO_2), 150.8% (HC), 136.4% (PMx), and 121.4% (NOx) less air pollutants than the following best approach, again the RR-30. Therefore, a higher rates of BEAVs with SIMP protocol is more sustainable than the competing approaches.

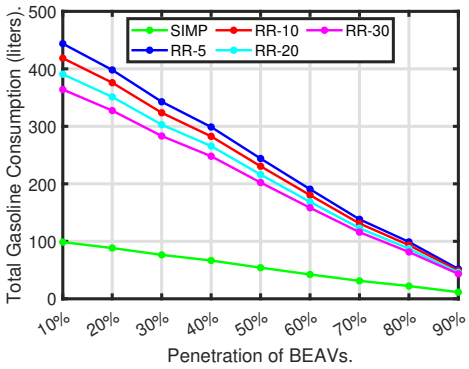

(a) Total gasoline consumption ($liters$).

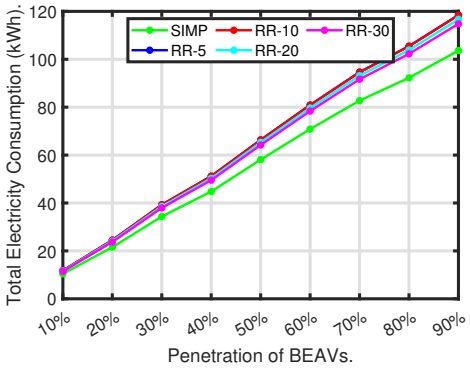

(b) Total electricity consumption (kWh).

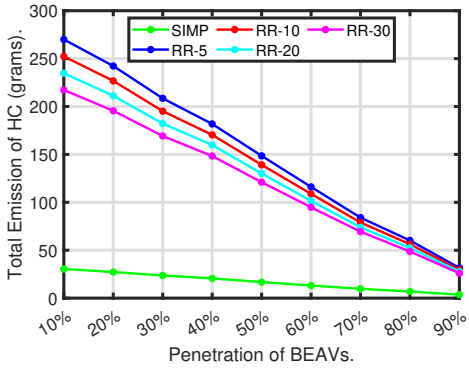

(c) Total HC emissions ($grams$).

Figure 8.4: Total gasoline and electricity consumption and HC emissions for 1000 vehicles for growing AV rates.

	Avg. emission of CO ($grams$).					**Avg. emission of PMx ($hgrams$).**				
	SIMP	RR-5	RR-10	RR-20	RR-30	SIMP	RR-5	RR-10	RR-20	RR-30
10%	5532	54007	50422.6	46901.2	43374.3	36.1	234.7	221.3	206	190.8
20%	4958.7	48467.8	45321.8	42204.4	39050.2	32.4	210.6	198.8	185.3	171.7
30%	4299.7	41711	39004.4	36400.6	33789.7	28	181.3	171	159.8	148.5
40%	3750.9	36368.8	34062	31944.5	29620.6	24.4	158	149.4	140.2	130
50%	3048.6	29715.2	27810.9	25994	24168.6	19.8	129	122	114	106
60%	2397.2	23225.9	21760.5	20291	18940.5	15.6	101	95.4	89	83
70%	1774.3	16809.6	15778.2	14765	13861.6	11.5	73	69.3	64.8	60.9
80%	1262.5	12038.6	11245.6	10473	9714.9	8.2	52.3	49.4	46	42.7
90%	660	6314.5	5897	5521.4	5189	4.2	27.4	25.9	24.2	22.8
	Avg. emission of CO_2 (kgs).					**Avg. emission of NOx ($grams$).**				
10%	22945.3	103243	97364.5	90879.8	84687.2	92.4	460	433.5	404	375.6
20%	20542	92608.8	87452.6	81704.8	76172.6	82.7	412.7	389.4	363.2	337.8
30%	17775.6	79737.4	75290.8	70478.8	65876	71.6	355.3	335.2	313.3	292.2
40%	15497.2	69519.7	65728.6	61806.9	57691.6	62.4	309.8	292.6	274.8	256
50%	12587.9	56759.8	53640.6	50268	47048	50.7	253	238.8	223.5	208.8
60%	9851.8	44350	41947	39227	36836	39.7	197.6	186.8	174.4	163.5
70%	7266.7	32160.3	30479.2	28588	26973.3	29.3	143.3	135.7	127	119.7
80%	5169.6	23022.4	21724	20294	18951.3	20.8	102.6	96.7	90.2	84
90%	2685.2	12052	11376.5	10658.7	10072	10.8	53.7	50.7	47.4	44.7

Table 8.5: Average emission of CO, PMx, CO_2 and NOx for **scenario 3** at $30km/h$ maximum speed.

8.2 Isolated Multi-lane Intersections

For studying the transportation sustainability of growing BEVs and BEAVs rates at isolated multi-lane intersections (Figs. 4.3 and 4.4), the simulation scenarios, parameters, and assigned values are now presented. Two simulation scenarios are designed by mixing BEVs and BEAVs with ICE HVs to analyze energy savings and emissions volume for one hour ($3600s$). Therefore, in the first scenario, both ICE and BEVs are HVs. This scenario showcases the increased energy efficiency and decreased emission of air pollutants obtained from employing human-driven BEVs. It is further discretized across the various IM approaches to characterize their performance in managing HVs. No start-stop is used in ICE vehicles. In the second scenario, ICE HVs are mixed with BEAVs. This scenario studies the impacts of autonomous-driver control on the whole traffic scenarios, fuel consumption, and emissions metrics. It presents this impact for each IM approach to understanding better how the IMs handle the change from HVs to AVs.

From [180], it is clear that most of the IM approaches saturate at $0.2veh/s$ (i.e., 12 vehicles per minute), so we choose the same traffic arrival rate. Tables 3.1 and 8.6 summarize the simulation parameters and allocated values of ICE, BEVs, and BEAVs. In Table 8.6, BEVs/BEAVs specific parameters and allocated values represent a passenger car with an average mass value [75]. The traffic is generated following a uniform distribution and randomly distributed for left (33%), straight (33%), and right (33%) crossings in all experiments. Finally, each experiment is run five times with different random seeds but with the same set of parameters; hence, each data point is the average of five runs.

Table 8.6: Simulation Parameters and assigned values for BEAVs.

Parameters	**Values**
Max. Battery Capacity	$64kWh$
Max. Power	$150kW$
Constant Power Intake	$100W$
Internal moment of Inertia	$0.01Kg.m^2$
Air drag coefficient	0.35
Radial drag coefficient	0.5
Roll drag coefficient	0.01
Propulsion Efficiency	0.98
Recuperation Efficiency	0.96
Stopping Threshold	$0.1km/h$

We now discuss intersection performance metrics (intersection throughput and waiting time), followed by energy savings (gasoline and electricity), and finally, emission of air pollutants (PM_x, NO_x, CO, HC, and CO_2). Understanding the intersection performance and driving behavior of human/autonomous vehicles induced by the various IM approaches is relevant to interpreting the corresponding fuel consumption and emission measurements afterward.

8.2.1 Intersection Performance Metrics

8.2.1.1 Intersection Throughput (veh/h)

Figure 8.5 shows the intersection throughput results (veh/h) for various rates of BEVs (Fig. 8.5a) and BEAVs (Fig. 8.5b) rates. The BEV scenario results (Fig. 8.5a) are presented as a reference to the results of the BEAV scenario (Fig. 8.5b), analyzing the impact of autonomous vehicle introduction and the performance of the selected IM approaches. In the BEV scenario, both ICEVs and BEVs have jerky driving behavior as they are human-driven vehicles following the same Krauss CFM. We observe that the best-performing approaches are SIMP duo (SIMP-D and SIMP-S) with the highest throughput values, and WTLC is the worst-performing IM approach with a difference of around 900 vehicles. The remaining IM approaches show intermediary performance. Overall, the throughput improvements of SIMP-S are 7.2% higher than the following best, the ITLC.

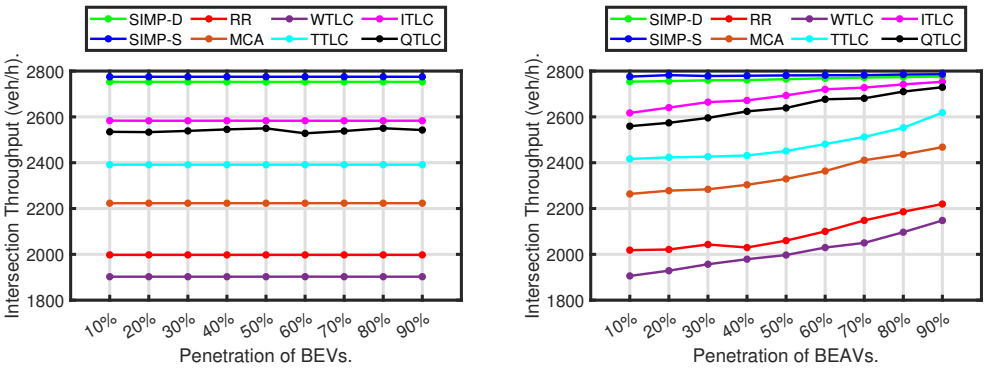

(a) Throughput for growing rates of BEVs. (b) Throughput for growing rates of BEAVs.

Figure 8.5: Intersection throughput (veh/h) of different IM approaches for growing rates of BEVs and BEAVs.

In the BEAV scenario (Fig. 8.5b), the intersection throughput improves due to autonomous vehicles more consistent driving behavior for their growing penetration rates. The following BEAVs employ shorter headway (respecting safety distance) to the leading vehicle, while the human-driven vehicles employ longer headway due to their jerky behavior. In the range of 10% to 90% BEAVs penetration, all IM approaches experience increased throughput, with TTLC (5.5%), ITLC (4.13%), and QTLC (4%) being the most positively impacted ones. However, SIMP dominates with 3.25% higher throughput than the next best, the ITLC.

SIMP's throughput performance is due to the lowest control cycle time, which serves the highest number of vehicles by synchronizing conflict-free vehicle movements. Also, whether vehicles are human-driven (BEVs) or autonomous (BEAVs), there is no significant improvement (i.e., 0.22% only) in throughput performance. SIMP induces much less speed variations on vehicles than other IMs. Therefore, while the 'jerkiness' typical of human-driven vehicles impacts other IMs, it impacts SIMP less.

Conventional IM approaches (RR and TTLC) block the road lanes other than the serving ones for longer based on their control cycle times, hindering their performance and serving fewer vehicles. Differently, the ITLC and QTLC adapt their control cycles using traffic characteristics (queue lengths, vehicle speed, and acceleration) and improve the throughput results. Adaptive approaches (MCA and WTLC) decisions are inefficient in tackling saturated traffic conditions. At 90% of BEAVs penetration, all IM approaches reach their peak and only the ITLC is close to SIMP.

8.2.1.2 Average Waiting Time (s)

Due to congestion and traffic signal configurations, vehicles must wait longer to access the intersection, particularly during the yellow/red phases. The apparent behavior of longer control cycle times is that they impose longer waiting times, while the shorter ones impose shorter waiting delays. Figure 8.6 displays the average waiting time (s) of vehicles that completed their journey in one hour (3600s) simulations.

In the reference BEV scenario (Fig. 8.6a), all IM approaches exhibit similar waiting time results regardless of the BEVs penetration rate, as both ICEVs and BEVs mimic human-driven vehicle driving behavior. SIMP duo has the lowest average waiting times of 5s (SIMP-S) and 7s (SIMP-D), serving vehicles based on their arrival. The intelligent approaches (ITLC and QTLC) have a higher waiting time of about 100s than SIMP, even though they are designed to reduce the waiting time of vehicles approaching the intersection. Employing SIMP is 182% more advantages in minimizing waiting delays than the next best approach QTLC.

The performance of conventional approaches (TTLC and RR) and the adaptive MCA is almost double the intelligent ones, and the worst-performing approach is the WTLC. TTLC and RR permit vehicles waiting at the intersection entrance in at most one control cycle cyclically; thus, not all vehicles suffer longer waiting times. In the case of MCA, it is possible that a waiting vehicle must spend more than one control cycle due to the acyclic nature of TLC signals adaptation that is based on the instantaneous traffic flow rather than a few stopped vehicles. The poor performance of WTLC shows an inadequate adaptive mechanism that considers specific traffic arrival rates the same as the previous time interval to decide signal timing and control cycle length. When the traffic flow pattern changes, the WTLC either adapts too frequently or occasionally.

In the BEAVs scenario (Fig. 8.6b), different IM approaches exhibit different waiting time behaviors for increasing BEAVs penetration. Firstly, SIMP protocols experience a slight increase in the waiting time values for increasing BEAVs. On average, 1s (SIMP-S) and 3s (SIMP-D) higher than the BEVs scenario. This apparent behavior can be expected as BEAVs increased average speed lets them join the queue faster, stop and wait to access the intersection. The number of vehicles SIMP serves does not change based on vehicle speeds. Moreover, SIMP performs 169.5% better than the following best approach, the ITLC, throughout the BEAVs transition.

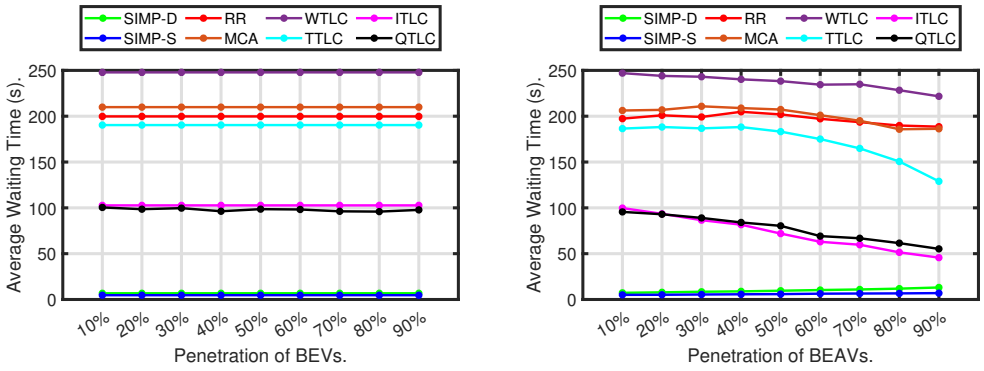

(a) Penetration of BEVs. (b) Penetration of BEAVs.

Figure 8.6: Average waiting time (s) imposed by different IM approaches for various BEVs and BEAVs penetration rates.

Over the BEAVs transition, the highly positively impacted IM approaches are TTLC, ITLC, and QTLC with 10%, 34.34%, and 23.7% with respect to the BEVs scenario. At 90% of BEAVs, TTLC, ITLC, and QTLC minimized 61.4s, 57s, and 42.5s average waiting delays with respect to the BEVs scenario. This means the smooth and less jerky driving movements imposed by the BEAVs that minimize the hard brakes and associated decelerations and accelerations lead to fewer speed deviations and consequent delays. The interchanging behavior of QTLC and ITLC performances after 20% of BEAVs penetration matches their original design to support either human-driven (QTLC) or autonomous (ITLC).

Interestingly, RR and MCA maintain closer performance behavior around 200s, and a slight decrease can be observed after 40% of BEAVs introduction. Finally, the WTLC shows a slight reduction in waiting time at each increasing BEAVs percentage. These poor behaviors represent conventional and adaptive IM approaches inability to reduce waiting times associated with traffic congestion.

8.2.2 Energy Efficiency

Figure 8.7 shows the average gasoline consumption (ml) results of ICEVs in BEVs and BEAVs scenarios. The results of both BEVs and BEAVs scenarios indicate a correlation with waiting time results, where a higher waiting time leads to higher fuel consumption values as the engine of the vehicle is kept in idling mode during the waiting time.

In BEVs results, a slight change can be observed after 60% of BEVs (Fig. 8.7a) for all IM approaches except the SIMP duo. This can be attributed to the least number of vehicles and poor statistical significance. Similar to the waiting time results, the performance order of intelligent approaches is QTLC and ITLC, with fuel consumption of roughly $100ml$ higher than the SIMP duo, and the remaining approaches values are above $200ml$ than SIMP. Overall, WTLC is the least sustainable option with the highest fuel consumption results.

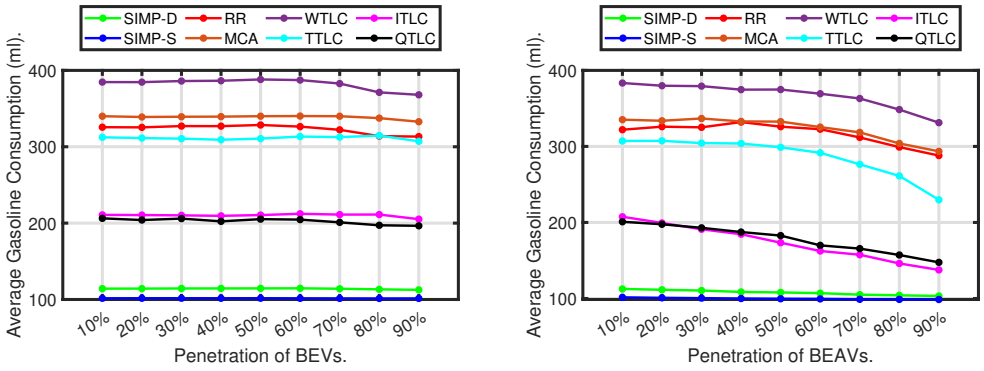

(a) Penetration of BEVs. (b) Penetration of BEAVs.

Figure 8.7: ICE vehicles average gasoline consumption (ml) of comparing IM approaches for BEVs and BEAVs scenarios.

In the BEAVs scenario, the results show that lower waiting delays and minimized engine idling time of BEAVs result in lower fuel consumption. The highly positively influenced ones are ITLC, QTLC, TTLC, and WTLC, with almost $50ml$ at 90% BEAVs. QTLC dominates over ITLC until 30% of BEAVs penetration, and then ITLC takes over due to its design supporting autonomous driving, matching the waiting time results (Fig. 8.6b). Overall, SIMP-S is the most sustainable approach, with the lowest fuel consumption results at $100ml$, followed by SIMP-D. This is due to the SIMP-induced lower waiting times leading to smoother movements among mixed vehicles and associated soft braking.

The average electricity consumption (Wh) results of BEVs and BEAVs scenarios are presented in Fig. 8.8. Note that we are comparing the electricity consumption of two different CFMs representing BEVs (Krauss CFM) and BEAVs (ACC CFM). It is also worth mentioning that the waiting time of vehicles at intersections does not increase electricity consumption as they employ regenerative braking.

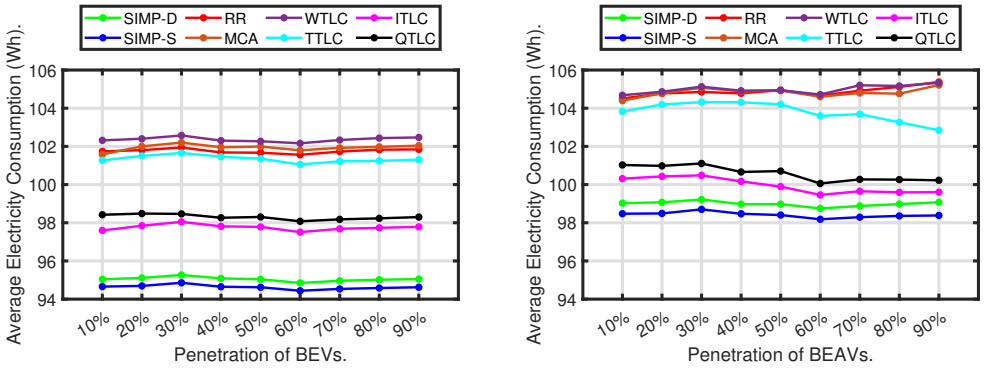

(a) Penetration of BEVs. (b) Penetration of BEAVs.

Figure 8.8: Average electricity consumption (Wh) of comparing IM approaches for various rates of BEVs and BEAVs penetration.

Figure 8.8a, shows the average electricity consumption results of the BEVs scenario. From the results, the SIMP duos performance is the best with average electricity consumption of $\sim 95Wh$. The ITLC and QTLC approaches consume between 97 to $99Wh$. This means the SIMP is 3.2% more energy efficient than the next best, the ITLC. Conventional RR and TTLC approaches consume around $101Wh$; thus, SIMP is 6.5% more energy efficient than conventional ones. Adaptive MCA and WTLC are the worst sustainable options with the highest electricity consumption of up to $102Wh$. In this case, SIMP is 7.8% more energy efficient than the adaptive IM approaches.

Figure 8.8b, shows the BEAVs average electricity consumption results. Compared with the BEVs, the BEAVs electricity consumption is higher. Respecting the same, for the entire transition of BEAVs from 10 to 90%, the higher electricity consumption values in Wh are ~ 4 (SIMP being the highest consumer), 3.13 (RR), 2.9 (MCA), 2.63 (WTLC), 2.5 (TTLC), 2.3 (QTLC), and 2.2 (ITLC being the least consumer). The average speeds of BEAVs are higher than those of BEVs, which led to higher throughput values, shown in Fig. 8.5b, consequently increasing the aerodynamic drag and resistance, and are responsible for more electricity consumption. Yet, SIMP is 1.613% more energy efficient than the next best approach, the ITLC. In this BEAVs scenario, both SIMP configurations and intelligent IM approaches (ITLC and QTLC) maintain similar electricity consumption behavior for increasing rates of BEAVs respecting the BEVs; while other IM approaches behave differently. For instance, TTLC observes a considerable reduction after 50% of BEAVs. Conversely, the conventional RR and adaptive MCA and WTLC approaches slightly increase for BEAVs by above 60%. We believe these behaviors are associated with the IM operations for higher penetration rates of autonomous vehicles and further studies on the micro level are needed to find out the real cause.

8.2.3 Emissions Efficiency

The average emissions result of two tested BEVs and BEAVs scenarios are presented in this section. The order of emissions discussions is as follows: PM_x (Fig. 8.9), NO_x (Fig. 8.10), CO (Fig. 8.11), HC (Fig. 8.12), and CO_2 (Fig. 8.13). The following observations are made from the average emission values of the tested BEVs and BEAVs scenarios.

In the BEVs scenario, all IM approaches exhibit the correlation between gasoline consumption and emission of air pollutants (PM_x, NO_x, CO, HC, and CO_2), respecting the directly proportional relation as specified in the fuel consumption models (section 3.5). For WTLC, RR, and MCA, above 70% of BEVs introduction, the reduced emission values show poor statistical significance matching the gasoline consumption.

The primary observation is about the environmental friendliness of IM protocols in the BEVs scenario. The emission results show that the SIMP duo offers the best performance due to the lower waiting time of vehicles and associated engine idling time before accessing the intersection. Unlike SIMP, the engine idling time of vehicles in QTLC and ITLC is higher, linked to their waiting times, so thus the air pollutants emissions. Then the

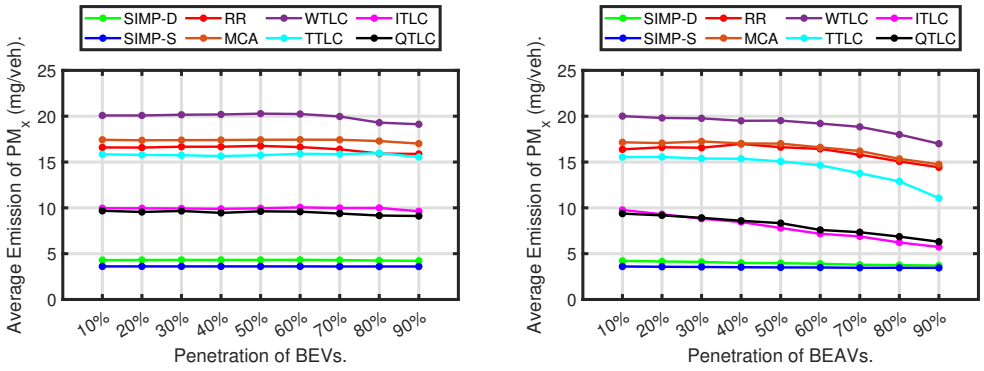

(a) Penetration of BEVs. (b) Penetration of BEAVs.

Figure 8.9: Average emission of PM_x (mg) per ICE vehicle of comparing IM approaches for BEVs and BEAVs scenarios.

conventional approaches TTLC and RR come before the adaptive approaches MCA and WTLC. This emissions behavior with the RR and TTLC is highly likely due to their fixed TLC cycles regardless of vehicles presence on inflow lanes, letting the vehicles engines in idling mode on blocked road lanes. In the case of MCA, it is possible that a few waiting vehicles must spend multiple control cycles (longer time) due to the acyclic nature of TLC signals adaptation which is based on the instantaneous traffic flow. This behavior leads to more engine idling time and associated emissions. The IM operating behavior of WTLC is similar to the RR but adapts between the minimum and maximum TLC cycle times. These adaptations are either more frequent or rare, leading to the worst-performing approach during saturated traffic conditions. Overall, SIMP minimizes 90% of PM_x, 72.7% of NO_x, 114.24% of CO, 108.4% of HC, and 66.4% of CO_2 against QTLC, the following best approach.

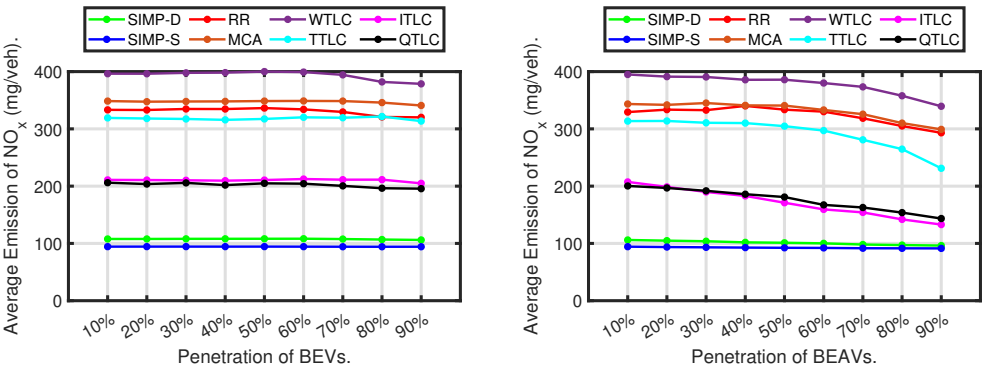

(a) Penetration of BEVs. (b) Penetration of BEAVs.

Figure 8.10: Average emission of NO_x (mg) per ICE vehicle for comparing IM approaches of BEVs and BEAVs scenarios.

From the emissions results of BEAVs scenario, decreasing emissions trends for the increasing rates of BEAVs can be observed. This is due to the zero-tailpipe emissions of BEAVs. The secondary observation is that the emissions results of the BEAVs scenario

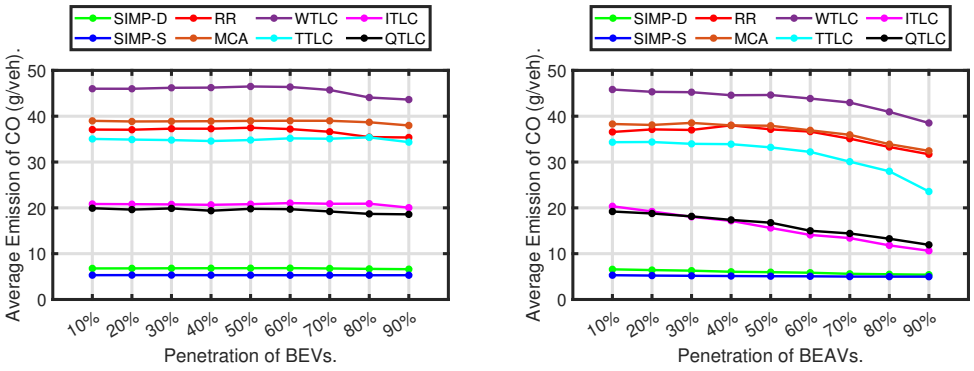

(a) Penetration of BEVs. (b) Penetration of BEAVs.

Figure 8.11: Average CO (g) emission per ICE vehicle for various IM approaches at various penetration rates of BEVs and BEAVs.

are lower than that of the BEVs scenario as autonomous driver control executes smoother movements and induces that behavior on human driver control agents correlating with the waiting delays (Fig. 8.6).

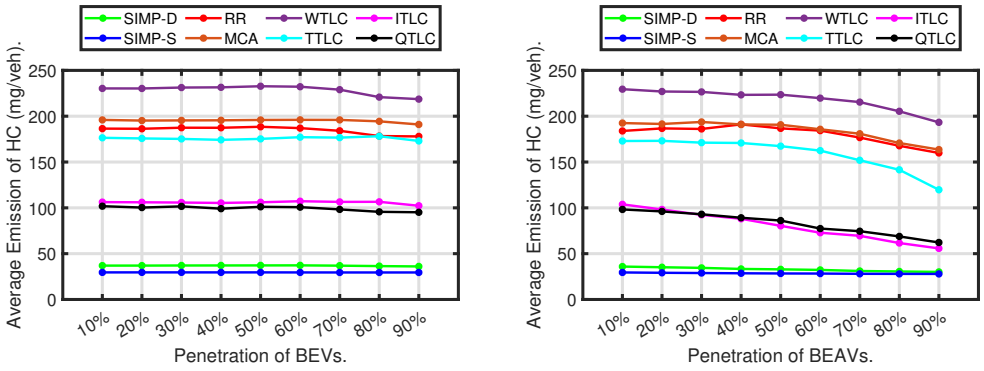

(a) Penetration of BEVs. (b) Penetration of BEAVs.

Figure 8.12: Average HC (mg/veh) emission per ICE vehicle for various IM approaches at various penetration rates of BEVs and BEAVs.

SIMPs emission values of the BEAVs scenario are almost similar to the emission values of the BEVs scenario. The performance behavior of QTLC and ITLC interchange after 30% of BEAVs. This means that the performance of QTLC is better until 30% of BEAVs, then the ITLC takes over. This behavior can be explained again by their design, i.e., the ITLC is designed to support autonomous vehicles while QTLC is designed to support human-driven vehicles. Like other IM approaches, TTLC, RR, MCA, and WTLC show the correlation between gasoline consumption and the associated emission of air pollutants. Overall, WTLC is the worst-performing approach with the highest emissions of air pollutants. In this scenario, SIMP minimizes 76% of PM_x, 59.6% of NO_x, 101.45% of CO, 95.2% of HC, and 53.8% of CO_2 against ITLC, the following best approach.

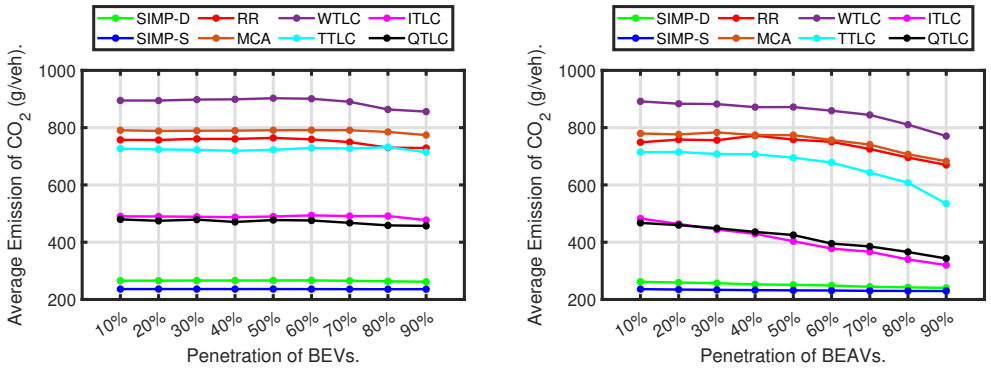

(a) Penetration of BEVs.

(b) Penetration of BEAVs.

Figure 8.13: Average CO_2 (g) emission per ICE vehicle for various IM approaches at various penetration rates of BEVs and BEAVs.

8.3 Networks of Multi-lane Intersections

We designed two scenarios to study the growth rates of BEVs and their impacts on achieving transportation sustainability in a network of intersections. These scenarios indicate whether the left-crossing lane is dedicated or shared, same as scenarios 1 and 2 presented in Section 6.3. We chose the traffic arrival rate of $0.1veh/s$ and $30km/h$ maximum speed. From Fig. 6.6, this $0.1veh/s$ indicate a medium (close to saturation) traffic arrival rate. The simulation parameters and associated values for HVs and ICE vehicles are exhibited in Table 3.1 and BEVs in Table 8.6. Energy efficiency and emissions efficiency are studied for increasing BEVs and decreasing ICE vehicles in a total of 2500 vehicles.

Note that we are not presenting the results of the growing rates of BEAVs due to the similar performance behavior and varying absolute values in relation to the BEAVs at isolated single-lane intersections presented in previous sections.

8.3.1 Energy Efficiency

Figures 8.14 and 8.15 exhibit the average gasoline and average electricity consumption results. The gasoline consumption behavior is expected due to the reduced rates of ICE vehicles. Interestingly, the gasoline consumption graphs are similar to those observed in scenario-3 of the single-lane intersection case but have different absolute values for different IM approaches (Fig. 8.4a). However, the question is which IM approach is more energy efficient. From the graphs, it is clear that SIMP is the more energy-efficient approach, again. In contrast, the WTLC is the worst-performing approach with the highest gasoline consumption values in both scenarios. The other approaches (RR, TTLC, and MCA) show intermediary performance with relatively closer values. At the 10% of BEVs, the differences between consumption values are higher and keep reducing, reaching very close at 90%. Overall, in the dedicated left-lane case, SIMP is up to 47% more energy efficient

than the following best approach, TTLC. In the shared left-lane case, the improvements of SIMP are up to 43%, in which the MCA is the following best approach.

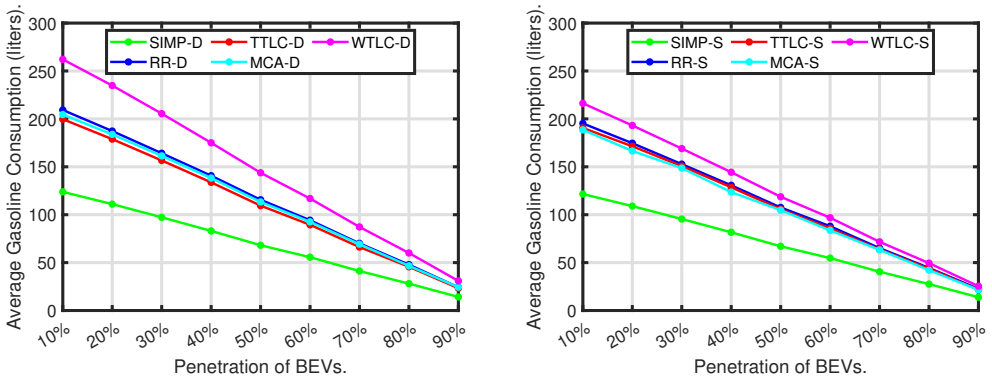

(a) Penetration of BEVs. (b) Penetration of BEVs.

Figure 8.14: ICE vehicles average gasoline consumption (*liters*) for growing BEVs rates.

In Fig. 8.15, we can observe roughly linear growth in the average electricity consumption for growing BEV rates. The behavior of these results is similar to the ones observed at the single-lane isolated intersections. However, the difference between IM approaches is relatively very close. Overall, SIMP is up to 1.45% energy efficient. The main reason is the regenerative braking that BEVs utilize.

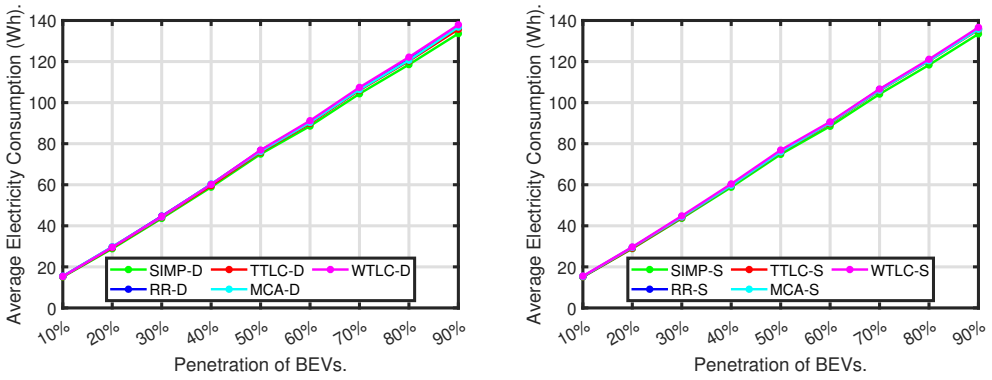

(a) Penetration of BEVs. (b) Penetration of BEVs.

Figure 8.15: ICE vehicles average gasoline consumption (ml) of comparing IM approaches for BEVs and BEAVs scenarios.

8.3.2 Emissions Efficiency

The average emissions of air pollutants (CO, CO_2, HC, PMx, and NOx) for the BEVs scenarios (dedicated and shared left lanes) are exhibited in Table 8.7. The emissions results correlate with the gasoline consumption results. This means that the decreasing rates of ICE vehicles considerably reduce the emission of associated air pollutants. Similar to the

fuel consumption results, these emissions results also show corresponding behavior with the single-lane intersections, scenario 3.

In the dedicated left lane case, the emissions efficiency that can be achieved using the SIMP protocol is up to 89.4% (CO), 46.8% (CO_2), 83.9% (HC), 69.5% (PMx), and 52.6% (NOx). These values in the shared left lane case are 85% (CO), 42.6% (CO_2), 79.5% (HC), 64.9% (PMx), and 48.2% (NOx). From these results, we can emphasize that the emission of air pollutants can be minimized by employing shared left-lane intersections, specifically when the SIMP (i.e., SIMP-S) manages them.

8.4 Discussion

This section combines the discussion of all simulation scenarios of this chapter. The simulation results show that SIMP outperforms all the competing IM approaches in all the tested intersections, scenarios, speeds, and performance metrics. The results clearly indicate that it is better, at low-speed urban conditions, to synchronize vehicles intersection access from all the non-conflicting roads than permitting one road at a time sequentially or opposite road lanes parallelly. Synchronous intersection access leads to more fluid traffic flows, i.e., smoother acceleration/deceleration and braking with fewer stops that efficiently reduce the spillback effect and are adequate for reducing the corresponding time loss, which is one reason for SIMP's highest average speed. The other advantage of using the synchronous framework is that the travel time loss and waiting time of vehicles accessing the intersection are short. On the one hand, SIMP allows multiple vehicles, one from each lane. On the other hand, CDM identifies possible conflicting paths as vehicles enter the intersection area and execute the synchronous movement when they approach the intersection.

The fuel consumption results prove that the SIMP is more sustainable, with the lowest fuel consumption in all cases due to smoother acceleration/deceleration, braking, and less engine idling time, better preserving vehicle momentum and improving the controllability of transient engine operations. The leader and follower relation is broken at the intersection, saving AVs' fuel that follows an HV. In the leader/follower relation, if the leader decelerates to a stop, the follower also must decelerate to a stop by maintaining the safety headway; and the follower's acceleration depends upon the leader's relative velocity. Hence, the followers' driving behavior depends on the leader's behavior, consumes more fuel and associated emissions, and breaking this dependency makes the follower vehicle independent. SIMP's fuel consumption is slightly reduced in high traffic densities for increased AV penetration as they have perfect or near-perfect driving behavior. All these elements lead to lower gasoline consumption and the associated emission of dangerous air pollutants like PMx, NOx, and CO, as well as other emissions, i.e., CO_2 and HC.

On the other hand, sequential (RR, MCA, and WTLC) and parallel (TTLC, ITLC, and QTLC) IM approaches show inferior performance due to the conservative nature of allowing vehicles from one road at a time or from opposite road lanes, which forces vehicles to come

	Avg. emission of CO ($grams$).									
	SIMP-D	RR-D	TTLC-D	MCA-D	WTLC-D	SIMP-S	RR-S	TTLC-S	MCA-S	WTLC-S
10%	9	25.6	23.7	24.7	36	8.7	23	22	21.7	27.2
20%	8.1	22.9	21.3	22.3	32.2	7.8	20.5	19.9	19	24.2
30%	7.1	20.1	18.6	19.6	28.1	6.8	17.9	17.5	17.1	21.2
40%	6.1	17.2	15.8	16.8	23.9	5.8	15.3	14.9	14	18.1
50%	5	14.1	12.9	13.7	19.6	4.8	12.6	12.3	12.1	14.9
60%	4	11.5	10.6	11.2	15.9	4	10.4	10	9.5	12.1
70%	3	8.6	7.8	8.4	11.9	2.9	7.7	7.4	7.3	9
80%	2.1	5.9	5.4	5.6	8.2	2	5.2	5.1	4.8	6.2
90%	1	3	2.8	3	4.3	1	2.6	2.5	2.4	3.2
	Avg. emission of CO_2 ($grams$).									
10%	388.2	656.1	626.1	641.3	821.7	381.1	612.2	597.4	591.2	678.1
20%	348.2	587.2	560.8	576.2	736.1	341.6	547.5	537.4	522.1	605.5
30%	304.9	514.7	491	506	644.2	299.4	479	472.6	466.1	530
40%	260.5	441.1	419.4	433.5	548.8	255.9	409.7	403.1	387.5	452.4
50%	213.6	362.4	343.2	355.2	450.8	210.2	337.2	331.5	328.4	372.2
60%	174.4	295.4	280.5	290.1	366.5	171.6	275.8	268.7	262.3	303.6
70%	129.2	219.7	207.6	217	273.5	126.9	204.2	200.3	198.4	224.8
80%	88	150.1	143.1	146.2	188.3	86.5	139.2	136.9	132.2	155.1
90%	44.4	75.9	73	76.4	96.8	43.6	70.8	68.2	67.5	79.6
	Avg. emission of HC (mg).									
10%	50	131.6	122.4	127.2	182.7	48.1	118.6	114	112.4	139.4
20%	44.8	117.7	109.7	114.6	163.6	43.1	106	102.7	98.3	124.2
30%	39.2	103.1	95.8	100.7	143	37.2	92.6	90.5	88.7	108.7
40%	33.5	88.5	81.8	86.4	121.5	32.3	79.2	77.2	72.4	92.8
50%	27.4	72.7	66.7	70.4	99.8	26.5	65.3	63.4	62.6	76.4
60%	22.4	59.3	54.6	57.6	81.1	21.6	53.5	51.3	49.4	62.3
70%	16.6	44.2	40.4	43.3	60.6	16	39.7	38.4	37.8	46.1
80%	11.3	30.2	27.9	28.9	41.8	10.9	27	26.3	24.8	31.9
90%	5.7	15.2	14.2	15.5	21.6	5.5	13.7	12.9	12.7	16.6
	Avg. emission of PMx (mg).									
10%	5.6	12.3	11.6	11.9	16.5	5.4	11.2	10.8	10.7	12.9
20%	5	11	10.3	10.8	14.8	4.8	10	9.8	9.4	11.5
30%	4.4	9.7	9	9.4	12.9	4.2	8.8	8.6	8.4	10
40%	3.7	8.3	7.7	8.1	11	3.6	7.5	7.3	6.9	8.6
50%	3.1	6.8	6.3	6.6	9	3	6.2	6	6	7.1
60%	2.5	5.5	5.2	5.4	7.3	2.4	5.1	4.9	4.7	5.8
70%	1.9	4.1	3.8	4.1	5.5	1.8	3.7	3.6	3.6	4.3
80%	1.3	2.8	2.6	2.7	3.8	1.2	2.5	2.5	2.4	2.9
90%	0.64	1.4	1.3	1.4	1.9	0.62	1.3	1.2	1.2	1.5
	Avg. emission of NOx (mg).									
10%	152.7	275.8	261.9	269	351.9	149.4	255.6	248.8	245.9	285.8
20%	137	246.8	234.6	241.8	315.2	134	228.5	223.9	216.8	255.2
30%	119.9	216.3	205.3	212.3	275.8	117.4	199.9	196.9	193.9	223.3
40%	102.5	185.5	175.4	182	234.8	100.4	171	168	160.7	190.6
50%	84	152.4	143.4	149	192.9	82.4	140.7	138.1	136.7	156.9
60%	68.6	124.2	117.3	121.7	156.8	67.3	115.2	111.9	108.9	127.9
70%	50.8	92.4	86.8	91.1	117.1	49.7	85.3	83.5	82.6	94.7
80%	34.6	63.1	59.8	61.3	80.6	33.9	58.1	57.1	54.9	65.4
90%	17.5	31.9	30.5	32.2	41.5	17.1	29.6	28.4	28	33.6

Table 8.7: Average emission of air pollutants (CO, CO_2, HC, PMx, and NOx) for mixed ICE vehicles and BEVs at $30km/h$ maximum speed.

to a complete halt even if the intersection is free of other cars. The fact that multiple vehicles can cross consecutively also keeps leader/follower relationships. This combination imposes significant variations on the speed of the vehicles, with frequent slowdown, braking, and acceleration. Also, all other IM approaches suffer from the spillback generated by their TLC logic. The same spillback mechanism is responsible for higher time loss results and associated fuel consumption and air pollutants emissions.

In practice, existing IM approaches try to compensate for these issues by combining features of more fluid management, e.g., allowing them to turn right during red periods using a specific flashing yellow light. This combination leads to a hybrid behavior that improves traffic fluidity. However, it relies on the vehicles autonomous behaviors to avoid collisions; thus, it is not inherently safe.

Regarding electricity consumption, all IM approaches exhibit similar behaviors with minor differences. This is due to the regenerative braking of BEVs/BEAVs that capture the kinetic energy that would otherwise have been wasted when the vehicle decelerates or reaches a stoppage while braking. The trade-offs of employing the BEVs and BEAVs are debatable that BEVs are more energy savers than BEAVs. The BEAVs consume more electricity due to the higher levels of aerodynamic drag. On the other hand, employing BEAVs improves the throughput, travel time loss, and energy than that of BEVs due to smoother driving. Further studies on BEVs and BEAVs performance are required to understand these trade-offs better before adopting them.

8.5 Summary

This chapter studied the transportation sustainability of introducing growing rates of AVs, BEVs, and BEAVs at single-lane and multi-lane isolated intersections and networks of multi-lane intersections. The other dimension of the study is the operational efficiency of IM approaches for those growing rates of AVs, BEVs, and BEAVs. For the performance comparison, various metrics in various scenarios are considered. For isolated single-lane intersections, average speed, travel time loss, energy efficiency (gasoline and electricity), and associated vehicular emissions are considered. In the isolated multi-lane intersections case, we considered the intersection throughput, average waiting time, fuel efficiency, and emissions efficiency. In the case of networks of intersections, we considered only the efficiency of energy and emissions. The following observations are made from the simulation studies.

- Regarding the intersections, multi-lane intersections are more sustainable than single-lane intersections, where vehicles wait for less time, consume less gasoline, and emit less air pollutants. The saturation level of multi-lane intersections is also higher. The reason is the additional road lanes on which the traffic is distributed.

- The fuel consumption and associated emissions results correlate with the waiting time results. This is due to the engine idling during waiting. Therefore, the IM approach that imposes less waiting time is more sustainable.
- The SIMP protocol performs better than the competing IM approaches in all the tested scenarios, performance metrics, and intersections (isolated and networked) by synchronizing vehicles intersection access.

The following chapter emphasizes the conclusions drawn and the future directions to follow.

Chapter 9

Conclusions & Future Directions

This chapter first summarizes the main research contributions and discusses the thesis validation, then identifies limitations of this work and introduces future directions.

9.1 Contributions and Thesis Validation

Current urban transportation services are strained due to fossil fuel dependency, environmental challenges, and associated human health conditions. The urban future would bring disastrous consequences if not guided towards sustainability due to the further expected growth in the urban population. Therefore, sustainable transportation is a major concern demanding affordable energy-efficient transportation, emitting low- to zero-emissions of air pollutants, like electrical energy. In urban transportation, road intersections play a crucial role where growing trends in queue length, waiting delays, fuel wastage, and associated adverse effects can be observed. On the other hand, communication, electric and autonomous technologies are envisioned to provide new opportunities for sustainable transportation. In this context this work provides three research contributions to the state of the art in ITS, which are described below and used to validate our thesis statement.

9.1.1 Synchronous Framework

The primary contribution of our research was described in Chapter 4 and it consists of the Intelligent Intersection Management Architecture IIMA and the Synchronous Intersection Management Protocol SIMP. This is a *synchronous framework* that manages mixed traffic combining HVs and AVs in any percentage. IIMA employs roadside sensors such as induction loop detectors and cameras to detect vehicles positions in the intersection area and their crossing directions. SIMP employs the crossing directions and the Conflicting Directions Matrix CDM for decision-making and admit or block vehicles at the intersection entrance. This admission operates vehicle by vehicle, possibly with multiple vehicles in parallel, in cycles. This approach allows reacting quickly to vehicles present at the intersection entrance, indicating the reactive nature of the framework. A wide range of driving

contexts is simulated, including low to medium and congested traffic scenarios in urban flat road settings. The *synchronous framework* was extended from isolated single-lane [171; 178] to multi-lane [180] intersections in Chapter 5 and to grid networks of multi-lane intersections [179; 185] in Chapter 6. Simulation results of average metrics exhibit a clear dominance of the *synchronous framework* against the baseline conventional, adaptive, and intelligent IM approaches in all tested scenarios, speeds, and performance metrics, namely the traffic throughput (up to 30%), travel time loss (up to 129.2%), and fuel consumption (up to 67.4%). Therefore, applying the *synchronous framework* in real-world scenarios seems advantageous and easily applicable to any intersection type by knowing the vehicles crossing directions on road lane groups (using road/roadside sensors) and configuring the appropriate CDM.

9.1.2 Worst-Case Response Time

Another contribution of our research is a new delay metric that aims at characterizing the service efficiency of IM strategies. It equips city planners with an estimate of the worst service a given intersection can provide considering a known statistical traffic arrival pattern, particularly maximum waiting time and queue size. Knowing the maximum queue size allows tuning the IM configuration to prevent queue spillback at neighboring intersections. Knowing the maximum waiting time is relevant for all users, but particularly for safety-critical or mission-critical traffic. This new metric is called *Worst-Case Response Time* (WCRT) inspired in real-time systems analysis and it was presented in Chapter 7.

The analytical WCRT values were validated against simulation measurements for a fixed number of injected vehicles following the uniform distribution at varying intensities, from non-saturated to saturated. In the case of isolated multi-lane intersections (particularly dedicated left-lane intersections), two maximum speeds of 30 and $50km/h$ were employed [182]. The traffic was characterized using arrival curves that represent worst-case conditions. We utilized the IM-specific parameters and associated values to draw service curves, including the total control cycle time and the maximum number of vehicles each IM serves in one control cycle. Our analysis provides upper bounds for the response time of vehicles crossing the intersection.

Regarding the networks of intersections [184], both dedicated and shared left-lane intersections were considered. First, vehicles maximum waiting time when crossing a set of intersections was estimated to understand the efficiency of the IM approaches at $30km/h$ maximum speed. Then the WCRT values were obtained. A set of four traffic arrival rates were simulated, representing low to medium and close to saturated traffic conditions. Lastly, the simulation results were employed to validate the analytical values. The simulation results validate the estimated WCRT values with some pessimism that varies across scenarios.

9.1.3 Transportation Sustainability

The previous contributions dealt with mixed traffic of HVs and AVs in equal amounts (i.e., 50% each) and using ICE propulsion only. Thus, in our research we also provide a third contribution consisting of a study of the transitioning from ICE HVs to BEVs, and from ICE AVs to BEAVs to confirm the benefits these vehicles bring to transportation sustainability when their penetration increases. This contribution considered several mixed traffic scenarios in isolated single-lane and multi-lane intersections and grid networks of multi-lane intersections and was developed in Chapter 8.

At single-lane intersections, the first scenario set a baseline using equal numbers of HVs and AVs, both of which were ICE, and measured average fuel consumption and associated emissions [174]. The second scenario analyzed the impacts of growing rates of AVs mixed with HVs, again with ICE vehicles, only on the average speed, travel time loss, fuel consumption, and emissions. This scenario was repeated but using BEAVs instead of ICE AVs to analyze the advantages that autonomy with electrical propulsion could bring [173]. At isolated multi-lane intersections [183], we analyzed the impact of introducing growing rates of BEVs or BEAVs concerning intersection throughput, average waiting time, energy (gasoline and electricity) savings, and emissions efficiency for heavy traffic conditions. Finally, the same study was carried out in a grid network of multi-lane intersections with both dedicated and shared left lanes.

In all these experiments, the *synchronous framework* outperformed all other IM approaches in all the tested scenarios at all the intersections considered. We also observed that growing rates of AVs improve the performance of all IM approaches towards achieving the SUM. This is particularly visible with growing penetrations of BEAVs. Hence, our results indicate that the *synchronous framework* with BEAVs provides the most sustainable transportation management system among all configurations tested.

9.1.4 Thesis Validation

The contributions that we just summarized provide a validation of our thesis statement presented in Chapter 1. In fact, we proposed a reactive *synchronous framework* that was shown to provide smoother and more efficient intersection access for any combination of HVs and AVs, exhibiting improved throughput together with reduced delays, fuel wastage, and associated emissions of dangerous air pollutants. This constitutes a clear step toward SUM.

9.2 Limitations & Future Directions

In spite of all the benefits brought by the proposed *synchronous framework*, there are still pending limitations that would benefit from further research.

One limitation that was observed when applying the *synchronous framework* in a grid network of multi-lane intersections with dedicated left lanes was that some road lanes were lightly used while others were saturated. This is due to the random predefined routes between origin and destination without considering the actual traffic conditions at each intersection. Therefore, one way to solve the issue is by dynamically adapting the route based on traffic conditions at each intersection. The MAS and RL-based techniques have already proven their applicability in such scenarios. Applying them to this problem can improve performance and the applicability of the *synchronous framework* in a city-wide road network.

Another limitation is that the *synchronous framework* can only be applied to scenarios in which vehicle-to-vehicle interactions are prevalent, in practice without pedestrians. It is also necessary to incorporate emergency response vehicles (e.g., ambulances) and how the IM approach could prioritize serving them. These modifications seem non-trivial requiring specific sensing and then a clear definition of adequate maneuvers that preserve the safety of pedestrians and other vulnerable road users in the first case and cut delays to a minimum in the second case.

The analytical models of WCRT are no longer valid when the traffic demand is higher than the road capacity, causing spillbacks and overflows. In the future, we will adapt the analytical WCRT models to support such traffic conditions. We will also adapt the WCRT analysis to include unexpected road events such as emergency vehicle presence, road blockage, and accidents. A particular detail that also needs further work is the analytical estimation of the saturation speed, which is currently done by observation in the simulations. Overall, we would like to apply the WCRT analysis to a real-world city-wide general road network and assess its efficiency.

In what concerns the sustainability study, we are not considering the emissions of air pollutants in the BEVs and BEAVs scenarios, where the factors of mining, production, and disposal of batteries would have an effect. Considering such facts in the trade-off analysis concerning adopting BEVs and BEAVs could reveal new balances with potentially different results. Therefore, we plan to include those factors in the future and extend the study to a city-wide road network.

The proposed *synchronous framework* uses V2X communications in AVs. However, these communications have not been considered explicitly. Thus, another future direction is also model V2X communications between AVs and road infrastructure and consider the impact of disturbances in content delivery due to message losses caused by interferences, vehicular mobility, dynamic topologies, etc. These effects also make delivery, vehicular mobility, topology management, and consistent routing make using internet protocols (IP) for V2X communications more complex. New Information-Centric Networking (ICN) paradigms were introduced to cope with IP challenges and quality of service provisions. Named-Data-Networking (NDN) [96], a part of the ICN paradigm, has great potential to address IP challenges in V2X communications. Content name is the key element in the

NDN, and networking semantics are shifted from delivering the packet to a given destination address to fetching data identified by a given name. A consumer puts the name of the requested data into an interest packet and sends it to the network. Routers use this name to forward the interest toward the data producer(s). Once the interest reaches a node with the requested data, the node will return a data packet containing both the name and the content, together with a signature by the producer's key, which binds the data and security. Hence, NDN-based V2X communications seem to have a high potential for supporting new future research.

References

[1] Abdeljalil Abbas-Turki, Yazan Mualla, Nicolas Gaud, Davide Calvaresi, Wendan Du, Alexandre Lombard, Mahjoub Dridi, and Abder Koukam. Autonomous intersection management: Optimal trajectories and efficient scheduling. *Sensors*, 23(3):1509, 2023.

[2] Baher Abdulhai, Rob Pringle, and Grigoris J Karakoulas. Reinforcement learning for true adaptive traffic signal control. *Journal of Transportation Engineering*, 129 (3):278–285, 2003.

[3] Baher Abdulhai, Rob Pringle, and Grigoris J Karakoulas. Reinforcement learning for true adaptive traffic signal control. *Journal of Transportation Engineering*, 129 (3), 2003.

[4] Anton Agafonov, Alexander Yumaganov, and Vladislav Myasnikov. Cooperative control for signalized intersections in intelligent connected vehicle environments. *Mathematics*, 11(6):1540, 2023.

[5] Kyoungho Ahn, Sangjun Park, and Hesham A Rakha. Impact of intersection control on battery electric vehicle energy consumption. *Energies*, 13(12):3190, 2020.

[6] Aiman Albatayneh, Mohammad N Assaf, Dariusz Alterman, and Mustafa Jaradat. Comparison of the overall energy efficiency for internal combustion engine vehicles and electric vehicles. *Rigas Tehniskas Universitates Zinatniskie Raksti*, 24(1):669–680, 2020.

[7] Mohammed Albrahim, Ahmed Al Zahrani, Anvita Arora, Rubal Dua, Bassam Fattouh, and Adam Sieminski. An overview of key evolutions in the light-duty vehicle sector and their impact on oil demand. *Energy Transitions*, 3(1):81–103, 2019.

[8] Levente Alekszejenkó and Tadeusz P Dobrowiecki. Sumo based platform for cooperative intelligent automotive agents. In *SUMO*, pages 107–123, 2019.

[9] S Sheik Mohammed Ali, Boby George, Lelitha Vanajakshi, and Jayashankar Venkatraman. A multiple inductive loop vehicle detection system for heterogeneous and lane-less traffic. *IEEE Transactions on Instrumentation and Measurement*, 61(5): 1353–1360, 2011.

[10] Ala Abu Alkheir, Moayad Aloqaily, and Hussein T Mouftah. Connected and autonomous electric vehicles (caevs). *IT professional*, 20(6):54–61, 2018.

[11] Shaik Shabana Anjum, Rafidah Md Noor, Nasrin Aghamohammadi, Ismail Ahmedy, Laiha Mat Kiah, Nornazlita Hussin, Mohammad Hossein Anisi, and Muhammad Ahsan Qureshi. Modeling traffic congestion based on air quality for greener environment: an empirical study. *IEEE Access*, 7:57100–57119, 2019.

[12] Shunsuke Aoki and Ragunathan Rajkumar. V2v-based synchronous intersection protocols for mixed traffic of human-driven and self-driving vehicles. In *2019 IEEE 25th International Conference on Embedded and Real-Time Computing Systems and Applications (RTCSA)*, pages 1–11. IEEE, 2019.

[13] Shunsuke Aoki and Ragunathan Raj Rajkumar. A configurable synchronous intersection protocol for self-driving vehicles. In *2017 IEEE 23rd International Conference on Embedded and Real-Time Computing Systems and Applications (RTCSA)*, pages 1–11. IEEE, 2017.

[14] Ramin Arvin, Asad J Khattak, Mohsen Kamrani, and Jackeline Rio-Torres. Safety evaluation of connected and automated vehicles in mixed traffic with conventional vehicles at intersections. *Journal of Intelligent Transportation Systems*, 25(2):170–187, 2020.

[15] Mohammad Aslani, Mohammad Saadi Mesgari, and Marco Wiering. Adaptive traffic signal control with actor-critic methods in a real-world traffic network with different traffic disruption events. *Transportation Research Part C: Emerging Technologies*, 85:732–752, 2017.

[16] L Athanasopoulou, H Bikas, and P Stavropoulos. Comparative well-to-wheel emissions assessment of internal combustion engine and battery electric vehicles. *Procedia CIRP*, 78:25–30, 2018.

[17] Reza Azimi, Gaurav Bhatia, Ragunathan Rajkumar, and Priyantha Mudalige. Ballroom intersection protocol: Synchronous autonomous driving at intersections. In *2015 IEEE 21st International Conference on Embedded and Real-Time Computing Systems and Applications*, pages 167–175. IEEE, 2015.

[18] Fan Bai, Daniel D Stancil, and Hariharan Krishnan. Toward understanding characteristics of dedicated short range communications (dsrc) from a perspective of vehicular network engineers. In *Proceedings of the sixteenth annual international conference on Mobile computing and networking*, pages 329–340, 2010.

[19] Prateek Bansal and Kara M Kockelman. Forecasting americans' long-term adoption of connected and autonomous vehicle technologies. *Transportation Research Part A: Policy and Practice*, 95:49–63, 2017.

[20] Mirko Barthauer and Bernhard Friedrich. Presorting and presignaling: A new intersection operation mode for autonomous and human-operated vehicles. *Transportation research procedia*, 37:179–186, 2019.

[21] Abdullah Baz, Ping Yi, and Ahmad Qurashi. Intersection control and delay optimization for autonomous vehicles flows only as well as mixed flows with ordinary vehicles. *Vehicles*, 2(3):523–541, 2020.

[22] Assia Belbachir, Amal El Fallah-Seghrouchni, Arthur Casals, and Marcia Pasin. Smart mobility using multi-agent system. *Procedia Computer Science*, 151:447–454, 2019.

[23] Adam Berthelot, Andreas Tamke, Thao Dang, and Gabi Breuel. A novel approach for the probabilistic computation of time-to-collision. In *2012 IEEE Intelligent Vehicles Symposium*, pages 1173–1178. IEEE, 2012.

[24] Erik Björck and Fredrik Omstedt. A comparison of algorithms used in traffic control systems, 2018.

[25] Someswara Rao Bonela and B Raghuram Kadali. Review of traffic safety evaluation at t-intersections using surrogate safety measures in developing countries context. *IATSS research*, 2022.

[26] Marko AA Boon and Johan SH van Leeuwaarden. Networks of fixed-cycle intersections. *Transportation Research Part B: Methodological*, 117:254–271, 2018.

[27] Marko AA Boon, Ivo JBF Adan, Erik MM Winands, and Douglas G Down. Delays at signalized intersections with exhaustive traffic control. *Probability in the Engineering and Informational Sciences*, 26(3):337–373, 2012.

[28] Isabella Burch and Jock Gilchrist. Survey of global activity to phase out internal combustion engine vehicles. *Center of Climate Protection: Santa Rosa, CA, USA*, 2018.

[29] Sean Campbell, Niall O'Mahony, Lenka Krpalcova, Daniel Riordan, Joseph Walsh, Aidan Murphy, and Conor Ryan. Sensor technology in autonomous vehicles: A review. In *2018 29th Irish Signals and Systems Conference (ISSC)*, pages 1–4. IEEE, 2018.

[30] Fernando Castro-Alvarez, Shruti Vaidyanathan, Hannah Bastian, and Jen King. The 2018 international energy efficiency scorecard. *Report I1801, American Council for an Energy-Efficient Economy, Washington, DC*, 2018.

[31] Partha Chakroborty and Shinya Kikuchi. Evaluation of the general motors based car-following models and a proposed fuzzy inference model. *Transportation Research Part C: Emerging Technologies*, 7(4):209–235, 1999.

[32] Brian E Chandler, Matthew Myers, Jennifer E Atkinson, Tom Bryer, Richard Retting, Jeff Smithline, Jeff Trim, Peter Wojtkiewicz, Gary B Thomas, Steven P Venglar, et al. Signalized intersections informational guide. Technical report, United States. Federal Highway Administration. Office of Safety, 2013.

[33] Tang-Hsien Chang and Jen-Ting Lin. Optimal signal timing for an oversaturated intersection. *Transportation Research Part B: Methodological*, 34(6):471–491, 2000.

[34] Hrishit Chaudhuri, Vibha Masti, Vishruth Veerendranath, and S Natarajan. A comparative study of algorithms for intelligent traffic signal control. In *Machine Learning and Autonomous Systems: Proceedings of ICMLAS 2021*, pages 271–287. Springer, 2022.

[35] Lei Chen and Cristofer Englund. Cooperative intersection management: A survey. *IEEE transactions on intelligent transportation systems*, 17(2):570–586, 2015.

[36] Li-Wen Chen and Ta-Yin Hu. Flow equilibrium under dynamic traffic assignment and signal control—an illustration of pretimed and actuated signal control policies. *IEEE Transactions on intelligent transportation systems*, 13(3):1266–1276, 2012.

[37] Tom Cherrett, Hugh Bell, and Mike McDonald. Traffic management parameters from single inductive loop detectors. *Transportation Research Record*, 1719(1):112–120, 2000.

[38] Myungwhan Choi, Areeya Rubenecia, and Hyo Hyun Choi. Reservation-based autonomous intersection management considering vehicle failures in the intersection. In *2020 International Conference on Information Networking (ICOIN)*, pages 654–659. IEEE, 2020.

[39] Arthur John Hamblin Clayton. Road traffic calculations. *Journal of the Institution of Civil Engineers*, 16(7):247–264, 1941.

[40] Sina Dabiri, Kianoush Kompany, and Montasir Abbas. Introducing a cost-effective approach for improving the arterial traffic performance operating under the semi-actuated coordinated signal control. *Transportation research record*, 2672(18):71–80, 2018.

[41] C Daganzo and G Newell. Methods of analysis for transportation operations. *Institute of Transportation Studies, University of California at Berkeley*, 1995.

[42] GC D'ans and DC Gazis. Optimal control of oversaturated store-and-forward transportation networks. *Transportation Science*, 10(1):1–19, 1976.

[43] Saber Darmoul, Sabeur Elkosantini, Ali Louati, and Lamjed Ben Said. Multi-agent immune networks to control interrupted flow at signalized intersections. *Transportation Research Part C: Emerging Technologies*, 82:290–313, 2017.

[44] Sanhita Das, Alice Boruah, Arunabha Banerjee, Rahul Raoniar, Suresh Nama, and Akhilesh Kumar Maurya. Impact of covid-19: A radical modal shift from public to private transport mode. *Transport Policy*, 109:1–11, 2021.

[45] Bart De Schutter and Bart De Moor. Optimal traffic light control for a single intersection. *European Journal of Control*, 4(3):260–276, 1998.

[46] Taşkın Dirsehan and Ceren Can. Examination of trust and sustainability concerns in autonomous vehicle adoption. *Technology in Society*, 63:101361, 2020.

[47] Carlos Dora, Margaret A Phillips, and Margaret Phillips. Transport, environment and health. *WHO Regional Office Europe*, 89, 2000.

[48] Kurt Dresner and Peter Stone. Multiagent traffic management: An improved intersection control mechanism. In *Proceedings of the fourth international joint conference on Autonomous agents and multiagent systems*, pages 471–477, 2005.

[49] Kurt Dresner and Peter Stone. A multiagent approach to autonomous intersection management. *Journal of artificial intelligence research*, 31:591–656, 2008.

[50] Jinxiao Duan, Daqing Li, and Hai-Jun Huang. Reliability of the traffic network against cascading failures with individuals acting independently or collectively. *Transportation Research Part C: Emerging Technologies*, 147:104017, 2023.

[51] Fábio Duarte and Carlo Ratti. The impact of autonomous vehicles on cities: A review. *Journal of Urban Technology*, 25(4):3–18, 2018.

[52] Michael C Dunne and Renfrey B Potts. Algorithm for traffic control. *Operations Research*, 12(6):870–881, 1964.

[53] Patrick Emami, Mahmoud Pourmehrab, Marilo Martin-Gasulla, Sanjay Ranka, and Lily Elefteriadou. A comparison of intelligent signalized intersection controllers under mixed traffic. In *2018 21st International Conference on Intelligent Transportation Systems (ITSC)*, pages 341–348. IEEE, 2018.

[54] Myungeun Eom and Byung-In Kim. The traffic signal control problem for intersections: a review. *European transport research review*, 12:1–20, 2020.

[55] Ricardo Faria, Pedro Moura, Joaquim Delgado, and Anibal T De Almeida. A sustainability assessment of electric vehicles as a personal mobility system. *Energy Conversion and Management*, 61:19–30, 2012.

[56] Mahmood Fathy and Mohammed Yakoob Siyal. Measuring traffic movements at junctions using image processing techniques. *Pattern Recognition Letters*, 18(5):493–500, 1997.

[57] Paulo Fernandes, Tânia Fontes, Mark Neves, Sérgio Ramos Pereira, Jorge M Bandeira, Nagui M Rouphail, and Margarida C Coelho. Assessment of corridors with different types of intersections: Environmental and traffic performance analysis. *Transportation Research Record*, 2503(1):39–50, 2015.

[58] Christiaan M Fourie and Hermanus Carel Myburgh. An intra-vehicular wireless multimedia sensor network for smartphone-based low-cost advanced driver-assistance systems. *Sensors*, 22(8):3026, 2022.

[59] José Alberto Fuinhas, Matheus Koengkan, Nuno Carlos Leitão, Chinazaekpere Nwani, Gizem Uzuner, Fatemeh Dehdar, Stefania Relva, and Drielli Peyerl. Effect of battery electric vehicles on greenhouse gas emissions in 29 european union countries. *Sustainability*, 13(24):13611, 2021.

[60] Kaizhou Gao, Yicheng Zhang, Rong Su, Fajun Yang, Ponnuthurai Nagaratnam Suganthan, and MengChu Zhou. Solving traffic signal scheduling problems in heterogeneous traffic network by using meta-heuristics. *IEEE Transactions on Intelligent Transportation Systems*, 20(9):3272–3282, 2018.

[61] Nathen H Gartner. On-line and off-line urban traffic control. In *Computing in Civil Engineering*, pages 503–513. ASCE, 1981.

[62] F Garwood. An application of the theory of probability to the operation of vehicular-controlled traffic signals. *Supplement to the Journal of the Royal Statistical Society*, 7(1):65–77, 1940.

[63] Denos C Gazis. Optimum control of a system of oversaturated intersections. *Operations Research*, 12(6):815–831, 1964.

[64] Wade Genders and Saiedeh Razavi. An open-source framework for adaptive traffic signal control. *arXiv preprint arXiv:1909.00395*, 2019.

[65] Mina Ghanbarikarekani, Xiaobo Qu, Michelle Zeibots, Weiwei Qi, et al. Minimizing the average delay at intersections via presignals and speed control. *Journal of Advanced Transportation*, 2018, 2018.

[66] Peter G Gipps. A behavioural car-following model for computer simulation. *Transportation Research Part B: Methodological*, 15(2):105–111, 1981.

[67] Gary Golembiewski, Brian E Chandler, et al. Intersection safety: A manual for local rural road owners. Technical report, United States. Federal Highway Administration. Office of Safety, 2011.

[68] Sandra Vieira Gomes, Srinivas Reddy Geedipally, and Dominique Lord. Estimating the safety performance of urban intersections in lisbon, portugal. *Safety science*, 50 (9):1732–1739, 2012.

[69] Dominik Grether, Joschka Bischoff, and Kai Nagel. Traffic-actuated signal control: Simulation of the user benefits in a big event real-world scenario. In *2nd International Conference on Models and Technologies for ITS, Leuven, Belgium*, pages 11–12, 2011.

[70] Sonja Grossberndt and Alberto González Ortiz Bartonova, Alena. Public awareness and efforts to improve air quality in europe. *EEA and NILU*, 2021.

[71] Matt Grote, Ian Williams, John Preston, and Simon Kemp. A practical model for predicting road traffic carbon dioxide emissions using inductive loop detector data. *Transportation Research Part D: Transport and Environment*, 63:809–825, 2018.

[72] Juan Guerrero-Ibáñez, Sherali Zeadally, and Juan Contreras-Castillo. Sensor technologies for intelligent transportation systems. *Sensors*, 18(4):1212, 2018.

[73] Ammar Haydari and Yasin Yılmaz. Deep reinforcement learning for intelligent transportation systems: A survey. *IEEE Transactions on Intelligent Transportation Systems*, 23(1):11–32, 2020.

[74] Xiaozheng He and Xinkai Wu. Eco-driving advisory strategies for a platoon of mixed gasoline and electric vehicles in a connected vehicle system. *Transportation Research Part D: Transport and Environment*, 63:907–922, 2018.

[75] Eckard Helmers and Patrick Marx. Electric cars: technical characteristics and environmental impacts. *Environmental Sciences Europe*, 24(1):1–15, 2012.

[76] Peter Hemmerle, Micha Koller, Gerhard Hermanns, Michael Schreckenberg, Hubert Rehborn, and Boris S Kerner. Impact of synchronised flow in oversaturated city traffic on energy efficiency of conventional and electrical vehicles. In *Traffic and Granular Flow'15*, pages 539–546. Springer, 2016.

[77] Yunfei Hou, Salaheldeen MS Seliman, Enshu Wang, Jeffrey D Gonder, Eric Wood, Qing He, Adel W Sadek, Lu Su, and Chunming Qiao. Cooperative and integrated vehicle and intersection control for energy efficiency (civic-e 2). *IEEE Transactions on Intelligent Transportation Systems*, 19(7):2325–2337, 2018.

[78] PB Hunt, DI Robertson, RD Bretherton, and RI Winton. Scoot-a traffic responsive method of coordinating signals. Technical report, Transport Research Laboratory, 1981.

[79] Andrew Hursthouse and George Kowalczyk. Transport and dynamics of toxic pollutants in the natural environment and their effect on human health: research gaps and challenge. *Environmental Geochemistry and Health*, 31:165–187, 2009.

[80] Jessica N Hutton, Courtney D Bokenkroger, Melanie M Meyer, et al. Evaluation of an adaptive traffic signal system: route 291 in lee's summit, missouri. Technical report, Midwest Research Institute, 2010.

[81] Riccardo Iacobucci, Benjamin McLellan, and Tetsuo Tezuka. Modeling shared autonomous electric vehicles: Potential for transport and power grid integration. *Energy*, 158:148–163, 2018.

[82] IEA. Electric vehicles, iea, paris, license: Cc by 4.0. https://www.iea.org/reports/electric-vehicles, 2022. [Online; accessed 19-May-2023].

[83] Shahin Jalili, Samadhi Nallaperuma, Edward Keedwell, Alex Dawn, and Laurence Oakes-Ash. Application of metaheuristics for signal optimisation in transportation networks: A comprehensive survey. *Swarm and Evolutionary Computation*, 63:100865, 2021.

[84] Arshad Jamal, Muhammad Tauhidur Rahman, Hassan M Al-Ahmadi, Irfan Ullah, and Muhammad Zahid. Intelligent intersection control for delay optimization: Using meta-heuristic search algorithms. *Sustainability*, 12(5):1896, 2020.

[85] Arshad Jamal, Hassan M Al-Ahmadi, Farhan Muhammad Butt, Mudassir Iqbal, Meshal Almoshaogeh, and Sajid Ali. Metaheuristics for traffic control and optimization: Current challenges and prospects. *Search Algorithm-Essence of Optimization*, 2021.

[86] Udita Jana, Jyoti Prakash Das Karmakar, Pranamesh Chakraborty, Tingting Huang, Dave Ness, Duane Ritcher, and Anuj Sharma. Automated approach for computer vision-based vehicle movement classification at traffic intersections. *arXiv preprint arXiv:2111.09171*, 2021.

[87] Huifu Jiang, Jia Hu, Shi An, Meng Wang, and Byungkyu Brian Park. Eco approaching at an isolated signalized intersection under partially connected and automated vehicles environment. *Transportation Research Part C: Emerging Technologies*, 79: 290–307, 2017.

[88] Shan Jiang, Yufei Huang, Mohsen Jafari, and Mohammad Jalayer. A distributed multi-agent reinforcement learning with graph decomposition approach for large-scale adaptive traffic signal control. *IEEE Transactions on Intelligent Transportation Systems*, 23(9):14689–14701, 2021.

[89] Junchen Jin and Xiaoliang Ma. Hierarchical multi-agent control of traffic lights based on collective learning. *Engineering applications of artificial intelligence*, 68:236–248, 2018.

[90] Md Abdus Samad Kamal, Jun-ichi Imura, Tomohisa Hayakawa, Akira Ohata, and Kazuyuki Aihara. A vehicle-intersection coordination scheme for smooth flows of traffic without using traffic lights. *IEEE Transactions on Intelligent Transportation Systems*, 16(3):1136–1147, 2014.

[91] Takeshi Kano, Yuki Sugiyama, and Akio Ishiguro. Autonomous decentralized control of traffic signals that can adapt to changes in traffic. *Collective Dynamics*, 1:1–18, 2016.

[92] Thenuka Karunathilake and Anna Förster. A survey on mobile road side units in vanets. *Vehicles*, 4(2):482–500, 2022.

[93] Ryuji Kawamoto, Hideo Mochizuki, Yoshihisa Moriguchi, Takahiro Nakano, Masayuki Motohashi, Yuji Sakai, and Atsushi Inaba. Estimation of co2 emissions of internal combustion engine vehicle and battery electric vehicle using lca. *Sustainability*, 11(9):2690, 2019.

[94] John B Kenney. Dedicated short-range communications (dsrc) standards in the united states. *Proceedings of the IEEE*, 99(7):1162–1182, 2011.

[95] Manzoor Ahmed Khan, Hesham El Sayed, Sumbal Malik, Talha Zia, Jalal Khan, Najla Alkaabi, and Henry Ignatious. Level-5 autonomous driving—are we there yet? a review of research literature. *ACM Computing Surveys (CSUR)*, 55(2):1–38, 2022.

[96] Hakima Khelifi, Senlin Luo, Boubakr Nour, Hassine Moungla, Yasir Faheem, Rasheed Hussain, and Adlen Ksentini. Named data networking in vehicular ad hoc networks: State-of-the-art and challenges. *IEEE Communications Surveys & Tutorials*, 22(1): 320–351, 2019.

[97] Yong-Kul Ki and Doo-Kwon Baik. Model for accurate speed measurement using double-loop detectors. *IEEE Transactions on Vehicular Technology*, 55(4):1094–1101, 2006.

[98] Matheus Koengkan, José Alberto Fuinhas, Emad Kazemzadeh, Nooshin Karimi Alavijeh, and Saulo Jardim de Araujo. The impact of renewable energy policies on deaths from outdoor and indoor air pollution: Empirical evidence from latin american and caribbean countries. *Energy*, 245:123209, 2022.

[99] Pantelis Kopelias, Elissavet Demiridi, Konstantinos Vogiatzis, Alexandros Skabardonis, and Vassiliki Zafiropoulou. Connected & autonomous vehicles–environmental impacts–a review. *Science of the total environment*, 712:135237, 2020.

[100] Stefan Krauß. Microscopic modeling of traffic flow: Investigation of collision free vehicle dynamics. *TIB Hannover: RN 437(98-08)*, 1998.

[101] S Vasantha Kumar, P Priyadharshini, B Dhanalakshmi, and K Settu. Study of traffic flow at a three legged busy intersection in vellore, india. In *IOP Conference Series: Materials Science and Engineering*, volume 396(1), page 012015. IOP Publishing, 2018.

[102] SSP Kumara and Hoong Chor Chin. Application of poisson underreporting model to examine crash frequencies at signalized three-legged intersections. *Transportation Research Record*, 1908(1):46–50, 2005.

[103] Tamás Kurczveil, Pablo Álvarez López, and Eckehard Schnieder. Implementation of an energy model and a charging infrastructure in sumo. In *Simulation of Urban MObility User Conference*, pages 33–43. Springer, 2013.

[104] Tamás Kurczveil, Pablo Álvarez López, and Eckehard Schnieder. Implementation of an energy model and a charging infrastructure in sumo. In *Simulation of Urban MObility User Conference*, pages 33–43. Springer, 2013.

[105] Richard K Lattanzio and Corrie E Clark. Environmental effects of battery electric and internal combustion engine vehicles. Technical report, Congressional Research Service, 2020.

[106] Oscar Lazaro, Eric Robert, Lin Lan, Javier Gozalvez, Siebe Turksma, Fethi Filali, Fabio Cartolano, M. A. Urrutia, and Daniel Krajzewicz. itetris: An integrated wireless and traffic platform for real-time road traffic management solutions. *21st WWRF 2008*, October 2008.

[107] Choul Ki Lee, Ilsoo Yun, Jin-Hyung Choi, Se-jin Ko, and Jin-Yoo Kim. Evaluation of semi-actuated signals and pedestrian push buttons using a microscopic traffic simulation model. *KSCE Journal of Civil Engineering*, 17:1749–1760, 2013.

[108] Bai Li, Youmin Zhang, Yue Zhang, Ning Jia, and Yuming Ge. Near-optimal online motion planning of connected and automated vehicles at a signal-free and lane-free intersection. In *2018 IEEE Intelligent Vehicles Symposium (IV)*, pages 1432–1437. IEEE, 2018.

[109] Boyuan Li, Haiping Du, and Weihua Li. A potential field approach-based trajectory control for autonomous electric vehicles with in-wheel motors. *IEEE Transactions on Intelligent Transportation Systems*, 18(8):2044–2055, 2016.

[110] Shen Li, Keqi Shu, Chaoyi Chen, and Dongpu Cao. Planning and decision-making for connected autonomous vehicles at road intersections: A review. *Chinese Journal of Mechanical Engineering*, 34(1):1–18, 2021.

[111] Shen Li, Keqi Shu, Yang Zhou, Dongpu Cao, and Bin Ran. Cooperative critical turning point-based decision-making and planning for cavh intersection management system. *IEEE Transactions on Intelligent Transportation Systems*, 23(8):11062–11072, 2021.

[112] Yan Li, Lijie Yu, Siran Tao, and Kuanmin Chen. Multi-objective optimization of traffic signal timing for oversaturated intersection. *Mathematical Problems in Engineering*, 2013, 2013.

[113] Yuying Li and Qipeng Liu. Intersection management for autonomous vehicles with vehicle-to-infrastructure communication. *PLoS one*, 15(7):e0235644, 2020.

[114] Xiao Liang, S Ilgin Guler, and Vikash V Gayah. Joint optimization of signal phasing and timing and vehicle speed guidance in a connected and autonomous vehicle environment. *Transportation research record*, 2673(4):70–83, 2019.

[115] Xiao Joyce Liang, S Ilgin Guler, and Vikash V Gayah. An equitable traffic signal control scheme at isolated signalized intersections using connected vehicle technology. *Transportation Research Part C: Emerging Technologies*, 110:81–97, 2020.

[116] Wei-Hua Lin and Chenghong Wang. An enhanced 0-1 mixed-integer lp formulation for traffic signal control. *IEEE Transactions on Intelligent transportation systems*, 5 (4):238–245, 2004.

[117] Kai Liu, Dong Liu, Cheng Li, and Toshiyuki Yamamoto. Eco-speed guidance for the mixed traffic of electric vehicles and internal combustion engine vehicles at an isolated signalized intersection. *Sustainability*, 11(20):5636, 2019.

[118] Xi Liu, Ping-Chun Hsieh, and PR Kumar. Safe intersection management for mixed transportation systems with human-driven and autonomous vehicles. In *2018 56th Annual Allerton Conference on Communication, Control, and Computing (Allerton)*, pages 834–841. IEEE, 2018.

[119] Ying Liu, Lei Liu, and Wei-Peng Chen. Intelligent traffic light control using distributed multi-agent q learning. In *2017 IEEE 20th international conference on intelligent transportation systems (ITSC)*, pages 1–8. IEEE, 2017.

[120] Pablo Alvarez Lopez, Michael Behrisch, Laura Bieker-Walz, Jakob Erdmann, Yun-Pang Flötteröd, Robert Hilbrich, Leonhard Lücken, Johannes Rummel, Peter Wagner, and Evamarie Wießner. Microscopic traffic simulation using sumo. In *2018 21st international conference on intelligent transportation systems (ITSC)*, pages 2575–2582. IEEE, 2018.

[121] Melanie Lowe, Deepti Adlakha, James F Sallis, Deborah Salvo, Ester Cerin, Anne Vernez Moudon, Carl Higgs, Erica Hinckson, Jonathan Arundel, Geoff Boeing, et al. City planning policies to support health and sustainability: an international comparison of policy indicators for 25 cities. *The Lancet global health*, 10(6):e882–e894, 2022.

[122] Chaoru Lu, Jing Dong, and Liang Hu. Energy-efficient adaptive cruise control for electric connected and autonomous vehicles. *IEEE Intelligent Transportation Systems Magazine*, 11(3):42–55, 2019.

[123] Gongyuan Lu, Zili Shen, Xiaobo Liu, Yu Marco Nie, and Zhiqiang Xiong. Are autonomous vehicles better off without signals at intersections? a comparative computational study. *Transportation research part B: methodological*, 155:26–46, 2022.

[124] Hui Luo, Zhifeng Bao, Gao Cong, J Shane Culpepper, and Nguyen Lu Dang Khoa. Let trajectories speak out the traffic bottlenecks. *ACM Transactions on Intelligent Systems and Technology (TIST)*, 13(1):1–21, 2021.

[125] Highway Capacity Manual. Highway capacity manual. *Washington, DC*, 2(1), 2000.

[126] Charalampos Marmaras, Erotokritos Xydas, and Liana Cipcigan. Simulation of electric vehicle driver behaviour in road transport and electric power networks. *Transportation Research Part C: Emerging Technologies*, 80:239–256, 2017.

[127] Vito Mauro and C Di Taranto. Utopia. *IFAC Proceedings Volumes*, 23(2):245–252, 1990.

[128] Dave McKenney and Tony White. Distributed and adaptive traffic signal control within a realistic traffic simulation. *Engineering Applications of Artificial Intelligence*, 26(1):574–583, 2013.

[129] Claudio Meneguzzer, Massimiliano Gastaldi, Riccardo Rossi, Gregorio Gecchele, and Maria Vittoria Prati. Comparison of exhaust emissions at intersections under traffic signal versus roundabout control using an instrumented vehicle. *Transportation research procedia*, 25:1597–1609, 2017.

[130] Lei Miao and Dallas Leitner. Adaptive traffic light control with quality-of-service provisioning for connected and automated vehicles at isolated intersections. *IEEE Access*, 9:39897–39909, 2021.

[131] Panos G Michalopoulos and George Stephanopoulos. Oversaturated signal systems with queue length constraints—i: Single intersection. *Transportation Research*, 11 (6):413–421, 1977.

[132] Vicente Milanés and Steven E Shladover. Modeling cooperative and autonomous adaptive cruise control dynamic responses using experimental data. *Transportation Research Part C: Emerging Technologies*, 48:285–300, 2014.

[133] Vicente Milanés, Steven E Shladover, John Spring, Christopher Nowakowski, Hiroshi Kawazoe, and Masahide Nakamura. Cooperative adaptive cruise control in real traffic situations. *IEEE Transactions on intelligent transportation systems*, 15(1):296–305, 2013.

[134] Alan J. Miller. *A Computer control system for traffic networks.* University of Birmingham, Graduate School in Highway & Traffic Engineering Birmingham, England, 1963.

[135] Pitu Mirchandani and Larry Head. A real-time traffic signal control system: architecture, algorithms, and analysis. *Transportation Research Part C: Emerging Technologies*, 9(6):415–432, 2001.

[136] Roozbeh Mohammadi, Claudio Roncoli, and Milos N Mladenovic. User throughput optimization for signalized intersection in a connected vehicle environment. In *2019 6th international conference on models and technologies for intelligent transportation systems (mt-its)*, pages 1–10. IEEE, 2019.

[137] Roozbeh Mohammadi, Claudio Roncoli, and Miloš N Mladenović. Signalised intersection control in a connected vehicle environment: User throughput maximisation strategy. *IET Intelligent Transport Systems*, 15(3):463–482, 2021.

[138] Hossein Moradi, Sara Sasaninejad, Sabine Wittevrongel, and Joris Walraevens. Proposal of an integrated platoon-based round-robin algorithm with priorities for intersections with mixed traffic flows. *IET Intelligent Transport Systems*, 15(9):1106–1118, 2021.

[139] Benjamin Moseley and Shai Vardi. The efficiency-fairness balance of round robin scheduling. *Operations Research Letters*, 50(1):20–27, 2022.

[140] Edward A Mueller. Aspects of the history of traffic signals. *IEEE Transactions on Vehicular Technology*, 19(1):6–17, 1970.

[141] Akihito Nagahama, Daichi Yanagisawa, and Katsuhiro Nishinari. Dependence of driving characteristics upon follower–leader combination. *Physica A: Statistical Mechanics and its Applications*, 483:503–516, 2017.

[142] Elnaz Namazi, Jingyue Li, and Chaoru Lu. Intelligent intersection management systems considering autonomous vehicles: A systematic literature review. *IEEE Access*, 7:91946–91965, 2019.

[143] Gordon Frank Newell. Queues for a fixed-cycle traffic light. *The Annals of Mathematical Statistics*, pages 589–597, 1960.

[144] Tien Viet Nguyen, Patil Shailesh, Baghel Sudhir, Gulati Kapil, Libin Jiang, Zhibin Wu, Durga Malladi, and Junyi Li. A comparison of cellular vehicle-to-everything and dedicated short range communication. In *2017 IEEE Vehicular Networking Conference (VNC)*, pages 101–108. IEEE, 2017.

[145] National Highway Traffic Safety Administration (NHTSA). Automated vehicles for safety, 2019. URL https://www.nhtsa.gov/technology-innovation/automated-vehicles-safety.

[146] THEODOR-FABIAN Niculae. Edge server placement on traffic lights for smart city services. B.S. thesis, University of Twente, 2022.

[147] Chunting Nie, Heng Wei, Jianjun Shi, and Mengmeng Zhang. Optimizing actuated traffic signal control using license plate recognition data: Methods for modeling and algorithm development. *Transportation Research Interdisciplinary Perspectives*, 9: 100319, 2021.

[148] Mark Nieuwenhuijsen and Haneen Khreis. Urban and transport planning, environment and health. *Integrating Human Health into Urban and Transport Planning: A Framework*, pages 3–16, 2019.

[149] Mark J Nieuwenhuijsen. Urban and transport planning, environmental exposures and health-new concepts, methods and tools to improve health in cities. *Environmental health*, 15:161–171, 2016.

[150] Mark J Nieuwenhuijsen. Urban and transport planning pathways to carbon neutral, liveable and healthy cities; a review of the current evidence. *Environment international*, 140:105661, 2020.

[151] Ramin Niroumand, Mehrdad Tajalli, Leila Hajibabai, and Ali Hajbabaie. Joint optimization of vehicle-group trajectory and signal timing: Introducing the white phase for mixed-autonomy traffic stream. *Transportation research part C: emerging technologies*, 116:102659, 2020.

[152] Donncha O'Cinneide and Rod J Troutbeck. At-grade intersections/worldwide review. *Transportation research circular*, E-C003:26–1, 1998.

[153] European Court of Auditors. Urban mobility in the eu, 2019. URL https://www.eca.europa.eu/lists/ecadocuments/ap19_07/ap_urban_mobility_en.pdf.

[154] Cheol Oh, Seri Park, and Stephen G Ritchie. A method for identifying rear-end collision risks using inductive loop detectors. *Accident Analysis & Prevention*, 38(2): 295–301, 2006.

[155] World Health Organization et al. Who global air quality guidelines: particulate matter (pm2. 5 and pm10), ozone, nitrogen dioxide, sulfur dioxide and carbon monoxide: executive summary. *World Health Organization*, 2021.

[156] World Health Organization et al. World health statistics 2022: monitoring health for the sdgs, sustainable development goals. *World Health Organization*, pages 1–131, 2022.

[157] Carolina Osorio and Kanchana Nanduri. Energy-efficient urban traffic management: a microscopic simulation-based approach. *Transportation Science*, 49(3):637–651, 2015.

[158] Pratham Oza and Thidapat Chantem. A real-time server based approach for safe and timely intersection crossings. In *2019 IEEE 25th International Conference on Embedded and Real-Time Computing Systems and Applications (RTCSA)*, pages 1–12. IEEE, 2019.

[159] Pratham Oza and Thidapat Chantem. Timely and non-disruptive response of emergency vehicles: A real-time approach. In *29th International Conference on Real-Time Networks and Systems*, pages 192–203, 2021.

[160] Pratham Oza, Thidapat Chantem, and Pamela Murray-Tuite. A coordinated spillback-aware traffic optimization and recovery at multiple intersections. In *2020 IEEE 26th International Conference on Embedded and Real-Time Computing Systems and Applications (RTCSA)*, pages 1–10. IEEE, 2020.

[161] Ang Pan, Xin Zhang, Hideki Nakamura, and Wael Alhajyaseen. Investigating the efficiency and safety of signalized intersections under mixed flow conditions of autonomous and human-driven vehicles. *Arabian Journal for Science and Engineering*, 45:8607–8618, 2020.

[162] Aaron Parks-Young and Guni Sharon. Intersection management protocol for mixed autonomous and human-operated vehicles. *IEEE Transactions on Intelligent Transportation Systems*, 23(10):18315–18325, 2022.

[163] SM Patella, F Scrucca, F Asdrubali, and S Carrese. Carbon footprint of autonomous vehicles at the urban mobility system level: A traffic simulation-based approach. *Transportation Research Part D: Transport and Environment*, 74:189–200, 2019.

[164] Mahmoud Pourmehrab, Lily Elefteriadou, Sanjay Ranka, and Marilo Martin-Gasulla. Optimizing signalized intersections performance under conventional and automated vehicles traffic. *IEEE Transactions on intelligent transportation systems*, 21(7):2864–2873, 2019.

[165] H Chinthaka N Premachandra, Tomohiro Yendo, Mehrdad Panahpour Tehrani, Takaya Yamazato, Hiraku Okada, Toshiaki Fujii, and Masayuki Tanimoto. High-speed-camera image processing based led traffic light detection for road-to-vehicle visible light communication. In *2010 IEEE Intelligent Vehicles Symposium*, pages 793–798. IEEE, 2010.

[166] Syed Shah Sultan Mohiuddin Qadri, Mahmut Ali Gökçe, and Erdinç Öner. State-of-art review of traffic signal control methods: challenges and opportunities. *European transport research review*, 12:1–23, 2020.

[167] Hongsheng Qi, Rumeng Dai, Qing Tang, and Xianbiao Hu. Coordinated intersection signal design for mixed traffic flow of human-driven and connected and autonomous vehicles. *IEEE Access*, 8:26067–26084, 2020.

[168] Xiangjun Qian, Jean Gregoire, Fabien Moutarde, and Arnaud De La Fortelle. Autonomous intersection management for mixed traffic flow. *arXiv preprint arXiv:1407.5813*, 2014.

[169] SA Ramadhan, HY Sutarto, GS Kuswana, and E Joelianto. Application of area traffic control using the max-pressure algorithm. *Transportation planning and technology*, 43(8):783–802, 2020.

[170] Nedal T Ratrout and Imran Reza. Comparison of optimal signal plans by synchro & transyt-7f using paramics–a case study. *Procedia Computer Science*, 32:372–379, 2014.

[171] Radha Reddy, Luís Almeida, and Eduardo Tovar. Work-in-progress: Synchronous intersection management protocol for mixed traffic flows. In *2019 IEEE Real-Time Systems Symposium (RTSS)*, pages 576–579. IEEE, 2019.

[172] Radha Reddy, Luís Almeida, and Eduardo Tovar. An intersection management protocol for mixed autonomous and legacy vehicles. In *Proceedings of the 3rd Doctoral Congress in Engineering (DCE 2019)*, 2019.

[173] Radha Reddy, Luis Almeida, Miguel Gutiérrez Gaitán, Pedro Miguel Santos, and Eduardo Tovar. Impact of intersection management on energy-efficiency when mixing electric and combustion vehicles. In *23rd EURO Working Group on Transportation Meeting*, 2020.

[174] Radha Reddy, Luís Almeida, Pedro M Santos, and Eduardo Tovar. Comparing the ecological footprint of intersection management protocols for human/autonomous scenarios. In *2020 IEEE 23rd International Conference on Intelligent Transportation Systems (ITSC)*, pages 1–6. IEEE, 2020.

[175] Radha Reddy, Luís Almeida, Miguel Gaitan, Harrison Kurunathan, Pedro Santos, and Eduardo Tovar. Work-in-progress: Worst-case response time of intersection management protocols. In *2021 IEEE Real-Time Systems Symposium (RTSS)*, pages 556–559. IEEE, 2021.

[176] Radha Reddy, Luís Almeida, Miguel Gutiérrez Gaitán, Pedro Miguel Santos, and Eduardo Tovar. Synchronous framework extended for complex intersections. In *24th Euro Working Group on Transportation Meeting*, 2021.

[177] Radha Reddy, Luís Almeida, Miguel Gutiérrez Gaitán, Pedro Miguel Santos, and Eduardo Tovar. Sustainability analysis of complex multi-lane intelligent signalized intersections. In *Doctoral Congress in Engineering*, 2021.

[178] Radha Reddy, Luís Almeida, Pedro M Santos, Samia Bouzefrane, and Eduardo Tovar. Synchronous intersection management to reduce time loss. *Transportation Research Procedia*, 52:364–372, 2021.

[179] Radha Reddy, Luis Almeida, Pedro Santos, and Eduardo Tovar. Work-in-progress: Exploring the composition of synchronous intelligent intersections. In *2022 IEEE Real-Time Systems Symposium (RTSS)*, pages 523–526. IEEE, 2022.

[180] Radha Reddy, Luis Almeida, Miguel Gaitan, Pedro Santos, and Eduardo Tovar. Synchronous management of mixed traffic at signalized intersections towards sustainable road transportation. *IEEE Access*, 7:1–12, 2023.

[181] Radha Reddy, Luís Almeida, Pedro Miguel Gaitán, Santos, and Eduardo Tovar. Quality of service of im approaches under saturated traffic. In *25th Euro Working Group on Transportation Meeting*, 2023.

[182] Radha Reddy, Luis Almeida, Harrison Kurunathan, Miguel Gaitán, Pedro Santos, and Eduardo Tovar. Comparing the worst-case response time of complex intersections management. *IEEE Open Journal of Intelligent Transportation Systems*, 2023.

[183] Radha Reddy, Luis Almeida, Harrison Kurunathan, Pedro Santos, and Eduardo Tovar. Comparing energy savings and emissions efficiency of mixed icevs and bevs at complex intersections. *Under submission to TRPD*, 2023.

[184] Radha Reddy, Luís Almeida, Pedro Santos, and Eduardo Tovar. Waiting time analysis for a network of signalized intersections. *Procedia Computer Science*, 220:503–510, 2023.

[185] Radha Reddy, Luís Almeida, Pedro Miguel Santos, and Eduardo Tovar. Advantages of synchronizing vehicles intersection access. In *25th Euro Working Group on Transportation Meeting*, 2023.

[186] Hannah Ritchie and Max Roser. Urbanization. *Our world in data*, 2018.

[187] Dennis I Robertson. Transyt: a traffic network study tool. *RRL Report LR 253, Road Resarch Laboratory Crowthorne, Berkshire.*, 1969.

[188] Mohammad Sadeghi, Melike Erol-Kantarci, and Hussein T Mouftah. Connected and autonomous electric vehicle charging infrastructure integration to microgrids in future smart cities. In *Connected and Autonomous Vehicles in Smart Cities*, pages 1–17. CRC Press, 2020.

[189] Steven H Schot. Jerk: the time rate of change of acceleration. *American Journal of Physics*, 46(11):1090–1094, 1978.

[190] David Schrank, Bill Eisele, Tim Lomax, et al. Urban mobility report 2021. *Texas Transportation Institute*, 2021.

[191] Suvrajeet Sen and K Larry Head. Controlled optimization of phases at an intersection. *Transportation science*, 31(1):5–17, 1997.

[192] S Niggol Seo. Beyond the paris agreement: Climate change policy negotiations and future directions. *Regional Science Policy & Practice*, 9(2):121–140, 2017.

[193] Susan Shaheen and Rachel Finson. Intelligent transportation systems. *Elsevier*, pages 487–496, 2004.

[194] Neda Shahidi, Tsz-Chiu Au, and Peter Stone. Batch reservations in autonomous intersection management. In *The 10th International Conference on Autonomous Agents and Multiagent Systems-Volume 3*, pages 1225–1226, 2011.

[195] Palwasha W Shaikh, Mohammed El-Abd, Mounib Khanafer, and Kaizhou Gao. A review on swarm intelligence and evolutionary algorithms for solving the traffic signal control problem. *IEEE transactions on intelligent transportation systems*, 23(1):48–63, 2020.

[196] Guni Sharon and Peter Stone. A protocol for mixed autonomous and human-operated vehicles at intersections. In *International Conference on Autonomous Agents and Multiagent Systems*, pages 151–167. Springer, 2017.

[197] Ibrahem Shatnawi, Ping Yi, and Ibrahim Khliefat. Automated intersection delay estimation using the input–output principle and turning movement data. *International Journal of Transportation Science and Technology*, 7(2):137–150, 2018.

[198] Chaitrali Shirke, Nasser Sabar, Edward Chung, and Ashish Bhaskar. Metaheuristic approach for designing robust traffic signal timings to effectively serve varying traffic demand. *Journal of Intelligent Transportation Systems*, 26(3):343–355, 2022.

[199] MJ Shirvani Shiri and Hamid Reza Maleki. Maximum green time settings for traffic-actuated signal control at isolated intersections using fuzzy logic. *International Journal of Fuzzy Systems*, 19:247–256, 2017.

[200] Óscar Silva, Rubén Cordera, Esther González-González, and Soledad Nogués. Environmental impacts of autonomous vehicles: A review of the scientific literature. *Science of The Total Environment*, page 154615, 2022.

[201] Arthur G Sims and Kenneth W Dobinson. The sydney coordinated adaptive traffic (scat) system philosophy and benefits. *IEEE Transactions on vehicular technology*, 29(2):130–137, 1980.

[202] Ranjay Singh, Abhishek Kumar, Arvind R Singh, Raj Naidoo, Ramesh C Bansal, and Praveen Kumar. Environmental feasibility of incorporation of electric taxis in south africa. *The Journal of Engineering*, 2019(18):5078–5084, 2019.

[203] Hariom Kumar Solanki, Farhad Ahamed, Sanjeev Kumar Gupta, and Baridalyne Nongkynrih. Road transport in urban india: Its implications on health. *Indian journal of community medicine: official publication of Indian Association of Preventive & Social Medicine*, 41(1):16, 2016.

[204] Sebastian Sontges, Markus Koschi, and Matthias Althoff. Worst-case analysis of the time-to-react using reachable sets. In *2018 IEEE Intelligent Vehicles Symposium (IV)*, pages 1891–1897. IEEE, 2018.

[205] Morteza Taiebat, Austin L Brown, Hannah R Safford, Shen Qu, and Ming Xu. A review on energy, environmental, and sustainability implications of connected and automated vehicles. *Environmental science & technology*, 52(20):11449–11465, 2018.

[206] Mehrdad Tajalli and Ali Hajbabaie. Traffic signal timing and trajectory optimization in a mixed autonomy traffic stream. *IEEE Transactions on Intelligent Transportation Systems*, 2021.

[207] Ahmadreza Talebian and Sabyasachee Mishra. Predicting the adoption of connected autonomous vehicles: A new approach based on the theory of diffusion of innovations. *Transportation Research Part C: Emerging Technologies*, 95:363–380, 2018.

[208] Md Abu Sufian Talukder, Abhay D Lidbe, Elsa G Tedla, Alexander M Hainen, and Travis Atkison. Trajectory-based signal control in mixed connected vehicle environments. *Journal of transportation engineering, Part A: Systems*, 147(5):04021016, 2021.

[209] Eiichi Taniguchi, Tien Fang Fwa, and Russell G Thompson. *Urban transportation and logistics: Health, safety, and security concerns*. CRC Press, 2013.

[210] Manel Terraza, Ji Zhang, and Zongzhi Li. Intersection signal timing optimisation for an urban street network to minimise traffic delays. *Promet-Traffic&Transportation*, 33(4):579–592, 2021.

[211] Chunlin Tian, Zhilong Wang, and Liying Wei. Modeling and simulation on the bus priority based on actuated traffic signal control at intersections. In *Sixth International Conference on Traffic Engineering and Transportation System (ICTETS 2022)*, volume 12591, pages 469–474. SPIE, 2023.

[212] Mohamed Tlig, Olivier Buffet, and Olivier Simonin. Decentralized traffic management: A synchronization-based intersection control. In *2014 International Conference on Advanced Logistics and Transport (ICALT)*, pages 109–114. IEEE, 2014.

[213] Behnam Torabi, Rym Z Wenkstern, and Robert Saylor. A collaborative agent-based traffic signal system for highly dynamic traffic conditions. *Autonomous Agents and Multi-Agent Systems*, 34:1–24, 2020.

[214] Martin Treiber, Ansgar Hennecke, and Dirk Helbing. Congested traffic states in empirical observations and microscopic simulations. *Physical review E*, 62(2):1805, 2000.

[215] Martin Treiber, Arne Kesting, and Christian Thiemann. How much does traffic congestion increase fuel consumption and emissions? applying a fuel consumption model to the ngsim trajectory data. In *87th Annual Meeting of the Transportation Research Board, Washington, DC*, volume 71, pages 1–18, 2008.

[216] Pravin Varaiya. Max pressure control of a network of signalized intersections. *Transportation Research Part C: Emerging Technologies*, 36:177–195, 2013.

[217] Francisco José Lopes Veiga. Image processing for detection of vehicles in motion, 2018.

[218] Shrey Verma, Gaurav Dwivedi, and Puneet Verma. Life cycle assessment of electric vehicles in comparison to combustion engine vehicles: A review. *Materials Today: Proceedings*, 2021.

[219] Jacob Dirk Vreeswijk, MKM Mahmod, and Bart van Arem. Energy efficient traffic management and control-the ecomove approach and expected benefits. In *13th International IEEE Conference on Intelligent Transportation Systems*, pages 955–961. IEEE, 2010.

[220] Miroslav Vujić, Ivana Šemanjski, and Pero Vidan. Improving energy efficiency by advanced traffic control systems. *Transactions on maritime science*, 4(02):119–126, 2015.

[221] Walther Wachenfeld, Philipp Junietz, Raphael Wenzel, and Hermann Winner. The worst-time-to-collision metric for situation identification. In *2016 IEEE intelligent vehicles symposium (IV)*, pages 729–734. IEEE, 2016.

[222] Jian Wang, Wei Wang, Gang Ren, and Min Yang. Worst-case traffic assignment model for mixed traffic flow of human-driven vehicles and connected and autonomous vehicles by factoring in the uncertain link capacity. *Transportation research part C: emerging technologies*, 140:103703, 2022.

[223] Michael I-C Wang, Charles H-P Wen, and H Jonathan Chao. Roadrunner+: An autonomous intersection management cooperating with connected autonomous vehicles and pedestrians with spillback considered. *ACM Transactions on Cyber-Physical Systems (TCPS)*, 6(1):1–29, 2021.

[224] Qing Wang, Jianying Zheng, Hao Xu, Bin Xu, and Rong Chen. Roadside magnetic sensor system for vehicle detection in urban environments. *IEEE Transactions on Intelligent Transportation Systems*, 19(5):1365–1374, 2017.

[225] Yu Wang, Qi Zhang, and Xiao Huang. Research on traffic signal self-organizing control based on vanet acquisition information. In *IOP Conference Series: Materials Science and Engineering*, volume 392 (6), page 062159. IOP Publishing, 2018.

[226] Ziran Wang, Yougang Bian, Steven E Shladover, Guoyuan Wu, Shengbo Eben Li, and Matthew J Barth. A survey on cooperative longitudinal motion control of multiple connected and automated vehicles. *IEEE Intelligent Transportation Systems Magazine*, 12(1):4–24, 2019.

[227] Shannon Warchol, Nagui Rouphail, Chris Vaughan, and Brendan Kearns. Queue-based guidance for signalization consideration at two and three-legged intersections. *Transportation research record*, 2673(10):416–426, 2019.

[228] Fo Vo Webster. Traffic signal settings. Technical report, Road Research Lab Tech Papers, 1958.

[229] Axel Wegener, Michał Piórkowski, Maxim Raya, Horst Hellbrück, Stefan Fischer, and Jean-Pierre Hubaux. Traci: an interface for coupling road traffic and network simulators. In *Proceedings of the 11th communications and networking simulation symposium*, pages 155–163, 2008.

[230] Hua Wei, Chacha Chen, Guanjie Zheng, Kan Wu, Kai Xu, Vikash Gayah, and Zhenhui Li. Presslight: Learning max pressure control for signalized intersections in arterial network. In *Proceedings of the 25th ACM SIGKDD International Conference on Knowledge Discovery and Data Mining*, pages 1290–1298, 2019.

[231] Hua Wei, Guanjie Zheng, Vikash Gayah, and Zhenhui Li. A survey on traffic signal control methods. *arXiv preprint arXiv:1904.08117*, 2019.

[232] Kaige Wen, Shiru Qu, and Yumei Zhang. A stochastic adaptive control model for isolated intersections. In *2007 IEEE International Conference on Robotics and Biomimetics (ROBIO)*, pages 2256–2260. IEEE, 2007.

[233] Reiter Wiedemann and U Reiter. Microscopic traffic simulation: the simulation system mission, background and actual state. *Project ICARUS (V1052) Final Report*, 2:1–53, 1992.

[234] Marcus Wisch, Adrian Hellmann, Markus Lerner, Thomas Hierlinger, Volker Labenski, Michael Wagner, Harald Feifel, Oana Robescu, Pauline Renoux, and Xavier Groult. Car-to-car accidents at intersections in europe and identification of use cases for the test and assessment of respective active vehicle safety systems. In *26th International Technical Conference on the Enhanced Safety of Vehicles, Eindhoven, Netherlands*, pages 10–13, 2019.

[235] Jennifer R Wolch, Jason Byrne, and Joshua P Newell. Urban green space, public health, and environmental justice: The challenge of making cities 'just green enough'. *Landscape and urban planning*, 125:234–244, 2014.

[236] SC Wong. Group-based optimisation of signal timings using the transyt traffic model. *Transportation Research Part B: Methodological*, 30(3):217–244, 1996.

[237] Wei Wu, Yang Liu, Wei Liu, Fangni Zhang, Vinayak Dixit, and S Travis Waller. Autonomous intersection management for connected and automated vehicles: A lane-based method. *IEEE Transactions on Intelligent Transportation Systems*, 23(9): 15091–15106, 2021.

[238] Liping Xia and Yaping Shao. Modelling of traffic flow and air pollution emission with application to hong kong island. *Environmental Modelling & Software*, 20(9): 1175–1188, 2005.

[239] Lin Xiao, Meng Wang, and Bart Van Arem. Realistic car-following models for microscopic simulation of adaptive and cooperative adaptive cruise control vehicles. *Transportation Research Record*, 2623(1):1–9, 2017.

[240] Biao Xu, Xuegang Jeff Ban, Yougang Bian, Wan Li, Jianqiang Wang, Shengbo Eben Li, and Keqiang Li. Cooperative method of traffic signal optimization and speed control of connected vehicles at isolated intersections. *IEEE Transactions on Intelligent Transportation Systems*, 20(4):1390–1403, 2018.

[241] Urban Transport XVI. An investigation of the variability of start-up lost times and departure headways at signalized intersections in urban areas. *Urban Transport XVI: Urban Transport and the Environment in the 21st Century*, 111:59, 2010.

[242] Kento Yabuuchi, Masahiro Hirano, Taku Senoo, Norimasa Kishi, and Masatoshi Ishikawa. Real-time traffic light detection with frequency patterns using a high-speed camera. *Sensors*, 20(14):4035, 2020.

[243] Kaidi Yang, S Ilgin Guler, and Monica Menendez. Isolated intersection control for various levels of vehicle technology: Conventional, connected, and automated vehicles. *Transportation Research Part C: Emerging Technologies*, 72:109–129, 2016.

[244] Handong Yao and Xiaopeng Li. Decentralized control of connected automated vehicle trajectories in mixed traffic at an isolated signalized intersection. *Transportation research part C: emerging technologies*, 121:102846, 2020.

[245] Bao-Lin Ye, Weimin Wu, Keyu Ruan, Lingxi Li, Tehuan Chen, Huimin Gao, and Yaobin Chen. A survey of model predictive control methods for traffic signal control. *IEEE/CAA Journal of Automatica Sinica*, 6(3):623–640, 2019.

[246] Maram Bani Younes and Azzedine Boukerche. An intelligent traffic light scheduling algorithm through vanets. In *39th Annual IEEE Conference on Local Computer Networks Workshops*, pages 637–642. IEEE, 2014.

[247] Raid Zaghal, Khalid Thabatah, and Saeed Salah. Towards a smart intersection using traffic load balancing algorithm. In *2017 Computing Conference*, pages 485–491. IEEE, 2017.

[248] Jian Zhang, Xia Jiang, Ziyi Liu, Liang Zheng, and Bin Ran. A study on autonomous intersection management: planning-based strategy improved by convolutional neural network. *KSCE Journal of Civil Engineering*, 25(10):3995–4004, 2021.

[249] Ying Zhang, Zhaoyang Ai, Jinchao Chen, Tao You, Chenglie Du, and Lei Deng. Energy-saving optimization and control of autonomous electric vehicles with considering multiconstraints. *IEEE Transactions on Cybernetics*, pages 10869–10881, 2021.

[250] Yue Zhang and Christos G Cassandras. The penetration effect of connected automated vehicles in urban traffic: an energy impact study. In *2018 ieee conference on control technology and applications (ccta)*, pages 620–625. IEEE, 2018.

[251] Hong-Xing Zhao, Rui-Chun He, and Na Yin. Modeling of vehicle co2 emissions and signal timing analysis at a signalized intersection considering fuel vehicles and electric vehicles. *European Transport Research Review*, 13(1):1–15, 2021.

[252] Bowen Zheng, Chung-Wei Lin, Shinichi Shiraishi, and Qi Zhu. Design and analysis of delay-tolerant intelligent intersection management. *ACM Transactions on Cyber-Physical Systems*, 4(1):1–27, 2019.

[253] Yongtao Zheng, Xuedong Hua, Wei Wang, Jialiang Xiao, and Dongya Li. Analysis of a signalized intersection with dynamic use of the left-turn lane for opposite through traffic. *Sustainability*, 12(18):7530, 2020.

[254] Shaopeng Zhong, Ao Liu, Yu Jiang, Simon Hu, Feng Xiao, Hai-Jun Huang, and Yan Song. Energy and environmental impacts of shared autonomous vehicles under different pricing strategies. *npj Urban Sustainability*, 3(1):8, 2023.

[255] Zijia Zhong, Mark Nejad, and Earl E Lee. Autonomous and semiautonomous intersection management: A survey. *IEEE Intelligent Transportation Systems Magazine*, 13(2):53–70, 2020.